Spindle positioning in the ascidian zygote and its role in organelles repartition

Anne Rosfelter

Sorbonne Université

Ecole doctorale Complexité du Vivant (ED515)

Laboratoire de Biologie du Développement de Villefranche-sur-Mer UMR7009 CNRS/Sorbonne
Equipe Ascidian BioCell

Le positionnement du fuseau mitotique chez le zygote d'ascidie et son rôle dans la répartition des organelles.

Par Anne ROSFELTER

Thèse de doctorat de Biologie du Développement

Dirigée par Alex McDOUGALL
Co-encadrée par Hervé TURLIER

La thèse présentée et soutenue publiquement le 20/02/2023

Devant un jury composé de :

Dr. Marie DELATTRE,	Présidente du jury
Dr. Benjamin LACROIX,	Rapporteur
Dr. Guillaume HALET,	Rapporteur
Dr. Bénédicte CHARRIER,	Examinatrice
Dr. Hervé TURLIER,	Co-encadrant de thèse
Dr. Alex McDOUGALL,	Directeur de thèse

Acknowledgements

Merci Alex, Hervé, de m'avoir fait confiance et de m'avoir laissée détourner le projet initial vers mes sujets préférés. Merci de m'avoir chacun donné vos conseils ; Alex tu m'as permis de prendre confiance et de m'affirmer comme scientifique, Hervé, ton regard critique et ta disponibilité ont été d'une aide précieuse.

Merci aux membres du jury qui donnent de leurs temps pour critiquer mes travaux.

Merci aux membres de mon comité de thèse, Michel Gho pour ses idées d'expériences, Matteo Rauzi pour son enthousiasme et pour m'avoir accueillie dans son équipe le temps d'une expérience, et Yas pour sa prévenance tout au long de ma thèse.

Merci à toute l'équipe, Rémi, Lydia et Céline, d'avoir toujours été disponibles pour m'aider. Et je remercie particulièrement Janet, qui m'a inspirée à continuer la science, qui n'a jamais manqué d'intérêt et d'idées pour mes hypothèses les plus farfelues, et que je n'ai jamais vue à court de jeux de mots ou de citations, qui parsèment mails et paillasses.

Merci Ghislain, et merci Sébastien pour la simplicité et la gentillesse avec lesquelles vous m'avez aidée et conseillée.

Merci à chacun au laboratoire, qui rendez cet endroit convivial, tous toujours prêts à rendre service. Je n'oublie évidemment pas Jocelyne, Didier et Thierry.

Et enfin, merci à mes amis, plus qu'un merci, 100 000 mercis. Vous étiez là quand c'était dur avec le stress, le Covid, les couvre-feux. Et vous étiez aussi là pour rire, râler et sortir. Vous avez mis de la joie dans chacune des journées passées au labo. Vous avez rendu mes années de thèse inoubliables. Merci Manon, merci Julia, merci Angelica, merci Bastien. Merci Léa, loin des yeux près du cœur. Merci Nicolas, Sami et Anna, merci Camille, Charlotte, petite Marie, grande Marie, Cat, Vitoria, Marc, et Marianne et David.

Merci à ma famille, discrète et présente, sur qui je peux compter inconditionnellement.

Résumé :

Après la fécondation d'un ovocyte, un aster de microtubules se forme autour de l'ADN mâle. Cet aster spermatique permet d'amener le pro-noyau femelle jusqu'au pro-noyau mâle pour qu'ils puissent fusionner. Il permet aussi de déplacer l'ADN fusionné jusqu'au centre de la cellule pour assurer une division cellulaire équitable. Les mécanismes de centration d'un aster ou d'un fuseau ont donné lieu à de nombreuses recherches, que ce soit par modélisation, expérimentalement chez des espèces telles *C. elegans*, *P. lividus*, *M.musculus* ou *in vitro* sur des extraits de *Xenopus laevis.* Trois mécanismes principaux se dégagent : le *pushing*, le *cortical pulling* et le *cytoplasmic pulling* (ou *bulk pulling*).

En étudiant le déplacement de l'aster et du fuseau mitotique chez le zygote de l'ascidie *P. mammillata* j'ai découvert un système qui combine ces trois mécanismes en s'appuyant sur l'alternance des étapes du cycle cellulaire. En méiose, l'aster utilise la polymérisation des microtubules qui le composent pour pousser contre le cortex d'actine et s'en décoller (*pushing*). Arrivé en interphase, l'aster retourne contre le cortex grâce à une traction qu'exerce la membrane sur les microtubules (*cortical pulling*). Enfin à l'entrée en mitose, la traction membranaire cesse et libère les asters du fuseau mitotique, qui cèdent donc aux forces exercées par le transport d'organelles vers le centre de l'aster (*cytoplasmic pulling*) qui semblent constantes durant le cycle cellulaire. Cela permet de centrer le fuseau.

En même temps que l'aster se forme et se déplace, une réorganisation des compartiments intracellulaires se met en place. Pour comprendre de quelle manière l'organisation intracellulaire peut être perturbée par la formation de l'aster, j'ai étudié le cas du vitellus. En effet, le vitellus, qui est présent sous forme de vésicules, est initialement abondant et homogène dans l'ovocyte non fécondé. Cependant, dès que l'aster apparaît, sa répartition change et les vésicules de vitellus sont exclues de la zone contenant l'aster. Cette exclusion générée à la formation de l'aster chez le zygote, est maintenue au cours du développement. Dans mes travaux, j'ai pu observer qu'elle est majoritairement due à l'accumulation à l'aster d'autres organelles comme le réticulum endoplasmique. La fonction de transport des microtubules de l'aster suffit donc à réorganiser complètement la cellule en excluant certaines organelles et en en accumulant d'autres.

Les déplacements de l'aster et du fuseau mitotique, leur régulation par le cycle cellulaire, et la réorganisation intracellulaire, identifiés ici chez le zygote d'ascidie, s'appuient sur le fonctionnement d'éléments fondamentaux d'une cellule, à savoir : les microtubules, le cortex d'actine, le réticulum endoplasmique, les protéines du cycle cellulaire, etc. Les découvertes présentées revêtent ainsi une portée universelle, adaptable aux spécificités de différents types cellulaires.

Summary:

After oocyte fertilization, a microtubule aster forms around the male DNA. The sperm aster brings the female pro-nucleus to the male pro-nucleus so they can fuse, but it also moves the fused nuclei to the cell center to ensure an equitable cell division. Numerous studies performed in vitro, by modeling or experimentally in species such as *C. elegans, P. lividus*, and *M. musculus*, addressed the aster and spindle centration mechanisms. Three main mechanisms emerged; pushing, cortical pulling, and cytoplasmic pulling. By studying aster centration in the zygote of the ascidian *P. mammillata*, I discovered a system that combines these three mechanisms based on the cell cycle stages. In meiosis, the aster uses the polymerization of its microtubules to push against the actin cortex and move away from it (pushing). Once in interphase, the aster returns to the cortex by a pull exerted by the membrane on the microtubules (cortical pulling). At mitosis entry, cortical pulling stops, and releases the mitotic spindle's asters. In consequence, the asters give in to the forces exerted by the transport of organelles to the aster center (cytoplasmic pulling), that appeared constant during the cell cycle. Cytoplasmic pulling hence participate in centering the spindle

While the aster forms and moves, the intracellular compartments reorganize. To understand how intracellular organization can be disrupted by aster formation, I studied the case of yolk. The yolk, in the form of vesicles (called granules or platelets), is initially abundant and homogeneous in the unfertilized oocyte. However, as soon as the aster appears, its distribution changes and the yolk platelets are excluded from the region containing the aster. This exclusion generated by the aster formation in the zygote is maintained during development. I observed that yolk exclusion is mainly due to the accumulation at the aster of other organelles such as the endoplasmic reticulum. The transport function of the aster microtubules is therefore sufficient to completely reorganize the cell by excluding some organelles and accumulating others.

The movements of the aster and the spindle, their regulation by cell cycle, and the intracellular reorganization, identified here in the ascidian zygote, rely on basic elements of a cell, namely: the microtubules, the actin cortex, the endoplasmic reticulum, the proteins of the cell cycle, etc. Thus, the discoveries presented here cover a broad scope, and seem adaptable to the specificities of different cell types.

Table of contents

List of Figures

Introduction

0.1 The large field of developmental biology

Developmental biology addresses how to obtain a fully functioning organism. This question holds innumerable research paths. First, we can distinguish research on the formation of specialized cell-structures, like organogenesis or regeneration, from research with a focus on the development of an organism as a whole. To develop a new individual from a mature organism, either the species involved can perform asexual reproduction, like strobilation (in *Aurelia aurita*) (Kroiher et al., 2000), fragmentation (for example in some sponges and corals) (Wulff, 1991) or even like budding and non-embryologic development (NED, in colonial ascidian) (Alié et al., 2018), or they perform sexual reproduction. Sexual reproduction is defined by the encounter of male and female gametes, each carrying a set of chromosomes, to produce one totipotent cell which possess two sets of chromosomes (Gilbert & Barresi, 2016). In this context, the big question of developmental biology finds a clear start: the egg. From the egg, embryonic development can be summed up in four main steps: fertilization, segmentation (also named cleavage), gastrulation, and organogenesis, that are adjusted and tailored to each species. Using the basic example of a bilaterian, these steps can be described as follows:

- At fertilization, the male gamete, called spermatozoid, breaks the female gamete's state of inertia by triggering physiological responses for the entry of its DNA. The female gamete, also called egg or oocyte, now has two sets of chromosomes and as it possesses a new genome and it is therefore considered to be a new individual, called the zygote (Foucrier et al., 2019).
- Cleavage (or Segmentation) starts when the zygote initiates a succession of divisions. The cells do not grow between divisions and they divide following a specific pattern that varies between species. This results in an embryonic stage called blastula where the embryo is about the same volume as the zygote (Foucrier et al., 2019). The blastula goes into mid-blastula

transition (MBT), meaning that the embryo will start expressing its own genes (Newport & Kirschner, 1982) and its cells will go through a longer cell cycle.

- After the MBT, the process of gastrulation enables extensive cell rearrangements into three distinct tissue layers (endoderm, ectoderm, mesoderm) (Gilbert & Barresi, 2016).
- These three germ layers signal to each other, they proliferate, rearrange, and differentiate into specific organs according to their origins and inductions (Gilbert & Barresi, 2016). Organogenesis finishes when the organism is relatively autonomous, that is, when it reaches a larval stage, hatches or at birth. After this step, the organism can undergo post-embryonic development or metamorphosis.

Looking into the history of developmental biology, it is manifest that these embryology topics have been central to the field. Fertilization and segmentation were already described in publication from the very early 1900's, while gastrulation and organogenesis, were foresaw from discussion on cell fate and cell lineage (Conklin, 1905a; Morgan, 1927). During this period, the concept of perturbation experiments was controversial (G. J, 1928) but booming as exemplified by this quote from the preface of "Experimental Biology" by T.H. Morgan:

> *"Hence not without a feeling of jealous regret, the old-fashioned embryologist sees these gems of nature consigned to test tubes for chemical analyses, to centrifuges to disturb their arrangement, to microdissecting instruments to pick them to pieces, and to endless tortures by alterations in the environment to disturb the orderly, normal course of events. For, it is the automatic self-contained perfection of the developmental process that holds our interest."*

This author also refers extensively to Wilhelm Roux as a pioneer in experimental embryology for his work on "developmental mechanics" performed in 1885, thus indicating that the booming of perturbation experiments probably originates in the late 19th century. Experiments were mostly performed on frogs or on various marine invertebrates, like ascidians, nereis or amphioxus, due to their accessibility, size and external development (Fisher & Smith, 1984).

Ascidians embryos were a recognized model of embryology studies, as shown by the abundant and international literature mentioned by Conklin in 1905 (Conklin, 1905a; Fisher & Smith, 1984). Developmental biology on ascidian continued through the 20th century, with a highlight in cell biology from the 90's until now (Nishikata et al., 1999; Roegiers et al., 1999; Sardet et al., 1989; Sawada & Schatten, 1988; Speksnijder et al., 1993), and it currently benefits

from a new impetus with the input of biomechanics into the field (Fujii et al., 2021; Godard et al., 2020a; Pierre et al., 2016a).

Following the first embryologists, and the line of researchers that continued and modernized the field, the study described in this manuscript focuses on the ascidian zygote, between fertilization and cleavage, with the global aim to better understand the cellular and mechanical cues that can shape an embryo. J.M.W. Slack classed people interested in embryos in two groups; people that share the concern of medical research scientist, that want to know how similar to human an embryo can be, and the ones who find delight in the differences of developmental strategies supposed attuned to the concern lifestyle (Slack, 1991). Whether you want to know how similar or how different ascidian embryos are from your favorite species, I wish you will find interest in this work on ascidian, a curious invertebrate that few people can recognize, but that is not so far from human.

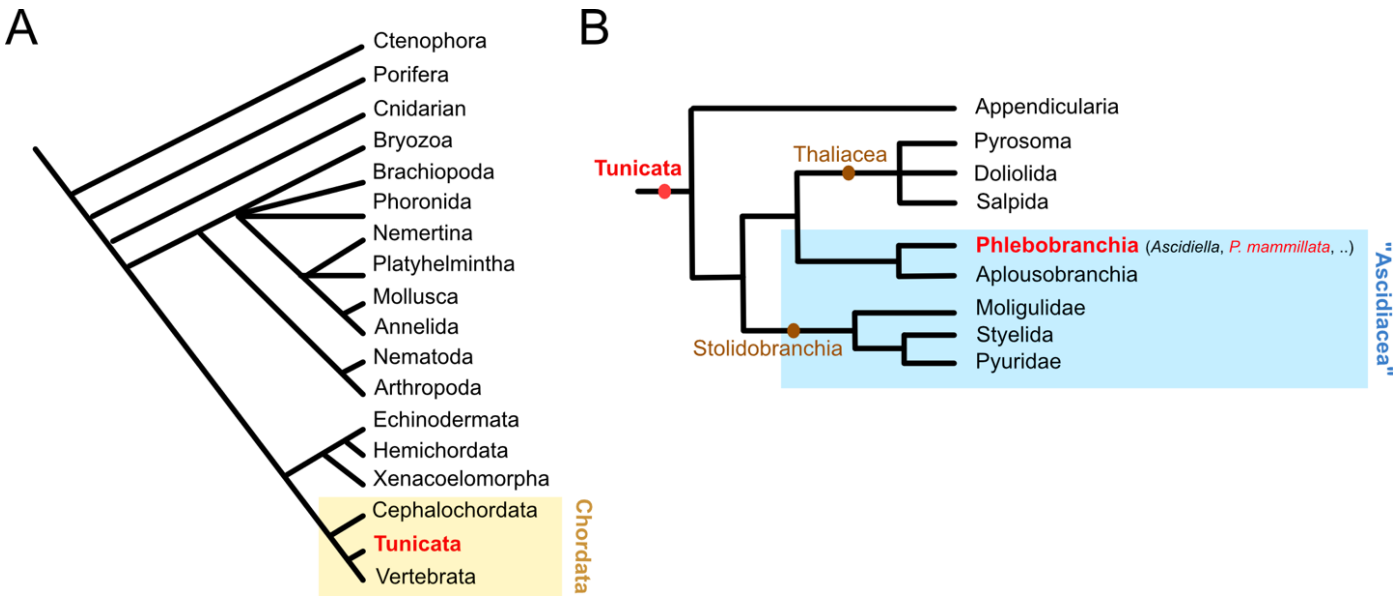

Figure 0.1: Tunicata phylogeny

A- Current view of Tunicata position in the metazoan tree built from molecular phylogenies. B- Simplified tree of the current understanding of the tunicate relationships according to (Stolfi & Brown, 2015). Dashed lines represent possible relationship

0.2 The ascidian *Phallusia mammillata*

0.2.1 Phylogeny

Ascidians, also designated by the vernacular name sea squirt, belong to the phylum of chordates and the subphylum of tunicates. The chordates regroup species notably recognizable by the presence of a notochord and a dorsal nerve cord at a moment of their development. Chordate separates in three sub-phyla: vertebrate, tunicate (also called urochordates) and cephalochordate. Tunicates is a monophyletic group of marine filter-feeding animals, united by the ability to synthesize cellulose. Originally, tunicates were divided into three classes Appendicularia, Thaliacea and Ascidiacea. The term "ascidian" is a common name for the paraphyletic class Ascidiacae. However, the Ascidiacea group has been revised after molecular phylogenies provided no support indicating its monophylogeny (Tsagkogeorga et al., 2009). Therefore, the phylogenetic relationship of the classes composing the Tunicata is not yet completely settled (Kocot et al., 2018; Stolfi & Brown, 2015). It is now thought that tunicate group has three clades: Appendicularia, Stolidobranche, and Thaliacea together with Phlebobranch and Aplousobranch ascidians (Figure 0.1) (Delsuc et al., 2018; Stolfi & Brown, 2015; Tsagkogeorga et al., 2009).

The Ascidiacea paraphyletic class regroups species from Phlebobranch, Stolidobranch, and Aplousobranch that share morphological traits. They are fixed, they possess two siphons, and, as implied by the greek etymology ἀσκός, askós, their body looks like a goatskin. They can be colonial or solitary. Among all ascidians, I exclusively worked with the specie *Phallusia mammillata* which belongs to the Phlebobranch suborder, characterized by a vascular branchial sac. In the same way as aplousobranchs, their gonads are surrounded by the gut (Figure 0.2). To sum up, the taxonomic classification of *P. mammillata* is:

Chordata > Tunicata > Phlebobranchia > Ascidiidae > *Phallusia mammillata*

0.2.2 Description

P. mammillata, the white sea squirt, can live on various substrates (sand, rocks, mud, …), from 2 to 200 meters under sea level. It is found on coasts of the Northeastern Atlantic, the

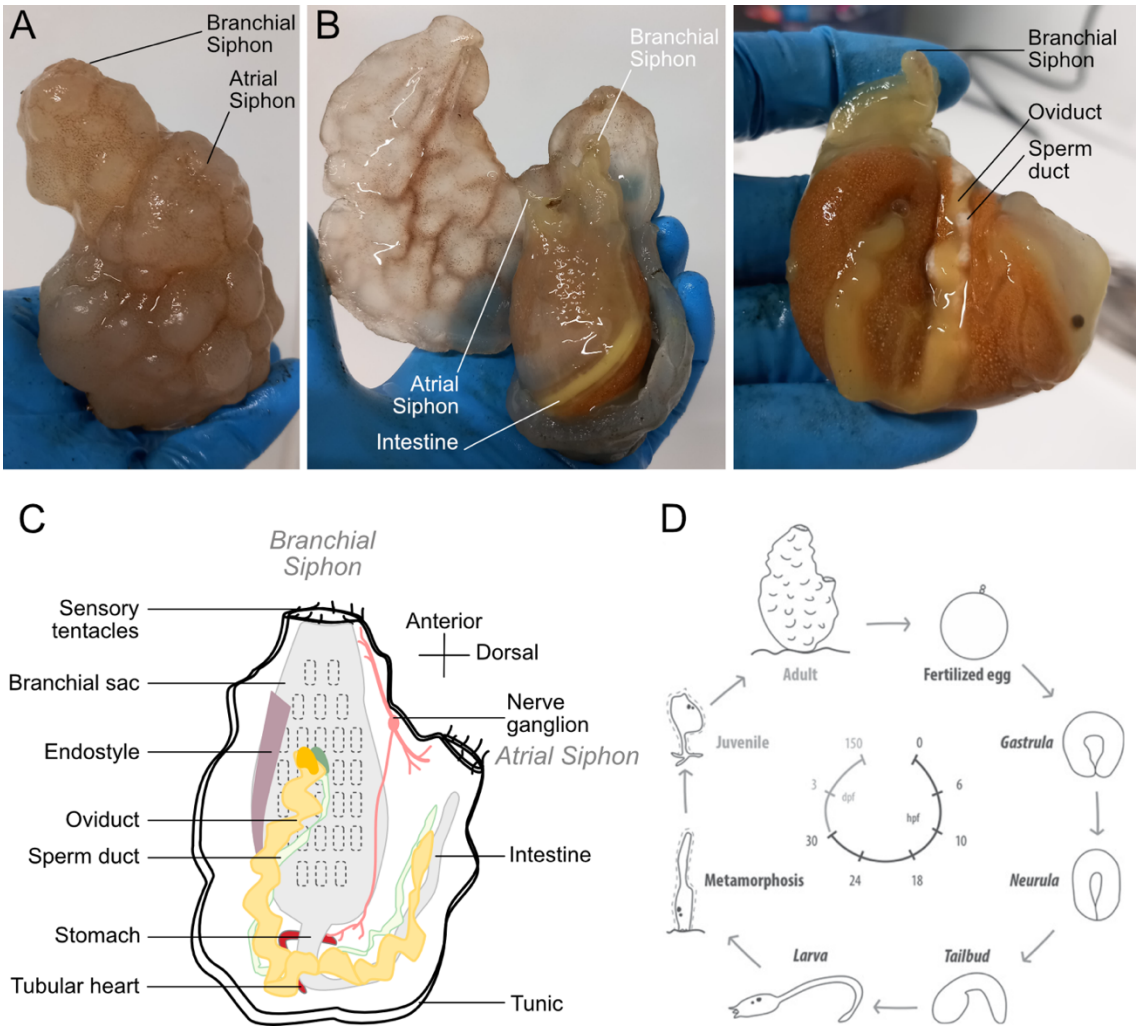

Figure 0.2: *P. mammillata* body plan and life cycle

A- Wild type specimen from Banyuls, B- Body of the animal after removal of the tunic. Several organs are visible C- Simplified diagram of the body plan of an adult, D- Diagram of life cycle from (Gomes et al., 2019)

North Sea, the Channel and around the Mediterranean Sea, mainly on French coasts (Reguieg et al., 2021).

It was first described by GL Cuvier in 1815 (Cuvier, 1815). It is a solitary ascidian whose adults measure around 15 cm in height and are 6-9 cm wide (Figure 0.2). It has an irregular and bumpy white tunic, sometimes thicker than 1cm in places. Fixed on its posterior region, it has two clearly separated siphons, the branchial and the atrial siphon. The branchial one is on top of the animal and defines the anterior, the atrial siphon is more in the middle of the body, and defines the dorsal side of the animal. In *Phallusia*'s simple body plan, the two contractile siphons, surrounded by sensory tentacles, create a current leading the water to a branchial sac (pharynx) (Figure 0.2 C). The water is filtered through the openings of the branchial sac and ejected through the atrial siphon. Particles suspended in the water are retained in the sac and recovered by a mucus produced by the nearby endostyle (Harant & Vernières, 1933). In continuation from the bottom of the branchial sac there is a stomach and a curved intestine where the mucus and suspended food particles are digested. Digestion wastes are expelled through the atrial siphon (Goodbody, 1975). Ascidians are hermaphrodites and self-fertile, although fertilization is more efficient between different individuals. *P. mammillata* sex glands are in the antero-ventral side, they fill the oviduct and sperm duct that follow a very wavy path leading to the atrial siphon. Spermatozoids and oocytes are spawn under light simulation. The brain and the nervous system regressed after the larval stage, only leaving one ganglion located between the two siphons. The nerve fibers arising from this ganglion innervate both siphons, the muscle of the mantle between the tunic and the branchial sac, and they also innervate the branchial sac itself, together with the visceral mass (Goodbody, 1975). The circulatory system consists of a tubular heart enclosed in a pericardium, connected on both sides to vessels and channels ramified throughout the body. The heart pumps circulating cells by peristaltic contractions that regularly changes direction.

0.2.3 Life cycle

Unfertilized oocytes are surrounded by an acellular envelope called chorion or vitelline coat, to which follicle cells adhere externally and test cells internally (Honegger & Koyanagi, 2008). After fertilization, the development of *P. mammillata* is globally similar to *Ciona intestinalis* that was described in two parts by the same author, Kohji Hotta, with indicative

times (Hotta et al., 2007, 2020). Embryonic development starts within the chorion, and is divided into six periods: Zygote period (0 - 55min), Cleavage period (55min - 4h30), Gastrula period (4h30 - 6h20), Neurula period (6h20 - 8h30), Tailbud period (8h30-17h30) when trunk and tail start to be distinguishable, and the Larva period defined by hatching from the chorions (from 17h30). Then the organism enters post-embryonic development. Five periods can be defined, first a pre-metamorphosis period where the tadpole is swimming in search of a suitable substrate on which to metamorphose. It has a notochord, a nervous system, and sensory organs (otholith, ocellus and adhesive papillaes). The tadpole then adheres trunk first onto a substrate (24h-27h), the tail regress (27h-30h), the body axis rotates (30h-60h), and finally, a post-metamorphosis juvenile period starts (3-7 days after fertilization) (Hotta et al., 2020). The juvenile becomes a young adult and then a mature adult several month later. The hermaphrodite mature adult spawns both male and female gametes, for an external fertilization in sea water, and self-fertilization is prevented partly by the chorion's presence (Ban et al., 2005).

0.2.4 *P. mammillata* as a model for embryo cleavage

Ascidians follow an invariant cleavage pattern. This means that they have a stereotyped development, and the cleavage pattern of *P. mammillata* early embryo (a phlebobranch) is the same as the cleavage pattern of stolidobranchs ascidians despite phlebobranch and stolidobranch last sharing a common ancestor 400 million years ago (Delsuc et al, 2018; Kumano & Nishida, 2007). Thus, the multiples cues determining the orientation of individual cell division must be controlled. This make ascidian embryos a powerful tool to understand the factors involved in the emergence of an embryo shape. First, since divisions are precisely the same from one embryo to the other, it offers the opportunity to study specific characteristics in a reproductive manner. Parameters such as cell shape (Guignard et al., 2020), cell tension (Godard et al., 2020), apico-basal polarity(Dumollard et al., 2017), organelle or domain repartition (Pierre et al., 2016), that are known to be crucial to determine the cell division axis will be reproducible whether the research is performed on the zygotic stage to the gastrula. And second, this reproducibility permits elucidation of prevailing factors that orient cell division, since perturbing a major actor will have visible consequences on the embryo shape (Nishikata et al., 1999). As opposed to the ascidian invariant cleavage, other species can have different and more variable cleavage patterns despite being closely related, such as the nematodes (K.

Yamamoto & Kimura, 2017), or some amphibians that display noise in the cleavage pattern (Desnitskiy & Litvinchuk, 2015).

In addition to being useful to understand embryo shape emergence, ascidian embryos have been studied in research concerning cell fate and differentiation (Esposito et al., 2017; Nishida, 2002). Thanks to the invariant cleavage, and to recognizable axes, each blastomere can be precisely identified based on its position. This allowed the introduction of a cell-lineage nomenclature that is still in use today (Conklin, 1905a) (Figure 0.3 C). After the cleavage stage, gastrulation occurs at the 110-cell stage. 94 out of the 110 blastomeres are already tissue-restricted (i.e: fated to be only a single tissue type) (Nishida, 1987). A model with a defined cell lineage coupled with a tissue-restriction on a small number of cells is ideal to understand cell differentiation and cell inductions and interactions (Guignard et al., 2020; Williaume et al., 2021). Ascidian embryos were mentioned as an example of an organism with a "mosaic" development; where cell fate is determined by cytoplasmic factors contained within the cell itself rather than by cell-cell interactions. This view originated from an old experiment on a 2-cell stage embryo where the death of 1 cell shows mosaic development as the embryo becomes a lateral half of a tadpole (Conklin, 1905b; Fisher & Smith, 1984; Slack, 1991). This view was revised when cell-cell interactions were proven to also play a role in neuronal cell differentiation (Guignard et al., 2020; Nishida, 2005; Slack, 1991).

0.2.5 Advantages and drawbacks

Advantages

The ascidian embryo is a minimal system, it is self-sufficient, isolated and has a small number of cells (only 110 cells at gastrulation for stolidobranchs (Hotta et al., 2007)). These characteristics simplify and limit the inputs that one may need to take in account when trying to understand a specific phenomenon. For the same reason, using a simple organism is an advantage in modeling, since a limited number of variables may give global conclusions. In addition to these first advantages, the invariance of the cleavage pattern allows us to immediately detect a defect in embryo development, that could be in the axis of cell divisions, in the timing of cell division, in the cell size, etc. This is useful for any perturbation experiment on that affects the emergence of the embryo shape. The phylogeny of ascidians, placing them

among the closest animals to vertebrates, is also an advantage since the protein families of vertebrates share a common ancestor with the ascidians.

On a technical side, *P. mammillata* also provides several advantages. The animal can generate gametes all year round, and a single animal generates thousands of eggs, and sperm. *In vitro* fertilization is straightforward, so embryos are accessible for observation and manipulation from the zygote stage. Moreover, cell cycles are rapid, leading to a quick development, therefore experiments can easily be performed throughout different stages. The embryos of *P. mammillata* are also convenient for imagery by their size and transparency. Finally, most modern techniques are operable on the embryos since the genome has been sequenced, micro-injections are possible whether it is with mRNAs, morpholinos or proteins (McDougall et al., 2014a).

Drawbacks

The animals used are wild specimens, and the life cycle is not often carried out in the lab. First this leads to variabilities between individuals, especially in terms of health and egg quality, and it hinders the use of powerful genetic tools, such as creating genetically modified lines. Moreover, the animals are sensitive to environmental conditions since changes in water quality (like presence of heavy metals) that affects their mortality rate and the production of gametes (Franchet et al., 1997). It also seems that gamete production is partly seasonal, oocytes are of a better quality in spring and fall. No protocol is established to collect the oocyte after the spawning for the main reason that the animals are hermaphrodite and we need the two type of gametes separately to fertilize *in vitro* at the desired time. Hence, the adult animal must be dissected for gamete collection. About the oocytes and embryos, they stick on uncoated surfaces and to one another, they are fragile and die easily from micro-injection or air contact or after being stuck to a surface, therefore requiring careful manipulation.

0.3 From cleavage pattern to cellular cues

0.3.1 The cleavage pattern is determined at the cellular level

The determination of the division planes must be precisely regulated to generate a highly reproducible cleavage pattern. The division plane is perpendicular to the spindle axis (Figure 0.3) (Strome, 1993), except in some particular cases (Bhavsar-Jog & Bi, 2017). The spindle is an intracellular microtubules structure that forms to separate DNA between daughter cells during mitosis. Therefore, to look into the spindle position, and into the cell cycle, is necessary to understand how embryo shape emerges. In addition to the spindle axis, the yolk abundance is also an important factor to determine embryonic cleavage pattern. Indeed, traditionally, cleavage patterns are regrouped in categories that are related to the yolk abundance and its cytoplasmic repartition in the zygote (Foucrier et al., 2019; Gilbert & Barresi, 2016). Briefly, there exist two types of cleavage: holoblastic cleavage, that completely splits the zygote, and meroblastic cleavage, where the cleavage is partial so cells are not completely split (Figure 0.3 B). Embryos with meroblastic cleavage generally contain a dense yolk cell. The yolk may be in the zygote center (centrolecithal eggs, like in *D. melanogaster*) leading to superficial cleavages, or it can be dense throughout most of the cell and partial cleavages take place in a discoidal area on an oocyte pole (in telolecithal eggs, like in *D. rerio* or in the chick embryo). There are also subtypes among the holoblastic cleavages, depending on the yolk distribution as well. The yolk is sparse allowing complete cleavages, and it is either evenly distributed (in isolecithal eggs) and the cleavage pattern seems independent of the yolk repartition, or it can be denser at one pole in mesolecithal eggs (*e.g. X. laevis*). In this second case, the cleavage axis cut completely the egg but is displaced according to the yolk distribution. In alecithes eggs where there is no yolk, like in the human ovocyte (Foucrier et al., 2019; Sathananthan et al., 2006), the cleavage is like in isolecithal eggs. To sum up, spindle position and yolk repartition are key points to understand the emergence of embryo shape, and I based the following up work on these two axes.

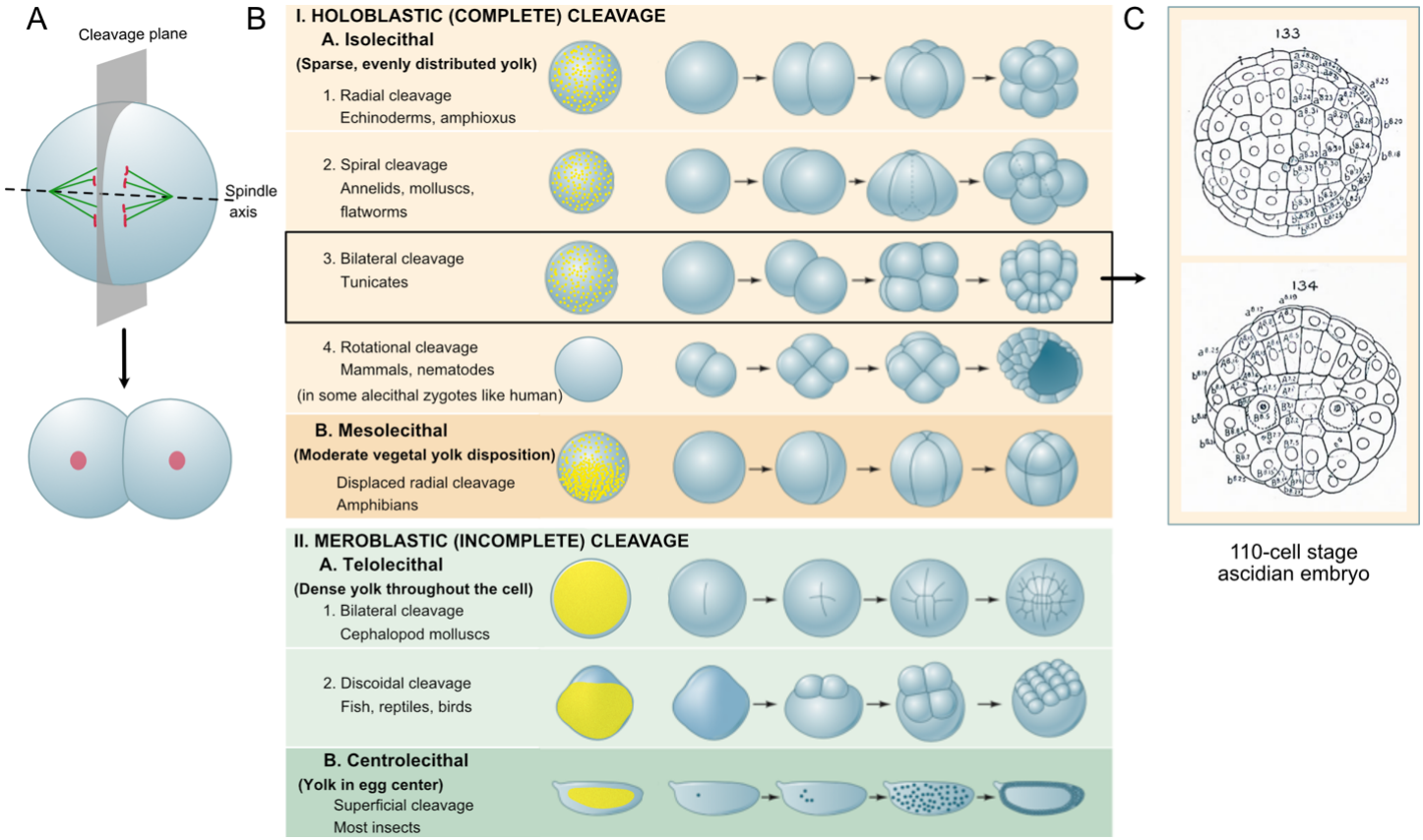

Figure 0.3: The variety of cleavage patterns

A- Cleavage plan is orthogonal to spindle axis, and centered on the spindle. The spindle (in green) separates the DNA (red) between the daughter cells. B– Type of cleavage pattern associated with yolk repartition (adapted from (Gilbert & Barresi, 2016). In the first column representative dispositions of the yolk are shown in yellow. C- Drawings of the ventral (Fig. 133) and dorsal (Fig. 134) views of one and the same embryo of 110 cells of the ascidian *Styela partita*, just prior the beginning of gastrulation. The drawing is annotated with the cell nomenclature to illustrate the ascidian invariant cleavage pattern (adapted from (Conklin, 1905a))

0.3.2 Why the zygote to understand spindle position?

Ascidian embryos, which have an invariant cleavage pattern and whose axes are determined from the zygotic stage (Nishida, 2005), must have a precise control of their spindle position from the first cell division. A variety of cues were discovered to influence the spindle orientation in different species, mainly proteins complexes (PCP proteins, LGN/NuMA/G protein complex, etc....) (di Pietro et al., 2016; Grill et al., 2001), but also mechanical cues like the cell shape (Minc et al., 2011) or tissue tension (Scarpa et al., 2018), or cytoskeleton dynamics (Holy et al., 1997; Laan et al., 2012), including spindle interaction with organelles (Kimura & Kimura, 2011a). The mechanisms of spindle centration often rely on interwoven cues, for example, cell shape and polarity domain can act simultaneously (Godard et al., 2021), or tissue tension can impact protein complex position and hence spindle position (Bosveld et al., 2016). In addition, all these cues can be altered through the cell cycle (Bosveld et al., 2016; Dumollard et al., 2017; Godard et al., 2020). In the ascidian embryo, the shape of the apical surface (Dumollard et al., 2017) the presence of a "centrosome attracting body" (CAB) (Hibino et al., 1998a; Nishikata et al., 1999), mitochondria distribution (Negishi & Yasuo, 2015) or the tissue tension changes that influence cell shape (Godard et al., 2020), have been found to guide spindle position. The yolk distribution, that can influence spindle position (Pierre et al., 2016) has not been extensively investigated in ascidians, despite a clear segregation from the spindle during the embryo segmentation (Conklin, 1905a). This may be explained by the fact that the ascidian egg is isolecithal (*i.e* yolk is relatively sparse and evenly distributed) and yolk did not obviously affect the three or four first cell divisions. None of the factors found to influence spindle position in ascidians are applicable to the first cleavage since the spherical zygote offers no long axis and has, for instance, no neighboring cells, no baso-lateral polarity, an initially homogeneous yolk, and an immature CAB. Hence the zygote may be used as a simplified version of the embryo to understand the basics of spindle positioning. Furthermore, since the yolk influence on the spindle has not yet been tested, to work on the zygote offers an opportunity to investigate how the yolk and spindle segregation is established, and thus to provide a basis for further work on the role of yolk in the ascidian cleavage pattern. Finally, embryos of *Phallusia* are transparent, and fertilization to cytokinesis takes about 50 min whereas the next cell cycles last approximatively 20 min, these combined features provide the technical advantage to monitor the precise moment of entry in interphase since all nuclei are visible. To

sum up, I used the ascidian zygote as a simplified version of the embryo to investigate the mechanisms of spindle positioning and yolk segregation.

In the zygote or in later stages, the positioning cues are mainly intra-cellular elements (organelles, MTs, protein complex, ...), they influence the spindle through their interaction with the dynamic astral microtubules that emanate from the centrosomes. In the zygote no tissue-level factors can influence the spindle position, so the spindle position can only be studied at the cell level. For this reasons, a thorough presentation of the cell is laid out in the next part.

0.4 At the cellular level

This section introduces the intracellular components of a cell, and more specifically, of the ascidian zygote, that will be mentioned throughout the work I performed. It is inspired from textbook materials (Alberts, 2014; Alberts et al., 2014; Cooper & Hausman, 2013). Indeed, zygotes are not yet specialized cells, therefore their organization is rarely ultra-specific, except that they can contain yolk, as for the ascidian case (Berg 1960).

0.4.1 Cytosol

The cell content, delimited by the plasma membrane, is called cytoplasm. This term regroups the cell medium called cytosol, and all the elements bathing in it. The cytosol is composed of 85% water and has a neutral pH. It is the main site of protein synthesis and degradation. The cytosol, hosts large and small molecules, organelles, and a cytoskeleton.

0.4.2 Cytoskeleton

The cell cytoplasm is dynamic. To illustrate its constant motion, we can highlight the transport of some organelles throughout the cell (Terasaki, 2000), the exchanges between the different organelles, and also the intracellular fluxes that cell division can create (Pelletier et al., 2020). To maintain a certain organization and adapt to circumstances, the cells have a cytoskeleton made of three main protein filaments with specific properties: the intermediate

filaments, the actin filament, and microtubules. The three types of filaments function together, and, in interaction with other proteins and motors attached to them, they guide intracellular organization (Tolić-Nørrelykke, 2008). They also give the cell the ability and strength to move and to maintain its shape (Alberts, 2014; Alberts et al., 2014). The cytoskeleton's role in cell division is a dramatic example of the regulation of the different filaments. It shows their coordination and their influence on the cell shape and organization (see cytokinesis section 0.5.2).

Intermediate filament

Intermediate filaments (IFs) are 10nm thick; thinner than microtubules (24 nm), but wider than actin microfilaments (7nm). They were named according to this characteristic. Unlike microtubules and microfilaments, intermediate filaments have a cell-type specific expression pattern. They are also the most stable and flexible type of filament. They are made of fibrous subunits, each containing a head domain, a rod domain (an extended α-helix), and a tail domain. The subunits pairs into dimers by the winding of rod domains of the same orientation. Dimers laterally associate to other dimers in opposite direction, to form tetramers. The tetramers assemble side-by-side to generate the filament formation. Because of this organization IFs are apolar. There are four main types of IF: keratin mostly in epithelial cells, vimentin, neurofilaments in nerve cells and nuclear lamins. The first three are found in the cytoplasm, whereas the fourth is found in nuclei. In addition to the different type of IF, there are splicing variants, and a variety of post-translational modifications. The IFs functions are modulated by their composition (Etienne-Manneville, 2018).

IF are known to serve as a structural and mechanical cell support. IFs can also interact with organelles such as mitochondria (Godsave et al., 1984). In certain cell types they form elaborated networks that connect the cell cortex to intracellular organelles or to adhesion complexes (Etienne-Manneville, 2018). The many human disease associated with IFs defects shed light on signaling cascades targeting IFs expression, suggesting that in addition to their structural roles, IF also participate in dynamic processes (Etienne-Manneville, 2018). Lamins strengthen the nucleus and provide it with mechanical stability by covering the inner side its envelope. Lamins offer an anchoring point for chromatin and transcription factors (Dobrzynska et al., 2016). Cytoplasmic and nuclear IFs can interact together (Dobrzynska et al., 2016). Taken

together, all these characteristics question the role of IF in maintaining intracellular organization and their influence on nucleus positioning.

The presence of IFs in eggs is confirmed in several animal groups. In mouse oocytes, IFs associate with the cell cortex, with the germinal vesicle, and later with the metaphasic plate (Markova et al., 2015). In *Xenopus* eggs IFs are distributed with mitochondria, they also arrange in a fine network throughout the cytoplasm that is suspected to help maintain the asymmetric egg organization (Godsave et al., 1984). In ascidians, IFs first associate to the cortex but seem segregated with mitochondria after fertilization as mentioned in (Sardet et al., 2002). Whether IFs influence intracellular organization or no, their recognized structural role, in association with mitochondria or with the cortex, may not be negligible when considering the supports that can help spindle centering.

Actin

Actin filaments are present in all eukaryotic cells. They are formed from the assembly of globular actin monomers (G-actin). Each monomer has an arrowed-head shape, hence their assembly is oriented, and this gives rise to a polar actin filament with a pointed end (- end), and a barbed end (+ end). The actin filament (F-actin) is not a simple column of actin monomers, it can be thought of as a two-stranded helix with a twist. The microfilament assembles faster at the plus end, and it can disassemble from both ends. Actin monomers carry a tightly bound adenosine triphosphate (ATP) that is hydrolyzed into adenosine diphosphate (ADP) soon after the monomer is incorporated into the filament. The ATP hydrolysis decreases polymer stability, thereby promoting microfilament depolymerization. The stability and assembly of the filament is regulated by associated proteins that can for example cap filaments or bind monomers. An actin microfilament is rarely found alone, it is generally part of bundles and/or network, the structure of which is organized by associated proteins. For instance, the Arp2/3 complex mediates the nucleation of new filaments on the existing ones and, in doing so, creates a branched actin network. On the opposite, formins nucleate the growth of straight, unbranched filaments to form parallel bundles. The F-actin networks can build stiff and stable structures like a muscle contractile apparatus or microvilli from an intestine epithelium, or temporary and dynamic structures like the protrusions of a crawling cell and the contractile ring that pinches the cell in two during cytokinesis (Glotzer, 2004). The actin contractility comes from its interaction with myosins in an actomyosin network.

In most animal cells, an actomyosin meshwork called the cellular cortex is present directly under the plasma membrane (Chugh & Paluch, 2018). The heterogeneity of cell cortices across cell types makes difficult to describe a unique organization (Svitkina, 2020). Moreover, the actin cortex is dynamic and capable of remodeling (e.g, in blebbing membrane with a thin cortex retracts thanks to recruitment of actin (Ikenouchi & Aoki, 2022)). It is also responsible for the cortical surface tension, which is one of the major focus in the research about the cortex, along with other mechanical properties like stiffness and viscoelasticity (Svitkina, 2020). The cortical actomyosin meshwork seems finely regulated, indeed a contractility asymmetry can lead to cell shape instabilities, and reorganization of the meshwork can have consequences like a change in cell polarity, as seen in *C. elegans* one-cell embryos (Chugh & Paluch, 2018; Reymann et al., 2016). F- actin is also present in the cytoplasm and around and in the nucleus (Davidson & Cadot, 2021). In certain cases, it can position the nucleus (Kawashima et al., 2014). In addition to being capable of moving a nucleus, actin can also move other organelles, such as the yolk granules by the formation of actin comets (Shamipour et al., 2019). Directly concerning spindles, a well-known example of actin importance occurs during the meiotic spindle formation and orientation in mouse oocytes. A F-actin cloud surrounding the meiotic spindle conducts it to its final position (Bezanilla & Wadsworth, 2009). In most mammals and in other groups like sea urchin, actin filaments also promote the formation of the MTs responsible for chromosome alignment (Dunkley et al., 2022; Mogessie & Schuh, 2017). In ascidians, F-actin also plays a role in meiotic maturation. Like in mammals, microfilaments are present near the chromosomes during spindle formation, but before that, a mysterious actin bundle emanates from the germinal vesicle and moves toward the oocyte vegetative pole while carrying nucleus pore complex protein (Prodon et al. 2009). After fertilization, the re-organization of the actin cortex of *P. mammillata* eggs has been described to be crucial in the localization of specific RNAs and maternal determinants (Sardet et al., 2005). This gives a first insight into the importance of the cortex in ascidian development.

In 16-cell stage embryos, Godard et al., revealed that cell tension regulation, and especially apical relaxation, is necessary to obtain reproductible cell shape, cell division orientation and overall embryo shape (Godard et al., 2020). In parallel to this result, it is known that the spindle position correlates with apical cell shape in 16-cell stage embryo (Dumollard et al., 2017). Cell and tissue tension can affect the spindle position as it has been observed in other models, mainly in epithelium (Scarpa et al., 2018). Thus, a dynamic actomyosin cortex is very likely to be involved in the emergence of ascidian embryo shape. A more direct implication

of the cortex on the spindle position is encountered in the asymmetric divisions that create germline precursors (Hibino et al., 1998b). These asymmetric divisions depend on spindle positions, which rely for one part on induced microtubule depolymerization at one side of the spindle (Costache et al., 2017) and for another part on a mechanism of cortical pulling (team unpublished data, Chenevert et al, in preparation). Hence, beyond its necessity in cell division (Turlier et al., 2014), the cortex is involved in many processes that regulate ascidian embryo shape throughout the segmentation stages, and it is even sometimes directly involved in the mechanism of spindle positioning. Although actin microfilaments are known to be present in oocytes, in eggs, as well as in zygotes and later stages, its fine structure, its width and density and its molecular organization depending on the stage have not been described, leaving thereupon open questions about actin interaction with other cell components at the cortex or in the cytoplasm to position the spindle and organize organelles during ascidian embryo cleavage.

Microtubules (MTs)

After IFs, and actin microfilaments, the third main type of filaments are the microtubules (MTs). Microtubules direct intracellular transport, and form the mitotic spindle that segregates chromosomes during cell division. MTs are cylindrical and hollow, and are the thickest and most rigid filaments in the cytosol. The wall of the tubular MTs is made of 13 parallel protofilaments, composed of heterodimers of globular proteins from the tubulin family. The dimers are made of one α-tubulin and one β-tubulin associated with a guanine triphosphate (GTP). To form a protofilament dimers are stacked head to tail, this creates a polarity: protofilaments have an α and a β side. The 13 protofilaments align in the same direction with respect to polarity, therefore providing a polarity to the whole MT (Alberts et al., 2014). Instead of using α and β terms, MT polarity is described with "minus" and "plus". Like in microfilaments, MTs assemble faster at the plus end, and its stability is affected by hydrolysis of the GTP bound to each subunit. GTP hydrolysis reduces the affinity of the dimers for their neighbors and thereby promotes microtubule disassembly. Such a shrinkage is called a catastrophe. Reciprocally, phases of MT growth called rescue are observed. Certain microtubule associated proteins (MAPs) can promote MT catastrophe, or help MT stabilization. MTs converts between growing and shrinking phases (Mitchison & Kirschner, 1984), this dynamic instability can be characterized by the velocity and frequency of the rescues and catastrophes (Lacroix & Dumont, 2022). Yet, not only MTs are dynamic, but also their dynamic instability evolves throughout cell cycle (Rusan et al., 2001).

In addition to a change in MTs dynamic instability, entry in mitosis also provokes the formation of the mitotic spindle. Prior to mitosis, MTs are generally organized in an aster around a microtubule organizing center (MTOC), a centrosome in ascidians. Centrosomes are protein matrix which contains γ-tubulin ring complex, that are nucleation site for MTs, they embed MTs minus-end, and thus become the center of spherical MTs array: the MT asters (Alberts et al., 2014). The centrosome duplicates during interphase and the two centrosomes polymerize their own aster to form the two poles of the spindle. Between the poles, MTs capture the DNA and form the interpolar spindle that will segregate DNA between the daughter cells. MTs can also form other type of structures like bundles, axons or cilium, and they can nucleate from pre-existing microtubules, like was demonstrated in oocyte meiotic extracts (Petry et al., 2013).

In addition to their crucial role in segregating DNA, and to their role in intracellular organization through transport (Minin, 1997), MTs, naturally, are key actors in mechanisms of spindle or nucleus positioning. The astral MTs of the spindle explore the cell, and push, or are pulled by other cell components (Dogterom et al., 2005; Laan et al., 2012). MTs, and hence the whole aster or spindle can be pulled by the dragging force of minus-end directed transport of cargoes, like during the female PN migration (De Simone et al., 2018). In this case the direction of the spindle depends on the length of MTs and the distribution of the cargoes in the cell (Kimura & Kimura, 2011b; Minc et al., 2011; Tanimoto et al., 2018). MTs can also be pulled by minus-end directed motors bound to the plasma membrane supported by the cell cortex (Redemann et al., 2010). If the motors are concentrated in a region, the aster decenters (Gotta et al., 2003; Sallé et al., 2019), otherwise the cortical pulling seem to also be capable of centering an aster (Laan et al., 2012). Finally, since I am interested in understanding spindle position to decipher a cleavage pattern, it is worth mentioning that another role of the spindle, more precisely of the interpolar spindle, is to indicate the site of furrow ingression for cleavage (Glotzer, 2004)(section 0.5.2).

In ascidians zygotes, the sperm delivers the centrosome at fertilization, and the aster polymerizing around it is called the sperm aster (Roegiers et al., 1995). The mechanisms of spindle positioning have not yet been investigated in the zygote, but cortical pulling and cytoplasmic pulling were shown to be involved in specific cells in later stages. At the 4-cell stage, presence of cortical pulling was demonstrated on the whole cortex except in a precise region (Godard et al., 2021). At the 24-cell stage, in the future neuro ectoderm, the spindle

rotates following an enrichment in mitochondria and dynein (Negishi & Yasuo, 2015). The presence of a cortical MT array, like the one that control cortical rotation in, can be debated (Sardet et al., 1994)(see Discussion in chapter1).

Molecular motors

Molecular motors are molecular machines that convert the energy of ATP hydrolysis into mechanical force. Motors are associated with cytoskeleton filaments, the repetition of ATP binding to the motor and its hydrolysis permits a repetitive change of conformation of the motor that dissociates and binds its filament, thus creating a movement. There are three families of cytoskeletal motor protein; dyneins, kinesins and myosins. Dynein and kinesin both move along the microtubules, dynein moves towards the minus-end, while kinesin towards the plus-end. Myosin moves towards the plus end of actin filaments. However, myosins and kinesins have structurally more in common than kinesin with dynein. All possess on their heavy chains subunits the head region or "motor domain" that binds the associated filament and hydrolyzes the ATP. Myosin have two heavy chains and four light chains, kinesin have two heavy chains and two light chains. And dynein has one, two, or three heavy chains and a variable number intermediate and light chains. Cytoskeleton motors are employed in many different ways, and it exists sub families for each type of motors. Moreover, their functions can be adjusted by adapter proteins, this explains how motor's functions can range from the basic transport and delivery of organelles to the functioning of super-structures such as flagellum or muscles. Pavin & Tolíc-Nørrelykke suggest three possible ways in which motors can exert forces on the cytoskeleton: the transport of cargos, the pulling of filaments as a rope, or the formation of higher-order structures like a MT spindle or an actin cortex (Pavin & Tolíc-Nørrelykke, 2013).

0.4.3 Organelles

Nucleus/ and Pronucleus

The nucleus is delimited by a nuclear envelop. It contains and protects the DNA from chemical agents. It also possesses a nucleolus, an area dense in ribosomal RNAs and ribosomal subunits where ribosome biogenesis occurs. Ribosomes perform the translation of RNAs into proteins. The nucleus can exchange with the cytosol through pores on the nuclear envelop.

The pronucleus is a nucleus present in the zygote after fertilization, containing either the DNA delivered by the spermatozoid or the DNA of the oocyte. The haploid male and female pronuclei are destined to fuse form the zygote nucleus with a complete diploid genome. It is interesting to note that each pronucleus contain an immature nucleolus called NPB (nucleolar precursor bodies) (Koné, 2016).

The endo-membranous system

Endoplasmic reticulum

The nucleus is connected to another organelle, the endoplasmic reticulum (ER). The outer nuclear membrane extends into the cytoplasm like a maze of branching tubules and flattened sacs that form the ER. The ER has several main functions. It completes the synthesis of proteins to be secreted or integrated in the plasma membrane, it ensures their transport to the right destination, and the ER can also evacuate misfolded proteins after a quality check and help detoxify the cell. It produces lipids for the whole endomembranous system (composed of the ER, Golgi apparatus and traffic vesicles). Finally, it acts as a reservoir ready to uptake or release calcium ions. The ER is not a homogenous organelle and two types of ER can be distinguished in the same cell, the rough and the smooth ER. The rough ER (RER) carries many ribosomes on its cytosolic surface, so the RER is mostly involved in some protein production, protein folding, quality control and dispatch. ER regions that lack bound ribosomes are called smooth ER (SER). The SER is associated to more metabolic functions like lipid synthesis and cell detoxification. Both stock Ca^{2+} ions.

The distinction between SER and RER is rarely made in ascidian zygotes, before fertilization ER is mainly RER, but after fertilization ER organization changes towards more sheets and, to my knowledge, the type of these sheets was not clearly defined. Instead the ER is defined by its localization, cytoplasmic or cortical, although both are connected. This was necessary to describe the ER reshaping at fertilization. Indeed, the cortical ER enriches on the vegetal pole at fertilization (Speksnijder et al., 1993). Cytoplasmic ER is found around the meiotic spindle and accumulating at the sperm aster, as well as in clusters spread in the cell (Speksnijder et al., 1993). The cortical ER brought to the vegetal cortex contains a large amount of Ca^{2+}, as shown by its pacemaker activity provoking several calcium waves after a first trigger by a sperm-induced calcium wave (McDougall & Sardet, 1995).

Golgi

The ER sends many of the newly-synthesized protein and lipids to the Golgi apparatus for maturation. There, they are subject to post-translational modifications, like glycosylation. The proteins ready to be secreted are concentrated at the extremities of the disc-like compartment (i.e. cisternae) composing the Golgi apparatus, from which they will be released through exocytosis. Golgi distribution, like other organelles, depends on MT transport (Minin, 1997).

Lysosomes/Endosomes (&Peroxisomes)

A continual exchange of materials takes place between the endoplasmic reticulum, the Golgi apparatus, lysosomes and the outside of the cell. Lysosomes, as well as endosomes and peroxisomes are mobile single membrane-enclosed organelles that can be defined by their functions.

Lysosomes contain enzyme capable of breaking down any biological polymer, like bacteria or damaged or useless cell elements. They degrade intracellular material for either recycling within the cell or excretion from the cell. The majority of the material to degrade is taken up from the outside by endocytosis. On the way to lysosomes, endocytosed material must first pass through a series of organelles called endosomes. The endocytosed vesicles tether to endosomes and fuse with them to discharge their contents. From there, endosomes can still recycle the material or fuse with a lysosome to start degradation. They offer an environment to sort material before degradation. After fusion with a lysosome, endosomes can themselves become lysosomes by lowering their pH from about 6 or 5.5 to 5 thanks to a proton pump. Endosomes can also receive material from the Golgi apparatus. Endosomes are transported throughout the cell thanks to MTs transport function.

In addition to lysosome and endosomes, organelles called peroxisomes can be found in the cell. They are involved in metabolic pathways, particularly, they detoxify the cell by carrying out oxidative reactions. Despite emerging from the ER and being structurally similar to the two previous organelles, peroxisomes do not clearly participate in membrane exchanges with the Golgi or the plasma membrane. Hence, peroxisome's belonging to the endomembranous system is open to question.

Mitochondria

Mitochondria are organelles present in essentially all eukaryotic cells. Their shape, size and number vary, but there are recognizable by their structure. A mitochondrion is an enclosed organelle with double-membrane and the inner membrane forms extensive invaginations. These organelles produce adenosine triphosphate (ATP) from the oxidation of nutrients like sugar and fatty acids in a process called cellular respiration. The ATP is necessary in every synthesis activity of the cell and for active transport. The mitochondria transform nutrients into an exploitable source of energy for the cell. Although mitochondria contain their own DNA, ribosomes, and other components required for protein synthesis, most of their proteins are encoded in the cell nucleus and imported from the cytosol. They reproduce by simply splitting in two. In ascidians zygotes, mitochondria settle in the vegetal pole just after fertilization, and form the myoplasm, together with maternal mRNAs (Sardet et al., 1989).

Yolk

Yolk's role is to provide the embryo with nutrients to unsure its survival before the organism become capable of feeding itself. The yolk is present in most oocytes, and its consumption is regulated to supply nutrients to a developing tissue at the right time throughout embryonic development. The yolk as an organelle is rarely described in textbooks as it is not present in typical cells, and also probably because there is no clear consensual definition. Indeed, the terms and vocabulary around the yolk thematic vary depending of the field, the species, and the time of publication. In the next paragraph, I attempt to sum up the main conceptions about the yolk.

First of all, many vertebrate species, especially the amniotes species, develop a **yolk sac** that acts like an extraembryonic gut and intake yolk proteins. The yolk sac is an extraembryonic tissue, derived from the primitive endoderm that is defined at the blastocyst stage (Gilbert & Barresi, 2016). Since the yolk sac is a tissue or an organ-like structure and not an intracellular organelle, it falls out of the scope of the determination of a cleavage pattern, thus the yolk sac will not be considered in the following work. In animal groups that do not develop a yolk sac, like nematodes amphibians or sea urchins, the yolk is present as an organelle inherited from the oocyte cytoplasm and it is distributed between daughter cells at each division. It is consumed intracellularly (Jorgensen, 2008). The development of a yolk sac and the presence of intracellular yolk are not mutually exclusive, as shown by many species like the hen, zebrafish or marsupials.

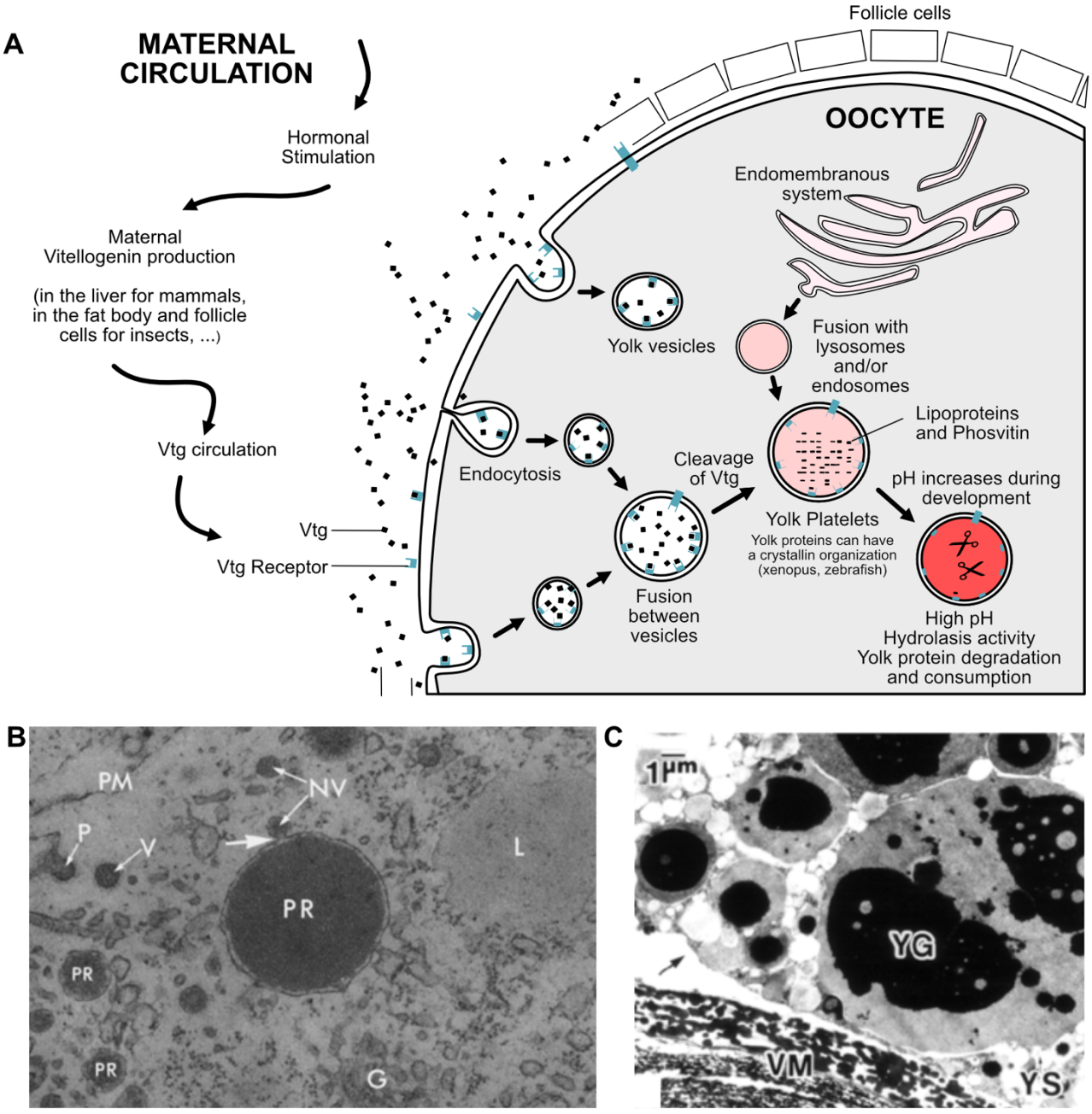

Figure 0.4: Yolk structure and formation.

A- schematic of a generic oocyte vitellogenesis. B- Micrograph of the mosquito *Aedes aegypti* oocyte from (Roth & Porter, 1964), showing the process of vitellogenesis. Vesicles (V) are endocytosed (P) from the plasma membrane (PM) and eventually fuse with yolk platelets ((PR), yolk droplet or yolk granules). Here the white arrow indicates fusion between PR and what Roth and Porter called a naked vesicle (NV), that could be a vesicle originating from endomembranous system. The micrograph also shows the presence of lipid droplets ((L), or lipid bodies) and of Golgi components (G). (X56,500).C- Micrograph of the oocyte of the Japanese quail *Coturnix japonica* (from Yoshizaki et al., 2004)), showing a different type of yolk granules. Here a yolk granule (YG) is a protein inclusion into a yolk sphere (YS, which could be assimilated to a yolk platelet). VM: vitellin membrane. Arrows indicate the cell membrane.

When talking about the yolk as an intracellular organelle, some generalities can be drawn, despite the presence of exceptions of any kind. Most of the yolk descriptions comes from oogenesis literature. The oocyte intracellular yolk originates from a process called **vitellogenesis**. During vitellogenesis, the oocyte grows in size due to a **vitellogenin (Vtg)** uptake. Vtgs are large multidomain apolipoproteins that are the precursors of the major egg yolk proteins (Jessus et al., 2020). They are highly nutritious, they provide the essential amino acids and associate with ~50 lipid molecule (Jorgensen et al., 2009). Vtg is cleaved to make mainly phosvitin and lipovitellin, and as there are Vtg isoforms (Perez & Lehner, 2019), yolk protein composition can vary despite the maternal circulation being constant. There is a regulation of the isoform intake from the oocyte receptors (Hiramatsu et al., 2015). The Vtg domains are not all conserved between species (Akasaka et al., 2013). In the case of vertebrates, Vtg production is induced in the mother's liver under oestrogen simulation, in molluscs it is induced in oocyte follicle cells and in insects in the fat body (Hara et al., 2016; Jessus et al., 2020). In some insects and maybe in hydrozoans Vtg is thought to be produced by the oocyte itself (Kessel, 1968; Postlethwait & Giorgi, 1985). The Vtgs secreted in maternal circulation are captured by the oocyte's Vtg membrane receptors and are endocytosed (Wallace, 1985) (Figure 0.4A). As in a classical endocytosis, the Vtgs bound to their receptors are encompassed by the plasma membrane to form an intracellular **yolk vesicle**. The yolk vesicles then fuse with endosomes or lysosomes. Hence the yolk proteins are now present within organelle-size membrane-bound lumps termed **yolk platelets**, or **yolk granules (YG)** in more recent literature**.**

The 1960's literature about yolk consist mainly of electronic microscopy descriptions (Berg & Humphreys, 1960; Karasaki, 1963; Kessel, 1966; Roth & Porter, 1964; K. Yamamoto & Oota, 1967). From these descriptions, the term **yolk bodies,** or yolk globules, emerged to describe YG of lighter density (Wallace et al., 1983), and it was defined as an intermediate YG containing Vtg not yet cleaved into different yolk proteins. This term is rarely used, and it is unclear if it describes a yolk vesicle, a yolk granule or a proper intermediary stage. The electronic microscopy observation also mentioned the structure of the yolk proteins in the YG, the yolk proteins assemble in a crystallin (organized) way, as seen in mosquito or in xenopus, and this criterion was sometime used to differentiate the YG between themselves, as a crystallin form of yolk would denote a mature YG (Roth & Porter, 1964). A crystallin organization of yolk proteins permits reaching a high density of yolk protein (Jorgensen et al., 2009).

Apart from their content in yolk proteins, the YG resemble lysosomes. Indeed, both share a hydrolase activity meant to degrade the organelle contents, and they both become more and more acidic (YG go from pH 5.7 to 5 in xenopus). However, YGs do not degrade their content until specific developmental stages, sometimes weeks after their formation, or even at post-embryonic stages (Perez & Lehner, 2019). The YG acidification correlates with yolk degradation, and as Fagotto suspected when he mentioned a latent enzyme in mild pH, and sleepy lysosomes (Fagotto, 1995; Fagotto & Maxfield, 1994), acidification and enzymatic activity coincide in YG (Abreu et al., 2004).

Yolk proteins coming from Vtg are lipoproteins, they are a major source of lipid. So are the lipoprotein coming from **lipid droplets** (LDs), also called **fat droplets.** This common feature between YG and lipid droplets often creates a confusion, despite the presence of clear element of distinction. Lipid droplets generally characterize an adult tissue. LDs arise from the ER and they are filled with neutral, low-density, or very-low-density lipoproteins, on the contrary of YG containing high-density protein. To protect their hydrophobic core, LDs adopt a micelle conformation. Most cells can make LDs (Jackson, 2019). Oocytes can contain LDs in addition to YG, like it is the case in several ascidians (Berg & Humphreys, 1960). On the opposite it has been reported that LDs are never seen within the zebrafish *Brachydanio rerio* at any developmental stage (Selman et al., 1993). The oocyte's LDs seem to originate from a lipoprotein uptake from maternal circulation in a process called oocyte lipidation which is thought to work by diffusion or by transporter and not by endocytosis (Hiramatsu et al., 2015).

A last source of confusion needs to be addressed. It stems from the use of the term YG to describe both yolk platelets, and a dense aggregate of yolk protein. The second definition is still in use, specially into food industry because it illustrates the structure of the hen yolk. The bright yellow hen yolk is quite peculiar and possesses a specific vocabulary. By centrifuging hen's yolk, two components are separated; a plasma and a granular substance. When looking into details, the plasma is made of soluble proteins and of **lipid micelles** mainly containing low density lipoproteins (LDLs), that are similar to the lipid droplets (Anton, 2013). About the granular substance, it is sometimes non-specifically called "yolk granules", it is, or contains tightly packed membrane-bound **yolk spheres or yolk globules** (Yoshizaki et al., 2004), which could be assimilated to yolk platelets. Into a yolk sphere there are non-soluble protein aggregates of high-density lipoproteins (HDL), that are called **yolk granules,** and a matrix (Yoshizaki et al., 2004). In teleosts the yolk platelets are yolk spheres.

In a nutshell, yolk composition, structure, origins and its other facets are studied in parallel, and no norm has been established to unify the yolk nomenclature. This observation is supported in (Ramos et al., 2022) where the authors remark that "The literature traditionally refers to all vesicle-like organelles within an oocyte as YG", and that this impacted the research on the diversity and function of YG-like vesicles. In the bio-mechanic field, in the subdomain where the forces exerted on and in a cell and its organelles are questioned, the **yolk** is the totality of individual YG-like vesicles that overall behave the same way and are stained by the same dyes (Pierre et al., 2016b; Shamipour et al., 2022). These vesicles are called yolk granules, but they probably also regroup the lipid droplets, yolk vesicles, and maybe lysosomes. Since the present work is framed by the question of the influence of yolk as whole on the spindle position, and since the yolk organelles were only defined by dyes, I used the term **Yolk Granules** throughout the thesis in coherence with the field.

About ascidians yolk, to my knowledge, the literature is quite sparse. A study addressed the presence of various organelles in different species of ascidian. Homogenous yolk platelets were recognized, their sizes varied from one species to the other (Berg & Humphreys, 1960). No description of the *Phallusia mamillata* yolk has been performed, however my estimation of the size of the yolk granules (section 2.2), seems to fit the *Ciona* yolk platelets description, that is of a size of 1.5 µm. Lipid droplets were also found in ascidian oocytes. They accumulate with the mitochondria to form a yellow crescent in *Styela*, but not in C*iona* (Berg & Humphreys, 1960). The presence of LDs has not been assessed in *P.mammillata***.** One study suggested that, in *Ciona*, yolk originate from the oocyte's own Golgi (Kessel, 1966), but in light of the current knowledge, the process described fits with a classical vitellogenesis which was actually mentioned as an alternative hypothesis in conclusion of Kessel's yolk description. It is currently implicitly thought that yolk platelets arise from vitellogenesis in several ascidian species (Akasaka et al., 2013; Sardet et al., 2002). The yolk consumption in ascidian was assessed in *Ciona* through vitellogenin proteomic profile in oocyte, 16 cell-stage and tadpole (Nomura et al., 2009), showing that yolk protein digestion occurs throughout the whole of embryonic development, but some yolk protein are still present at the tadpole stage.

0.5 Spatio-temporal framework

Throughout the introduction, we have seen that the shape of the embryo during segmentation stage is mainly determined by the embryo cleavage pattern. The cleavage pattern is itself dependent on the spindle position. I decided to work on the spindle position in the zygote to address the interactions between the mitotic apparatus and the other cell components, rather than the tissue-level positioning mechanisms. The presence of a spindle is characteristic of the M-phase of mitosis and meiosis. Hence this section presents the cell cycle in the zygote from fertilization until cell division to provide a precise temporal framework of the phenomenon studied and better explain how the position of the spindle affects cleavage orientation. Furthermore, in the considered time-window the ascidian zygote undergoes several intracellular reorganizations that I will evoke to provide an overview of the setting in which the first mitosis occurs.

0.5.1 Cell cycle

The cell cycle is the process that allows one cell to divide into two daughter cells, each containing a complete genome. The cell cycle is composed of several phases, generally four, in the following order; G1, S, G2, and M-phase. G1, S and G2 compose the interphase. During the **S**-phase, DNA is duplicated (another version of the genome is **S**ynthesized). The two **G**-phase flank the S phase, these phases permit to control and check the DNA duplication and they give time (a **G**ap) for the cell to grow before the cell division. The duplicated genome is then split between the daughter cells during the M-phase. The M-phase can be subdivided into five stages of mitosis plus the cytokinesis that will be developed later. The five stage of mitosis are associated with recognizable events. During prophase the DNA condense to form chromosomes in the nucleus and the mitotic spindle assembles, prometaphase starts with the nuclear envelop breakdown (NEB or NEB), the interpolar MTs can now bind the chromosomes, then at metaphase the chromosomes aligned on a plate in the middle of the spindle. Chromosomes split during anaphase when the microtubules to which they are attach retract towards the spindle poles, and spindle poles move apart. Finally, telophase is defined by the formation of a new nuclear envelop around the DNA. In early embryos, during the cleavage stage, the S and M-phase are conserved but it is common to observe extremely reduced G-phases. Hence,

blastomeres have no time to grow between cycles the oocyte is subdivided into smaller cells (Alberts, 2014).

The alternation of phases is controlled by the activity of several protein. These protein kinases activate when they form a complex with the cyclin proteins, they are thus called the CDKs, cyclin-dependent kinases. Unlike CDKs, the concentration of cyclins (Cyc) varies during the cell cycle. The association of distinct cyclins with different CDKs rules the course of event during the cell cycle. In vertebrate the association of CDK1 with Cyclin B forms a complex called the mitosis promoting factor (MPF), whereas the association of CDK2 with Cyc A or Cyc E promotes the S-phase. To exit the S or the M-phase, the corresponding CDK/Cyc complex must be inactivated. The CDK/Cyc inhibition can be done by the anaphase-promoting complex (APC), which is especially important for the exit of M-phase. APC tags the cyclins with a chain of ubiquitin to provoke subsequent cyclin degradation, the CDK/Cyc complex is therefore dissociated, and CDK inactivated (Alberts, 2014). The cell can also employ CDK inhibitor proteins that can phosphorylate the CDK/Cyc complex on inhibitory sites. Conversely, specific phosphatases can activate the complex. In section 1.2 (Figure 2 & 4) I perturbed the cell cycle by injecting p21 in the cell that inhibits the entry in S-phase by binding the CDK/Cyc complex, thus it maintains the cell in interphase kinase (Figure 0.4). I also maintained the cell in M-phase by injecting a truncated CycB deprived of its site of ubiquitination by APC, therefore the CDK1/cycB cannot be degraded and the complex activity is maintained.

While the cell cycle progress and enters mitosis, the cytoskeleton is employed to specific tasks. Indeed, the actomyosin cortex will be requisition to pinch the cell to form the two daughter cells, and MTs must form the mitotic spindle that will segregate the chromosomes. The interphasic MT array disassembles and MTs reassemble around the centrosomes previously duplicated (in S-phase) to organize a bipolar array with MTs minus ends focused at the poles and plus ends overlapping in the center or connecting chromosomes (Alberts, 2014).

0.5.2 Cytokinesis

Cytokinesis is the final step of cell division during which the two daughter cells become physically separated. It begins right after chromosome segregation in anaphase (D'Avino et al., 2015). The role of MTs in defining the cleavage plane was suspected because of early investigations showing that the presence of two opposing asters are sufficient to induce the

formation of a membrane furrow (Rappaport, 1961). MT depolymerization during metaphase or very early anaphase was then shown to prevent cleavage furrow formation, but MT depolymerization in late anaphase did not (Glotzer, 2004). This indicates that microtubules are essential to induce furrow formation, but they are not required for ingression. Supporting the connection between the spindle and the cell cortex, some proteins such as ECT2 (a guanine-exchange factor for the rho protein controlling actomyosin contractility RhoA) were detected in association with both spindle and cell cortex (Glotzer, 2004). The main components of a mitotic spindle are the DNA, the central spindle, the centrosomes, and the astral MTs. Centrosome and chromosomes were shown to be dispensable for furrow ingression (Glotzer, 2004), but the central spindle and probably to a lesser extent astral MTs, were essential. The mechanism that connects the spindle and the cortex was later found. While CDK1 is active and chromosome are not segregated, CDK1 inhibits the transport to the central spindle of the centralspidlin complex composed of the kinesin Kif23 and a Rac (Rho activating protein), and of proteins inducing the formation of MTs bundles (D'Avino et al., 2015). At anaphase the chromosomal passenger complex (CPC) promotes recruitment at the central spindle of these previously inhibited protein, thus the centralspindlin complex is able to travel to the plus ends of interpolar and central spindle microtubules (D'Avino et al., 2015). At the MT plus end the Rac component of centralspidlin interacts with the RhoGEF ECT2, that in turn associates with the plasma membrane and activates RhoA. RhoA commences the actomyosin contractility pathway, and triggers the rearrangement of the cortex to form an actomyosin belt, the contractile ring, which constricts and pinches the cell in two (Alberts, 2014). To prevent association of ECT2 with the membrane before anaphase, CDK1 also inhibits ECT2 through a phosphorylation (D'Avino et al., 2015). About astral MTs, they have been described to be able to inhibit RhoA where they contact the cortex (D'Avino et al., 2015). Other organelles like the secretory system also plays a role during cytokinesis: it brings membrane vesicles to the furrow to permit membrane expansion. Finally, the constriction of the ring finishes around remnants of the central spindle; a bundle of MTs called the midbody. The midbody permits the recruitment of proteins that regulate the abscission of the daughter cells (D'Avino et al., 2015). This widely spread mechanism of cytokinesis illustrates how the position of the spindle can influence the orientation of the cell cleavage. In ascidian cell division is indeed inhibited by MT inhibition (Chenevert et al., 2020), however this is not universal, for example the budding yeast cleaves in a MT-independent way (Bhavsar-Jog & Bi, 2017).

0.5.3 Zygotic Cell Cycle

As mentioned previously, early embryos are particular since they often have no or extremely reduced gap phases. But even more particular is the case of the zygote. Indeed, at fertilization, zygotes first resume meiosis before to enter interphase and the mitotic M-phase. Oocytes are haploid gametes, but like most cells they are originally diploid and thus need to extrude half of their genome in a process called meiosis. First the genome is duplicated, and then two successive division called Meiosis I and II occur. Both meiosis I and meiosis II, slightly differ from a classical M-phase in terms of chromosome segregation, but also because of their highly asymmetric cell divisions; one cell, the oocyte, inherits most of the cytoplasm while the 2nd cell, called the polar body, receives only a set of chromosomes (Gilbert & Barresi, 2016). Depending on the specie, the oocyte reach maturity and stops cycling at different moments of meiosis. Mammal oocytes are generally arrested in Metaphase II, in contrast the

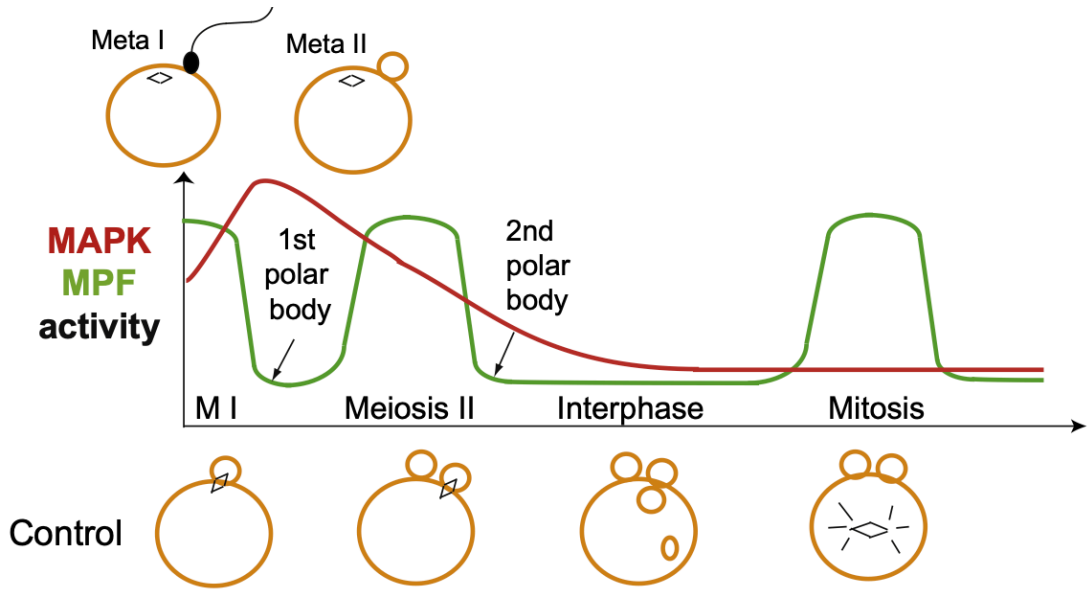

Figure 0.5: Correlation between CDK1/CycB activity and cell cycle stage in ascidian zygote.

Diagram representing the CDK1/CycB (MPF) activity in function of the cell cycle stage. Cell cycle stages appear on the x-axis. Fertilization occurs in Metaphase I (cartoon above the graph). Below the graph, visual cues of each cell cycle stage after fertilization are illustrated: extrusions of the polar bodies, pronucleus formation and spindle centration. Figure taken from (McDougall et al., 2012)

sea urchin oocytes are arrested after completion of the two meiosis, while ascidian oocytes are arrested in Metaphase I (Figure 0.5) (Dumollard et al., 2011; McDougall et al., 2012). Hence in ascidians, at fertilization, the zygote cell cycle starts with the resumption of Meiosis I with the extrusion of a first polar body (PBI), and continues with the second meiosis (II) and extrusion of PBII before to finally enter interphase and then mitosis (Figure 0.5). The oocyte and sperm DNA must meet prior to mitosis, precisely before NEB to allow the segregation of a diploid genome in the daughter cells, thus it mainly leaves the time of interphase for both haploid genomes to reach each other.

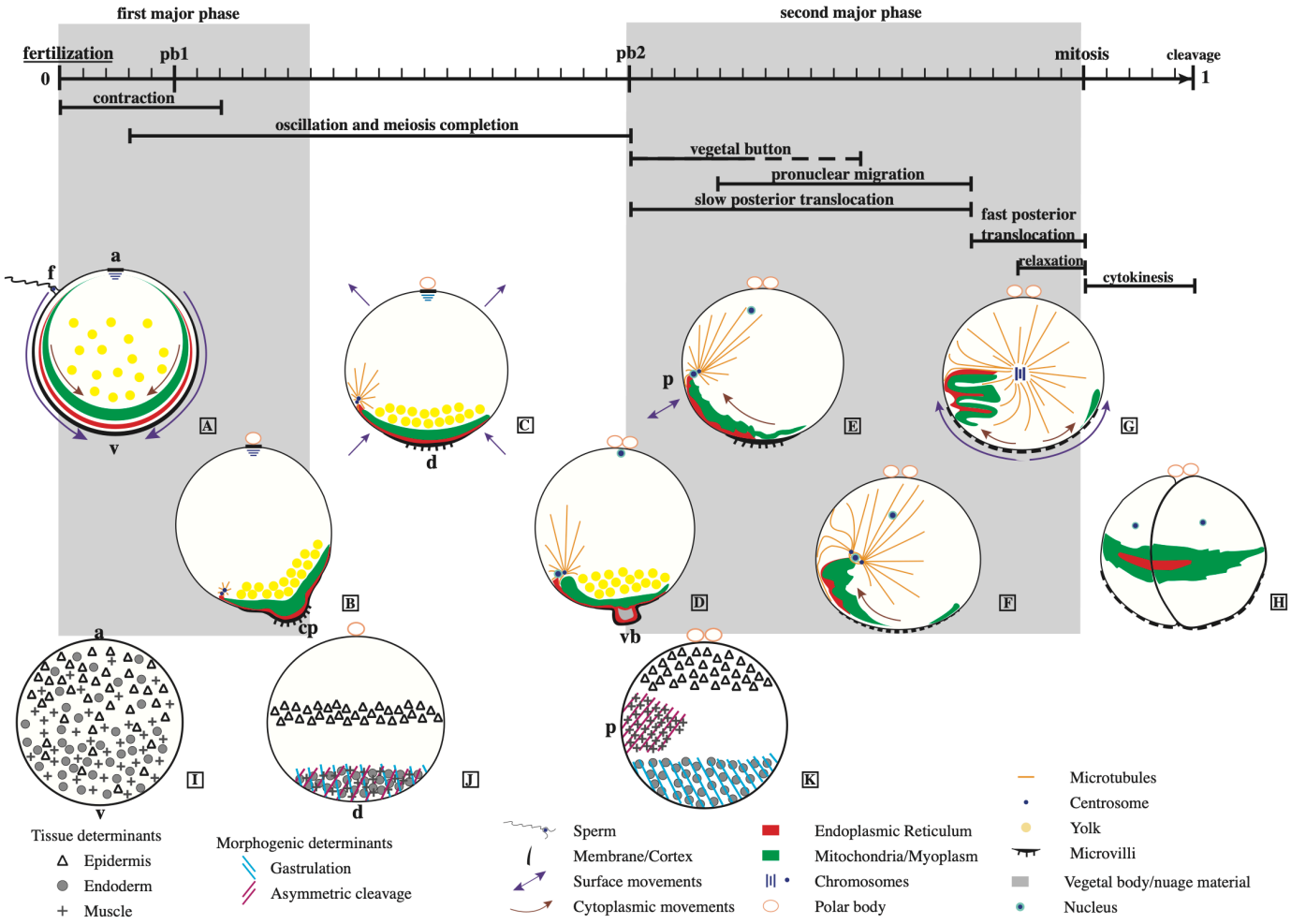

Figure 0.6: Phases of intracellular reorganization in *P.mammillata* zygote.

Diagram representing the cortical and cytoplasmic reorganization in the zygote (A-G), and illustrating how this reorganization affects determinant distribution, and thus cell fate (I-K). More details are provided in the text. Arrows perpendicular to the surface indicate constriction or bulging, other arrow indicate coordinated movement. Taken from (Roegiers et al., 1999).

0.5.4 *P. mammillata* zygote

During the first cell cycle, the ascidian zygote undergoes several intracellular reorganizations; using *P.mammillata,* Roegiers et al. provided a cellular description of the course of events during and following fertilization (Figure 0.5) (Roegiers et al., 1995, 1999). Note that intuitions about these reorganizations were already discussed and tested in several ascidian species in 1905 (Conklin, 1905a, 1905b).

Before fertilization the animal-vegetal (A-V) axis is already defined, cortical ER and a sublayer of mitochondria are localized rather homogeneously below the plasma membrane except near the animal pole, where they are absent (Prodon et al., 2006) (Figure 0.5A). At fertilization, a calcium wave propagates in the egg from the point of sperm entry, that is in the animal hemisphere (Roegiers et al., 1995), to the vegetal pole (McDougall & Sardet, 1995). This calcium wave triggers an actin-dependent contraction (Prodon et al., 2005; Yoshida et al., 2003) that creates a brief animal deformation, and travels to vegetal where it forms a "contraction pole" (Figure 0.6 B). The wave brings the male nucleus and centrosome to the vegetal hemisphere, and it enhances the A-V polarity by concentrating the previously cortical components to the vegetal pole. In turn, during 20min, the concentrated ER acts as a pacemaker and releases calcium in several waves (McDougall & Sardet, 1995), that are thought to be involved in meiosis completion (Roegiers et al., 1999). The contraction pole is an important cue in the axes formation because it defines the future site of gastrulation, and also holds the components that will define the posterior pole (Sardet et al., 2007). The contraction pole resorbs few minutes after its formation, and the zygote pursues its cell cycle through meiosis II, while the sperm aster starts growing (Figure 0.6 C). After Meiosis II, so at the beginning of interphase, a "vegetal button" forms (Figure 0.6 D). Like the contraction pole it is a transient actin-dependent deformation, however it is not seen in every zygote (Movie 9B). With its resorption a second phase begins, first the vegetal components moves slowly towards the sperm aster (that indicates the future posterior side) (Figure 0.6E), and then a fast posterior translocation is observed when the aster centers before cytokinesis (Figure 0.6 F,G). This fast translocation is associated with a "vegetal relaxation phase", that is described as an actin-dependent broad dispersion of cytoplasmic components, no cell deformation was mentioned (Roegiers et al., 1999). The precise sequence of events from interphase to cytokinesis, and especially the timing and mechanisms of aster or spindle centration are unknown.

Other works focused on precise points of the ascidian zygote development. Cell cycle (Chambon et al., 2013; Dumollard et al., 2011; McDougall et al., 2012) and calcium wave (Levasseur & McDougall, 2000; McDougall & Levasseur, 1998) were studied. Together with the mitochondria and cortical ER, maternal mRNAs are also brought to the vegetal pole, their identity, repartition and associated fates were largely investigated (Negishi et al., 2007; Nishida, 2005) (Figure 0.6 FI,J,K). More recently, studies on the cellular reorganization of *C. intestinalis* zygote were performed (Goto et al., 2019, 2022; Ishii et al., 2017). Even though the discoveries made in *C. intestinalis* do not contradict Roegiers et al. findings, and that no formal comparison has been established, some details on the mechanisms described do not seem to fit personal observations on *P.mammillata* zygote. Briefly, two main points stand out; during the second phase of cortical reorganization aster position in *Ciona* seems more in the animal hemisphere (Ishii et al., 2014), than on the cell equator like seen in *P.mammillata*, and the second phase is thought to be caused by a cortical rotation induced by a cortical MT array (Ishii et al., 2017). This array have not been observed in *P.mammillata*. Hence, they may be slight differences between ascidian species, nevertheless for sake of simplicity I called *P.mammillata* zygote, the ascidian zygote.

This description gives an insight into the complexity of the zygote stage, but overall it provides information on the context in which the sperm aster and then the spindle form, develop and position.

0.6 Thesis aims and content

As seen in the introduction, cleavage pattern is key to understand embryo development and morphogenesis. Cleavage orientation is most often dependent on spindle position (Strome, 1993), that itself relies on various cues, that range from the position of protein complexes that attract the spindle (di Pietro et al., 2016), physical constraints (cell shape, tissue tension, ...) (Finegan et al., 2019; Minc et al., 2011; van Leen et al., 2019), and cytoskeleton dynamics (Chaigne et al., 2016; Holy et al., 1997), to organelles transport and distribution (Kimura & Kimura, 2011; Pierre et al., 2016). Since the spherical zygote displays only an animal-vegetal axis, with no neighboring cells, or apicobasal polarity, an initially homogeneous yolk distribution, and an immature CAB, few of the factors known to influence spindle position in ascidian cleavage are applicable to the first cleavage. Hence the zygote may be used as a simplified version of the embryo to understand the basics of spindle positioning in the absence of many cues.

In this context, the **general aim** of the present study was to understand **how the spindle positions in the zygote** and **how it interacts with the other cell components**, especially with a major organelle, the yolk, to get a better understanding of how organelles, the cortex and MTs could be harnessed to position the spindle throughout the whole embryo segmentation stage.

Objectives

The general aim was split in two targeted objectives:

1-**Find the mechanism(s) that position the spindle in the zygote.** More precisely I wanted to first describe the steps of the DNA migration throughout the first cell cycle from sperm aster formation to spindle centration, and then perturb the migration to find the key elements of the mechanisms involved. It was necessary to take the sperm aster into account since in some species, like the sea urchin, the sperm aster first centers and only then the mitotic spindle forms (Minc et al., 2011), thus the sperm aster position participated in spindle positioning.

2- **Find the mechanism(s) by which the yolk and spindle are segregated from each other**. In order to investigate the formation of the segregation and not only how it is maintained, I had to focus on the sperm aster polymerization rather than on the spindle itself. In this work, yolk

can be perceived as both a potential actor constraining spindle position in later stages, and an example of how organelles can reshape their distributions and interact with MTs.

Contents

Following the two objectives the manuscript is composed of two main parts.

The first chapter addresses the question of the spindle position, it is divided in three parts; a main part where the aster/spindle migration was described and several key mechanisms were unraveled. This main part is formatted in such a way as to be directly submitted to a journal. The article is followed by complementary data. The chapter ends by describing preliminary data and a hypothesis on an event concomitant to the spindle centration, whose implication in the process of migration is unknown. These data could be developed into an interesting stand-alone project.

The second chapter concentrates on the yolk distribution around the sperm aster. It is composed of one section only, divided in subparts as for an article. With some modifications, the chapter should yield a second article.

Contributions

H.T and A.M supervised the thesis work, they suggested or designed many experiments, as well as provided feedbacks and corrected the manuscript.
C.H and L.B made all the mRNAs and proteins used during my thesis
All simulations were done by G.L except the simulation in chap.2.

In the article, the experiment testing the presence of cortical pulling by visualization of membrane invaginations in the zygote (section 1.2, Figure 4B) was performed by R.D and Z.M and quantified by R.D. The same experiment on two-cell stage embryo was performed and quantified by J.C and myself. S.S extracted and plotted the endocytosed vesicles parameters (section1.2, Figure 3). GL wrote the modeling methods, and A.D and myself wrote the rest of the manuscript with inputs from R.D, D.B, and H.T. The project was designed by H.T, A.M, D.B and myself.

In the rest of the manuscript: on the experiment monitoring pronuclei NEB (section 1.4, Figure 1.10), J.C produced control data and data on fused eggs. J.C tested the anti-dynein antibody. R.D measured the yolk exclusion throughout cell cycle in 3D (section 2.6, Figure 2.9)

Chapter 1:

Aster and mitotic apparatus migration in *P. mammillata* zygote

1.1 Introduction

In this chapter, I attempted to answer my first aim, that is to understand through which mechanism(s) the spindle positions in the ascidian zygote. I addressed this question by testing the three main MT-dependent mechanisms of aster or spindle centration. These mechanisms were previously described in other models and named cytoplasmic pulling, cortical pulling, and cortical pushing (Kimura & Kimura, 2011b; Reinsch & Gönczy, 1998). In addition, I paid attention to their variation through the cell cycle for several reasons: cues guiding the spindle position, like cell shape, or cell junction positions were shown to change through the cell cycle (Bosveld et al., 2016; Dumollard et al., 2017); MTs dynamic also change in cell cycle (Rusan et al., 2001); and it seemed that aster migration in time in the ascidian was not linear. This latter reason also made me differentiate the spindle migration from the spindle centration, since the aster can move in the cell in other directions than towards the cell center. The MTs-dependent mechanisms alone were not sufficient to completely explain aster migration. Since MTs and the cell cortex interact in the processes of aster centration mentioned above (Laan et al., 2012), I also began studying the actomyosin cortex during the spindle centration. The two types of mechanisms taken together give an overview of the spindle centration in the ascidian zygote.

Graphical abstract

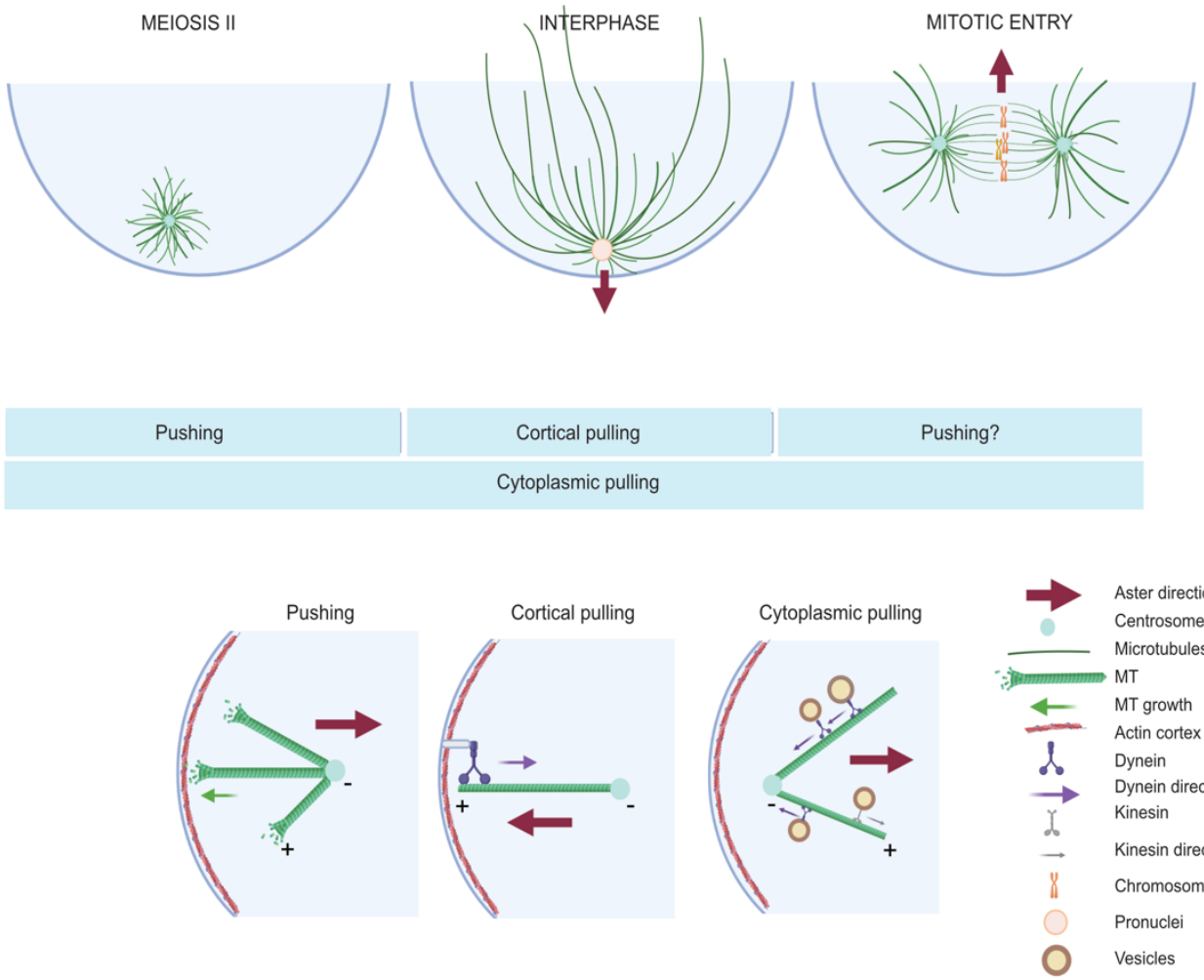

1.2 Reduction of cortical pulling at mitotic entry facilitates aster centration

Anne Rosfelter[1], Ghislain de Labbey[2], Janet Chenevert[1], Rémi Dumollard[1], Sebastien Schaub[1], Zoltan Machaty[1], Lydia Besnardeau[1], Céline Hebras[1], Hervé Turlier*[2], David Burgess*[3] and Alex McDougall*[1]

[1]Laboratoire de Biologie du Developpement de Villefranche-sur-mer, Institut de la Mer de Villefranche-sur-mer, Sorbonne Université, CNRS, 06230 Villefranche-sur-mer, France

[2]Center for Interdisciplinary Research in Biology (CIRB), Collège de France, CNRS, INSERM, Université PSL, Paris, France

[3]Department of Biology, Boston College, Chestnut Hill, Massachusetts, USA

Corresponding authors: dougall@imev-mer.fr; herve.turlier@college-de-france.fr; david.burgess@bc.edu

Keywords
Sperm aster/Mitotic apparatus/Nuclear migration/Cell cycle

Abstract

Although it has been studied for more than a century, the question of how one cell divides into two equal parts is still not fully resolved. Zygotes have provided much of the mechanistic insight into how the mitotic apparatus finds the center of the cell since the centrally-located mitotic apparatus is created from a large sperm aster that forms at the cortex and thus far from the zygote center. Here we show that in ascidians, the sperm aster extends throughout the cytoplasm during interphase yet remains located near the cortex and does not migrate towards the zygote center. It is only at mitotic entry, when the sperm aster has duplicated and the mitotic apparatus is being assembled, that most of the migration and centration occurs. This temporal pattern of centration behavior is mirrored by primate zygotes (including human). The current mechanisms of aster centration include cytoplasmic pulling that scale with microtubule (MT) length, MT pushing against the proximal cortex or MT-based cortical pulling. However, it is not yet known whether and how these 3 mechanisms are coordinated to prevent aster migration during interphase and trigger migration at mitotic entry. By monitoring quantitatively all three mechanisms (cytoplasmic pulling, pushing and cortical pulling) we have discovered that cortical pulling is switched off as the zygote enters mitosis while both cytoplasmic pulling and proximal cortical pushing remain active. Physical simulations could recapitulate both the static and migratory aspects of sperm aster and mitotic apparatus behavior. We therefore surmise that the reduction in cortical pulling at mitotic entry represents a switch that allows proximal cortical pushing forces and cytoplasmic pulling forces to center the nascent mitotic apparatus.

Introduction

Asters are intracellular structures of microtubules (MTs) radially organized around a microtubule organizing center (MTOC), generally a centrosome (Bornens, 2012), or self-organized in presence of molecular motors (Mitchison and Field, 2021; Nédélec et al., 1997). The cell may contain a single aster, as in the case of the sperm aster, or two asters following centrosome duplication, which localize at each pole of the mitotic spindle (Meaders and Burgess, 2020). Asters are involved in many essential functions in the cell including intracellular trafficking and organization (Hamaguchi 1986, Smyth 2015), polarity establishment (Wodarz, 2002), guidance of nuclei (Reinsch and Gönczy, 1998), and determination of the cleavage axis during cell division (Devore et al., 1989; Strome, 1993). Although we have known for more than a century that the protoplasmic mass of the cell becomes equally segregated to the two daughter cells following cell division (Hertwig, 1884), the precise details of the mechanism of migration and centration of the mitotic apparatus is still not fully resolved.

Elegant experiments in amphibians, echinoderms, and *C.elegans* zygotes, as well as in yeast and *in vitro* studies, have reported three possible mechanisms of how MTs can generate forces to displace nuclei and whole asters/MTOCs. One mechanism is based on cytoplasmic pulling (Li and Jiang, 2018; Minc and Piel, 2012; Minc et al., 2011; Pelletier et al., 2020; Wühr et al., 2009), one on cortical pulling (Grill et al., 2001; Kotak and Gönczy, 2013; Redemann et al., 2010), and one on MT pushing (Garzon-Coral et al., 2016; Laan et al., 2012; Meaders and Burgess, 2020; Tran et al., 2001). During centration of the sperm aster cytoplasmic pulling exerts forces on the aster by taking advantage of the transport of organelles that travel on the MTs (Kimura and Kimura, 2011; Tanimoto et al., 2016). A cargo moving towards the MTs minus-end at the centrosome experiences an opposing drag force from the cytoplasm (Longoria and Shubeita, 2013; Palenzuela et al., 2020). Cytoplasmic pulling force thus scales with MT length as more cargoes cover longer MTs (De Simone et al., 2018; Kimura and Onami, 2005). Cortical pulling occurs when MTs contact a minus end directed molecular motor localized on the plasma membrane (Laan et al., 2012) often via interaction with cortical LGN/Pins/GPR1-2 and NuMA/Mud/Lin-5 complexes (Pietro et al., 2016). Such minus-end directed motor activity, supported by the rigidity of the actin cortex, can pull on MTs bringing the whole aster and mitotic apparatus (notably during asymmetric cell division) towards the cell membrane (Grill and Hyman, 2005; Grill et al., 2001; Kiyomitsu, 2019). Finally, due to the inherent dynamic instability of MTs (Burbank and Mitchison, 2006) and their polymerization against the membrane and its actomyosin rich cortex (Rosenblatt et al., 2004), MTs can exert a pushing force in the opposite direction to MT growth (Sulerud et al., 2020) and thus lead to displacement of asters away from the cell surface (Meaders and Burgess, 2020). Such force generation may be limited however by MT buckling when the MTs exceed about 20µm in length (Dogterom et al., 2005), although this would be more difficult to interpret if short branched MTs were also present (Field and Mitchison, 2018; Petry et al., 2013).

Striking examples of sperm aster or mitotic apparatus centration occur following fertilization and have been studied in a number of species. Following fertilization a sperm aster forms from the sperm-derived centriole (in many species) at the site of sperm-egg fusion and thus near the plasma membrane and as a consequence far from the center of the fertilized egg (Ishihara et al., 2014). Interestingly however, the cell cycle phase during which aster migration occurs towards the center of the fertilized egg varies depending on species and is independent of the timing of fertilization. For example, sperm aster centration occurs during first interphase in sea urchin

immediately after fertilization (Minc et al., 2011) and in mouse oocytes during interphase following exit of meiosis II (Scheffler et al., 2021) whereas it occurs during first prophase in *C.elegans* (Gönczy et al., 1999). In *C. elegans* the sperm aster remains close to the cortex during interphase. In human oocytes (Asch et al., 1995) as well as those of other primates (Hewitson and Schatten, 2002; Simerly et al., 2019) centration also occurs at entry into mitosis (Asch et al., 1995; Simerly et al., 2019) when the sperm aster has duplicated to become the first mitotic apparatus. It is currently unknown how centration of these highly asymmetrically-positioned sperm asters in primates is 1) prevented during interphase and 2) triggered at mitotic entry.

To understand the mechanism of sperm aster/mitotic apparatus centration we analyzed the fertilized eggs of ascidians, which are a sister group to the vertebrates (Delsuc et al., 2006). As in mammals, fertilization occurs during meiotic metaphase in the ascidian (Meta I for ascidians, Meta II for primates/humans). We discovered that the sperm aster in ascidians behaves in a similar manner to those in primates/humans: the sperm aster remains cortical during interphase and migrates as a duplicated mitotic apparatus at mitotic entry. By combining experiments and numerical simulations, we investigated how the asymmetrically positioned sperm aster is prevented from migrating towards the center of the zygote during interphase and in addition how centration is triggered at mitotic entry. We found that cortical pulling is switched off at mitotic entry facilitating aster centration at mitotic entry when both cytoplasmic pulling and pushing are active.

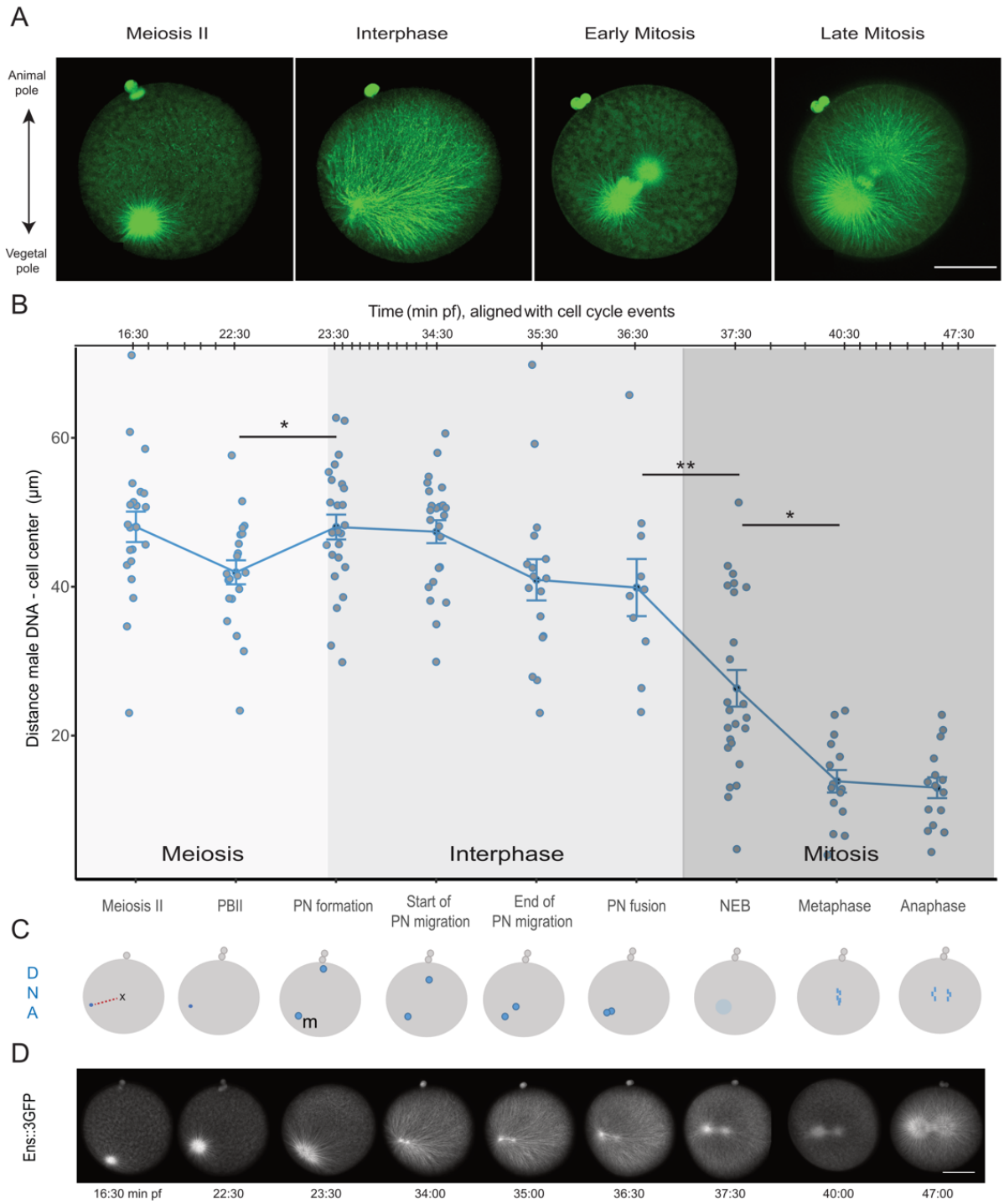

Figure 1. Migration of the sperm aster correlates with the cell cycle

A. Confocal z-sections from a timelapse 3D+time series showing microtubules in live zygotes labeled with Ens::3GFP. Meiosis II, interphase and mitosis (early and late) are displayed. Scale bar is 50µm. See Movie 1.

B. Quantification of the distance between the male DNA and cell center measured in 3D (see Materials and Methods) during the first cell cycle in 28 zygotes. Graph showing the distance of the male DNA from the cell center (in µm) at each cell cycle event. The x-axis shows the cell cycle phases corresponding to the time points measured (bottom of the graph) and the timing of the zygote shown in Fig 1D (top of the graph). The graph is colored according to the cell

cycle phases: meiosis II (light grey), interphase (medium grey) and mitosis (darker gray). Error bars represent SEM. Paired t-test adjusted with bonferroni, p-value ≤ 0.05 (*), ≤ 0.01 (**), ≤ 0.001 (***), p-value > 0.05 (ns). C. Schematic representation of the zygotic events that mark the first cell cycle and how they associate with DNA displacement in the cell. D. Confocal images from a timelapse movie of a microtubules labelled with ENS::3GFP corresponding to the schematic in C. Also see Movie 1.

Results

Aster migration in *Phallusia mammillata* correlates with the cell cycle

To monitor sperm aster and then mitotic apparatus migration while observing cell cycle stages during the first cell cycle, oocytes of *Phallusia* were co-injected with mRNAs encoding MT-binding protein Ensconsin (Ens::3GFP) and Tomato-tagged histone H2B mRNA (H2B::Tom). These oocytes were fertilized and imaged from 10 minutes post fertilization (mpf) until cytokinesis. We observed that the aster changes shape, size and position throughout the cell cycle as detailed in the next paragraph (Figure 1A, Movie 1). These changes were associated with cell cycle stages based on recognizable events: polar body (PB) extrusions, pronuclei formation, female pronucleus (PN) migration, nuclear envelope breakdown (NEB), metaphase and anaphase (Figure 1C, 1D).

In ascidians, during the completion of meiosis, the sperm aster grows in the vegetal hemisphere, on the opposite side of the fertilized egg from the meiotic spindle which defines the animal pole (Roegiers et al., 1995). During meiosis I, the aster is in the egg cortex (Dumollard and Sardet, 2001) whereas at meiosis II (7 to 20 min after fertilization), the aster is spherical and located a few microns (5-10 µm) from the egg cortex (Fig 1A « meiosis II »). Upon entering interphase, when the pronuclei form (Figure 1A "interphase"), the aster remains close to the plasma membrane in the vegetal hemisphere and MTs elongate. Later in interphase, the MTs reach the opposite side of the zygote thus allowing the capture of the female PN formed at the animal pole (Movie 2). This leads to a highly asymmetric aster with long MTs toward the cell center and animal pole, and shorter MTs towards the vegetal pole. The centrosome then duplicates and the two resulting centrosomes position on each side of the male PN which gives the aster an oblong shape extended along the vegetal cell membrane (Figure 1A, "interphase"). Finally, in prophase, which as in subsequent embryonic mitoses occurs 3-4 minutes before NEB (Dumollard et al., 2013), two asters with short MTs are linked by a central mitotic spindle (Figure 1A "late mitosis"). On the time series shown in Fig. 1A the aster does not move between meiosis and interphase whereas between interphase and early mitosis the aster migrates towards the cell center. The separation of the two centrosomes and the formation of the nascent mitotic apparatus both occur during the studied time period, for clarity purposes we refer to the globality of the aster and subsequent spindle migration as "aster migration".

Aster migration was quantified by measuring the distance between the cell center and the male DNA from 28 different embryos at several cell cycle stages (Figure 1B, Figure S1A). In the embryos pooled in the dataset the DNA was labelled either by expressing H2B::Tomato or H2B::Venus or by staining with Hoechst in live zygotes. The first noticeable event in the course of aster migration was the movement of the aster toward the cell cortex upon entry in interphase. Indeed, between the extrusion of the second polar body and the formation of the pronuclei, the

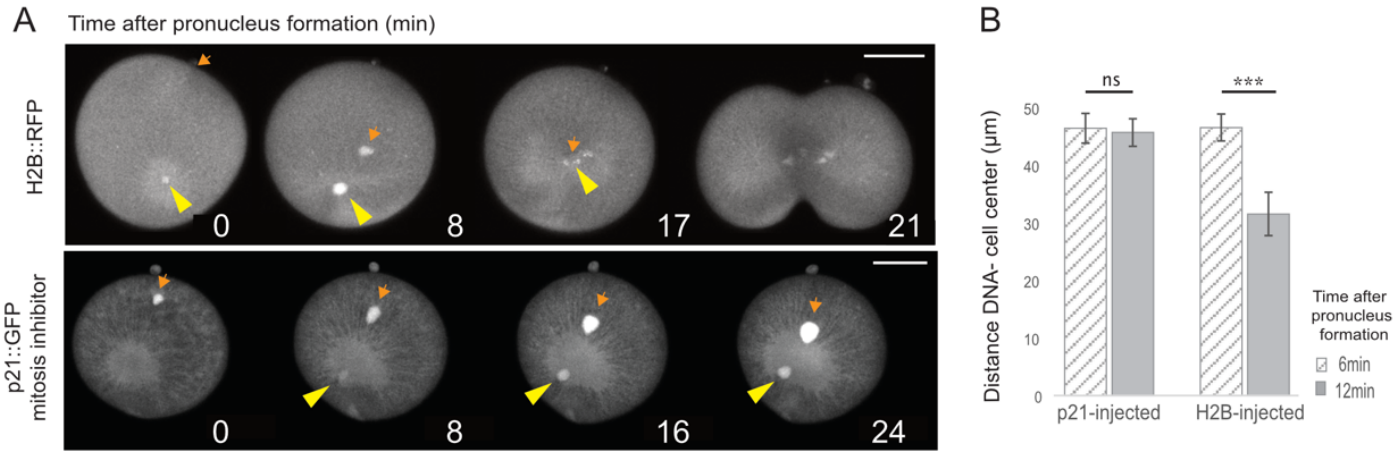

Figure 2. Entry into mitosis triggers aster migration

(A) Representative time-lapse series of a zygote expressing either H2B::RFP (top panel) and of a zygote injected with the cyclin-dependent kinase inhibitor p21::GFP protein (bottom panel). The male PN position, reflecting the aster position is shown by the DNA signal in H2B::RFP zygote and by the nuclear localization of p21::GFP in p21 injected zygotes. Male PN is indicated with a yellow arrowhead, female PN with an orange arrow. Times are indicated on each panel. Scale bar is 50µm.

(B) Quantification of the distance of the male DNA from the cell center (in µm) during interphase (6 min after PN formation) and during mitosis entry (on average at 12 min after PN formation) for p21-injected zygotes and in zygotes with an unaltered cell cycle. Error bars represent SEM. Paired t test. n=17 p21-injected embryos and n=17 control embryos.

aster moved away from the cell center (Fig. 1B). Then, during interphase (9 minutes duration), the distance between the male DNA and the cell center did not change significantly (Fig. 1B) suggesting that the aster did not significantly migrate. The main movement of migration occurred after pronuclei (PN) fusion, at mitosis onset. The distance of the DNA from the cell center decreased between the PN fusion and NEB and further declined between NEB and metaphase (Fig. 1B). Thus, after its initial growth in meiosis which displaces the aster slightly from the cortex, the sperm aster follows three phases of migration: a first movement brings the aster back to the cortex during which the aster changes shape (between 22 min. and 23 min. in Fig. 1D), then the aster does not move relative to the cell center during interphase (between 23min. and 35 min. in Fig 1D), and finally the aster starts centering at mitosis entry (after 35 min. in Figure 1C, 1D). This temporal sequence of aster migration was confirmed by the quantification of fixed samples from batches of zygotes sampled every 10 min and immuno-stained to label MTs and DNA (Figure S1B).

Aster migration requires mitosis entry

The main movement of migration starts at mitosis entry (Figure 1). Therefore, we investigated the causal role of mitosis entry on the aster migration. We monitored DNA position as a read out for aster migration and perturbed the cell cycle by injecting oocytes with p21 protein, a cyclin-dependent kinase (CDK) inhibitor (Figure 2). The presence of p21 perturbs CDK activity (Levasseur et al., 2007) and thus prolongs interphase by delaying entry into first mitosis. The injection was considered successful when interphase lasted more than twice the mean duration between PN formation and NEB in control zygotes or greater than 24 min (Table S1).

In zygotes with an unaltered cell cycle (Figure 2A, top panel) the pronuclei formed, the female PN (orange arrow) migrated and reached the male PN (yellow arrowhead), then the mitotic apparatus migrated towards the cell center during mitosis (t00:17 post PN formation). In the p21-injected zygotes with prolonged interphase (Figure 2A, bottom panel), the male and female pronuclei formed and the female PN migrated toward the male PN until it reached the centrosome (Figure 2, t00:16) or the male PN. However, the aster and the male PN never migrated, the aster remained asymmetric and uncentered and astral MTs continued to grow (Figure 2, t00:24).

Quantification of the aster migration in the two conditions revealed that in control embryos the distance between the cell center and the male PN decreased from 45+/- SEM µm to 30 +/- SEM µm from interphase to mitotic entry (Fig 2B). In contrast, during the same timing of interphase in p21-injected zygotes the distance remained at 45 +/-SEM µm, showing an absence of aster migration. Thus, prolonging interphase prevents DNA centration and aster migration.

Cytoplasmic pulling is constant during the cell cycle

Given that the aster specifically centers at mitotic entry, we wondered what could cause the absence of migration in interphase. The three mechanisms able to move the aster are cytoplasmic pulling (Li and Jiang, 2018; Minc et al., 2011; Wühr et al., 2009), cortical pulling (Grill et al., 2001; Kotak and Gönczy, 2013; Redemann et al., 2010) and cortical pushing (Garzon-Coral et al., 2016; Laan et al., 2012; Meaders and Burgess, 2020). Since the aster is highly asymmetric and has long MTs directed towards the animal hemisphere throughout the interior of the zygote during interphase (Figure 3A, Fig. 1A), one could expect to observe an

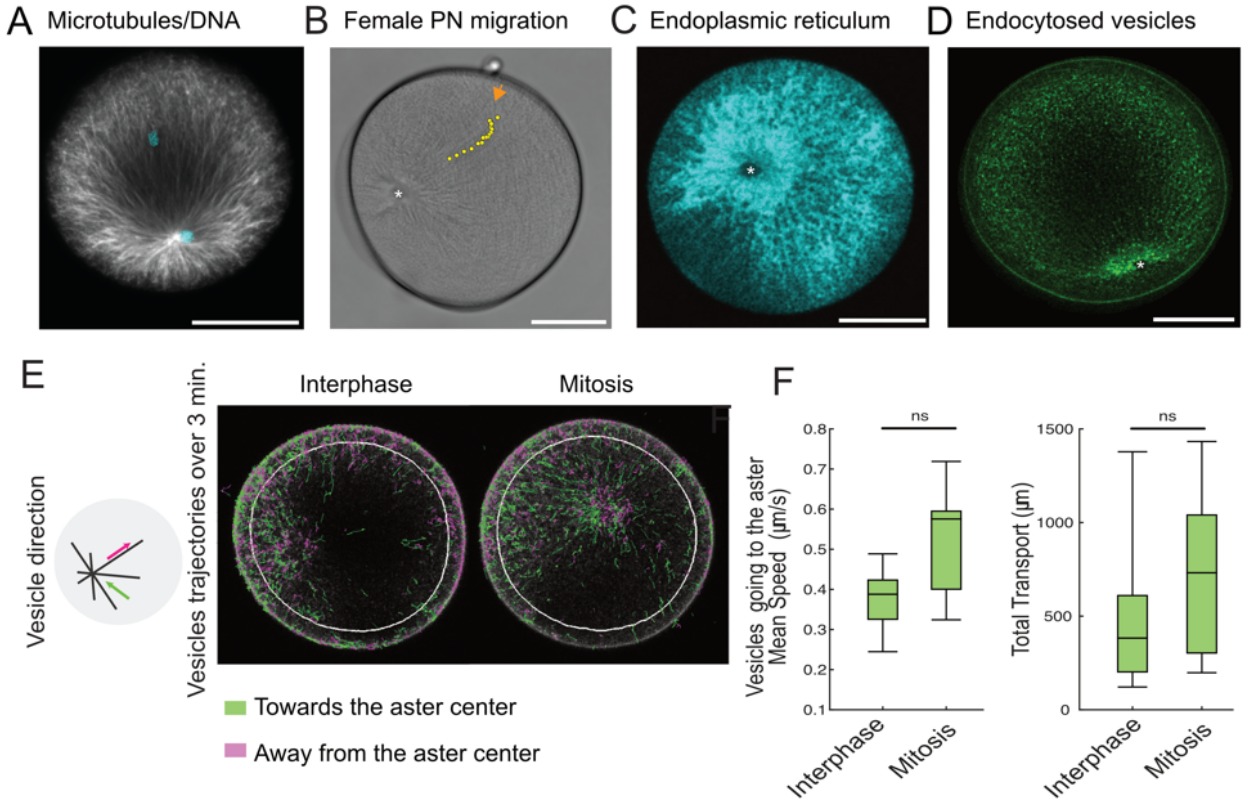

Figure 3. Characterization of minus-end directed transport in zygotes

A. Confocal image of a zygote fixed in interphase and immuno-labeled with the microtubule antibody DM1a (white), and stained for DNA with Hoechst (blue). Long microtubules crossing the whole zygote are observed during interphase. Scale bar 50µm.

B. Time projection of a bright field movie of a zygote during female PN migration towards the male PN during interphase. Yellow dots show the female PN position at several time points. Male pronucleus is indicated by a white asterisk. Also see Movie 2. Scale bar 50µm.

C. Confocal image showing ER distribution in a zygote expressing Venus::Reticulon. Note that most of the ER is accumulated around the aster at this stage. Male PN is indicated by a white asterisk (*). Scale bar 50µm.

D. Confocal image of a zygote stained with Cell Mask Orange showing endocytic vesicles accumulated at the sperm aster. Male PN is indicated by a white asterisk (*). Also see Movies 3A and 3B. Scale bars 50µm.

E. Cartoon explaining the experiment to quantify vesicle movement (left panel). Vesicles were classified as moving towards the aster center (retrograde in green), away from the aster center (anterograde in pink) or as stationary (not shown). Time projections over 3 min of a zygote treated with Cell Mask Orange in interphase (center panel) and in mitosis (right panel) showing the tracks of vesicles endocytosed from plasma membrane. Tracks of anterograde vesicles are in green, retrograde vesicles in pink.

F. Quantification of the speed (in µm/sec) and total transport of CM vesicles going towards the aster. Vesicles were imaged during 3 minutes of interphase and during 3 minutes of mitosis. Speed is measured over the complete vesicle trajectory, including pauses (left graph) and Total transport is the cumulated distance travelled by all retrograde vesicles in direction of the aster center (right graph). Box plot central mark indicates the median, bottom and top edges of the box indicate the 25th and 75th percentiles. The whiskers extend to the most extreme data points without considering outliers. Paired Wilcoxon test. n=8 embryos.

aster migration by cytoplasmic pulling (Minc et al., 2011). Thus, we first tested whether the absence of migration during interphase was caused by a lack of cytoplasmic pulling.We examined whether these long interphasic MTs accumulated or transported organelles towards the aster center, which would indicate minus-end directed transport and cytoplasmic pulling (Kimura and Kimura, 2011). The accumulation of organelles was tested by characterizing minus-end directed transport in different contexts. First, during interphase the sperm aster captured the female PN which migrated towards the sperm aster center and male PN (Figure 3B). When imaging endoplasmic reticulum during interphase, most of the ER was accumulated around the aster (Fig 3C). Finally, and in order to characterize more precisely the dynamics of organelle movement towards the sperm aster, we imaged the transport of vesicles endocytosed from the plasma membrane (labeled with the membrane dye Cell Mask Orange) and characterized their movement towards the sperm aster in the zygote (Movie 3A and 3B, Figure3D and Figure S2). The presence of minus-end directed transport of the female PN, the ER, and the endocytosed vesicles along the MTs during interphase demonstrated the presence of cytoplasmic pulling forces during interphase. We then wondered if cytoplasmic pulling may be weaker in interphase than in mitosis perhaps explaining the lack of sperm aster movement during interphase versus mitosis. As a proxy for a conserved cytoplasmic pulling we assessed whether the vesicle traffic changed throughout cell cycle. We imaged endocytic vesicles at high-speed (1 image/sec) in one confocal plane and made time projections to visualize vesicle trajectories over the course of 3 minutes (Fig 3E). We categorized the vesicles as vesicles moving towards the aster, moving away from the aster or static (Figure 3E, F, Figure S2). The projection of vesicle tracks in an interphasic versus mitotic zygote illustrated that there is no major difference in interphase versus mitosis (Figure 3E). We then compared the speed and transport of the endocytosed vesicles (Figure 3F). The speed measured is the mean speed of the vesicles on their total trajectories, and the total transport represents the sum of the distance traveled by all vesicles towards the aster center during the 3 min period. No statistically significant difference between interphase or mitosis was found for vesicle speed or the distance travelled (Figure 3F and Figure S2).

To conclude, we have demonstrated that there is retrograde transport and hence, active cytoplasmic pulling forces during interphase, and that the organelle transport is not significantly different in interphase and mitosis. This indicates that another mechanism must account for the difference of aster migration between interphase and mitosis, and especially, for the lack of aster migration in interphase.

Cortical pulling is strong in interphase and weak in mitosis

The asymmetric configuration of the sperm aster in interphase together with the accumulation of organelles at the aster center (Figure 1A, “interphase”) should favor an interphasic aster migration by cytoplasmic pulling in the direction of the longer MTs (Kimura and Kimura, 2011; Tanimoto et al., 2016). Since there was no aster migration despite the presence of cytoplasmic pulling, we hypothesized that some mechanism must prevent aster migration. A candidate mechanism to counteract the centering forces of cytoplasmic pulling is cortical pulling, which is able to off-center an aster (Laan et al., 2012). Cortical pulling occurs when minus-end directed motors bound to the cortex interact with MTs (Laan et al., 2012). The transport of the plasma membrane to the centrosome is prevented by the thick actin cortex which provides a support that resists membrane deformation. Hence, with an intact cortex, instead of bringing the plasma membrane towards the MTs minus-end, the molecular motors pull the centrosome to the plasma membrane (Figure 4A). We analyzed whether such cortical pulling forces would

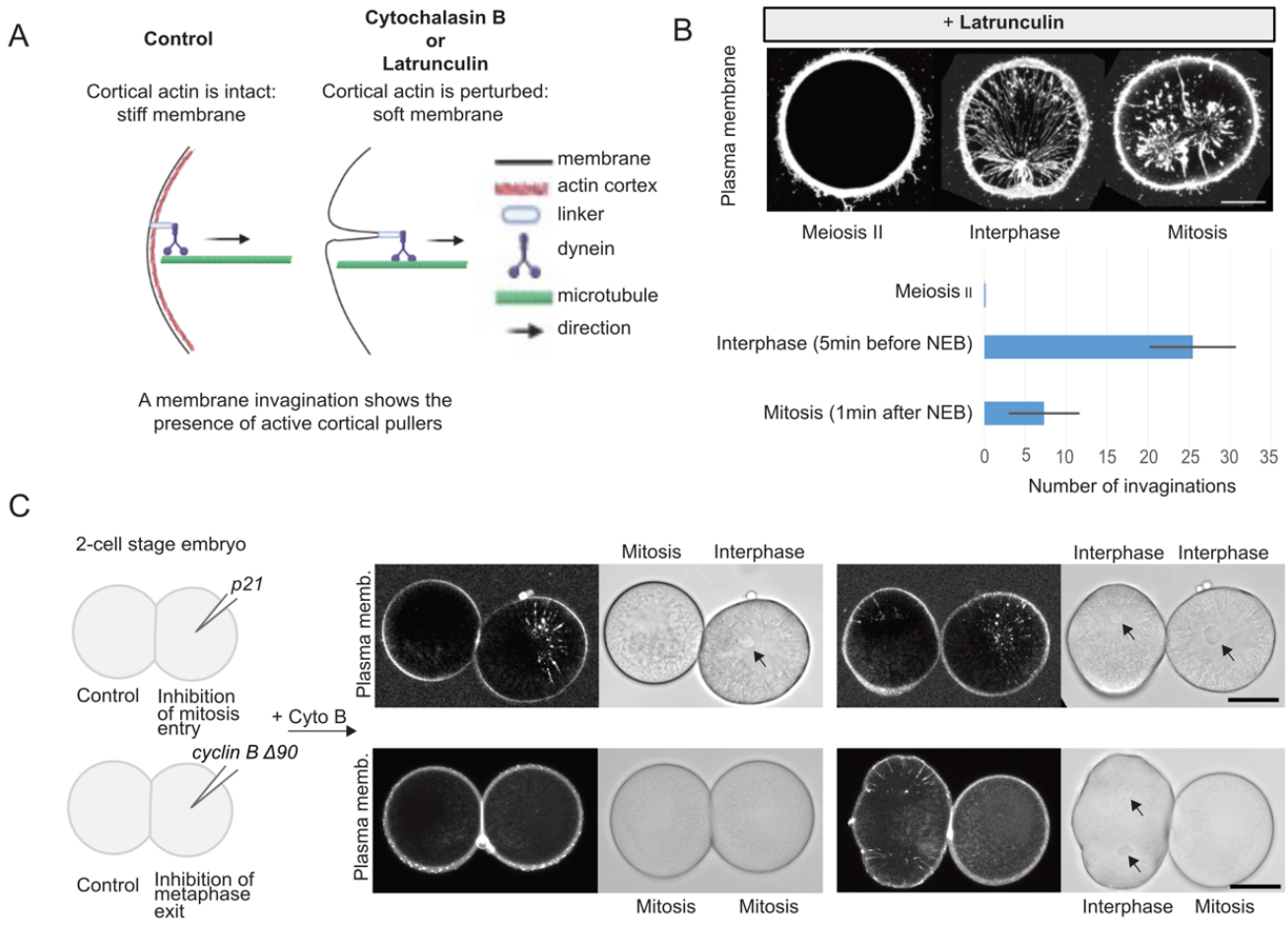

Figure 4. Cortical pulling is stronger in interphase

A. Schematic representation of the invagination assay that tests the presence of cortical pullers attached to the membrane.

B. Top panel: Confocal images of the membrane invaginations in meiosis, interphase and mitosis, in a representative zygote treated with latrunculin and labelled with CMo. Images are a projection of 10 images from a 25 μm-thick z-stack of confocal images. Bottom panel: Number of invaginations in meiosis (meiosis II), in interphase (5 min before NEB) and in mitosis (1 min after NEB). Error bars represent +/- SD. n=7 embryos. Also see Movie 4.

C. Schematic representation of the injection experiment that perturbs cell cycle in one cell of 2 cell stage embryo. Plasma membrane was labelled with prior microinjection of PH::GFP. Images displayed show the appearance of invaginations in both the injected cell and the control sister cell. Images are a projection of 10 images from a 10μm-thick z-stacks of confocal images at different time points extracted from xyzt movies. The cell cycle stage of each cell of the embryos are indicted above and below the BF images. Plasma membrane invaginations are observed only in cells in interphase (whether from control side or injected side of the embryos). Black arrow indicates the presence of a nucleus. n=11 embryos for p21 and n=9 embryos for □90. Also see Movies 5A and 5B.

thus restrain the aster from migrating to the cell center. We examined cortical pulling over the zygote cell cycle using a membrane invagination assay (Godard et al., 2021; Redemann et al., 2010; Rodriguez-Garcia et al., 2018).

We used two pharmaceutical compounds to disrupt the actin cortex: cytochalasin B or latrunculin B. Both perturbed the cortical resistance necessary to prevent membrane deformation. Thus, by labeling the membrane, invaginations of the plasma membrane towards the centrosome could be observed at sites of cortical pulling (Figure 4B, Figure 4C). Depolymerization of MTs with nocodazole completely inhibits such invaginations (Godard et al., 2021). In zygotes treated with latrunculin, the plasma membrane invaginations appear in a cyclic manner (Figure 4B, Movie 4). These data are shown as the mean number of invaginations per cell cycle phase, observed in zygotes (n=7) (Figure 4B bottom). Invaginations were never observed at meiosis II (6 minutes before PN formation) while an average of 25 +/- 5 (SEM) invaginations was counted during interphase (5 minutes before NEB) that decreased to 7 +/- 5 (SEM) invagination at mitosis (1 minute after NEB) (Figure 4A, 4B bottom). These observations demonstrate that cortical pulling is correlated with the cell cycle as it is not active in meiosis and mitosis but very active in interphase.

To test the causality between the cell cycle phases and the presence of active cortical pullers, we performed the membrane invagination assay on 2-cell stage embryos in which one cell was either blocked in mitosis or stalled in interphase while the sister cell kept cycling and served as a non-injected control cell. To manipulate the cell cycle we injected either p21 protein, to delay entry into mitosis, or a truncated non-destructible form of cyclin B protein (Δ90-cycB) to prevent exit from metaphase (Figure 4C and Figure S3) (Levasseur and McDougall, 2000). As for the zygotes (Figures 4B) non-injected cell displayed invaginations in interphase while none were visible in mitosis. We found that in p21-injected cells membrane invaginations were detected all throughout the prolonged interphase (Figure 4C top row and Movie 5A). On the contrary, in cyclin B Δ90 protein injected cells, no invaginations were visible during the prolonged metaphase, while the non-injected sister cell displayed invaginations during interphase (Figure 4C bottom row and Movie 5B). The absence or presence of plasma membrane invaginations as a function of time and cell cycle phase is displayed for each 2-cell stage embryo (Figure S3). In non-injected cells the invaginations disappeared around time of NEB (stars in Figure S3), and reappeared about 10-15 min after NEB at mitosis exit. We conclude that cortical pulling is cell cycle dependent, it is up-regulated during interphase and down-regulated at mitotic entry, prometaphase and metaphase.

Evaluation of the necessity of both cortical pulling and MT pushing against the cortex for aster migration

Cortical pulling is active in interphase therefore it could be responsible of preventing aster migration before mitotic entry. By inhibiting cortical pulling an early aster migration is expected. The inhibition of cortical pulling was performed by adding latrunculin which perturb the actin cortex, this drug also inhibited the pushing mechanism since it also requires an intact cortex. By examining aster migration in the presence of latrunculin, we evaluated the necessity of both cortical pulling and MT pushing against the cortex for aster migration. We found that

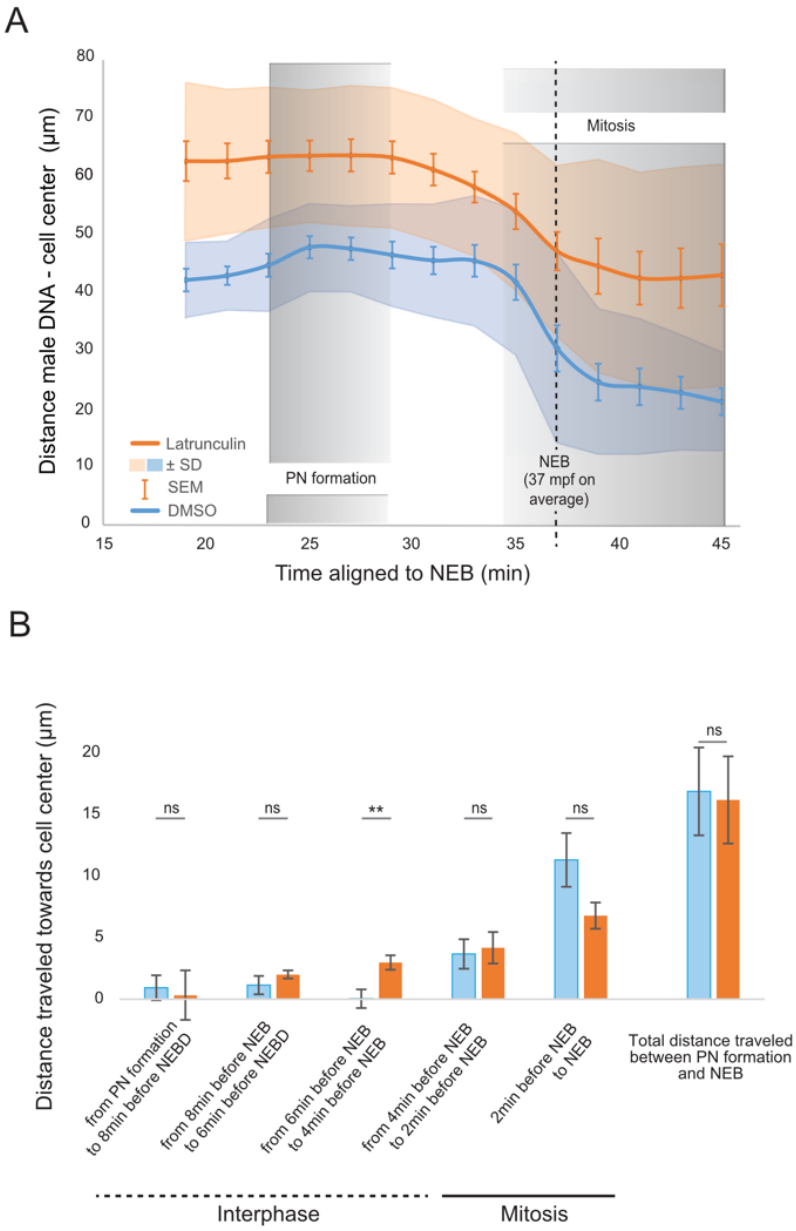

Figure 5. In absence of cortical pulling and pushing the aster migration is reduced but not advanced.

A. Average distance from DNA position to cell center in time. The distances are measured in two conditions; in control (blue curve, n=16) and in presence of latrunculin (orange, n=20), an actin polymerization inhibitor. To do the average, individual curves were aligned with respect to the time of NEB, here represented by a dotted line. The time PN-NEB is not equivalent in each embryo, thus PN formation is indicated as a span in grey shadow. Mitosis is also indicated with a grey shadow. The orange and blue shades represent = +/- SD, Error bars = +/- SEM.

B. Sperm aster distance travelled towards the cell center following latrunculin (orange bars) treatment versus control (blue bars) DMSO treated. All comparisons are not statistically different except for the 6 to 4 min before NEB timepoint which corresponds to the time that the sperm aster is flattened against the cortex following latrunculin treatment. Error bars = +/- SEM. Wilcoxon test.

when latrunculin was added during meiosis, the sperm aster was on average 60 µm away from the cell center and remained so for more than 10 minutes. Then the aster migrated throughout interphase and mitosis (Figure 5A, orange). In contrast, the aster in control DMSO-treated zygotes (blue in Figure 5A) was on average 40 µm away from the center and first migrated slightly towards the cortex at interphase entry (to 45 µm away from the center) and remained in position until mitotic entry, when the asters moved toward the cell center. The initial cortex-directed movement (just before PN formation) was not as pronounced in latrunculin-treated zygotes (Figure 5A). Nevertheless, in both latrunculin and DMSO conditions, the aster migrated approximately 15µm (total distance) between PN formation and NEB (Figure 5B), suggesting that cytoplasmic pulling is sufficient to move the aster towards the cell center. Since latrunculin inhibited cortical pushing we suggest that the closer proximity of the sperm aster to the plasma membrane is caused by the lack of efficient cortical pushing in meiosis. Finally, the slower pace of migration at mitotic entry in latrunculin-treated zygotes suggests that an additional mechanism supports aster migration at mitotic entry in control condition.

To sum up, the absence of a clear early aster migration when cortical pulling is inhibited (Figure 5A, 5B) shows that, in addition to cytoplasmic pulling which can center the aster (Figure 5A), a second mechanism is involved at mitotic entry to permit the fast aster migration. Since the inhibition of cortical pulling is accompanied by the inhibition of pushing, we hypothesized that the pushing mechanism could be an actor of aster centration at mitotic entry, thus we sought to determine when the pushing mechanism is active.

Cortical pushing is active in meiosis and mitosis

Following latrunculin treatment the aster was closer to the membrane than it was in control zygotes. We suggest that the closer proximity of the sperm aster to the plasma membrane caused by latrunculin could be explained by the lack of cortical pushing during meiosis II (Figure 5A). Indeed, we observed during meiosis II that the presence of an aster close to plasma membrane with a perturbed actin cortex creates thin membrane protrusions (i.e., a membrane deformation towards the exterior, Figure 6A). These deformations were not stable as they grew and shrunk (Movie 6) and co-localized with MTs (Figure 6B). This co-localization of MTs and plasma membrane as well as the dynamic nature of the protrusions suggested that the protrusions were caused by MTs dynamic polymerization. It also supported the notion that an actin cortex was required for the pushing mechanism to move the nascent sperm aster away from the cortex. The protrusions were visible in meiosis, and in cases where the aster did not migrate during the cell cycle, thus permitting to observe protrusions throughout the complete cell cycle, protrusions were absent in interphase and present again just after NEB (Figure 6B, Movie 6). These deformations thus appeared to follow the cell cycle as do microtubules themselves, being more dynamic during mitosis but long and stable during interphase (Figure 1). These latter observations must however be taken with caution since the absence of protrusion in interphase could also be due to the presence of the nucleus that may prevent direct contact of MTs on the membrane.

A computer simulation to challenge the contribution of cortical pulling

Based on all the results, we propose the following mechanism for aster migration (see graphical abstract). The sperm aster grows in meiosis and moves off the cortex by pushing and potentially by cytoplasmic pulling. In interphase, cortical pulling brings the aster back to the cortex, despite the constant presence of cytoplasmic pulling. Finally, entry into mitosis triggers the migration of the spindle away from the cortex: cortical pulling stops at mitotic entry, MTs become more

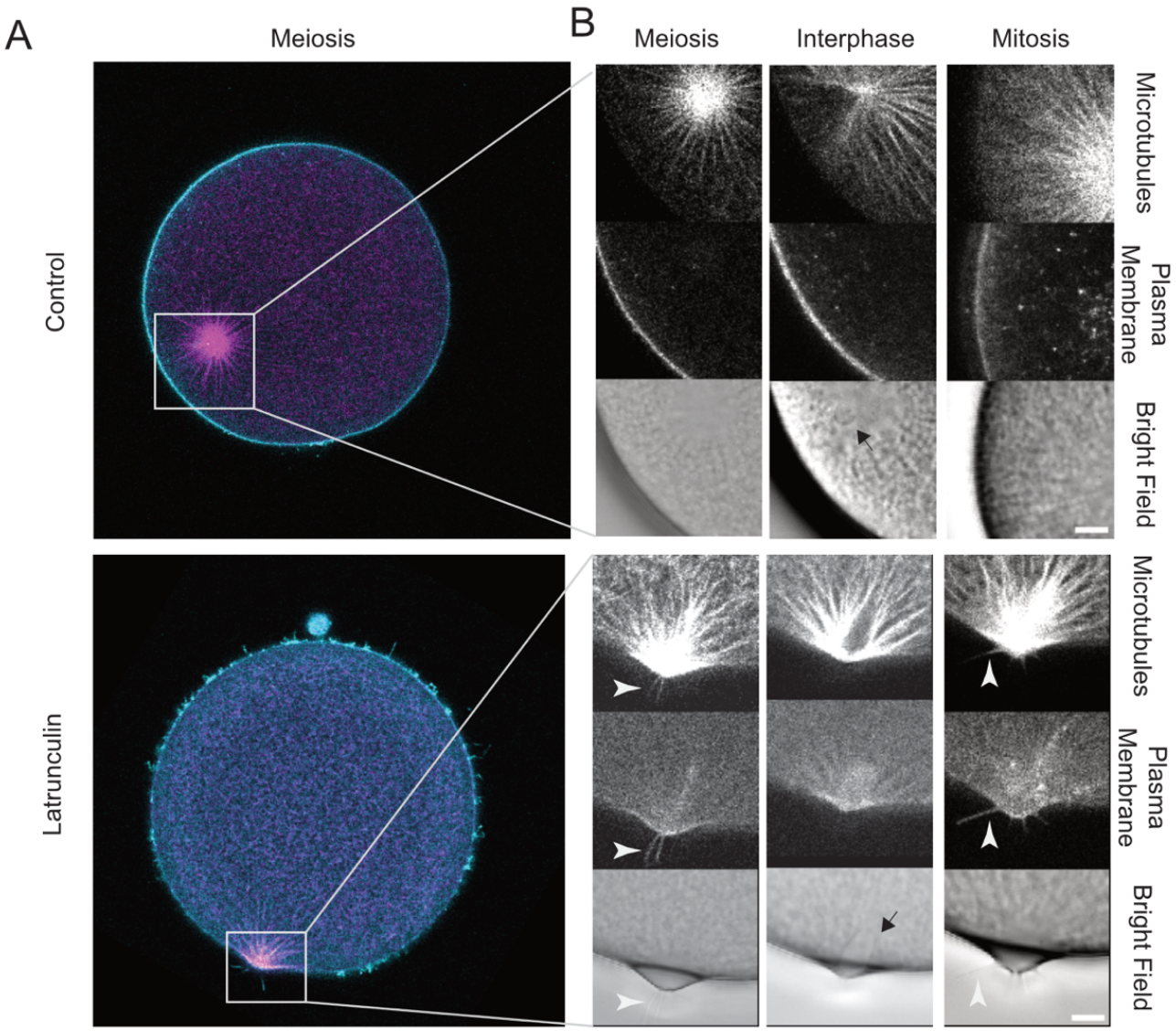

Figure 6. MT push on the plasma membrane

A. Representative confocal images of a control zygote (top panel) and of a zygote treated with latrunculin (bottom panel, n=9 embryos), both in meiosis and expressing the microtubule marker Ens::3GFP and labeled with the plasma membrane dye Cell Mask Orange.

B. Close-up of A on the area containing the sperm aster and the closest piece of plasma membrane in meiosis (first column). Adjacent images of the aster in interphase (second column), and mitosis (third column) are extracted from time-series of the same zygotes. Black arrow indicates the presence of a nucleus, white arrowhead indicates the presence of thin protrusions. Also see Movie 6. Scale bar is 10 µm. n=3 embryos.

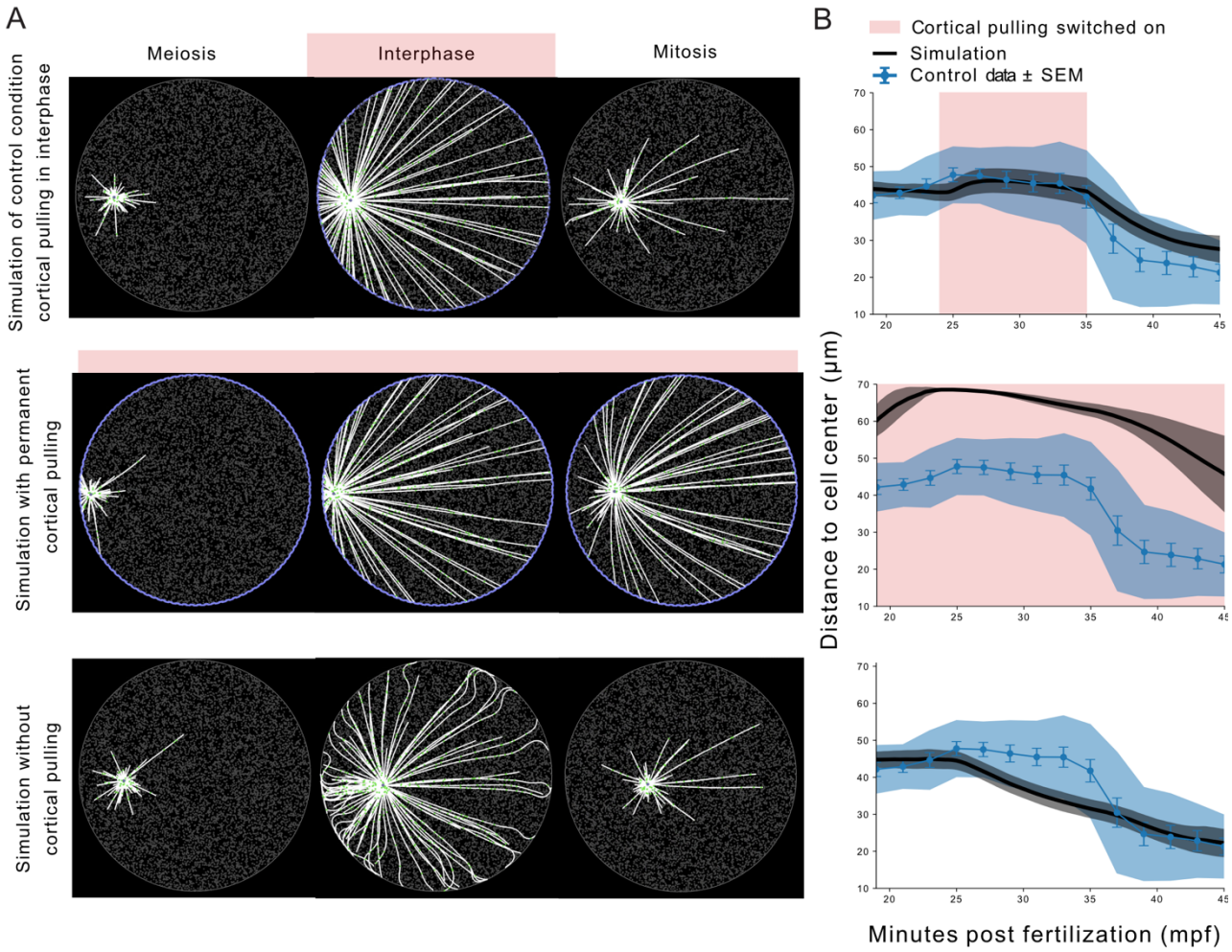

Figure 7. Cortical pulling dictates the pattern of aster migration

A. Stills from simulations testing the contribution of cortical pulling in the aster migration pattern. The selected frames correspond to times of meiosis, interphase and mitosis in the simulation. The mitotic apparatus was simplified as an aster. The aster core (centrosome) is represented by a purple dot at the center of the MTs structure. MTs are in white, they are set to become more stable in interphase and when they touch the cortex. The purple cell border illustrates the activity of cortical dyneins, and thus an active cortical pulling. The many grey dots show the presence of cytoplasmic pulling in the cell since these dots are fixed dyneins. They become green when attached to MTs. Three condition were tested; a transient cortical pulling in interphase (first row), a permanent cortical pulling (second row), and an absence of cortical pulling (third row)

B. Comparison of the aster migration, as the distance of the aster from the cell center through time, in control data (blue curve), and in the simulations (black curve). The blue and grey shades represent +/- SD. The red margin represents the cortical pulling activity in the corresponding simulation. The graphics are aligned with A so that the simulation corresponding to the graphic appear on the same row.

dynamic, and the mitotic apparatus moves by combined cytoplasmic pulling and cortical pushing. We designed a 2D agent-based stochastic computer model of aster migration based on the software *Cytosim* (Foethke et al., 2009) (Figure 7A, Movie 7). The parameters of model simulations were set according to past studies on different species (Sup Table S2), and adjusted to our data to match the timing of cell cycle and the cortical pulling activity. We verified the equivalence of the simulated and observed cytoplasmic pulling by comparing a simulation to latrunculin data (Figure S4 A and B, first row). Once an average reference simulation was established, we could remove specific forces to test the contribution of cortical pulling in the global scenario of aster migration (Figure 7), or to explore other situations (Figure S4). With a permanent cortical pulling the aster is quickly brought to the cell cortex in meiosis and did not seem to leave the cortex during the cell cycle (Figure 7A 7B, second row). Thus, in this condition the migration did not fit the control profile of aster migration, the aster was always further from the cell center than in control (Figure 7B, second row).

In the complete absence of cortical pulling throughout the cell cycle (Figure 7, third row) the aster position was slightly more centered in interphase, and the overall aster centration hence reached the same distance from the cell center as in the average reference simulation (Figure 7 first and third rows). Indeed, in the absence of cortical pulling the aster centered as much as it did in the control dataset, however the centration began earlier, progressed at a constant velocity, and did not show the static phase prior to aster migration (Figure 7B, third row). The comparisons of simulations outputs to the data supported the scenario drawn from our results where aster centration is prevented by cortical pulling activity during interphase, and the inactivation of cortical pulling in mitosis permits aster movement. Only relying on simulations, we pushed the exploration of our model on questions still experimentally unanswered. These theoretical explorations suggested that cytoplasmic pulling is the main contributor to aster centration in mitosis compared to the pushing mechanism (Sup Figure S4A, S4B, bottom row). Finally, we used the simulation to examine a scenario where cortical pulling is nonuniformly inactivated at mitosis entry i.e., if cortical pulling is first turned off near the aster before being completely inactivated (Figure S4C). In this case, the aster centration during mitosis was faster than that obtained by simulating uniform inactivation (Figure 7 top) and the simulation best fitted the experimental data (Figure S4C).

Discussion

A central question in the field of cell biology is how a cell divides into two equal sized daughter cells which relies on positioning of the mitotic apparatus to the cell center. The mechanism(s) involved in centering are still not fully resolved although they often depend on MT-based cortical pulling, cytoplasmic pulling or cortical pushing depending on the species, cell type and cell cycle stage. Centration has been studied extensively in *Xenopus,* sea urchin and *C. elegans* zygotes. In the large oocytes of *Xenopus* (circa 1mm) cytoplasmic pulling forces provide the force for aster centration. For example, by microinjecting a dominant negative fragment of the dynactin complex (p150-CC1) sperm aster centration was blocked (Wühr et al., 2010). Also, since MTs of the sperm aster are too short to reach the cortex on the opposite side of the zygote the primary mechanism for centration in *Xenopus* is cytoplasmic pulling in the direction of the longest MTs (Wühr et al., 2010). Sea urchins have smaller zygotes (circa 100µm) and even though MTs of the sperm aster are long enough to reach the opposite cortex, cortical pulling has not been reported to be involved and instead the two mechanism reported to power sperm aster centration in sea urchin are based on cytoplasmic pulling (Tanimoto et al., 2016) and

cortical pushing (Meaders et al., 2020). In *C. elegans* centration occurs during prophase in a dynein-dependent manner (Gönczy et al., 1999). In order to distinguish between cortical and cytoplasmic dynein, factors that recruit dynein to the cortex have been depleted. RNAi knockdown of goa-1/gpa-16 to deplete cortical dynein led to a higher velocity of sperm aster centration suggesting that cytoplasmic dynein was the primary force generating mechanism for centration (De Simone et al., 2018). In addition, since depletion of cortical dynein increased the velocity of centration cortical pulling forces were suggested to counteract the cytoplasmic forces that power centration of the sperm aster (De Simone et al., 2018).

The examples of sperm aster centration in *Xenopus* and sea urchin occur during interphase while in *C elegans*, primates (Asch et al., 1995; Hewitson and Schatten, 2002; Simerly et al., 2019) and ascidian (here) centration occurs at mitotic entry. Moreover, the position and geometry of the ascidian sperm aster, with long MTs extending into the zygote interior and short MTs directed towards the proximal vegetal cortex, represents a configuration that should favor cytoplasmic pulling to displace the sperm aster towards the zygote center. We were therefore curious about what prevented sperm aster centration until mitotic entry. A cell cycle link that triggers an increase in cortical pulling had been reported previously in *C. elegans* one cell stage embryos (Bouvrais et al., 2021; McCarthy Campbell et al., 2009; Redemann et al., 2010). Posterior cortical pulling forces displaces the mitotic apparatus towards the posterior cortex during anaphase (Grill et al., 2003; McCarthy Campbell et al., 2009; Redemann et al., 2010). Indeed, the number of short-lived MT plus ends engaged in cortical pulling increased at the posterior pole of *C. elegans* one cell stage embryos at anaphase onset (Bouvrais et al., 2021). This increase in cortical pulling has been linked with the fall in cyclin-dependent kinase (CDK) 1 activity: either reducing the function of the proteasome, the APC (anaphase-promoting complex), or Cdc20 all delayed spindle displacement while inactivating CDK1 in prometaphase caused premature spindle displacement (McCarthy Campbell et al., 2009). Although these findings indicate that cortical pulling increases at anaphase (Keshri et al., 2020; Kotak et al., 2013) one key additional point may be that cortical pulling is less prominent when CDK1 activity is elevated. Here in the ascidian, we have noted a similar phenomenon whereby cortical pulling is elevated during interphase and reduced at mitotic entry when CDK1 activity increases.

In the ascidian *P. mammillata*, the sperm aster forms in the vegetal hemisphere of the zygote during meiosis II (Roegiers et al., 1995). Here we demonstrate that during meiosis II the sperm aster grows and remains roughly spherical as it moves slowly away from the proximal vegetal cortex (Figure 1). At this stage the sperm aster remains relatively small (approx. 1/3 zygote diameter) and located in the zygote vegetal hemisphere. Such a vegetal location and relatively small size ensures that sperm astral MTs do not reach the animal pole and thus interfere with the segregation of the meiotic chromosomes, which in smaller *C.elegans* zygotes is accomplished by preventing sperm aster growth during meiosis II (McNally et al., 2012). At entry into interphase astral MTs extend throughout the zygote and capture the female PN located at the animal pole (Figure 1). The female PN then migrates towards the center of the sperm aster during a short interphase (about 10 min) while the cortically-located and highly asymmetric sperm aster remains in position near the vegetal pole (Figure 1). Just prior to NEB, during prophase, the sperm aster begins abruptly to migrate accompanied by NEB and formation of a bipolar mitotic apparatus (Figure 1).
What triggers the switch to induce migration at entry into mitosis? First, we delayed entry into mitosis to determine if a causal relationship existed between entry into mitosis and sperm aster migration. Delaying entry into mitosis with the CDK inhibitor p21 prevented sperm aster migration (Figure 2). Next, we teased apart the relative contributions of cortical pushing,

cytoplasmic pulling, and cortical pulling to determine which of these three mechanisms displayed a cell cycle-dependent change at mitotic entry that could explain how mitotic entry triggered sperm aster migration. Cortical pushing is present in Meiosis II, and is responsible for the initial aster displacement from the cortex (Figure 6). Even though it seems this mechanism is also active in mitosis (Figure 6B), its contribution to spindle migration at mitosis entry seems minor (Figure S4). We therefore focused on cytoplasmic pulling and cortical pulling. Cytoplasmic pulling can be visualized through the movement of three different endomembrane structures towards the center of the sperm aster: the female PN, endoplasmic reticulum and vesicles (Figure 3). Taking advantage of the opportunity to monitor a large number of vesicles (labelled with Cell Mask Orange) we quantified the movement of the cytoplasmic vesicles to determine whether there was a measurable difference in cytoplasmic pulling between interphase and mitotic entry (Figure 3 and Figure S2). The data demonstrated that vesicles transport was unchanged between interphase and mitotic entry, suggesting a constant cytoplasmic pulling. We then sought to determine whether cortical pulling was more prominent during interphase or mitosis. To do so we exploited the membrane invagination assay following weakening of the cortex (Godard et al., 2021; Redemann et al., 2010; Rodriguez-Garcia et al., 2018). Interestingly, we noted that cortical pulling was greater during interphase than mitotic metaphase (Figure 4). We therefore devised a 2-cell stage assay to determine whether cortical pulling was a feature of interphase and switched off at mitotic entry. By either delaying mitotic entry with p21 or blocking exit from metaphase with Δ90 cyclin B in one sister cell (Figure 4) we demonstrated that cortical pulling is elevated during interphase and switched off at mitotic entry when CDK1 activity is elevated. This observation could explain the switch-like behavior in migration and suggest that it is the increase in CDK1 activity at mitotic entry that switches off cortical pulling thus liberating the sperm aster from its cortical tethers facilitating centration. Moreover, these data develop further the findings from *C. elegans* where cortical pulling was decreased when CDK activity was elevated (McCarthy Campbell et al., 2009).
By using the software *Cytosim* we tested whether cortical pulling could prevent aster migration mediated by cytoplasmic pulling. Simulations showed that cortical pulling was capable of preventing migration caused by long MT-mediated cytoplasmic pulling and re-enforce the data showing that the sperm aster does not migrate during interphase when cortical pulling is elevated (Figure 7). This supports the idea that switching off cortical pulling at mitotic entry is necessary for sperm aster migration. Furthermore, the simulation indicated that a total absence of cytoplasmic pulling prevented aster migration in mitosis (Figure S4). Overall, these findings demonstrate that mitotic apparatus migration in the ascidian occurs at mitotic entry which causes the switching off of cortical pulling while cytoplasmic pulling and pushing remain active. It would be interesting to examine the relationship between mitotic entry and sperm aster migration in primate zygotes to determine whether cortical pulling is also switched off at mitotic entry.

Acknowledgments

We thank members of the Turlier and McDougall groups for technical advice and discussion. We are grateful to the Imaging Platform (PIM) and animal facility (CRB) of Institut de la Mer de Villefranche (IMEV), which is supported by EMBRC-France, whose French state funds are managed by the ANR within the Investments of the Future program under reference ANR-10-INBS-0, for continuous support. This work was supported by a collaborative grant from the French Government funding agency Agence National de la Recherche to McDougall (ANR ‘‘MorCell’’: ANR-17-CE 13-0028), by a MITI award from the CNRS (Modélisation du vivant) by an Assemble + grant 9632 to Burgess, and by Sorbonne Université which provided a doctoral

stipend. HT has received funding from EMBRC-France (AAP Découverte 2020) and from the European Research Council (ERC) under the European Union's Horizon 2020 research and innovation program (Grant agreement No. 949267).

Materials and Methods

Biological material

Phallusia mammillata were collected in Roscoff or Sète and kept at 16°C in an open system of aquarium in the animal facilities. The gametes were collected by puncturing separately the oviduct and the sperm duct. The sperm was kept dry at 4°C and could be used for fertilization up to 1 week after collection. Oocytes were used the day of collection after undergoing dechorionation by incubation in 0.1-0.2% trypsin in micro-filtered natural sea water (MSFW) at 19°C for 90 minutes, and subsequent washes in MSFW supplemented with 5mM TAPS (tris(hydroxymethyl)methylamino] propanesulfonic acid) pH 8.2. All the subsequent manipulations of live embryos were performed in MSFW 5mM TAPS, using pipette tips, dishes, slides and coverslips coated with 0.1% gelatin and 0.1% formaldehyde (Sardet et al., 2011). For fertilization, a small volume of activated sperm (circa 5µl) was added to the oocytes in a 5ml petri dish. To activate the sperm, 6 µL of dry sperm was incubated for 20 minutes at 19°C in 500µL of MSFW pH9.2. Time post fertilization was measured starting when the oocyte first showed a shape change. For fixation of fertilized cultures, time post fertilization started when about 30% of the oocytes showed simultaneously the first deformation.

mRNA synthesis and injections

Synthetic mRNAs for microinjection were prepared using the mMESSAGE mMACHINE T3 kit (Ambion), from plasmids containing the gene of interest (EB3::3GFP, Ensconsin::GFP, PH::GFP, Histone H2b::Rfp1, Venus::Reticulon) coupled to a T3 promotor and a polyA tail. mRNA yield was estimated by spectrophotometry. The mRNAs were stored at high concentration (>10µg/µL) in 1 µl aliquots at −80 °C, then thawed and diluted in distilled water for use. The mRNAs were micro injected into dechorionated oocytes transferred to small glass wedges mounted onto 400 µl Perspex mounting chambers designed for horizontal microinjection (see detailed protocols in McDougall et al., 2014). They were injected with a micropipette at a pipette concentration of 5-6 µg/µl (~1–2% injection volume) using a high pressure system (Narishige IM300). mRNA-injected oocytes were left for 5 h or overnight before fertilization and subsequent confocal imaging.

Protein purification and injections

The p21::Cherry protein (cyclin dependent kinase inhibitor 1a) was injected to arrest the cell cycle in interphase. The human p21 protein fused with mCherry was cloned in a pET11a vector with 6 His-tag, and purified with a silica-based resin column (MACHEREY-NAGEL, protino Ni-IDA). Aliquots were flash frozen in liquid nitrogen and stored at –80°C. The protein was used at a concentration of 30mg/ml.

The construction and synthesis of the Δ90 cyclin B1::GFP plasmid has been described previously (Levasseur and McDougall, 2000). The Δ90cyclin B::GFP fusion protein was stored at –80°C at a final concentration of approximately 11 mg/ml.

The microinjection system described above for mRNAs injection was also used for protein injection. Protein-injected oocytes were left for 45min at 18°C before fertilization and subsequent confocal imaging.

Invagination experiments

Eggs were fertilized in MSFW, and at deformation transferred into a solution of MSFW TAPS with 5µM of latrunculin B (Sigma Aldrich) diluted from a 10mM stock solution in DMSO. The embryos were then mounted on a slide in the latrunculin solution. The zygote membrane was visualized either by microinjection of the PH::Tomato mRNA, or by addition of the membrane dye Cell Mask orange (Thermofisher, Invitrogen) at 1:1000. For controls, zygotes labeled with PH::Tomato or Cell Mask were treated with DMSO at a dilution of 1:1000.

In the case of the embryo injected at the two-cell stage, the fertilized eggs were left to develop at 16°C in MFSW until they started cleaving. Then they were mounted on the injection chamber, and injected with p21 or Δ90cyclinB as soon as the division finished. When two or three embryos were injected they were immediately transferred in MFSW with 5µM of Cytochalasin B (Sigma Aldrich) diluted from a 10mM stock solution in DMSO, and mounted on a slide in this solution.

Confocal microscopy imaging

All imaging experiments were performed at 19°C using a Leica TCS SP8 inverted microscope fitted with Hybrid detectors and 40×/1.1NA water objective lens. To measure the aster migration, each fertilized egg or 2-cell stage embryo was scanned by 4D live imaging (xyzt) with a frame rate of at least every 210s on a whole embryo. The imaging parameters were adapted to each fertilized egg: z step was between 0.5 and 2µm and time step between 1 min and 3.30 min. For fixed samples, z-stacks were acquired at step size of 0.5 µm.

Quantification of aster migration

The quantification of the distance between the center of the zygote and the DNA throughout the cell cycle was performed in three steps, using Fiji (Schindelin et al., 2012). First, the center of mass of zygotes were determined at each time point. To do so, a Gaussian Blur (sigma =2) was applied to each xyz stack of the timelapse movie. Stacks were then made binary with the "Triangle" method of the "Auto Threshold" function. The Fiji plugin "3D Roi Manager" (Ollion et al., 2015) created objects from the binary stacks, and output their center of mass. This method was verified by comparing the center of mass of the 3D zygote to the centroid of the 2D equatorial section with widest diameter.

Secondly, using the Fiji "Point tool" and the "measure" function, the xyz coordinates of the DNA label were obtained at each time point. When DNA was not labeled (in p21-injected embryos), or weak (at NEB), DNA position was approximated to be at equal distance between the two spindle poles, or at the center of the aster when the spindle was not yet formed. The DNA label was chosen over the MT label to measure the aster migration because centrosome duplication occurs before the centration of the spindle, therefore while the spindle as a whole centers, each spindle pole starts centering and then diverge from the cell center to center the DNA.

Finally, the distance between the DNA coordinates and the center of mass was computed using the 3D Pythagorean theorem: $d=\sqrt{((x2-x1)^2+(y2-y1)^2+(z2-z1)^2)}$.

Quantification of the number of invaginations

To monitor the membrane invaginations in zygotes or 2-cell stage embryos, confocal images were acquired with a z step between 0.5 and 1 µm and time step was between 30 seconds and maximum 2min. Presence or absence of invagination was determined visually on multiple z projections covering about 10µm.

Quantification of the vesicle traffic

To image vesicle trafficking, eggs were fertilized, washed once, and immediately transferred to a GF-coated slide/coverslip in a MFSW containing Cell Mask orange (1/1000). Then, we acquired 2D images every second for 3 min. The imaged plane was selected to contain the center of one aster.

To measure relative movements of the vesicles, we combined 3 approaches. 1) For vesicles, we used the Fiji tool TrackMate with LoG particle detection and simple LAP tracker (Tinevez et al., 2017). 2) For aster localization we wrote (using Matlab) a manual periodic tracking, with interpolation for intermediate time frames. 3) For cell contour, we developed another Matlab algorithm based on threshold optimization to extract the cell mask. We combined information from those tools to quantify movement.

For each vesicle track, we measured the relative path with respect to the aster. In more detail, we defined a radius from the aster center to the centroid of the track, which naturally crosses the cell contour. On this radius, we projected the path to estimate the radial component of the vesicle movement. We also measured the temporal evolution of the contour. To take into account the cell deformation and its impact on vesicle movement, we subtracted from each relative path a yield drift. Considering an elastic behavior on the aster-contour axes, the yield drift of a vesicle at a radius r was defined as follows:

$$Y\_drift\ (r,t)=Y\_contour\ (t)\times r/(R(t))$$

with R(t) the distance of the cell contour from the aster center. To segregate vesicles just endocytosed, stagnant below the membrane, from the vesicle moving on the aster, we kept only the tracks 10µm away from the contour. Based on the path projection on the radius and its orientation (positive if the last position is further from the aster than the first position), we then sorted the tracks as going to (retrograde) or from (anterograde) the aster. For path projection smaller than 1µm we defined them as stationary (note that this category includes the static vesicles and vesicles moving orthogonally to the radius).

Modeling

Agent-based simulations were performed in 2D using a custom version of the software *Cytosim* - www.cytosim.org (Foethke et al., 2009) with the parameters provided in Table S2. *Cytosim* is a stochastic simulation engine that includes constituting elements of the cytoskeleton. It has already been used to study spindle and centrosome dynamics and position (Khetan and Athale, 2016; Lacroix et al., 2018; Letort et al., 2016).

Aster and microtubules

MTs are modeled as worm-like chains, characterized by a bending stiffness (see Table S2) and inextensibility. MTs can (de)polymerize and their instability is modeled by a stochastic alternation of growing and shrinking phases. The plus-end polymerizes until a catastrophe

happens, starting a shrinking period. The aster is modeled as a bead, from which MTs are nucleated. MTs minus-ends are anchored to the aster while their plus-end are directed outward from the aster.

A pushing force is generated by MTs' plus end polymerizing against the edge of the cell. When MTs push strongly on the cortex, polymerization is slowed down and they have a higher chance to undergo a catastrophe. Previous work (Letort et al., 2016) suggests that pushing cannot center the aster if MTs can glide along the cell membrane. In their work, gliding was prevented by pinning MTs' tips to the point where they first reached the edge of the cell. Pinning and cortical pulling were not activated at the same time though, as pinning would make cortical pulling inefficient. In our case, we didn't model control cells as a proper circle, but as a crenelated polygon, representing the actomyosin cortex Once a tip enters an alcove, it cannot slide anymore, as if it were stuck by intertwined actin filaments.

Dynein distributed in the cytoplasm

Dyneins are placed at random position in the cytoplasm. When a MT comes close, a dynein can bind to the MT and start moving towards its minus end. As in previous work cited above, a spring-like force pulls the dyneins back to their assigned position when they are displaced. The dynein's velocity depends on the load and the projection of the restoring force along the direction of the MT.

$$v = v_{max}\left(1 - \frac{f}{f_s}\right)$$

$$f = -k(\vec{x} - \overrightarrow{x_0}).\vec{u}$$

v_{max} is the unloaded speed, ie the speed when there is no applied force. f_s is the stall force, the maximal force the dynein can withstand before it stops moving. k is the spring stiffness, $\vec{x}$ the position of the dynein, $\overrightarrow{x_0}$ the rest position it has been assigned and $\vec{u}$ the direction of the MT.

Control of MT dynamics by cortical dynein to generate forces

If cortical pulling is implemented by usual dynein, it often makes the aster spin around the cell. This is due to the fact that MTs tend to align with the cell's edge, as more and more cortical dynein becomes attached to the MTs. The pulling force becomes higher and higher and the aster spins around. *In vitro* experiments suggest that dynein placed in front of a rigid barrier can control MTs' dynamics (Laan et al., 2012). Such dyneins triggers a catastrophe when they bind to the end of a MT, and regulate its shrinking speed thereby generating pulling forces. We modified *Cytosim* to implement such a behavior: cortical dynein work like classical molecular motors except that they can only bind to a MT end, and they chew the MT as they move forward. Like cytoplasmic dyneins, they have a stall force and the load comes from a spring linking the dynein to its original position. However, unlike cytoplasmic dyneins, cortical dyneins cannot move backwards as it would imply the MTs polymerized again.

Code availability and simulation reproducibility

The custom version of *Cytosim* with this interaction implemented is available at https://gitlab.com/gslndlb/cytosim, in the branch *dynein_chew*. All configuration files used are in the cym folder.

Statistics and diagrams

Statistical tests and graphics were performed using the libraries rstatix, tidyverse, dplyr, ggpubr, and ggplot2 from R software (R Studio, 2020) as well as Microsoft Excel (2013). Tests are provided in the figure legends. Diagrams were created with BioRender.com

Data availability

All main figures are supplied with data used to generate the figures.

References

Asch, R., Simerly, C., Ord, T., Ord, V. A. and Schatten, G. (1995). The stages at which human fertilization arrests: microtubule and chromosome configurations in inseminated oocytes which failed to complete fertilization and development in humans. *Hum Reprod* **10**, 1897–1906.

Bornens, M. (2012). The centrosome in cells and organisms. *Science* **335**, 422–426.

Bouvrais, H., Chesneau, L., Le Cunff, Y., Fairbrass, D., Soler, N., Pastezeur, S., Pécot, T., Kervrann, C. and Pécréaux, J. (2021). The coordination of spindle-positioning forces during the asymmetric division of the Caenorhabditis elegans zygote. *EMBO Rep* **22**, e50770.

Burbank, K. S. and Mitchison, T. J. (2006). Microtubule dynamic instability. *Curr Biol* **16**, R516-517.

De Simone, A., Spahr, A., Busso, C. and Gönczy, P. (2018). Uncovering the balance of forces driving microtubule aster migration in C. elegans zygotes. *Nat Commun* **9**, 938.

Delsuc, F., Brinkmann, H., Chourrout, D. and Philippe, H. (2006). Tunicates and not cephalochordates are the closest living relatives of vertebrates. *Nature* **439**, 965–968.

Devore, J. J., Conrad, G. W. and Rappaport, R. (1989). A model for astral stimulation of cytokinesis in animal cells. *J Cell Biol* **109**, 2225–2232.

Dogterom, M., Kerssemakers, J. W. J., Romet-Lemonne, G. and Janson, M. E. (2005). Force generation by dynamic microtubules. *Curr Opin Cell Biol* **17**, 67–74.

Dumollard, R. and Sardet, C. (2001). Three different calcium wave pacemakers in ascidian eggs. *J Cell Sci* **114**, 2471–2481.

Dumollard, R., Hebras, C., Besnardeau, L. and McDougall, A. (2013). Beta-catenin patterns the cell cycle during maternal-to-zygotic transition in urochordate embryos. *Developmental Biology* **384**, 331–342.

Field, C. M. and Mitchison, T. J. (2018). Assembly of Spindles and Asters in Xenopus Egg Extracts. *Cold Spring Harb Protoc* **2018**,.

Foethke, D., Makushok, T., Brunner, D. and Nédélec, F. (2009). Force- and length-dependent catastrophe activities explain interphase microtubule organization in fission yeast. *Mol Syst Biol* **5**, 241.

Garzon-Coral, C., Fantana, H. A. and Howard, J. (2016). A force-generating machinery maintains the spindle at the cell center during mitosis. *Science* **352**, 1124–1127.

Godard, B. G., Dumollard, R., Heisenberg, C.-P. and McDougall, A. (2021). Combined effect of cell geometry and polarity domains determines the orientation of unequal division. *Elife* **10**, e75639.

Gönczy, P., Pichler, S., Kirkham, M. and Hyman, A. A. (1999). Cytoplasmic dynein is required for distinct aspects of MTOC positioning, including centrosome separation, in the one cell stage Caenorhabditis elegans embryo. *J Cell Biol* **147**, 135–150.

Grill, S. W. and Hyman, A. A. (2005). Spindle positioning by cortical pulling forces. *Dev. Cell* **8**, 461–465.

Grill, S. W., Gönczy, P., Stelzer, E. H. and Hyman, A. A. (2001). Polarity controls forces governing asymmetric spindle positioning in the Caenorhabditis elegans embryo. *Nature* **409**, 630–633.

Grill, S. W., Howard, J., Schäffer, E., Stelzer, E. H. K. and Hyman, A. A. (2003). The distribution of active force generators controls mitotic spindle position. *Science* **301**, 518–521.

Hertwig, O. (1884). *Untersuchungen zur Morphologie und Physiologie der Zelle: Das Problem der Befruchtung und der Isotropie des Eies, eine Theorie der Vererbung*. Fischer.

Hewitson, L. and Schatten, G. (2002). The use of primates as models for assisted reproduction. *Reproductive BioMedicine Online* **5**, 50–55.

Ishihara, K., Nguyen, P. A., Groen, A. C., Field, C. M. and Mitchison, T. J. (2014). Microtubule nucleation remote from centrosomes may explain how asters span large cells. *Proc. Natl. Acad. Sci. U.S.A.* **111**, 17715–17722.

Keshri, R., Rajeevan, A. and Kotak, S. (2020). PP2A--B55γ counteracts Cdk1 and regulates proper spindle orientation through the cortical dynein adaptor NuMA. *J Cell Sci* **133**, jcs243857.

Khetan, N. and Athale, C. A. (2016). A Motor-Gradient and Clustering Model of the Centripetal Motility of MTOCs in Meiosis I of Mouse Oocytes. *PLoS Comput Biol* **12**, e1005102.

Khetan, N., Pruliere, G., Hebras, C., Chenevert, J. and Athale, C. A. (2021). Self-organized optimal packing of kinesin-5-driven microtubule asters scales with cell size. *J Cell Sci* **134**, jcs257543.

Kimura, K. and Kimura, A. (2011). A novel mechanism of microtubule length-dependent force to pull centrosomes toward the cell center. *Bioarchitecture* **1**, 74–79.

Kimura, A. and Onami, S. (2005). Computer simulations and image processing reveal length-dependent pulling force as the primary mechanism for C. elegans male pronuclear migration. *Dev Cell* **8**, 765–775.

Kiyomitsu, T. (2019). The cortical force-generating machinery: how cortical spindle-pulling forces are generated. *Curr Opin Cell Biol* **60**, 1–8.

Kotak, S. and Gönczy, P. (2013). Mechanisms of spindle positioning: cortical force generators in the limelight. *Curr. Opin. Cell Biol.* **25**, 741–748.

Kotak, S., Busso, C. and Gönczy, P. (2013). NuMA phosphorylation by CDK1 couples mitotic progression with cortical dynein function. *EMBO J* **32**, 2517–2529.

Laan, L., Pavin, N., Husson, J., Romet-Lemonne, G., van Duijn, M., López, M. P., Vale, R. D., Jülicher, F., Reck-Peterson, S. L. and Dogterom, M. (2012). Cortical dynein controls microtubule dynamics to generate pulling forces that position microtubule asters. *Cell* **148**, 502–514.

Lacroix, B., Letort, G., Pitayu, L., Sallé, J., Stefanutti, M., Maton, G., Ladouceur, A.-M., Canman, J. C., Maddox, P. S., Maddox, A. S., et al. (2018). Microtubule Dynamics Scale with Cell Size to Set Spindle Length and Assembly Timing. *Developmental Cell* **45**, 496-511.e6.

Letort, G., Nedelec, F., Blanchoin, L. and Théry, M. (2016). Centrosome centering and decentering by microtubule network rearrangement. *Mol Biol Cell* **27**, 2833–2843.

Levasseur, M. and McDougall, A. (2000). Sperm-induced calcium oscillations at fertilisation in ascidians are controlled by cyclin B1-dependent kinase activity. *Development* **127**, 631–641.

Levasseur, M., Carroll, M., Jones, K. T. and McDougall, A. (2007). A novel mechanism controls the Ca2+ oscillations triggered by activation of ascidian eggs and has an absolute requirement for Cdk1 activity. *Journal of Cell Science* **120**, 1763–1771.

Li, J. and Jiang, H. (2018). Regulating positioning and orientation of mitotic spindles via cell size and shape. *Phys Rev E* **97**, 012407.

Longoria, R. A. and Shubeita, G. T. (2013). Cargo transport by cytoplasmic Dynein can center embryonic centrosomes. *PLoS One* **8**, e67710.

McCarthy Campbell, E. K., Werts, A. D. and Goldstein, B. (2009). A cell cycle timer for asymmetric spindle positioning. *PLoS Biol.* **7**, e1000088.

McNally, K. L. P., Fabritius, A. S., Ellefson, M. L., Flynn, J. R., Milan, J. A. and McNally, F. J. (2012). Kinesin-1 prevents capture of the oocyte meiotic spindle by the sperm aster. *Dev Cell* **22**, 788–798.

Meaders, J. L. and Burgess, D. R. (2020). Microtubule-Based Mechanisms of Pronuclear Positioning. *Cells* **9**, E505.

Meaders, J. L., de Matos, S. N. and Burgess, D. R. (2020). A Pushing Mechanism for Microtubule Aster Positioning in a Large Cell Type. *Cell Rep* **33**, 108213.

Minc, N. and Piel, M. (2012). Predicting division plane position and orientation. *Trends Cell Biol.* **22**, 193–200.

Minc, N., Burgess, D. and Chang, F. (2011). Influence of cell geometry on division-plane positioning. *Cell* **144**, 414–426.

Mitchison, T. J. and Field, C. M. (2021). Self-Organization of Cellular Units. *Annu Rev Cell Dev Biol* **37**, 23–41.

Nédélec, F. J., Surrey, T., Maggs, A. C. and Leibler, S. (1997). Self-organization of microtubules and motors. *Nature* **389**, 305–308.

Ollion, J., Cochennec, J., Loll, F., Escudé, C. and Boudier, T. (2015). Analysis of nuclear organization with TANGO, software for high-throughput quantitative analysis of 3D fluorescence microscopy images. *Methods Mol Biol* **1228**, 203–222.

Palenzuela, H., Lacroix, B., Sallé, J., Minami, K., Shima, T., Jegou, A., Romet-Lemonne, G. and Minc, N. (2020). In Vitro Reconstitution of Dynein Force Exertion in a Bulk Viscous Medium. *Curr Biol* **30**, 4534-4540.e7.

Pelletier, J. F., Field, C. M., Fürthauer, S., Sonnett, M. and Mitchison, T. J. (2020). Co-movement of astral microtubules, organelles and F-actin by dynein and actomyosin forces in frog egg cytoplasm. *Elife* **9**,.

Petry, S., Groen, A. C., Ishihara, K., Mitchison, T. J. and Vale, R. D. (2013). Branching Microtubule Nucleation in Xenopus Egg Extracts Mediated by Augmin and TPX2. *Cell* **152**, 768–777.

Pietro, F. di, Echard, A. and Morin, X. (2016). Regulation of mitotic spindle orientation: an integrated view. *EMBO reports* **17**, 1106–1130.

Redemann, S., Pecreaux, J., Goehring, N. W., Khairy, K., Stelzer, E. H. K., Hyman, A. A. and Howard, J. (2010). Membrane invaginations reveal cortical sites that pull on mitotic spindles in one-cell C. elegans embryos. *PLoS ONE* **5**, e12301.

Reinsch, S. and Gönczy, P. (1998). Mechanisms of nuclear positioning. *J Cell Sci* **111 (Pt 16)**, 2283–2295.

Rodriguez-Garcia, R., Chesneau, L., Pastezeur, S., Roul, J., Tramier, M. and Pécréaux, J. (2018). The polarity-induced force imbalance in Caenorhabditis elegans embryos is caused by asymmetric binding rates of dynein to the cortex. *MBoC* **29**, 3093–3104.

Roegiers, F., McDougall, A. and Sardet, C. (1995). The sperm entry point defines the orientation of the calcium-induced contraction wave that directs the first phase of cytoplasmic reorganization in the ascidian egg. *Development* **121**, 3457–3466.

Rosenblatt, J., Cramer, L. P., Baum, B. and McGee, K. M. (2004). Myosin II-dependent cortical movement is required for centrosome separation and positioning during mitotic spindle assembly. *Cell* **117**, 361–372.

Rusan, N. M., Fagerstrom, C. J., Yvon, A. M. and Wadsworth, P. (2001). Cell cycle-dependent changes in microtubule dynamics in living cells expressing green fluorescent protein-alpha tubulin. *Mol Biol Cell* **12**, 971–980.

Sardet, C., McDougall, A., Yasuo, H., Chenevert, J., Pruliere, G., Dumollard, R., Hudson, C., Hebras, C., Le Nguyen, N. and Paix, A. (2011). Embryological methods in ascidians: the Villefranche-sur-Mer protocols. *Methods Mol. Biol.* **770**, 365–400.

Scheffler, K., Uraji, J., Jentoft, I., Cavazza, T., Mönnich, E., Mogessie, B. and Schuh, M. (2021). Two mechanisms drive pronuclear migration in mouse zygotes. *Nat Commun* **12**, 841.

Schindelin, J., Arganda-Carreras, I., Frise, E., Kaynig, V., Longair, M., Pietzsch, T., Preibisch, S., Rueden, C., Saalfeld, S., Schmid, B., et al. (2012). Fiji: an open-source platform for biological-image analysis. *Nat Methods* **9**, 676–682.

Simerly, C. R., Takahashi, D., Jacoby, E., Castro, C., Hartnett, C., Hewitson, L., Navara, C. and Schatten, G. (2019). Fertilization and Cleavage Axes Differ In Primates Conceived By Conventional (IVF) Versus Intracytoplasmic Sperm Injection (ICSI). *Sci Rep* **9**, 15282.

Strome, S. (1993). Determination of cleavage planes. *Cell* **72**, 3–6.

Sulerud, T., Sami, A. B., Li, G., Kloxin, A., Oakey, J. and Gatlin, J. (2020). Microtubule-dependent pushing forces contribute to long-distance aster movement and centration in Xenopus laevis egg extracts. *Mol Biol Cell* **31**, 2791–2802.

Tanimoto, H., Kimura, A. and Minc, N. (2016). Shape-motion relationships of centering microtubule asters. *J Cell Biol* **212**, 777–787.

Tinevez, J.-Y., Perry, N., Schindelin, J., Hoopes, G. M., Reynolds, G. D., Laplantine, E., Bednarek, S. Y., Shorte, S. L. and Eliceiri, K. W. (2017). TrackMate: An open and extensible platform for single-particle tracking. *Methods* **115**, 80–90.

Tran, P. T., Marsh, L., Doye, V., Inoué, S. and Chang, F. (2001). A mechanism for nuclear positioning in fission yeast based on microtubule pushing. *J Cell Biol* **153**, 397–411.

Wodarz, A. (2002). Establishing cell polarity in development. *Nat Cell Biol* **4**, E39-44.

Wühr, M., Dumont, S., Groen, A. C., Needleman, D. J. and Mitchison, T. J. (2009). How does a millimeter-sized cell find its center? *Cell Cycle* **8**, 1115–1121.

Wühr, M., Tan, E. S., Parker, S. K., Detrich, H. W. and Mitchison, T. J. (2010). A model for cleavage plane determination in early amphibian and fish embryos. *Curr. Biol.* **20**, 2040–2045.

Supplementary Figures and Table

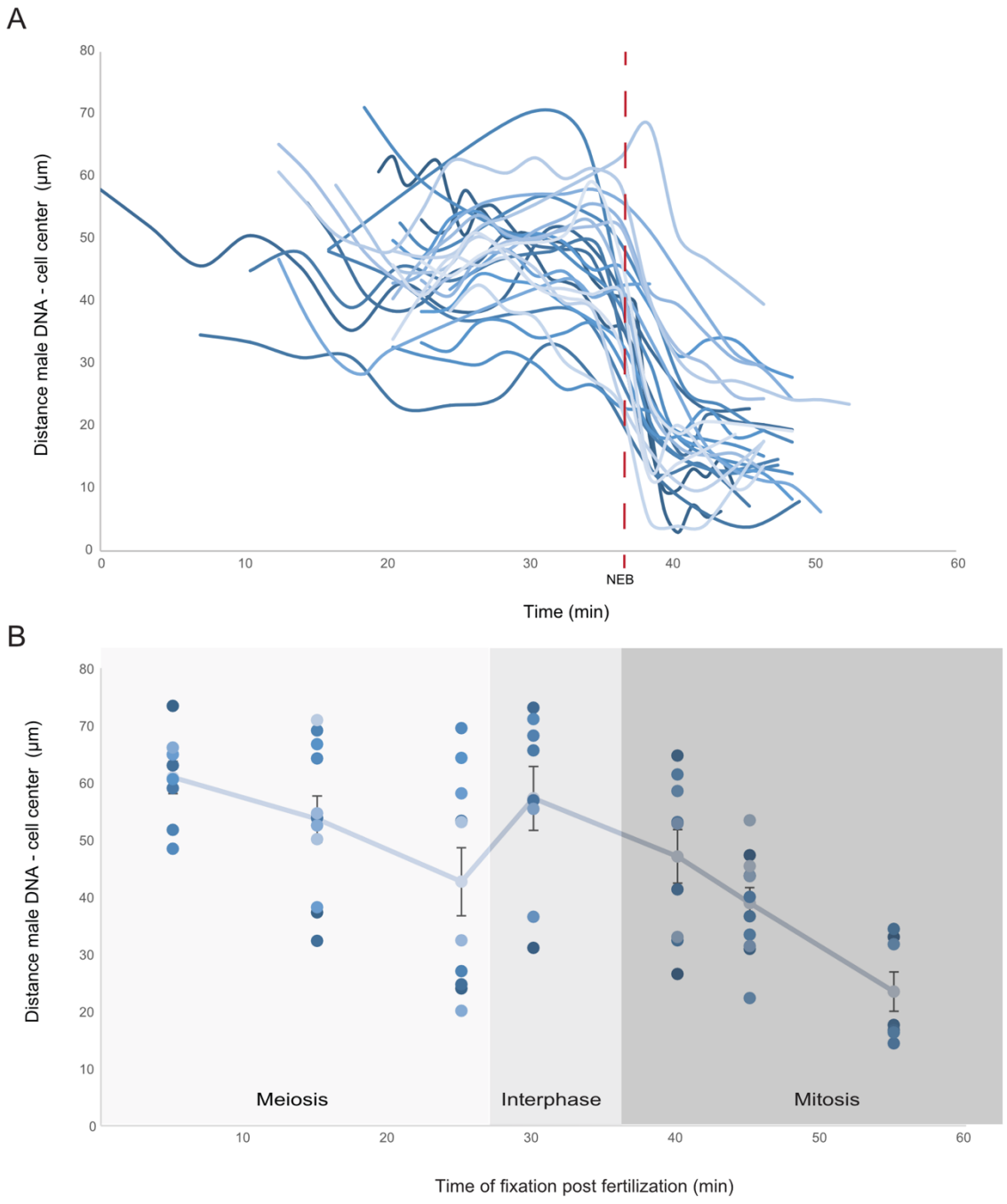

Supplementary Figure S1. Live and fixed data displaying sperm aster position following fertilization.

A. Graph of sperm aster position relative to the cell center as a function of time. All individual zygotes exploited in fig1 are displayed and aligned with respect to their time of NEB, indicated by a red dotted line.

B. Analysis of sperm aster position relative to the cell center in fixed zygotes.

Cell Cycle events	Control			p21-injected		
	min post fertilization	min after PN formation	n	min post fertilization	min after PN formation	n
PN formation	25 ± 2.8	0	22	34.9 ± 11.3	0	17
NEB	37.5 ± 4.2	12	23	65.8 ± 14.2	30	16
Cytokinesis	48 ± 4.5	23	24	65 ± 5.1	29	9
	min			min		
Time between PN formation & NEB	12.7 ± 2.6		20	26.9 ± 2		15
Time between NEB & Cytokinesis	10 ± 2		23	11.3 ± 1.8		9

Supplementary Table S1. Injection of p21 prolongs interphase

Analysis of the effect of p21 on the duration of cell cycle phases. Comparison between control and p21-injected zygotes for the duration between pronucleus formation to NEB and between NEB and cytokinesis. p21 significantly prolonged the duration of first interphase since the average duration from PN formation to NEB went from13 min to 28 min. n is displayed together with the SD.

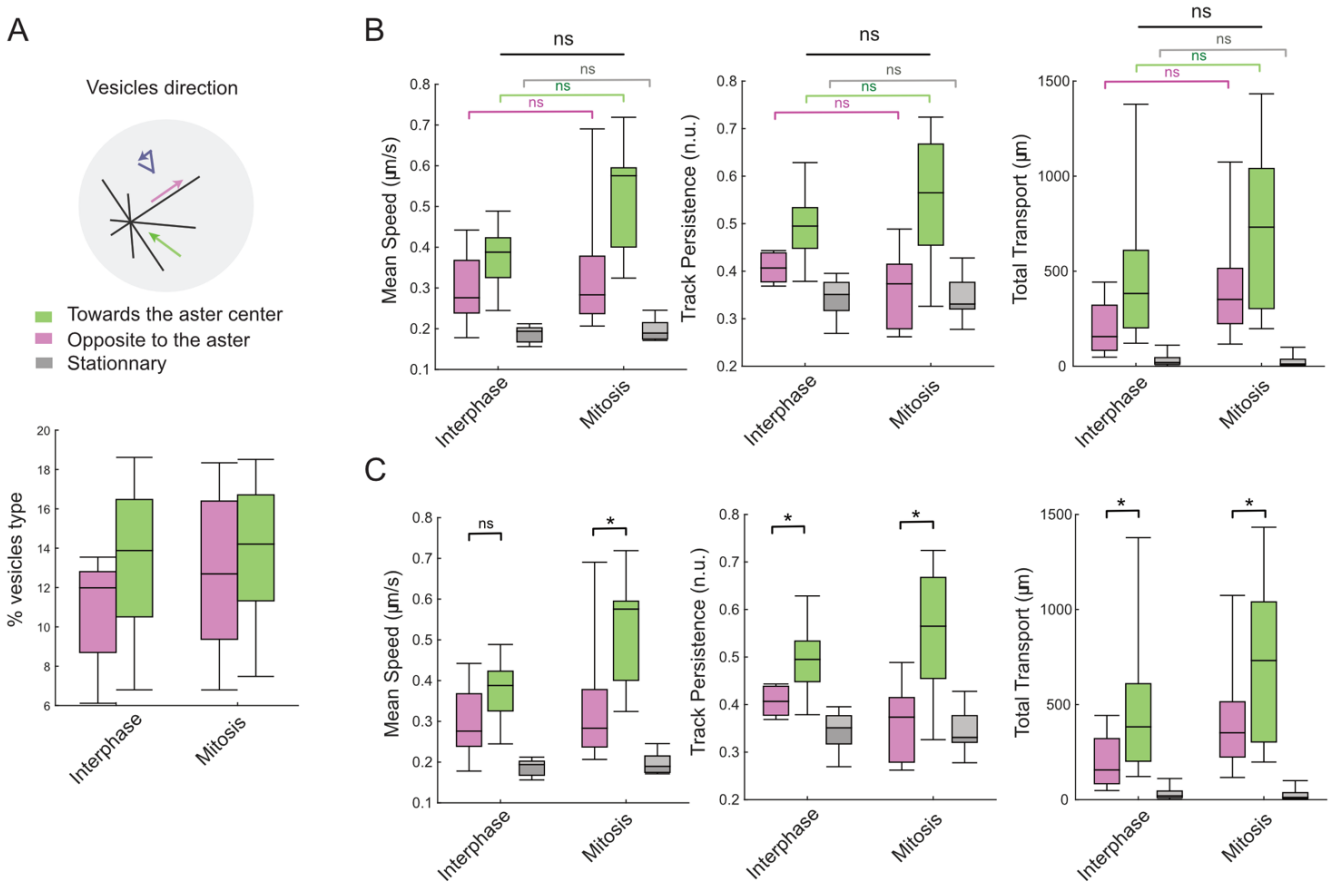

Supplementary Figure S2. Vesicle movement parameters

A. Schematic displaying vesicles either moving towards, away from the sperm aster center, or stationary. The graph below shows the mean percentage of each type of vesicle in interphase and in mitosis.

B. Statistical comparison of interphase versus mitosis for vesicle movement parameters: mean speed, track persistence, and total transport. Track persistence is the distance traveled towards the aster over the total trajectory of the vesicle. No significant difference was found. n=8 embryos, mean number of vesicles tracked per embryo = 1129 in interphase, 1734 in mitosis. Wilcoxon test.

C. Statistical comparison of vesicles moving towards or away from the aster center. From the same dataset as presented in B. Paired wilcoxon test.

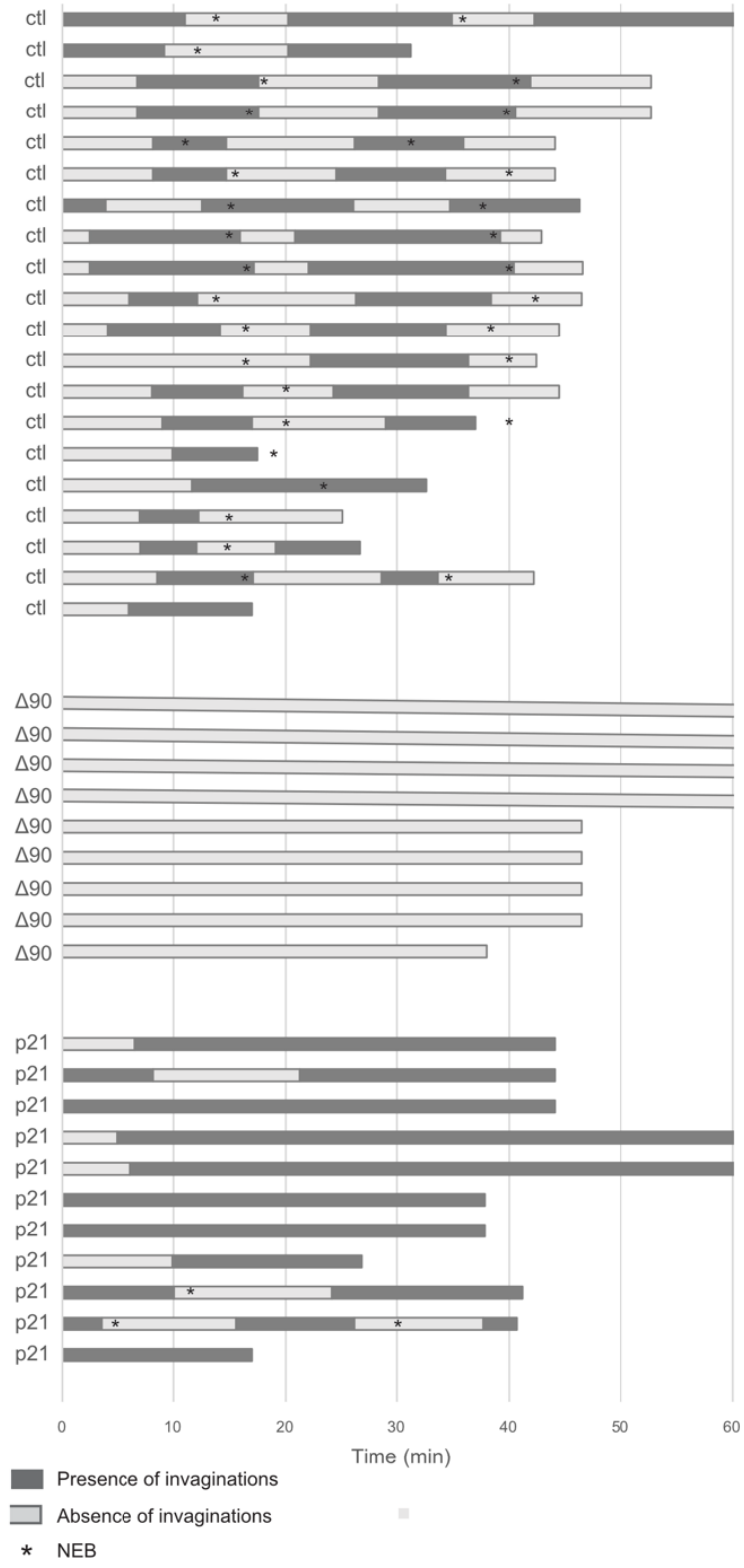

Supplementary Figure S3. p21 and D90 cyclin B to delay mitotic entry or block mitotic exit

Complied data displaying phases of apparitions of membrane invaginations as a function of time. Dark bars represent the presence of invaginations and light bars the absence of invaginations for control (control, n=20), D90 Cyclin B (n=9) and p21-injected cells (n=11). * represents time of NEB. Also see Movies 5A and 5B.

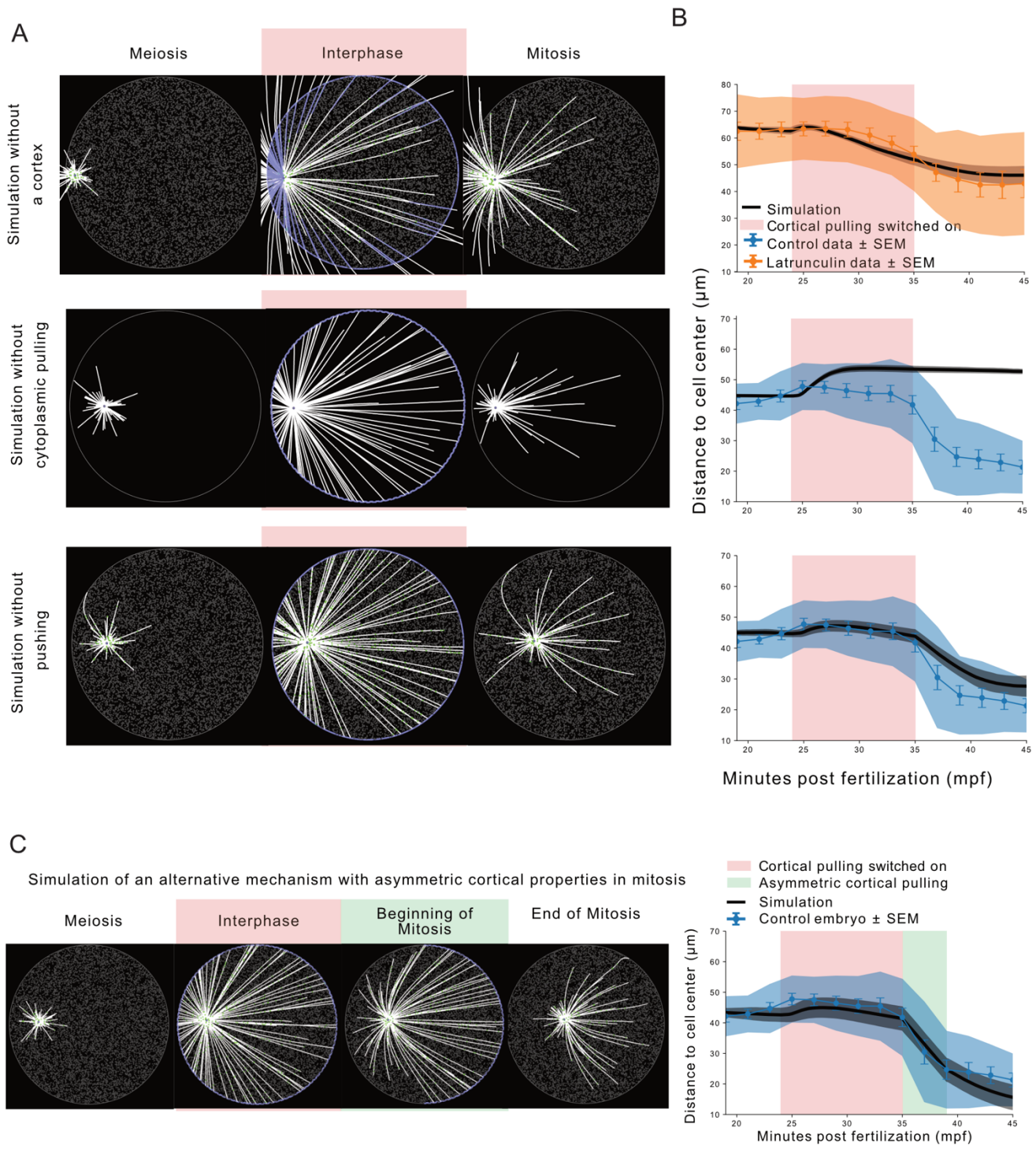

Supplementary Figure S4. Contribution of pushing and cytoplasmic pulling in aster centration

A.Stills from simulations testing the contribution of pushing and cytoplasmic pulling in the aster migration pattern. Like previously (Fig 7), the selected frames correspond to times of meiosis, interphase and mitosis in the simulation. The aster core (centrosome) is represented by a purple dot at the center of the MTs structure. MTs are in white, they are set to become more stable in interphase and when they touch the cortex. The purple cell border illustrates the activity of cortical dyneins, and thus an active cortical pulling. The many grey dots show the presence of cytoplasmic pulling in the cell since these dots are fixed dyneins. They become

green when attached to MTs. Three conditions were tested. To test the contribution of cytoplasmic pulling alone (first row), like we did experimentally by inhibiting the cell cortex (Figure 5), the pushing was removed by allowing MTs to ignore boundaries, and the cortical pulling was drastically reduced. Because MTs ignore boundaries, their plus-end is often located outside the cell at the interphase onset, so cortical dyneins were allowed to bind on all MTs, not only the plus-end. The counterpart is that they do not chew MTs anymore. The cortical motors were still allowed to bind MT but, as seen with the phenomenon of membrane invagination (Figure 4), they were pulled towards the MT rather than strongly attached to the cell boundary. The second row shows the inhibition of the cytoplasmic pulling, where the fixed cytoplasmic dyneins were removed. Finally, in the third row the inhibition of the cytoplasmic pulling was tested. However, since cortical dyneins only bind to the MTs plus-end, MTs could not be allowed to ignore the cell boundary, thus the inhibition of pulling was done by preventing the MT to have a grip on the cell boundary.
B. Comparison of the aster migration, as the distance of the aster from the cell center through time, in control data (blue curve), or with Latrunculin. Data (orange curve) and in the simulations (black curve). The blue, orange and grey shades represent +/- SD. The red margin represents the cortical pulling activity in the corresponding simulation. The graphics are aligned with A so that the simulation corresponding to the graphic appear on the same row.
C. Simulation exploring a mechanism of aster migration where at mitosis entry the cortical pulling is first turn off near the aster before to be completely inactivated. The associated migration (black curve) is compared to control data (blue). The green margin shows the moment of asymmetric cortical pulling.

Parameter	Value	Reference
General parameters		
Time step	0.01 s	
Cell Radius	70 µm	Average embryo radius
Temperature	18 ºC	To match experimental temp.
Viscosity	1 pN.s.µm^{-2}	(Lacroix et al,, 2018)
Centrosome		
Radius	0.5 µm	(Letort et al., 2016)
Number of MTs	100	(Letort et al., 2016)
MT anchoring stiffnesses	500, 500 pN/µm	(Letort et al., 2016)
Microtubules		
Bending stiffness	30 pN.µm^2	(Lacroix et al., 2018)
Minimal length	0.5 µm	
Maximal length	140 µm	
Polymerization speed	0.53 µm.s^{-1}	Approx .from unpublished data
Depolymerization speed	-0.53 µm.s^{-1}	
Growing force	5 pN	(Letort et al., 2016)
Catastrophe rates in meiosis and mitosis	0.12 s^{-1}, 0.48 s^{-1}	(Rusan et al., 2001), ratio between stalled and free (Letort et al., 2016)
Catastrophe rates in interphase	0.018 s^{-1}, 0.075 s^{-1}	
Rescue rate	0.064 s^{-1}	(Letort et al., 2016)
Cytoplasmic dyneins		
Unloaded speed	1.1 µm.s^{-1}	Approx. from instantaneous vesicle speed
Stall force	1.75 pN	(Khetan et al., 2021)
Attachment distance	0.02 µm	(Khetan et al., 2021)
Attachment rate	12 µm	(Khetan et al., 2021)
Detachment rate	1 s^{-1}	(Khetan et al., 2021)
Detachment force	1.75 pN	(Khetan et al., 2021)
Motor linker stiffness	100 pN/µm	(Khetan et al., 2021)
Membrane dyneins		
Unloaded speed	1.1 µm.s^{-1}	
Stall force	7 pN	4*cyto. dyneins
Attachment distance	0.02 µm	(Khetan et al., 2021)
Attachment rate	12 s^{-1}	(Khetan et al., 2021)
Detachment rate	0.01 s^{-1}	Approx. To match invagination lifetime (60s)
Detachment force	7 pN	4*cyto. dyneins
Motor linker stiffness (control)	100 pN/µm	(Khetan et al., 2021)
Motor linker stiffness (latrunculin)	0.222 pN/µm	To match latrunculin data

Supplementary Table S2. C*ytosim* parameters used in the simulations.
Related to Figure 7 and S5, parameters with corresponding references.
General units in Cytosim are seconds (s), micrometers (µm) and picoNewtons (pN).

Supplementary Movies

Movie 1. Confocal timelapse of aster formation and migration.

Confocal z-sections from a xyzt series showing microtubules in a live zygotes injected with Ens::3GFP. Scale bar is 50µm.

Movie 2. Female PN migration.

Confocal z-section from a timelapse series showing microtubule plus ends and associated brightfield showing female pronuclear migration. Microtubules are labelled with EB3::GFP.

Movie 3. Cell Mask Orange labelled vesicles accumulating at the sperm aster

A. Confocal timeseries with images collected every second in one z plane. The sperm aster is at the bottom and accumulates red fluorescence as vesicles become localized to the sperm aster. B. Confocal timeseries with images collected every second in one z plane. Here the zygote was compressed. The sperm aster is at the bottom and accumulates red fluorescence as vesicles become localized to the sperm aster. The female pronucleus in compressed zygotes formed karyomeres which can be seen migrating towards the sperm aster.

Movie 4. Cycling invaginations in the zygote

Zygote treated with latrunculin and labelled with Cell Mask Orange. No membrane invaginations are present during meiosis II. Membrane invaginations first become visible during interphase. The membrane invaginations are subsequently lost at mitotic entry. Scale bar = 50µm.

Movie 5. Membrane invagination during interphase in 2 cell stage embryo with one cell injected with either p21 or Δ90 Cyclin B.

A. Confocal timeseries of 2-cell embryo treated with latrunculin and labelled with Cell Mask Orange (rendered cyan). Membrane invaginations are present in the non-injected cell during interphase and are permanently present in the p21::GFP-injected cell (rendered magenta, right cell) during the prolonged interphase. Scale bar is 50µm.

B. Confocal timeseries of 2-cell embryo treated with latrunculin and labelled with Cell Mask Orange (rendered cyan). Membrane invaginations are present in the non-injected cell only during interphase, and not in Δ90 Cyclin B::GFP-injected cell (rendered magenta, cell on the right). Scale bar is 50µm.

Movie 6. MT pushing on plasma membrane in meiosis/interphase/mitosis.

Confocal timeseries of the outward membrane protrusions in the zygote. Microtubules are labelled with Ensconsin::3GFP, the plasma membrane is labelled with Cell Mask Orange and the zygote is treated with latrunculin.

Movie 7. Simulation of the aster migration

2D simulation of the aster migration from mid-meiosis to mitosis. The aster core (centrosome) is represented by a purple dot at the center of the MTs structure. MTs (in white), are set to become more stable in interphase and when they touch the cortex. The purple cell border illustrates the activity of cortical dyneins, and thus an active cortical pulling, also indicating interphase. The many grey dots represent fixed dyneins and thus the presence of cytoplasmic pulling in the cell. They become green when attached to MTs.

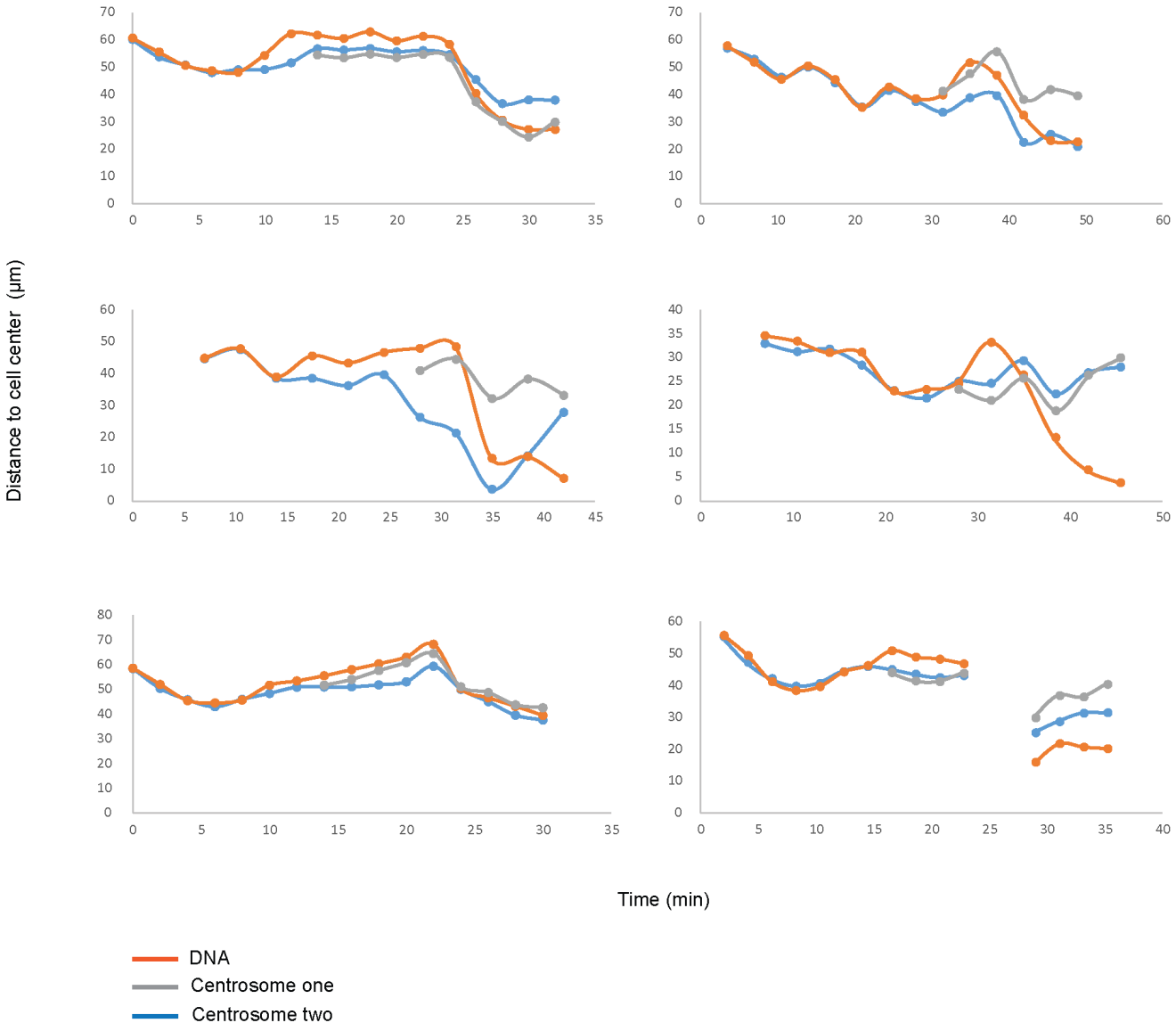

Figure 1.1: Comparison between centrosome and DNA as markers of aster migration.
Distance between centrosomes or DNA to cell center over time in 6 zygotes. Trajectories of the two centrosomes (approximated as centers of bright ensconsin foci) are shown in blue and grey, the trajectory of the DNA (H2B label) in orange. Time starts during meiosis, at the beginning of the microscopy acquisition and stops when the zygote started cytokinesis.

1.3 Additional information and troubleshooting

The work presented in the previous part was assembled in an article format, such as a reader could discover the aster migration in ascidian zygote and understand its mechanism through a direct storyline. In the following section, I will provide complementary data and detailed explanations on the quantification methods and specific drugs I chose to use. These data not only clarify the decisions taken in the article, but they also provide a better insight into the fine regulation of the aster migration mechanisms.

1.3.1 DNA position as a proxy for aster migration

The study of aster migration we performed is based on the measure of the distance from the aster to the cell center. This measurement was used to describe aster migration, and also to quantify phenotypes such as those induced by p21-injection or latrunculin treatment. The distance of the aster to the center was approximated by the distance from the male DNA to the cell center, whereas the centrosome is sometimes used to indicate aster position (Meaders et al., 2020). Several reasons account for the choice of DNA over the centrosomes: first and mainly, the two centrosomes separate before the end of the aster migration. The two centrosomes are indistinguishable, so to follow one centrosome forces a random choice and this could create variations if a centrosome is further from the cell center than the other. Then, the aim of the spindle centration is ultimately to center DNA, so each spindle pole, hence each centrosome, moves away from the cell center to surround the DNA, however the whole spindle centers. Therefore, the DNA best reflects spindle behavior. Finally, on a practical side, DNA and microtubule labels were used, as opposed to DNA and centrosome labels, because the DNA was useful to follow cell cycle stage, and MTs were necessary to understand the mechanism of aster movement. Also, the Ensconsin::3GFP label used for MTs was not adequate to locate precisely the centrosome because MTs are dense around the centrosome. Hence, the male PN and the chromosomes were chosen as a proxy for aster and spindle position. To illustrate the similarities and differences of the two measurements, I estimated centrosome position using ensconsin signal in 6 zygotes (Figure 1.1). On each graph the overall trajectories of DNA position and centrosome position are similar but when comparing different embryos, the movement of the DNA looked more reproducible.

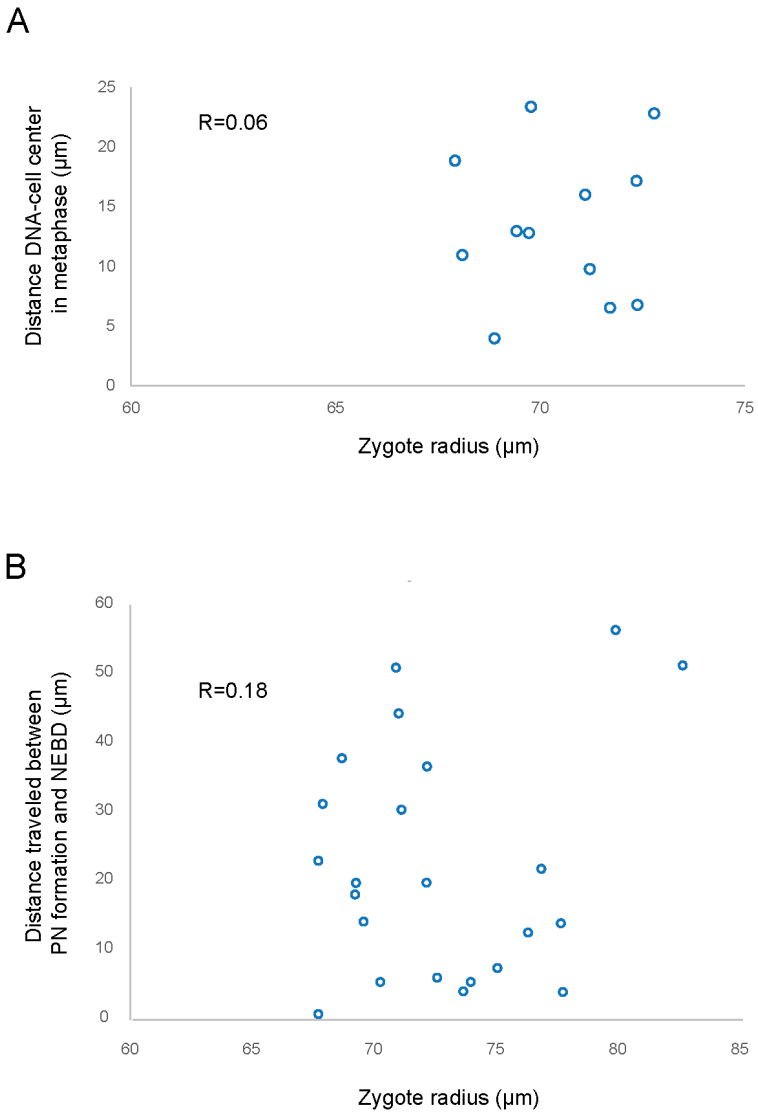

Figure 1.2: There is no correlation between cell size and the distance traveled by the aster
A- Distance DNA-cell center in metaphase as a function of the zygote radius (n=12). The distance in metaphase shows the position of the DNA after the aster migrated, and the zygote radius represents cell size. The aster is not closer to cell center in smaller zygotes B- Direct distance traveled between PN formation and NEB, as a function of the zygote radius (n=23). The distance traveled approximates the extent of aster migration, zygote radius represents cell size. The aster did not migrate more in bigger zygotes (n=23) Tests are Pearson correlations, R is included between 0 and 1, 0 indicate an absence of correlation, 1 a perfectly linear correlation.

1.3.2 Aster migration is independent of cell size

The quantification of the aster migration performed in the previous figure, as well as in the article section 1.2 (Figure 1.1, Figure 1) showed that the centration is rarely complete: in metaphase, the distance DNA-cell center was not of 0, but on average 14μm in live eggs ($\pm$6 sd, $\pm$2 sem, n= 15) (section 1.2, Figure 1 C). In fixed samples the minimum distance was reached at 55mpf and was on average 23μm ($\pm$9 sd, $\pm$3 sem, n= 7) (section 1.2, Figure S1 B). I hypothesized that in bigger zygotes the aster is further from cell center than it is in smaller zygotes, because it has more distance to travel from the membrane to the cell center. Thus, I checked whether there is a correlation between the radius of the zygote and the distance DNA-cell center in metaphase (Figure 1.2 A). The final position of the DNA did not correlate with the size of the zygote. I then investigated whether the direct distance traveled between PN formation and NEB was correlated to the radius of the zygote (Figure 1.2 B). Indeed, since the centration did not correlate with cell size, maybe the difference of size between zygotes is compensated by an increase in the distance traveled. No correlation was found between the zygote size and the distance traveled by the aster. These verifications tended to show that aster migration is independent of the zygote size, hence it was irrelevant to normalize the migration of the aster to the size of the cell.

1.3.3 Phenotypes of p21::Venus protein injection

Going further into the study of aster migration, I tested the correlation between the cell cycle and the migration. To do so, I perturbed the cell cycle using the p21 protein as a tool to delay the entry into mitosis (Figure 1.3, section 1.2, Figure 2 & 4). P21 inhibits cdk1/cycB that triggers mitosis (Levasseur et al., 2007). The success of the perturbation was assessed by the duration of interphase. Interphase is included in the period between PN formation and NEB, which lasted ~13 min in controls (section 1.2, Table S1). So only zygotes whose PN formation to NEB duration was twice the one in control (more than 24 minutes) were studied. The aster migration of all p21-injected zygotes that were quantified are displayed in Figure 1.3 A. On the graph when an individual curve stops, it is not necessarily because the interphase or the movie stopped, but sometimes because the nucleus became too big to mark a precise position, so

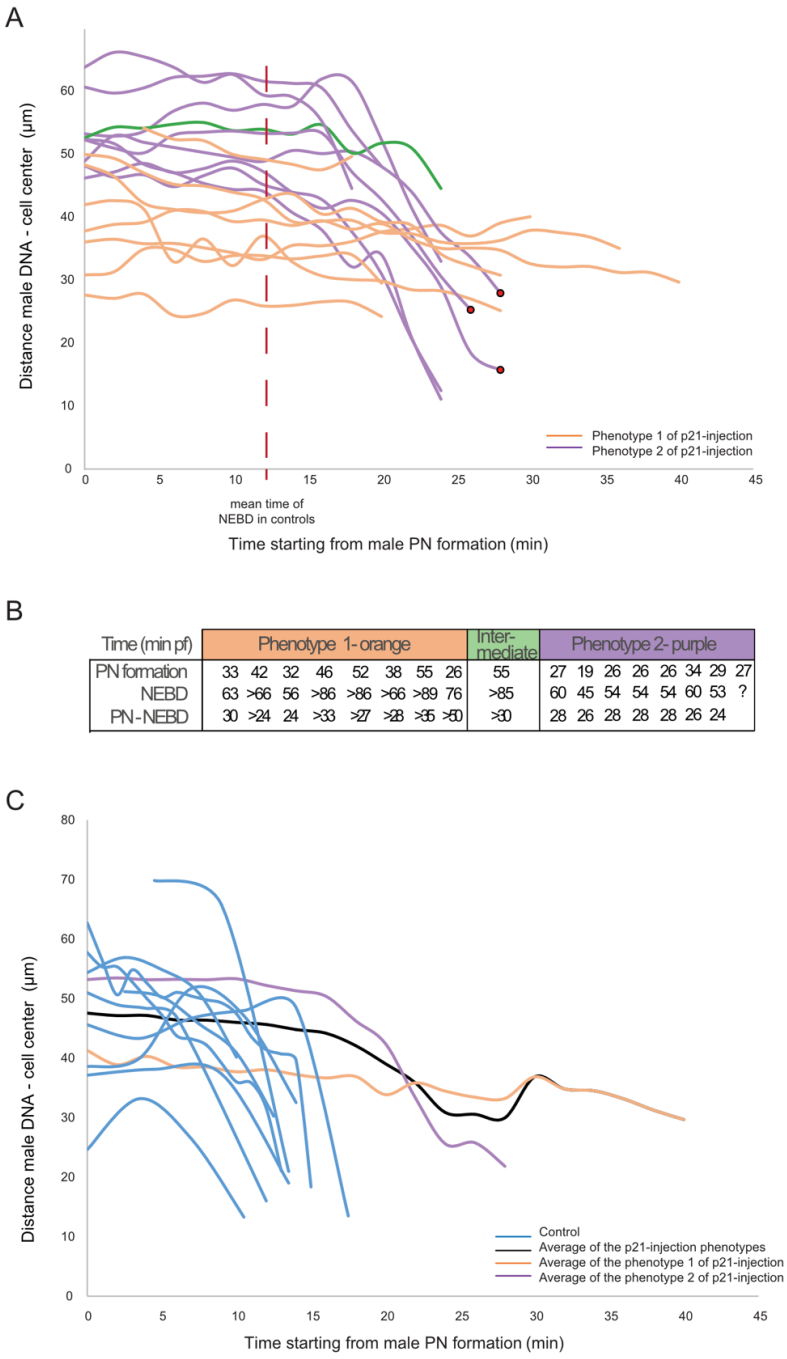

B

Time (min pf)	Phenotype 1- orange								Inter-mediate	Phenotype 2- purple							
PN formation	33	42	32	46	52	38	55	26	55	27	19	26	26	26	34	29	27
NEBD	63	>66	56	>86	>86	>66	>89	76	>85	60	45	54	54	54	60	53	?
PN-NEBD	30	>24	24	>33	>27	>28	>35	>50	>30	28	26	28	28	28	26	24	

Figure 1.3: Aster migration in p21-injected zygotes

Distance from male DNA to cell-center over time, in p21 injected zygotes. Curves are aligned on the time of PN formation (time 0) A- Aster migration was quantified in 17 injected zygotes. 8 asters showed no migration (orange curves), 8 migrated (purple curves), 1 has an intermediate phenotype (green curve). For purple curves, migration occurred mostly after the time when control embryos would have undergone NEB (red dotted line). NEB is represented on the curves as a red dot when it occurred during acquisition. B- Table of the timing of key cell cycle events (PN formation and NEBD) in each embryo sorted by their type of migration. C- The two types of migration are averaged separately with the same color code as in (A), and the average aster migration of all p21-injected zygotes is shown in black. Curves of aster migration in control embryos are shown for reference in blue. Whatever the type of aster migration in the p21-injected zygotes, the delay of entry in mitosis provoked a delay in aster migration.

to continue the measurement further in time would create great imprecision. In the article, only the 12 first minutes of the PN formation to NEB period were used to establish a comparison with control zygotes. Also, in the first 10 to 15 minutes of this period all the p21-injected zygotes behaved the same way. However, when looking at the aster migration on a longer timescale, that is, until the PN migration could not be followed anymore or the film ended, I observed that there were two distinguishable phenotypes. One, drawn in orange showed no change of DNA position through time, and no NEB. The other phenotype, drawn in purple, showed eventual DNA centration that may be related to the delayed entry into mitosis, however only three embryos out of the nine in purple entered mitosis during migration (time of NEB of each zygote was marked on the graph with a red dot). Difference in cell cycle timing were indeed found between the two phenotypes (Figure 1.3 B). In 7/8 zygotes where no aster migration was visible (orange), the PN formation occurred after more than 30 mpf, and NEB occurred more than 60mpf. In zygotes that showed an aster migration, PN formation occurred before 30mpf in 7/8 cases and NEB at or before 60mpf. A hypothesis to explain the difference of phenotypes is that the variability of injection created strong and weak inhibition, the embryo strongly inhibited (orange curves) went through a longer meiosis, maybe allowing some centration before PN formation, hence the smaller distance to the center at PN formation (Figure 1.3 A). And they also go through longer interphase since NEB happened after more than 30min after PN formation in 4/8 cases compared to 0/8 in embryos showing the other phenotype. During these long interphases, the aster often slowly disassembled. In zygotes with a weak inhibition, NEB happens within 30min after PN formation, testifying that CDK1/CycB did increase in the cell, but the aster migration occurred within 15 min before NEB. In addition to support the main result of the p21 experiment, that is, entry into mitosis is necessary for aster migration, this second phenotype may hint that there is a threshold in CDK1/CycB concentration where the aster can migrate.

Control data for the p21 injection experiment were xyt films in bright field that followed the timing of development of uninjected zygotes from the same batch of oocytes. These control embryos allowed me to define the criterion for a successful cell cycle perturbation, but the aster migration quantification could not be done on this type of 2D dataset. Therefore, I used the quantification and data from the aster migration description (section 1.2, Figure 1) to compare the migration in zygotes with an extended interphase and zygotes with a regular cell cycle

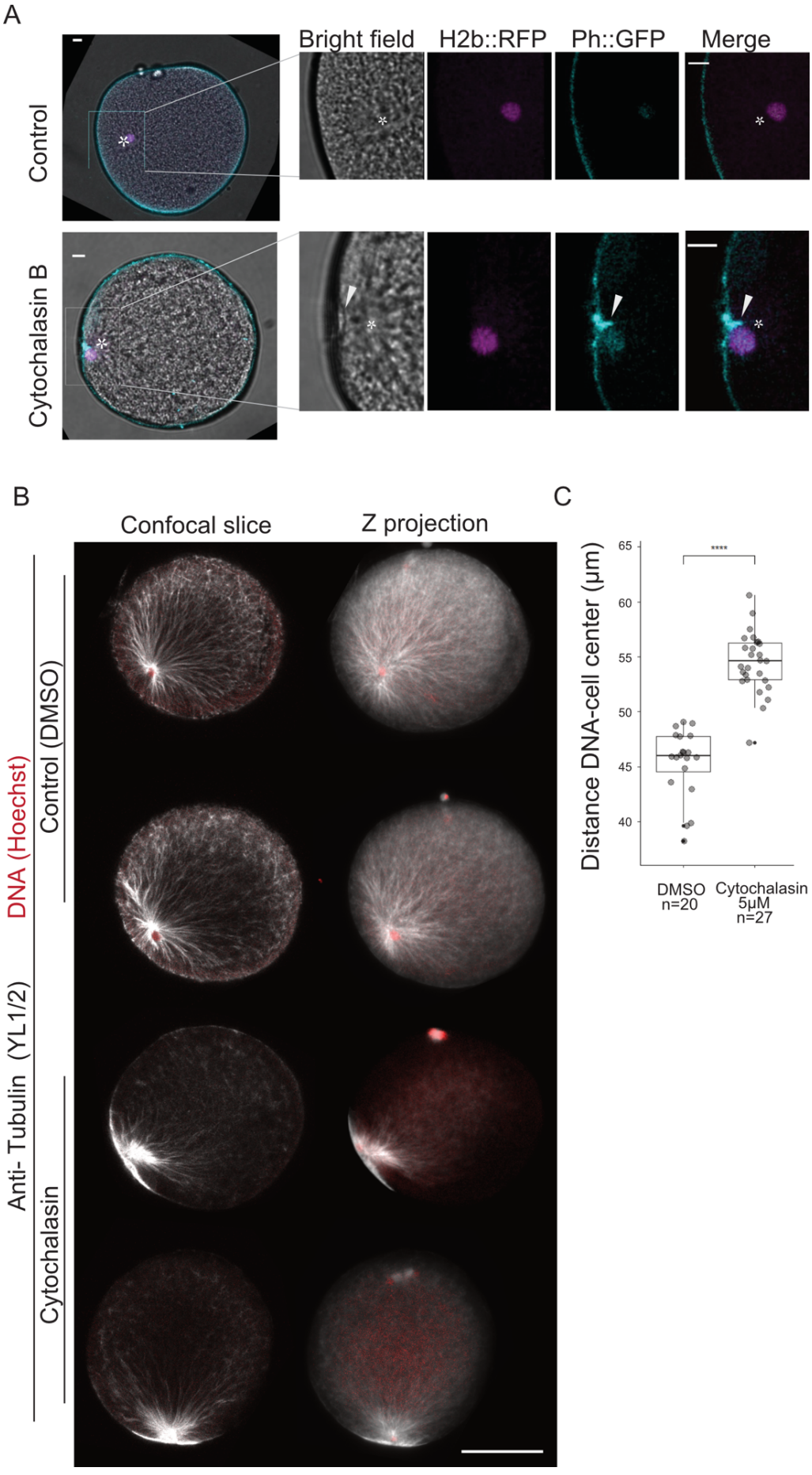
A
Bright field
H2b::RFP
Ph::GFP
Merge
Control
Cytochalasin B
B
Confocal slice
Z projection
DNA (Hoechst)
Anti- Tubulin (YL1/2)
Control (DMSO)
Cytochalasin
C
Distance DNA-cell center (µm)
****
65
60
55
50
45
40
DMSO
n=20
Cytochalasin
5µM
n=27

←

Figure 1.4: Aster position after treatment with Cytochalasin B to perturb the actin cortex
A-Confocal images representative of zygotes injected with mRNA encoding the membrane marker PH::GFP (blue in the figure) and the histone marker H2B::RFP (magenta), and treated with either DMSO for controls or with cytochalasin B to inhibit actin. Scale bar is 10µm. White stars indicate the aster center B- Confocal images and associated z-projections of zygotes treated for 20 min in DMSO or cytochalasin, then fixed and immuno-stained for microtubules (white in the figure) and labeled with Hoechst (red). Scale bar is 50µm. C- Quantification of aster position at 20mpf, in zygotes treated as described in (B). Wilcoxon test

(Figure 1.3 C). The orange and purple curves represented the average of each behavior described earlier (Figure 1.3 A), the black curve is the average of all the p21-injected embryos, and the blue curves represent controls. In the phenotype marked in purple, it appeared that aster migration was of the same extent as the controls. The difference in migration profile, with a slope less steep in p21-injected embryos, suggested that the mechanism of migration used for the p21 zygotes was different from that used in control embryos.

Taken together, the details of the p21-injection experiment suggest that there may be a threshold of CDK1/CycB concentration above which aster migration is possible. Depending on this concentration the cell may use different mechanism to center its aster. The CDK1/CycB complex is involved in numerous pathways that can notably affect MTs dynamics and actomyosin contractility so the question of the mechanisms at work in function of the CDK1/CycB concentration is still open. Given the slow slope of the migration of the p21 purple curve, the simplest hypothesis is that a small concentration of CDK1/ CycB switched off the cortical pulling and allowed a migration by cytoplasmic pulling.

1.3.4 The effects of actin inhibition on aster migration

Once we found that aster migration is correlated and triggered by the cell cycle, the next step was to investigate the mechanisms that drives the migration. There are three main MT-dependent forces: cytoplasmic pulling (also called bulk pulling), cortical pulling, and the pushing mechanism. Two of them, cortical pulling and pushing, require an intact actin cortex to be effective, and they are therefore affected by actin inhibition. To perturb the F-actin, latrunculin or cytochalasin drugs are commonly used, which both prevent actin filament polymerization (Wakatsuki et al., 2001).

The first aim of the F-actin perturbation was to reveal the presence of sites of cortical pulling by observing the formation of membrane invaginations (section 1.2, Figure 4). I treated

zygotes with 5μM cytochalasin B just after fertilization and saw one wide invagination emerging from the membrane just behind the aster (Figure 1.4 A). It also seemed that in cytochalasin the aster was closer to the membrane than in control embryos.

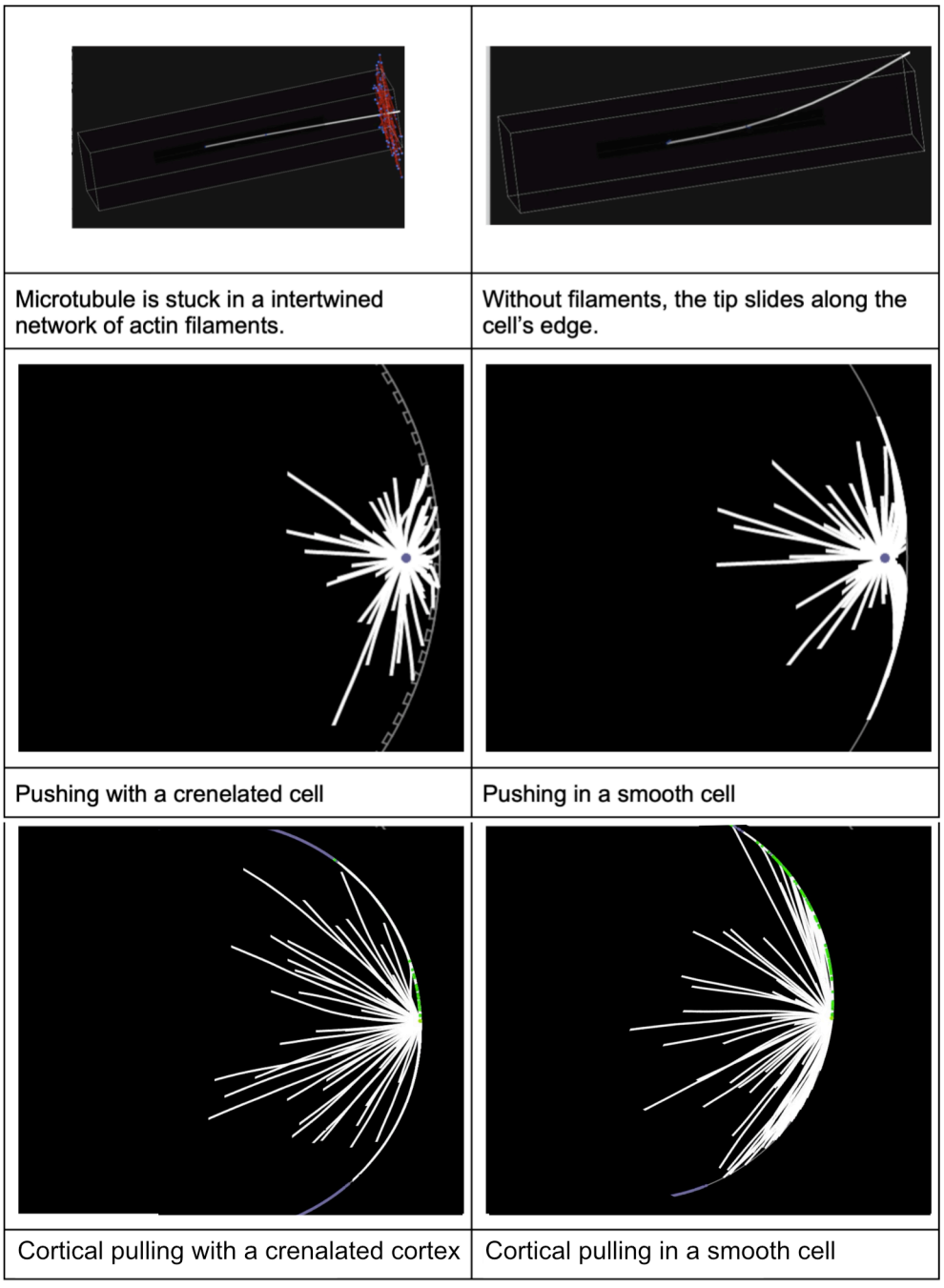

Figure 1.5: Simulation of the actin cortex outputs the cytochalasin phenotype
Stills from *Cytosim* simulation where the actin cortex was simulated with a serrated cortex added below the membrane to recreate the roughness of the actin cortex (left panels). Or without cortex, only a stiff membrane (right panel). First row shows a 3D simulation of an individual MT interacting with cell edges in absence or presence of an actin cortex. Second row shows 2D simulations of the aster pushing on the cortex. Third row shows 2D simulations of the aster pulled by the cortex.

To test if this difference starts in meiosis or begins in first interphase, I fertilized a batch of oocytes and treated them with 5μM cytochalasin. 20 minutes into treatment I fixed the batch of zygotes and labeled the microtubules by immunofluorescence. This allowed me to work on a larger scale to quantify the possible lack of aster migration. The control zygotes were at the end of meiosis II, with asters that started to take the shape they hold in interphase: the microtubules were spread in the zygote and the DNA was close to, but not directly against, the membrane (Figure1.4 A). In zygotes treated with cytochalasin, the asters did not migrate, the DNA was against the cortex. The microtubules that were towards the cell cytoplasm spread and extended similarly as in controls, but the thickness of the microtubule label on the membrane suggested that the many microtubules that were on the membrane side spread against it. This first experiment showed a difference of aster position in the two conditions at the end of meiosis II (20mpf); the aster is further from cell center in cytochalasin than it is DMSO-treated zygotes (Figure 1.4 B). This was not due to a change in cell size since cytochalasin did not affect the cell diameter (data not shown). This result was consistent with the quantification of live imaging movies of zygotes in latrunculin B (Figure 1.6, section1.2, Figure 5).

Simulations were used to test at once pushing, cortical pulling and cytoplasmic pulling mechanisms. To model an efficient pushing mechanism, a serrated circle was added as a layer below the membrane (Figure1.5 second row). Without this cortex, *Cytosim* simulation reproduced the phenotype of microtubules spreading on the cortex (Figure 1.5). On the one hand, MTs could not push on a smooth edge, thus they were gliding along the cortex (Figure1.5 first row), this caused a MT enrichment on the cell edge. (Figure1.5 second row). On the other hand, cortical pulling without cortex also lead to an increase of MT on the cell edge (Figure1.5 third row). Indeed, cortical pulling was represented by motors able to bind MTs, and attached to the membrane (which is rendered rigid in Cytosim). In simulation without cortex, instead of just capturing the tip of MTs, motors could also capture the length of MTs sliding along the membrane, therefore leading to an increase of MTs on the cell edge (Figure 1.5 third row). In brief, the absence of serrated cortex leads to MTs sliding on the membrane, hence to an increase of MTs density on the membrane. This resembles the cytochalasin phenotypes (Figure 1.4). The roughness of the serrated circle stopped the sliding of microtubules (Figure 1.5), so the lengths of the microtubules were not automatically caught by the motors bound to the membrane, and pushing was efficient, and hence the density of microtubules spread along the cortex decreased (Figure 1.5). The process of creation of the simulation led me to distinguish

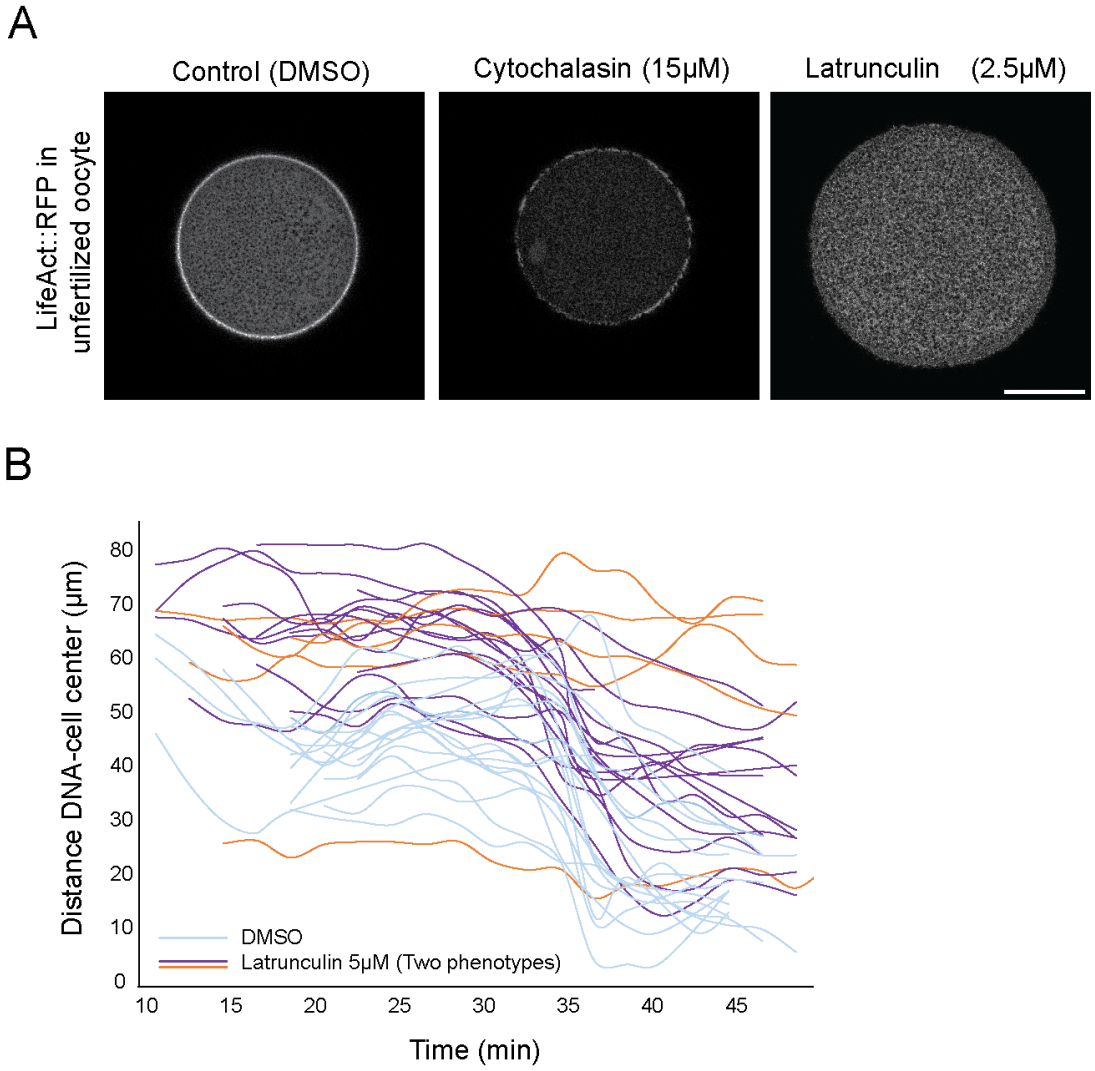

Figure 1.6: Aster position after treatment in Latrunculin to inhibit actin cortex
A-Confocal images of oocytes injected with LifeAct::RFP protein that labels actin, when treated with DMSO, 15µM cytochalasin B or 2.5 µM Latrunculin. Scale bar is 50 µm. (B) Distance from male DNA to cell-center over time, in zygotes that developed in latrunculin (purple and orange curves) or in DMSO (blue curve). Curves are aligned with respect to the time of NEB (37min). Out of the 19 zygotes treated with latrunculin, 5 showed no aster migration (orange curves), 14 migrated (purple curves).

several functions of the cortex: it provides rigidity to the membrane, and it may prevent the sliding of microtubules through its organization. This raised the question of the quality of the actin inhibition, by revealing that the actin cortex inhibition may be partial, and more precisely, that a medium of 5μM cytochalasin may perturb the proper actomyosin organization, but not its rigidity. A partial inhibition of the actomyosin cortex in cytochalasin would also explain why the invagination experiment performed in cytochalasin showed one small invagination (Figure 1.4 A) compared to the many drastic invaginations observed in latrunculin (section 1.2, Figure 4).

To overcome the potential partial perturbation of the actin cortex, I started using latrunculin B instead of cytochalasin B since latrunculin toxins are known to be more powerful (Wakatsuki et al., 2001). The drastic effect of latrunculin was confirmed by testing the drugs on oocytes injected with the protein LifeAct::RFP that labels actin (Figure 1.6 A). In controls, the actin label was homogenous and cortical. In presence of cytochalasin, it was punctated on the cortex, whereas in latrunculin the label was absent from the cortex and distributed in the cytoplasm. Hence the inhibition of the actin cortex was less pronounced in cytochalasin than in latrunculin. This observation had been previously reported on 16 cell-stage *Phallusia* embryos fixed in formaldehyde and stained with phalloidin (Patalano et al, 2006).

The aster migration in zygotes treated with 1μM latrunculin was quantified from xyzt imaging, and all curves were aligned with respect to their time of NEB (Figure 1.6 B). In latrunculin, the aster was further from the cell center than it was in control condition, and this difference was globally maintained through the whole migration. This result supported the quantification of the samples fixed after a cytochalasin treatment that showed that the difference in aster position starts in meiosis. However, like the p21 experiment, the latrunculin experiment brought a problem of dual phenotypes. In absence of actin, most asters migrated (purple curves), and even seemed to start migration earlier than in controls. A minority of asters did not migrate (orange curve) (Figure 1.6 B). A candidate parameter that could create various phenotypes is the time of drug addition. Indeed, one could imagine that inhibiting the actin before the aster had time to be pushed away from the membrane in meiosis gives a different outcome than inhibiting the actin after the aster was pushed away. In latrunculin live experiments, I aimed at adding the drug 10 min post fertilization. Because *P. mammillata* oocytes fertilization is not exactly synchronous, there was a window of several minutes around the time of drug addition.

To sum up, the use of cytochalasin gave interesting results with the apparition of only one main invagination, and a phenotype of MTs sliding on the membrane. This phenotype may result from a partial perturbation of the actin cortex which would still provide membrane

stiffness, but no roughness to prevent MTs sliding. Other origins are also contemplated as the simulation may gave a pertinent output but not necessarily for the right biological reasons. The uncertainty surrounding this phenotype lead me to use latrunculin, which has a more drastic effect, to pursue the study. Using latrunculin, the sliding MTs phenotype seemed reduced but there were variations in aster migration behavior: either it migrated, or it did not. I suspect that to harmonize the phenotypes, the time of drug addition requires higher precision than the one obtained using the protocols I established for actin perturbation. Finally, we should note the possibility that the quality of each batch of gametes may influence the phenotypes of aster migration in absence of an actin cortex.

1.3.5 Conclusion

The details and troubleshooting of the experiments clarified the decision taken at each step of the study presented in the main section of this chapter (section 1.2). In brief, the choices made were the following; I chose to use the DNA position to follow the aster migration, I checked that aster migration was independent of cell size, I focused on the first minutes of the aster migration in p-21 injected zygotes, and finally I chose to use latrunculin over cytochalasin to inhibit the actin cortex and perturb aster migration. In addition, to provide more explanations on these choices, each analysis brought new hypothesis and insights into the mechanism of aster migration. Among these hypotheses, the actin cortex partial perturbation, that may uncouple its properties of stiffness and roughness *in vivo*, seems especially interesting. First it is interesting because it would give an in-depth understanding of the mechanical actin-MT interactions at the cortex, which starts to be addressed *in vitro* (S. Yamamoto et al., 2022). And second, such an uncoupling of rigidity and roughness, if mastered, could be used as a tool in many fields as the actin cortex is quite universal and impacts cell and tissue tension, cytokinesis, movement of protein below the membrane, etc. Another interesting idea emerged from the study of phenotypes from p-21 injected zygotes; different migration mechanism could be involved depending on the CDK1/CycB concentration in the cell.

1.4 A concomitant mitotic contraction wave?

Actomyosin networks are major actors in the process of aster, nucleus, or spindle positioning. For instance, during oocyte maturation in the mouse an actin cloud surrounds the meiotic spindle and brings the spindle to the cortex in a myosin-dependant process (Bezanilla & Wadsworth, 2009b; Schuh & Ellenberg, 2008), and in the plant *Arabidopsis* the male PN is transported by an aster-like F-actin structure (Kawashima et al., 2014). Actin also plays a role in the positioning mechanisms in a less direct manner: it can create a space for the spindle through the movement of organelles by polymerisation of actin comets (Shamipour et al., 2019). Finally, actin also provides a circumferential scaffold, the actomyosin cortex, for MT traction or pushing force balance (Laan et al., 2012; S. Yamamoto et al., 2022).

The relevance of the actin cortex in *P. mammillata* spindle centration was demonstrated by inhibiting actin polymerisation in the zygote (section 1.2, Figure 5). I found that aster migration in the absence of F-actin was possible by cytoplasmic pulling. However, aster migration did not exhibit its usual pattern. Indeed, migration appeared more gradual and lacked the characteristic jump observed at mitosis entry. While imaging zygotes throughout the first cell cycle, one could notice changes in cell shape at several moments. First a well-characterized actomyosin contraction initiated by the sperm-triggered calcium wave takes place at fertilization (McDougall & Sardet, 1995; Sardet et al., 1989; Sawada & Osanai, 1981) to form the "contraction pole" that quickly resorbs. Then the embryo seems to flatten in interphase to finally deform briefly around the time of mitosis entry. Cell contraction creates intracellular flows and dynamics that can influence cytoplasmic organization (Longhini & Glotzer, 2022; Prodon et al., 2008). Although the fertilization-induced contraction wave has been characterized, the change in shape observed around the time of NEB has not been previously described and could indicate the presence of an actomyosin contraction wave and associated flows. Because of the timing of this phenomenon which seems to fit with the beginning of the spindle migration, such a contraction could affect or maybe trigger the spindle centration. Thus, further investigation was necessary to refine our understanding of the mitotic apparatus migration. In this section I will present the preliminary data obtained on this matter.

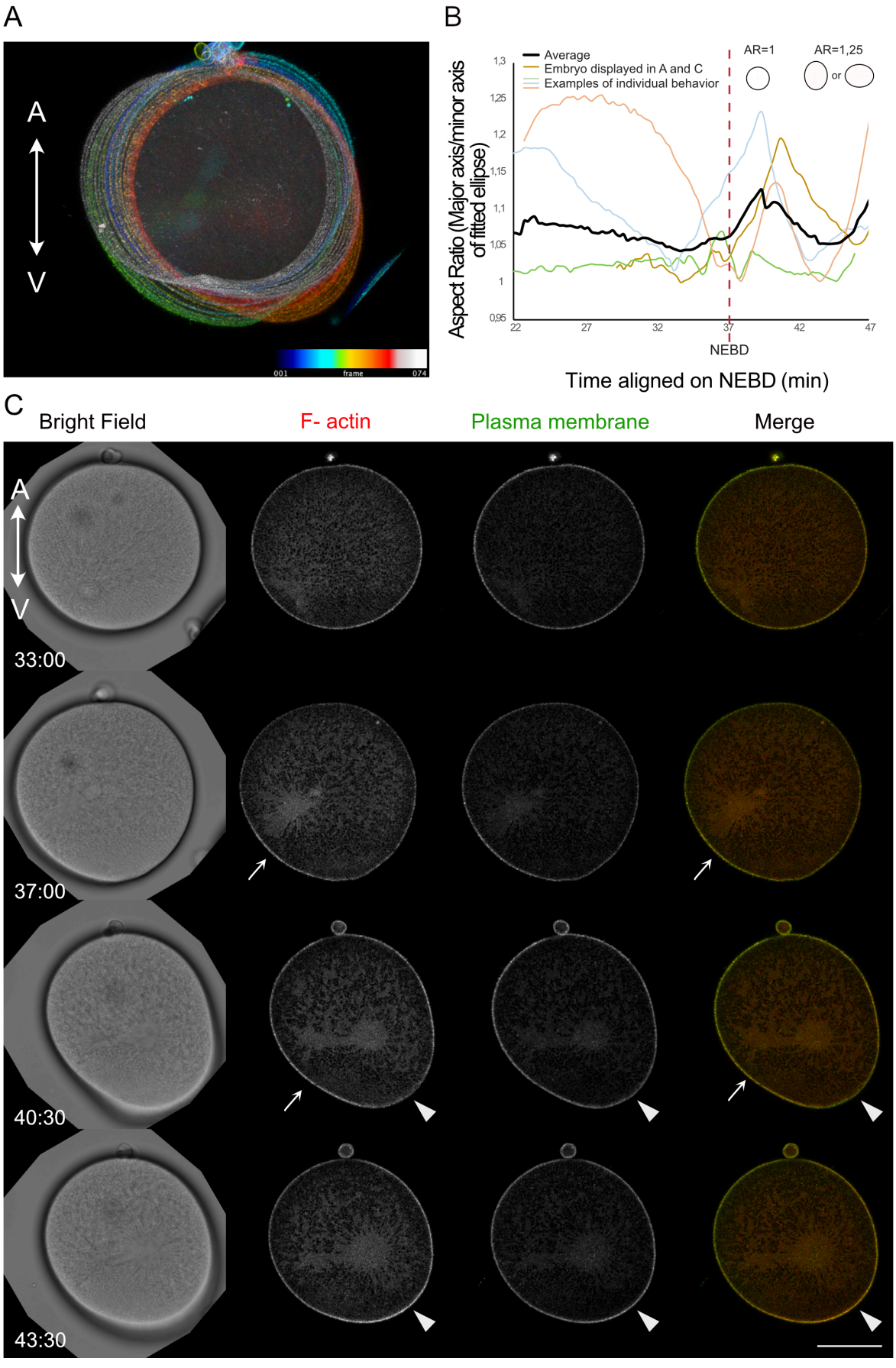
A
A
V
001
frame
074
B
Average
Embryo displayed in A and C
Examples of individual behavior
AR=1
AR=1,25
or
Aspect Ratio (Major axis/minor axis of fitted ellipse)
1,3
1,25
1,2
1,15
1,1
1,05
1
0,95
22
27
32
37
42
47
NEBD
Time aligned on NEBD (min)
C
Bright Field
F- actin
Plasma membrane
Merge
A
V
33:00
37:00
40:30
43:30

←

Figure 1.7: The zygote deforms during mitosis

Zygote is oriented with the animal pole on the top. A-Time projection of membrane label of one zygote, from interphase to cytokinesis. Time scale is color coded; the first movie frame is dark blue and the last frame is in white. B- Aspect ratio (AR) of the 2D ellipse that best fit the zygote shape as a function of time. Curves are aligned with respect to the time of NEB (dotted line). The average AR of 14 zygotes is represented in black. Colored curves represent the AR of individual zygotes including in brown the curve of the zygote presented in A and C. C- Selected movie frames showing the shape changes of a zygote in BF (first column). The zygote was injected with LifeAct to label the F-actin (second column, in red on the merge), and treated with Cell Mask deep red to label the plasma membrane (third column, green on the merge). The merge of F-actin and membrane label is presented in the fourth column. White arrows indicate an area with intense signal, white arrowheads indicate a dynamic area with a loss and recovery of F-actin and maybe of membrane signal. Scale bar is 50 µm.

1.4.1 The zygote deforms at the vegetal pole at the beginning of mitosis. The deformation could be correlated to a local actin loss.

Before the characterization of a potential contraction wave, the first step was to confirm the observation of a change of shape in ascidian zygotes around the time of NEB. To monitor cell shape changes during the first cell cycle, the zygote contour was labeled with a plasma membrane dye (cell-mask deep red), and the embryo was imaged every 15s. In parallel, the presence of F-actin was also monitored because in many cases shape changes involve the actomyosin network. To this purpose, the eggs were injected with LifeAct::RFP fusion protein before fertilization. By superimposing membrane label images of one zygote, we get a first idea of the shape progression in time (Figure1.7 A). The images superimposed are extracted from a movie starting at the beginning of interphase, and ending at the beginning of cytokinesis. At the beginning of interphase the zygote seems fairly round (blue shape). Then when the embryo transitions to mitosis (midway through the green), the embryo starts to extend in the vegetal hemisphere and shows a slightly oblong shape. Consecutively, a more drastic extension is visible in red. Finally, the vegetal extension regresses and the embryo flattens to proceed with cytokinesis that bisects the zygote along the animal-vegetal axis. To understand more precisely when the deformation starts with respect to the entry into mitosis, which occurs about 3min before NEB, I approximated the zygote shape around NEB time in 14 embryos, and tested whether there is a recurrent pattern of shape change (Figure 1.7 B, Figure Annex 3). The shape approximation was done by finding the ellipse that fitted best the 2D embryo shape at each time frame. The axes of the ellipse were extracted as minor and major axes; the ratio of the major axis over the minor axis gave an aspect ratio (AR) that approaches 1 when the zygote shape is

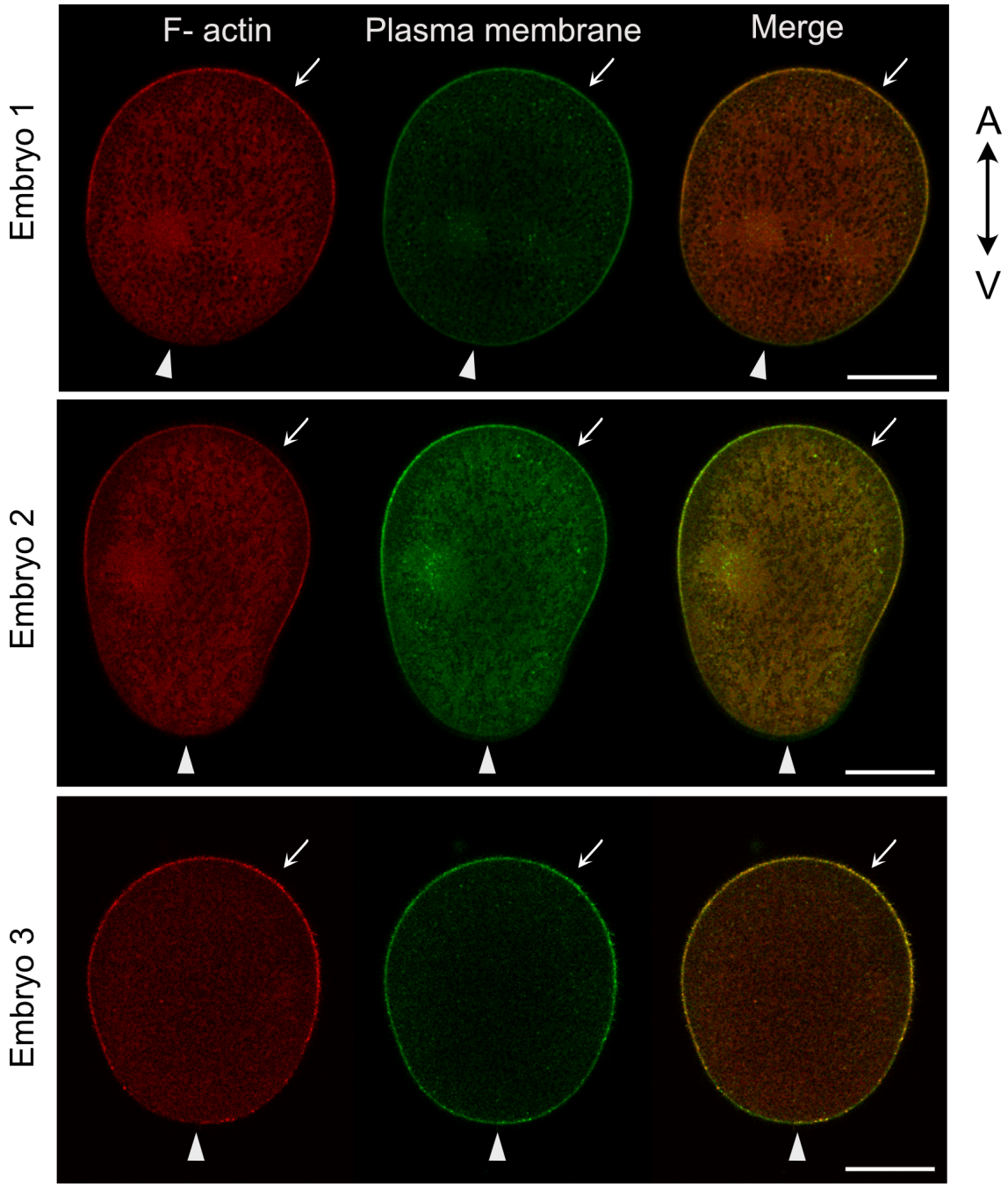

Figure 1.8: The zygote deformation correlates with a vegetal loss of F-actin
Images of three different zygotes during the shape change observed after NEB. The zygotes are derived from eggs injected with LifeAct to label the F-actin (in red, first column), and dyed with Cell Mask deep red to label the plasma membrane (in green, second column). The merge is presented in the third column. The brightness was adjusted. White arrows indicate the animal pole area where F-actin and membrane fluorescent signals are present. This is to compare with the area indicated by white arrowheads where there is no F-actin signal. Scale bar is 50 µm.

close to a circle, and the AR increases when the ellipse shape is oblong, no matter the orientation of the ellipse. The time of NEB was assessed for each embryo, and the aspect ratio curves were aligned with respect to the time of NEB (around 37 mpf (section 1.2, Table S1)). Only a few curves are displayed for clarity, while individual curves can be found in appendix (Annex 3). The striking differences between the 4 individual curves shown on the graph express how the deformations are heterogeneous from one zygote to another, in extent as well as in timing and duration. The variability observed among the curves can also arise from differences in zygote orientation during image acquisition. Hence for these two reasons, the average curve is to be taken as a trend and not as a characteristic behavior. The average AR decreases through interphase until it reaches its lowest point (nearing 1) before NEB. Then, the average AR increases, plateaus at NEB and increases again in a peak. In individual curves, the halt on the increasing slope is sometimes observed as a lower point between two peaks, like in the brown or green curves, or there is only one direct peak with no decline, like the blue curve. Overall, in interphase the zygote is slightly oblong, before reforming a circle by the end of interphase. The deformation starts again in the four minutes preceding NEB, and then increases drastically after NEB. The zygote then reforms a circle to transition to cytokinesis which also starts with a shape deformation as seen on the graph at around 45 min. A zygote matching the average behavior determined in B was selected to show an example of the deformation, with the associated F-actin and membrane label (Figure 1.7 C, Movie 8). During interphase at 33:00, the zygote is rather round and actin and membrane labels look homogenous. At 37:00 (NEB time), after mitosis started, there was already a deformation: the zygote was oblong in the Animal-Vegetal axis. The F-actin cortex looked less homogenous than it was before. After NEB (40:30) the zygote deformation was dramatic, and there may be a loss of F-actin at the extremity of the deformation, which was visible when comparing with the sides of the zygote. On the other hand, the membrane label still seemed rather homogenous. Finally, when the deformation was resorbing (43:30) the F-actin label appeared stronger in the region that was previously deprived of F-actin while the membrane label was still homogenous. This observation tentatively suggests that the shape change may be related to the loss of F-actin at the vegetal pole. When adjusting the brightness of the imaging samples, the loss of the actin label was regularly seen during the zygote deformation, as indicated by the arrowhead on the three embryos displayed (Figure 1.8). However, whether the signal loss was an F-actin loss is still to be determined. Indeed, the plasma membrane label also diminishes in some cases like in the second, and maybe in the first embryo (Figure 1.8). The decrease of the plasma membrane

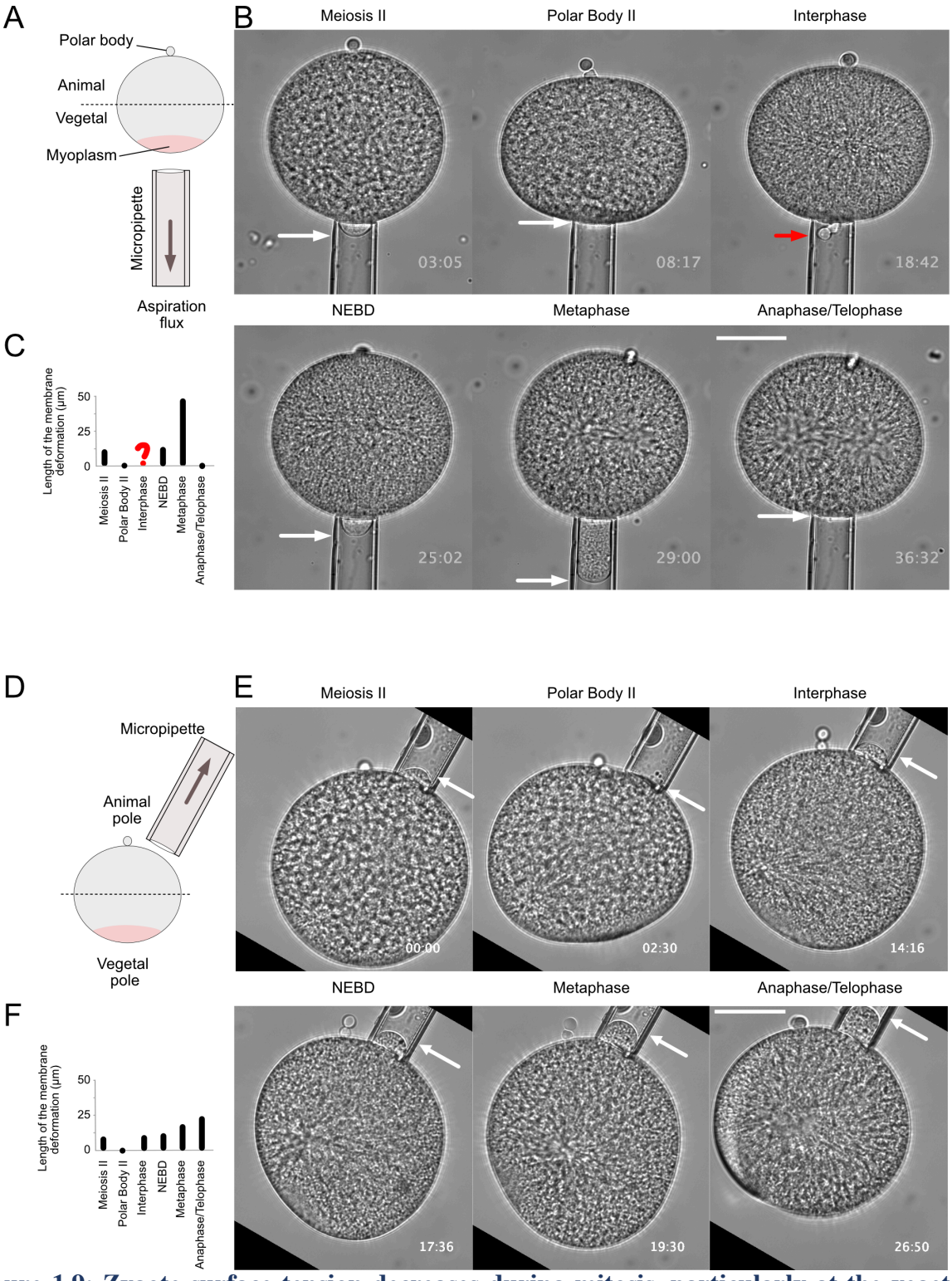

Figure 1.9: Zygote surface tension decreases during mitosis, particularly at the vegetal pole.

A-Schematic of the micropipette aspiration experiment performed on the vegetal side of the zygote. B- Frames from a BF movie showing the deformation created by the constant aspiration of the zygote by the micropipette. Frames were selected to represent specific cell cycle events. Arrows indicate the extremity of the deformation in the micropipette. C- Side-by-side comparison of the length between the tip of the micropipette and the extremity of the cell deformation into the micropipette, at the cell cycle events shown in B. D,E,F are like A,B,C except the measurement is performed on the animal pole. Scale bar is 50 µm.

signal could be explained by the extension of the membrane size for a maintained quantity of membrane, this could also explain the decrease in F-actin signal. The decrease of the membrane signal could also be caused by membrane advection by the necessary cortical divergent flows generated by the actin (and hence tension) loss. To test whether the decrease of F-actin and membrane signals is only due to cell shape extension, a zygote could be confined in a narrow mold to prevent any change of shape. This would also simplify the image analysis, since in the present case a fluorescence intensity analysis on a curved and moving cortex is challenging.

In conclusion, this experiment confirmed the presence of a deformation in 14 of the 15 embryos tested, to some degree along the animal-vegetal axis. The localization of the deformation site with respect to the aster position (that is posterior) is still undetermined. A loss of F-actin in the vegetal side of the actomyosin cortex seems to be a plausible explanation for the deformation but a profound analysis is required to draw a conclusion on this hypothesis. My observations nicely overlap with the brief mention of a vegetal actin-dependent cortical relaxation made in (Roegiers et al., 1999), however the previous description did not mention a change shape, only the dispersal of vegetal cytoplasmic components.

Given the difficulties of performing a fluorescence intensity analysis, I used an alternative strategy which was to determine whether the shape change at entry into mitosis was associated with changes in surface tension and indeed whether there were differences in surface tension between the animal and vegetal hemispheres at entry into mitosis.

1.4.2 Cell tension decreases in mitosis, especially at the vegetal pole.

The shape of an isolated cell, like an oocyte or a zygote, is generally attributed to its surface tension (Lecuit & Lenne, 2007; Thompson, 1942). The surface tension is thought to be determined by the cortical actomyosin contractility and by the tension of the membrane itself (Kelkar et al., 2020). This idea is supported by the phenomenon of mitotic rounding, where isolated cells in culture become rounder when entering mitosis, thanks to an increase in their cortical actomyosin contractility (Ramanathan et al., 2015; Stewart et al., 2011). Another instance where surface tension shapes a cell is provided by a model designed to qualitatively reproduce the surface contraction waves (SCW) observed in sea star zygotes. The model indicated that an increase of tension in a band perpendicular to the A-V axis and moving at constant speed could explain the cell shape changes associated with the sea star contractions

(Bischof et al., 2017). Changes in surface tension are also thought to be associated with contraction waves in the *Xenopus* zygotes (Yoneda et al., 1982). Hence, in parallel to the possible actin loss in the *Phallusia* zygote, a change in the cortical tension is likely to be involved in the zygote deformation. Using the technique of micropipette aspiration (Mitchinson & Swann, 1954), I estimated the variation of cell tension variation over time (Figure 1.9, Movie 9). In this experiment a constant negative pressure is applied by a micropipette in contact with the cell surface. By aspiring the zygote surface with a known and constant pressure, the cell deforms and reaches a steady state. The relation between the pressure applied and the deformation radius allows the calculation of surface tension (Guevorkian & Maître, 2017; Mitchinson & Swann, 1954), while the speed of deformation and retraction can give dynamic information about cortical and cytoplasmic viscoelastic properties.

The experiment was performed on the vegetal hemisphere of the cell (Figure 1.9 A,B,C, Movie 9A) and on the animal hemisphere (Figure 1.9 D,E,F, Movie 9B). On the vegetal hemisphere, in meiosis II a pressure where the deformation was in a steady state was found (Figure 1.9 B). At the extrusion of the second polar body, which marks the beginning of interphase the deformation resorbed. This indicates that the cortical tension increased since the membrane resisted more to the pressure that stayed constant. In interphase, an unusual deformation (red arrow in B, question mark in C) grew slowly from the membrane until the zygote transitioned to mitosis and the deformation quickly filled the micropipette as seen at NEB. Around metaphase, the deformation brutally extended and then resorbed in anaphase in preparation for cytokinesis. Looking at the size of the deformation throughout the cell cycle, it appeared that the zygote has a highly dynamic surface tension, which strikingly decreases after NEB and during metaphase (Figure 1.9 C). The timing of this decrease in tension corresponds to the zygote shape change. Of the three embryos tested, this pattern of tension was reproducible, including the strangely-shaped deformation observed in interphase. I then performed micropipette aspiration, but on the animal hemisphere of different zygotes (Figure 1.9 E, n=2). As on the vegetal hemisphere, the deformation resorbed at the extrusion of the second polar body. Then throughout interphase it grew to reach a new steady state. When entering mitosis, the tension decreased, this led to a progressive increase of the deformation size that did not decrease when cytokinesis started. On the animal hemisphere the tension appeared more constant since the steady state in meiosis II and in interphase led to deformations of about the same size. A decrease of surface tension is perceivable in mitosis despite not being as striking as on the vegetal side (Figure 1.9 F). Since the deformation continued to grow during

anaphase, one could hypothesize that the animal hemisphere is delayed compared to the vegetal hemisphere. The delay in the response of the deformation can be interpreted as a delay in local tension change, however the extension/retraction of the tongue in the pipette also depends on the pressure in the cell (Mitchinson & Swann, 1954). Since cytokinesis is starting when the delay is observed, the cell pressure increases with furrow ingression, hence it exists an alternative interpretation of the delay observed: it may arise from a delay in cytoplasmic pressure homogenization.

In conclusion, the vegetal loss of tension at mitosis entry supports the hypothesis of a loss of actin in that region that could create a cell extension (Figure 1.8, 1.9). On the animal hemisphere the decrease in tension in mitosis but with a deferred resorption of the cell deformation in the micropipette suggests that the tension decrease propagates from the vegetal towards the animal hemisphere. These results have not yet been analysed in depth since the protocol needs further development. In fact, even though the deformation observed in metaphase was what is expected from a decrease of tension due to a lack of actin, this result is to be regarded with caution. Indeed, considering the strong difference in surface tension between the beginning of interphase and metaphase, it may be worthwhile to perform this analysis with more brief observations of deformation (1-3 min) using a pressure adapted to each cell cycle stage to obtain precise measurements, rather than using a continuous pressure throughout the cell cycle as I have done here. A more refined pressure choice may also allow to use identical pressure parameters between animal and vegetal hemispheres for each stage, and thus permit a direct comparison of the deformations. Furthermore, a measurement should also be performed on the vegetal hemisphere just below the limit between vegetal and animal, in order to avoid interference by the dense myoplasm which may influence the extent of deformation into the pipette, as may be the case at the vegetal hemisphere during interphase (Figure 1.9 B interphase). Finally, the global shape change of the zygote throughout the cell cycle as described above (Figure 1.7) is again visible on this figure (Figure 1.9 E).

Given these observations that a contraction wave appears to propagate from the vegetal towards the animal hemisphere at entry into mitosis, I was interested in testing the hypothesis that the contraction wave was similar to the surface contraction waves found in other zygotes at entry into first mitosis.

A

Cytochalasin treated embryos fixed 37mpf

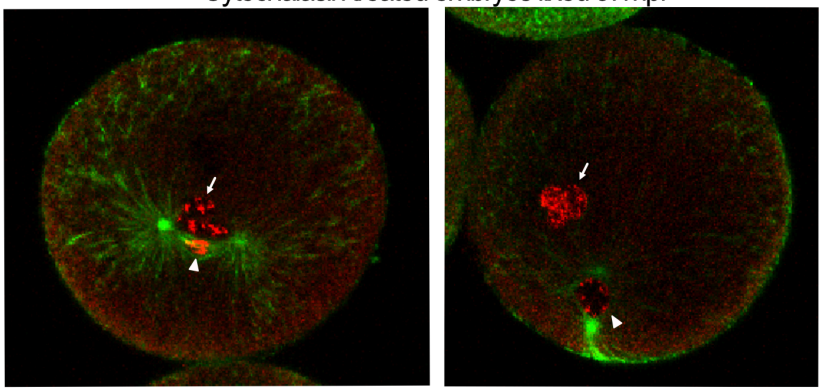

B

Compressed embryos

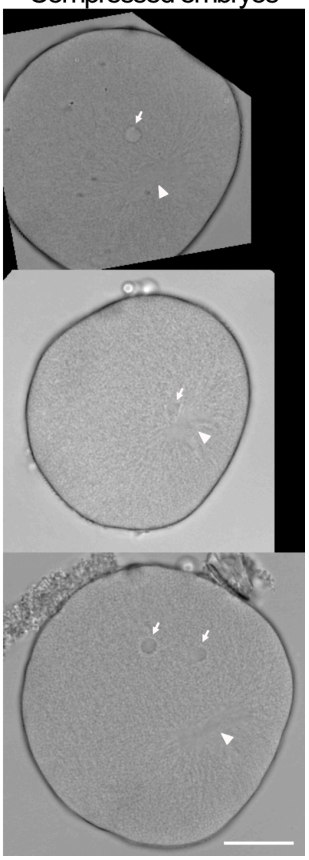

C

Condition	Number of zygotes with at least 1 PN delayed	In zygotes with at least 1 PN delayed		
		Male PN delayed	Female PN delayed	Simultaneous
Control	14 / 24 (58%)	0 / 14	14 / 14	X
Compressed	10 / 34	0 / 17	17 / 17	0 / 17
Fused eggs	6 / 6	3 / 12	7 / 12	2 / 12
Cytochalasin	6	0 / 15	13 / 15	2 / 15
2ME	3	0 / 4	4 / 4	0 / 4
Total	30/64 (47%)	3/62 (5%)	55/62 (89%)	4/62 (6%)

Figure 1.10: Male and female DNA can exihibit different cell cycle stage.
A-Immunofluorescence of samples treated with cytochalasin and fixed 37 min post fertilization. Microtubules are in green and DNA (labelled with Hoechst) in red. White arrows indicate the female DNA, arrowheads the male DNA. B-BF images extracted from time lapse of 3 different untreated embryos, compressed between slide and coverslip. White arrows indicate the female pronucleus. White arrowheads indicate the spindle which holds the male DNA, the nucleus having already broken down. Scale bar is 50um. C- Table comparing which of the male or female PN undergo NEB first in live embryos subjected to different conditions. Zygotes often create several female PNs, each of them has been considered in the data gathered from treated zygotes, whereas in controls only the first PN NEB was considered.

1.4.3 The female pronucleus breakdown is delayed compared to the male

If the first elements obtained about the zygote's change of shape prove to be accurate, then the shape change starts at mitosis onset (M-phase), and becomes more pronounced after NEB. It is accompanied by a decrease in cell tension that propagates on the vegetal-animal axis, and correlates with a local loss of actomyosin contractility. These characteristics resemble the SCWs of fertilized eggs of the sea star *Patiria miniate,* the jellyfish *Clytia Hemisphaerica* and the amphibian X*enopus laevis*. These species all present a contraction wave during M-phase except that unlike *Phallusia* the wave initiates on the animal hemisphere (Amiel & Houliston, 2009; Bischof et al., 2017; Pérez-Mongiovi et al., 1998; Yoneda et al., 1982). The SCW have been shown to rely on a gradient or a wave of CDK1/CycB, the cell cycle complex promoting M-phase (Bischof et al., 2017; Pérez-Mongiovi et al., 1998). In the cases of *Clytia* and the sea star, the contraction occurs in meiosis during oocyte maturation, and the meiotic spindle undergoing M-phase is at the animal pole. CDK1/CycB concentrates at the nucleus during prophase in HeLa cells (Hagting et al., 1998), starfish oocytes that are arrested in prophase of meiosis I, also concentrate CycB in their nucleus (Terasaki et al., 2003), thus at NEB a gradient of CDK1/CycB can form starting from the spindle, at the animal hemisphere.

In the case of *Xenopus*, the sperm aster with the male nucleus is also in the animal hemisphere, therefore the cell cycle wave goes from animal to vegetal. If the ascidian contraction is regulated by the same mechanism as in the three cases mentioned above, it would only be logical that the cell cycle wave goes from vegetal to animal since the sperm aster is positioned in the vegetal hemisphere. This also predicts that the wave and the actin depletion should start near the aster on the zygote posterior side, but this is still to be determined.

I wondered whether pronuclear breakdown could be used as a proxy for the increase of CDK1 activity, and hence as a tool to indirectly identify a wave of mitotic entry. Routinely working with ascidian zygotes, I noticed two things: first that zygotes possessing multiple female PNs were not rare occurrences, especially when the zygote is developing in non-control conditions, and second that the female PNs often seemed to go through NEB after the male PN. Based on this observation I gathered data from different experiments to analyse if this was a recurrent phenomenon (Figure 1.10). In several zygotes treated with cytochalasin and fixed 37 mpf (time of NEB) the male and female PN (mPN and fPN) showed differences in DNA condensation that testified of a difference in cell cycle stage (Figure 1.10 A). The image on the left shows a male DNA in metaphase while the female DNA is in prophase, the picture on the

right shows a male DNA in prophase, but the female DNA is still in interphase. In live embryos, the difference in cell cycle can be assessed by the time of NEB of each PN (Figure 1.10 B,C).

Four approaches were used to increase the distance between male and female PN before NEB in order to determine whether the male consistently entered mitosis ahead of the female. I compressed zygotes or fused unfertilized eggs before fertilization: both led to increased distance between male and female PNs. I also treated zygotes with 2 methylestradiol (2ME) to prevent sperm aster growth and hence fPN migration or with cyochalasin with which I initially observed the delay. In untreated zygotes compressed between slide and coverslip the distance between fPN and sperm aster is increased when the zygote is in a certain orientation, hence the encounter of fPN and mPN is disfavored, and the fPN remains far from the mPN by the end of interphase. Under these conditions and despite a time point interval of 3 min, I observed mPN NEB before fPN NEB in 10/34 (29%) of the cases (Figure 1.10 B, C). In the remaining of cases (24/34), the male and female nuclei underwent NEB within the 3 min time interval; the fPN NEB was never seen to preceded the mPN NEB. The fused egg experiment consisted of fusing two eggs followed by fertilization to obtain bigger zygotes with fPN separated from the male by greater distance. In the fused egg experiment, 7/12 fPN went through NEB after the mPN, but the opposite case was also seen: 3/12 fPN went through NEB first, though this did not occur in any other condition. In cytochalasin, the aster and spindle are less centered than in control embryo (section1.3, Figure 1.4), so they are also further from fPN, which simplifies NEB detection. Moreover, the inhibition of the PBs extrusion causes the apparition of many fPNs. In 2ME, the microtubules are shorter and this hinders the capture of the fPN. In each experiment, a difference in cell cycle was detected between male and female pronuclei. In addition to all the gathered data, new control data were acquired to check that the delays observed were not consequences of the embryo manipulations. In control embryos imaged in BF every 30s, the mPN went through NEB first in more than 50% of the cases. (Figure 1.10C). No correlation between the time of NEB and the distance was detected. Indeed, cell cycle delay was seen even when male and female PN were merging, likewise, when there were several fPN at unequal distances to the mPN, no preferential order of NEB was detected.

To sum up, there is a delay of mitosis between the male and female PN. The various treatments created more distance between fPN and mPN, and sometimes enhanced the number of fPNs, but were not responsible for the delay of mitosis. I hypothesize that, like in other species, the observed delay of fPN breakdown relative to the mPN originates from a gradient

in Cdk1/CycB concentration, with a strong concentration at the vegetal hemisphere of the zygote where Cdk1/CycB can accumulate perhaps due to the sperm aster presence.

1.4.4 Microtubules are necessary for DNA centration.

I was finally curious about what was the role of this contraction wave with associated reduction in surface tension at entry into mitosis. Since actomyosin contraction can create intracellular flows, I wondered whether the contraction could aid in centration of the sperm aster through cytoplasmic streaming, and thus, if a cytoplasmic stream could center the DNA without MTs that are the key element of aster migration. Nocodazole was added to the medium 25 min after fertilization to inhibit MT polymerization at the beginning of interphase (Figure 1.11). After measurement of the distance of the male DNA to the cell center at each time for each embryo, each curve was aligned on the time of NEB. The DNA did not center in the absence of MTs (Figure 1.11). This confirms the necessity of MTs for the process of DNA centration. This experiment holds the strong assumption that the contraction wave is MT-independent. However, even if MTs role was limited to the creation of a cell cycle gradient, their inhibition would impact the contraction, and thus the intracellular flow. On movies of embryos in nocodazole, contractions were still visible. However, a detailed analysis will be required to determine whether the change of shape and pattern of actin depletion are identical in control embryo versus in embryos treated with nocodazole.

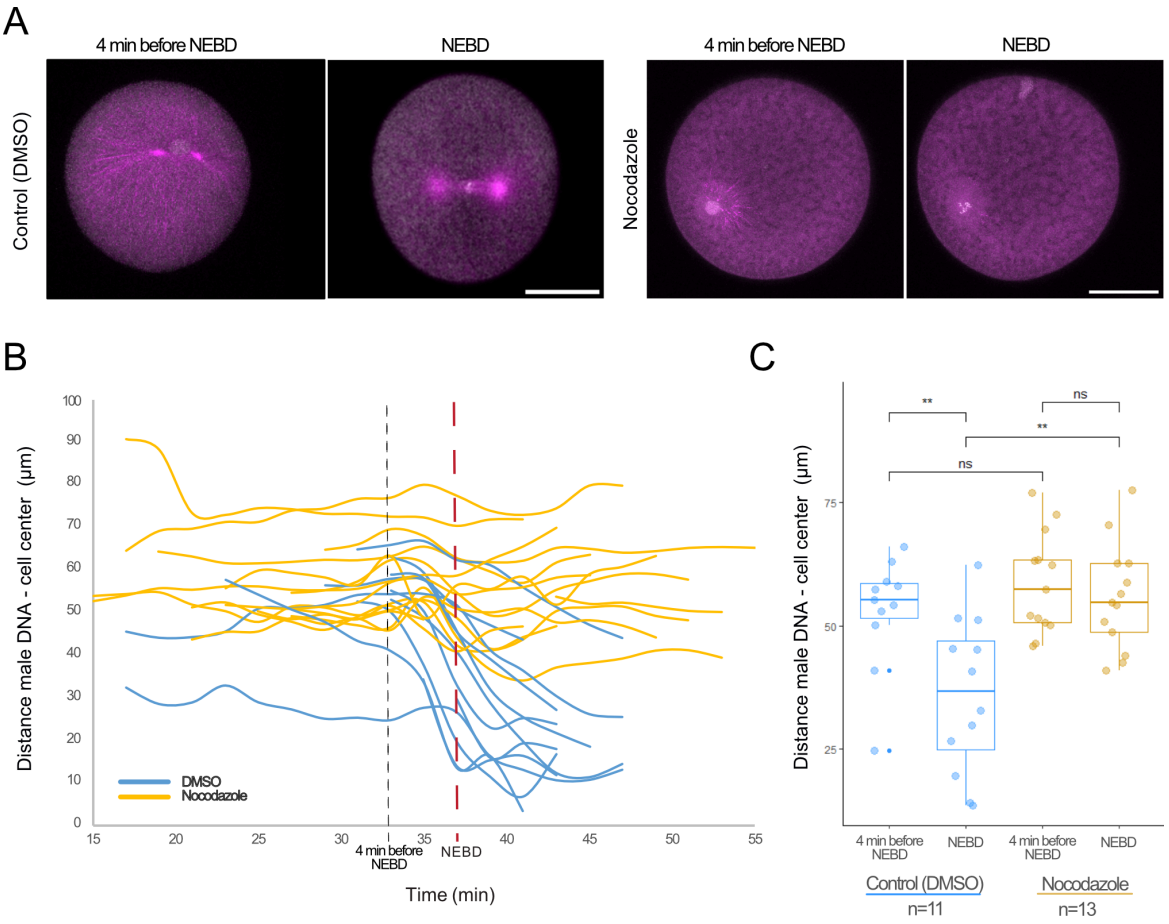

Figure 1.11: Microtubules are necessary for DNA centration

A-Images representative of zygotes expressing mRNA encoding the MT marker Ens::GFP (magenta in the figure) and the histone marker H2B::RFP (white), and treated from 25mpf with either DMSO for controls or with nocodazole to inhibit MT polymerization. Images just before and during the time of migration are shown for each condition. Scale bar is 50µm. B- Distance from male DNA to cell-center over time, in zygotes that developed in nocodazole (yellow curves, n=14) or in DMSO (blue curves, n=12). Curves are aligned with respect to the time of NEB (dotted line, 37min). C- Comparison of the DNA position before (4 min before NEB) and during (NEB) the expected time of migration in zygotes treated as described in (A). Paired Wilcoxon test for intra-condition comparison, and unpaired Wilcoxon test for inter-condition test.

1.4.5 Conclusion

I showed previously that spindle centration in the ascidian zygote starts at mitosis entry. Cortical pulling stops and the spindle is free to center at mitosis entry. Yet, we did not determine the exact mechanism of centration (section 1.2). The observation of a transient cell shape change around the time of mitosis could indicate the presence of an actomyosin contraction whose timing matches the beginning of the spindle centration. I wondered whether this potential contraction could participate in centering the mitotic spindle, so I aimed at describing the contraction to address in future works the interaction between the two events.

To explore the contraction, I first verified the initial observation of a cell shape change. The presence of a deformation, to some degree along the animal-vegetal axis, was confirmed. However, the overall extent of the deformation was quite variable. The deformation may be accompanied by a loss of F-actin in the actomyosin cortex at the vegetal side (Figure 1.7, 1.8). Meanwhile, during mitosis, the zygote cortical tension decreased at the vegetal pole, and then, in a more progressive fashion, at the animal pole. This suggested that tension drops in a propagating wave from the vegetal towards the animal hemisphere (Figure 1.9). If the change of shape, the loss of actomyosin cortex and a cortical tension wave correlate, then the phenomenon described here strongly resembles the surface contraction waves (SCWs) observed in sea stars, jellyfish and X*enopus* (Amiel & Houliston, 2009; Bischof et al., 2017; Pérez-Mongiovi et al., 1998). These SCWs are triggered by a local activation of the M-phase, hence, I monitored the time of NEB of the male PN (at the vegetal side) compared to the female PN (coming from the animal pole). I found that fPN NEB is delayed relative to the mPN NEB (Figure 1.10). This supported the idea of local activation of the M-phase at the vegetal hemisphere. Finally, since a local contraction can cause intracellular reorganization (Sawada & Osanai, 1981), I verified that the DNA centration was a MT-dependent mechanism and not only a result of intracellular flows, and indeed no DNA centration was observed in absence of MTs (Figure 1.11). Each conclusion remains uncertain and needs further research, however taken together they depict a coherent story of a SCW in the ascidian zygote entering mitosis. Also, it remains unknown what role a reduced cortical tension plays during first mitosis since surface tension is reported to increase in tissue culture cells at mitotic entry (Ramanathan et al., 2015). However, the apical surface tension falls at mitotic entry in ascidian embryos at the 16-cell stage (Godard et al., 2020) and a similar phenomenon has been reported in *Drosophilia* during germ band extension/gastrulation (Ko et al., 2020).

Considering that the preliminary data are consistent with each other and supported by a plausible mechanism, it seems reasonable to think that at entry in mitosis there is a SCW going from vegetal to animal hemisphere. Before to tackle whether the contraction wave accounts for the spindle migration impulse in mitosis, the SCW needs to be more thoroughly described.

1.5 Methods

Live F-actin and membrane staining

LifeAct protein injection

The LifeAct::RFP fusion protein was injected to label F-actin (McDougall et al., 2015; Riedl et al., 2008). The fluorescent protein was produced in bacteria from a plasmid containing the yeast Abp140 coding sequence (Saccharomyces cerevisiae NP_014882) fused to RFP sequence.

The microinjection system mentioned in the section 1.2 and described in (Yasuo & McDougall, 2018) was also used for protein injection. Protein-injected oocytes were left for 45min to 2h at 18°C before fertilization and subsequent imaging.

Membrane label

The membrane dye Cell Mask Deep Red (C10046, Invitrogen) was added 1:1000 in microfiltrated sea water (MFSW). After fertilization, the zygotes were bathed in this solution and immediately mounted with the solution between slide and coverslip (spaced by lines of grease).

Mounting Slide for live imaging

For the mounting, two lines were drawn on the slide with a syringe filled with grease (High Vacuum Grease, Dow Corning). Just after fertilization, zygotes were dropped with MFSW (complemented or not with dyes and chemical inhibitors) between the lines. The coverslip was put over the grease lines and gently pressed to prevent zygote movement. Slide and coverslip, and any material in contact with zygotes were coated beforehand with a 0.1% gelatin and 0.1% formaldehyde solution (GF).

Immunofluorescence

A batch of oocytes was put in presence of activated sperm. When about 30% of the oocytes showed simultaneously the fertilization deformation the batch was considered fertilized. At the desired time post fertilization, embryos were harvested (with a 20µl pipette with a GF-coated tip), and fixed in 2mL cold methanol (-20°C, and placed immediately at –20°C). Fixed samples were rehydrated in PBS-Tween (0.1%), blocked in PBS-Tween-BSA (1%), and incubated with anti-tubulin (mouse monoclonal DM1A (Sigma), 1:500), or rat monoclonal YL1/2 (Sigma), 1:200) for 2 hours at room temperature (RT) with shaking and overnight at 4°C. Zygotes were then washed three times in PBS Tween, incubated with appropriate FITC or

TRITC secondary antibody (1:1000, Jackson Laboratory) for 2h at RT, washed again twice in PBS Tween, once with PBS-Tween, treated with for 15 minutes with 5 μg/ml Hoechst 33342 (Sigma) to label DNA, washed once more in PBS Tween, and mounted in Citifluor (Chemlab).

Chemical treatments and perturbations

Chemicals

Several chemical inhibitors were used throughout the study; Cytochalasin B (Sigma 6762), Latrunculin B (Sigma 5163), Nocodazole (Sigma 1404), and 2-methoxyestradiol (2ME, Sigma 6383). Concentrated stock solutions were prepared in DMSO and kept at -20°C. For use, the inhibitors were diluted to the desired concentration in MFSW, then the oocytes were fertilized, and, at the right time post fertilization, zygotes were put into the corresponding drug solutions. Cytochalasin B and 2ME were used just after fertilization, respectively at final concentrations of 5 μM and 16 μM. Latrunculin B was used 10 mpf at a final concentration of 5 μM. In the experiment involving nocodazole, zygotes were added 25mpf to a 10 μM nocodazole/MFSW solution. In cases where other concentrations were used, it is mentioned on the figures (Figure 1.6). For negative controls for the use of these chemicals, zygotes were treated with DMSO.

Eggs Fusion

Dechorionated *Phallusia* eggs were incubated overnight, and some eggs spontaneously fused. These large eggs were selected, fertilized, and mounted for bright-field filming.

Zygote Compression

Zygotes were compressed while being mounted for imaging between slide and coverslip. The zygotes were compressed by pushing on the coverslip until few of the zygotes exploded.

Microscopy Imaging

The micropipette aspiration experiment was performed on the Olympus inverted microscope (IX70) equipped with Metamorph timelapse acquisition software. The experiment was imaged in BF on the 20X/0,75 air objective (UApo/340) with one frame every 2s and a 2x2 binning.
The control and fused eggs conditions of the cell cycle delay experiment were acquired on the Zeiss Axiovert 200M microscope, equipped with Hamamatsu ORCA digital Fusion camera and the Metamorph timelapse acquisition software. Every 30s a 2μm z-step stack was acquired in BF on the 40X/0,75 air objective (Neofluar).

Every other condition and experiment were imaged using the Leica TCS SP8 inverted microscope, and 40×/1.1NA water objective lens. Zygotes labeled with LifeAct::RFP and CMDR were imaged on a few z steps spaced 2 μm apart with a time constraint of a stack every 15s, to observe the zygote deformation at mitosis. For fixed samples, Z-stacks of the whole cell were acquired with a step size of 0.5 μm.

Finally, zygotes treated with 2ME, cytochalasin B, or compressed were imaged to capture the whole embryos with z-step size of 2 μm, and a time step between 30 sec and 3 min as described in the methods of section 1.2. For nocodazole treated embyos, the time interval between acquisitions was 2 min.

Quantification

Aster migration and DNA position were measured by computing the distance of male DNA to the cell center as described in the methods of the article section 1.2

Zygote Size Measurement

The radius of the zygote during meiosis (so when the zygote is round) was chosen as a proxy for cell size. The measurement of the radius was performed on a z-stack using a homemade Fiji macro. The macro first filtered a selected fluorescent channel (where the whole egg was distinguishable from the background) with a "gaussian blur" of $\sigma = 2$. Then it applied an auto-threshold on the blurred images with the "triangle white" method, and the surface of the threshold area was measured using the Fiji "measure area" function. The macro proceeded with these three steps for each z of the stack. The areas were sorted by size and exported on excel where the radius of the zygote was computed from the biggest area, with the assumption that the areas were disks. From a folder containing xyz acquisitions, the macro output one Excel table per file.

Aspect Ratio Analysis

The AR of the zygote as a function of time was computed using a homemade macro adapted from the one that measures the zygote radius. Using the channel showing the membrane label, the macro blurred the zygote image to apply a threshold on its surface. But, instead of measuring the surface area, the macro calls the Fiji function "fit ellipse" which outputs the aspect ratio of the ellipse. The macro then proceeded with these three steps for each time of the time-lapse (xyt) and for each file of the selected folder. It outputs an Excel table per file containing the

aspect ratio of the ellipse that best fits the zygote at each frame. The AR is computed as the length of the ellipse major axis over the length of the ellipse minor axis. The superimposition of the time-lapse images from one movie, shown in figure 1.7 was done using the Fiji Hyperstack function "Temporal Color Code" and the "16 colors" look up table (LUT).

Cell Cycle Delay

Zygotes often create several female PN. In all conditions except the control condition, each fPN was considered. The time points of NEB of each fPN were collected and compared one by one to the time point of the mPN NEB. For the control condition, the only information collected was whether the first NEB to occur was from a male or female PN, independent of the number of fPN. The annotation and collection of data was performed on BF images of xyzt files. Depending on the experiment, the time points varied from 30s to 3min. Delays were often observed within 30s to 1min, so larger time intervals caused an underestimation of the cell cycle delay occurrence. Furthermore, the occurrence of delays inferior to 30s was not assessed.

Surface Tension Measurement by Micropipette Aspiration

Oocytes were fertilized and immediately placed in a chamber filled with MFSW, identical to the wedge used for microinjection (Yasuo & McDougall, 2018). A layer of mineral oil (M8410, Sigma) was added to close the chamber and prevent water evaporation. The chamber was mounted on the inverted Olympus (IX70) microscope. Blunt-end glass pipettes with an internal diameter of 25µm (ES-blastocyst injection pipettes, blunt and straight, TL 12nm PL 55mm, Biomedical Instruments, BM1007-IOP) were filled with MFSW and then inserted into a pipette holder controlled by a hydraulic 3-way micromanipulator (MMO-203). The micropipette was connected to a sealed 15mL falcon tube, containing 6mL of SW, itself connected to a Microfluidic Flow Control System Pump (Fluiwell, Fluigent). The pipette was positioned on the zygote surface and a negative pressure was applied and adjusted until the zygote deformation inside the pipette reached a steady state for about 30s (for a steady state in meiosis the initial pressure was around -1.9 mbar on the vegetal side and -2.1 on the animal side).

Discussion

The Spindle Centration

The first objective of my thesis was to find the mechanism(s) that positions the spindle in the ascidian zygote. As a first step, I described the aster and spindle migration from the sperm aster formation in Meiosis II until anaphase (section 1.2, Figure 1). A few minutes after fertilization, the sperm-triggered calcium waves initiate a cortical contraction that brings the male centrosome to the vegetal side of the zygote (Roegiers et al., 1995). The description therefore started at MTs polymerization around the male centrosome at the vegetal side of the zygote. The sperm aster grew and detached from the cortex during Meiosis II but it did not move further. Then, entering interphase, the aster was brought back to the cortex. During interphase MTs extended to the far side of the cell and even reached the animal pole but crucially, the sperm aster did not migrate in the direction of these long MTs even though the cytoplasmic pulling model would have been predicted to displace the sperm aster. Instead, the sperm aster began to migrate a few minutes before NEB up until metaphase towards the cell center. The spindle rarely reached the cell center, and the spindle distance to the center was not correlated with cell size (section 1.3, Figure 1.2). After this initial description, the study was pursued by testing the implication of the three main MT-dependent mechanisms of spindle migration that cause centration (Reinsch & Gönczy, 1998). Namely, I tested cytoplasmic pulling, cortical pulling, and cortical pushing, on which I focused for three reasons; 1) these mechanisms were shown to center the nucleus or the spindle in zygotes of different species, 2) astral MTs, known to be capable of moving an aster, were present throughout the whole cell cycle, and 3) no particular cell cycle event was noted previously except the reshaping of the myoplasm, thought to be itself driven by the aster movement (Roegiers et al., 1999).

I found that during meiosis, MTs push on the cortex (section 1.2, Figure 6). Since at this time MTs are short and the aster rather symmetric, I suspected that the cytoplasmic pulling was minor, and that cortical pushing was the main mechanism that permits the aster to detach from the cell cortex. Then, I showed that cortical pulling was active during interphase, which explains how the aster was brought back to the cortex (section 1.2, Figure 4). However cortical pulling ceased at mitosis entry, when the spindle centered. The aster/spindle was capable of migrating by cytoplasmic pulling (section 1.2, Figure 5), and cytoplasmic pulling was present in both

interphase and mitosis without significant difference (section 1.2, Figure 3). Hence the reduction in cortical pulling at entry into mitosis permitted the centration of the spindle, and migration may be due to cytoplasmic pulling which remained active during mitosis. In mitosis cortical pushing also seemed active (section 1.2, Figure 6B), however, according to the simulations performed, its contribution to the spindle centering seems minor (section 1.2, Figure S5). These discoveries explain the global pattern of the spindle migration and revealed two major facts: spindle migration is cell cycle dependent in the zygote and it is facilitated by a cell cycle-dependent reduction in cortical pulling.

Nevertheless, I did not completely fulfill my aim since the mechanism of spindle centration I proposed is still hypothetical. Indeed, I showed that centration is possible by cytoplasmic pulling, but could not prove that this is actually the mechanism involved during the spindle centration. To experimentally tackle this aspect and remove cytoplasmic pulling, a solution was to inhibit dynein, but as shown later in this manuscript, my attempts to do so were unsuccessful (section 2.6 Figure 2.11). Although simulations suggested that cytoplasmic pulling was strongly involved (section 1.2, Figure S5), they also showed that this mechanism alone or with pushing could not recapitulate the curve of aster migration (section 1.2, Figure S5). A spindle centration solely due to cytoplasmic pulling is expected to be progressive and homogenous, like observed in Latrunculin (section 1.2, Figure 5), rather than show a sudden surge like in the control migration (section 1.2, Figure S1, Annex 2). The difference between the aster trajectory expected from a migration by cytoplasmic pulling and the actual aster trajectory hinted that some elements were missing in the centration process model established earlier.

Meanwhile, I discovered that the zygote transiently changed shape around the time of mitosis entry (section 1.4, Figure 1.7). A brief study of this event, based on preliminary data, suggested that the shape change was due to a local loss of cortical tension (section 1.4, Figure 1.9) (Bun et al., 2014) provoked by a diminution of cortical actin at the vegetal pole (section 1.4, Figure 1.8) triggered by CDK1/CycB activity (section 1.4, Figure 1.10). This phenomenon looked similar to the surface contraction waves (SCWs) observed in other species (Amiel & Houliston, 2009; Bischof et al., 2017; Yoneda et al., 1982). I hypothesized that CDK1/CycB complex might form and activate locally at mitosis entry, first on the vegetal side, presumably because of a Cyc B accumulation at the aster and in the nucleus. Local CDK1/CycB activity could inhibit the actin stabilization and actomyosin contractibility by inhibiting the RhoA and Rok pathways, as in the starfish (Bischof et al., 2017). In the present case, the actin

destabilization translated as a reduction of cortical actin. Accordingly, a reduction of cortical pulling is expected. Indeed, the complete F-actin inhibition performed with latrunculin was used to observe membrane invaginations (section 1.2, Figure 4), but their presence also testified that cortical pulling was inefficient without actin since the membrane-bound motors actively went towards the aster center. Hence, a local reduction of actin on the vegetal side could cause a local loss of cortical pulling, and thus lead to asymmetric cortical pulling, pulling the spindle away from the vegetal side.

Furthermore, the actin reduction and the end of cortical pulling both correlate with the entry into mitosis. It is tempting to hypothesize that at mitosis entry cortical pulling did not stop homogeneously, but it rather stopped progressively following the actomyosin relaxation, thus creating a transient asymmetric cortical pulling during a short time. This hypothesis was explored with a simulation established from the reference simulation created to test the initial model of aster migration (section 1.2, Figure 7 & S5C). The aster migration trajectory curve in this new simulation matched the data of aster migration better than in the reference simulation; precisely when cytoplasmic pulling could not explain the abrupt curve of migration, the brief asymmetric pulling did and matched the steep downward curve of the spindle centration (section 1.2, Figure S5C, Movie 10).

Other hypotheses

Despite the promising concordance between the simulation, the aster migration pattern and the preliminary data of a SCW, other reasons than cortical pulling may be considered to explain the spindle fast movement. Indeed, on the one hand, simulation has limitation: it is in 2D, only one aster is implemented, MTs were made more stable when binding a cortical motor, and especially, the cell shape change is not considered, and on the other hand the experimental data supporting the hypothesis are still quite minimal, especially concerning the F-actin decrease. Considering the zygote's fast deformation and reformation around the time of mitosis entry, cytoplasmic streaming may be involved in triggering spindle centration. This idea, addressed by inhibiting MTs around NEB time (section 1.4, Figure 1.11), needs to be further tested by inhibiting the SCW without inhibiting the MTs. A last actor potentially involved in centering the spindle is the myoplasm and cortical ER. Myoplasm, a mitochondria-rich mass initially at the vegetal pole, accompanies the spindle movements during centration and is therefore brought

to the equatorial region of the cell, that then defines the posterior side of the embryo. In *P. mammillata*, the myoplasm was thought to be pulled by the spindle (Roegiers et al., 1999; Sawada & Schatten, 1988), but a study performed on the ascidian *Ciona intestinalis* showed with an adapted immunofluorescence protocol the presence of a cortical array of microtubules in the posterior vegetal side of the zygote that correlated with the timing of aster centration. The authors therefore suggested that this cortical array was responsible for the translocation of the myoplasm and the fast movement of the aster (Ishii et al., 2014, 2017). The MTs array observed in *Ciona* was not visible with the live markers I used (Ensconsin::3GFP, Ensconsin::Tomato EB3::Venus, EB3:: Tomato), and at least not noticed with the routine immunofluorescence protocol I used (with anti-alpha tubulin antibodies) from previously published works (Patalano et al., 2006). In addition, they show that the inhibition of the cortical array with sodium azide prevented the myoplasm translocation but not the aster centration even though the migration pattern is different than in controls (Ishii et al., 2014). Finally, the authors did not mention the cortical relaxation we observed in *P. mammillata,* either because the work on fixed samples did not permit visualization of this event, or because this event does not occur in *Ciona*. To sum up, no element gave reason to believe that myoplasm translocation could be a trigger for spindle movement in *P. mammillata,* with the exception of the presence of a cortical array in *Ciona*, that has not yet been seen in *P. mammillata*. It is possible that, despite a similar output, the two ascidians species developed different processes to center their DNA at the zygotic stage.

Spindle Orientation

To determine the mechanisms that position the spindle in the ascidian zygote, I addressed the process of aster and spindle migration throughout the cell cycle, and found when and partially how spindle migration occurred. However, there is still a main unresolved question that I did not examine, that is how the spindle orients with respect to the zygote axes? Indeed, the spindle aligns perpendicular to the animal-vegetal (A-V) axis and perpendicular to the antero-posterior axis (A-P) to induce a cell division that bisects both axes, thus establishing the left-right bilateral symmetry of the ascidian embryo. No striking spindle rotation was seen after centration, and the spindle immediately centered in the correct orientation. How the aster senses and adjusts to the two axes in the zygote is unknown. Since this piece of information is crucial to get a global view of the aster positioning mechanism in the zygote, I propose a hypothetical

mechanism inspired by the literature about myoplasm reorganization and spindle position in later stages. The position of the sperm aster defines the future posterior pole, therefore, after centrosome duplication, if the two asters of the spindle behave the same way and leave the cortex at the same time, then the spindle would naturally position perpendicular to the A-P axis. While the spindle leaves the cortex, the myoplasm reshapes, and forms two immature domains; 1- the future centrosome attracting body (CAB), that ends up localized at the previous aster position, which is the posterior pole, and 2- the vegetal pole now free of myoplasm, that is known to later on become the site of gastrulation (Roegiers et al., 1999). Later, in the 4-cell stage *P. mammillata* embryo, a domain that repulses MTs, or at least that is not engaged in cortical pulling during anaphase was discovered at the vegetal pole (Godard et al., 2021). If this domain is already functional and repulsive during the zygotic stage, then it may be sufficient to explain the spindle orientation perpendicular to the A-V axis, as it would repulse an aster coming too close to the vegetal pole, therefore it may limit the spindle to the equatorial area. Finally, A. Pierre *et al.* modeled ascidian cleavage patterning from the zygotic stage, and to do so, they considered that MTs stopped growing when in contact with a domain at the vegetal pole (Pierre et al., 2016). They identify this domain as the yolk as mentioned in some early ascidian literature and more recent works (Roegiers et al., 1999). However, this description did not match the yolk position described in other studies, as well as in this manuscript (chapter 2) (Conklin 1905, Berg & Humphreys, 1960). Hence the model is consistent with the presence of a repulsive domain at the vegetal pole that is necessary for spindle position in the zygote. It has been shown at the 16-cell stage that Kif2A, a protein from the kinesin-13 family that depolymerizes MTs, localizes at the CAB that itself originates from the myoplasm (Costache et al., 2017). So, if the repulsive vegetal pole does exist at the zygotic stage, then Kif2 could be candidate to play the role of MTs repulsion.

A putative surface contraction wave

As previously mentioned, in addition to the MT-dependent mechanisms that drives aster migration, I found an actin-based phenomenon that is likely also involved. This phenomenon appeared similar to the surface contraction waves (SCWs) observed in other species (Amiel & Houliston, 2009; Bischof et al., 2017; Yoneda et al., 1982). However, the change of cell shape associated with SCWs are expected to be a result of a cortical contraction, as implied by their name. Although actomyosin contraction is best reflected by phospho-myosin label, an indicator

of activated myosin, no actomyosin contraction can occur without actin. Yet, I observed a loss of actin in the vegetal side of the mitotic ascidian zygote. In several works involving cell shape changes and showing actin staining (with phalloidin), a visible decrease of actin staining on the site of deformation was described as an actomyosin contraction on the other side (Pérez-Mongiovi et al., 1998; Yoshida et al., 2003). In addition, mitotic rounding has been shown to rely in some cases on an actomyosin increase (Ramanathan et al., 2015). Thus, I wondered whether a localized entry in M-phase in the ascidian zygote caused a proximal actin depolymerization, or an increase in the actomyosin network on the opposite side. To answer this question, I sought to determine if the well-described mechanism of SCW in the sea star, where M-phase induces an actomyosin contraction, was consistent with my data. In the sea star CycB accumulates in the nucleus localized at the animal pole. Thus, after cycB release at NEB, CDK1/CycB forms a gradient along the animal-vegetal axis. The complex inhibits ECT-2, a guanine nucleotide exchange factor (GEF), that in turn cannot activate the GTPase RhoA (Bischof et al., 2017; Yüce et al., 2005) that is responsible for actomyosin contraction and actin stability through the Rok (Rho kinase) activity pathway. At the end of metaphase, a lower threshold of CDK1/CycB activity is reached first at the animal pole where RhoA will activate and cause a local contraction. CDK1 loss of activity follows its own activity gradient in the cell, therefore propagating the contraction along the animal-vegetal axis (Bischof et al., 2017). At the rear of the contraction (towards the animal pole) the contractility is switched off by an inhibitory feedback downstream of RhoA. At first sight this mechanism does not correspond with the ascidian zygote, since the actomyosin contraction and the site of local M-phase co-localize. However, the sea star SCW starts after metaphase whereas in ascidian it starts at NEB. Thus, supposing that the ascidian zygote is sensitive to the CDK1/CycB activity, and not its inactivity, then the cortex could have reacted to CycB release by an actin destabilization through the RhoA, Rok pathway. One of the main actors of this pathway, Rho A, is present in ascidian zygote (Yoshida et al., 2003). This possible mechanism is consistent with what is known from the SCWs in *Xenopus*. There are two SCWs in the *Xenopus* zygote, one is called SCWa also named the relaxation wave, the second SCWb or contraction wave. They have been reported to correspond to the activation and inactivation of the MPF (the CDK1/CycB complex) (Pérez-Mongiovi et al., 1998; Rankin & Kirschner, 1997), but to my knowledge no details on the molecular pathway were provided. Finally, in *C elegans*, a resembling phenomenon occurs: a cortical flow is locally initiated when Aurora A, a mitotic kinase concentrated at the sperm aster, arrives in close proximity to the cortex and phosphorylates ECT-2. ECT-2 and myosins

are relocated to the opposite side by the cortical flow. ECT-2 seems to participate to the initiation of the cortical flow but also to depend on it for its localization (Longhini & Glotzer, 2022). This localization is thought to be involved in the formation of the cleavage furrow, however, its consequence on the spindle position that heads to the ECT2-depleated posterior side was not discussed.

Conclusion

In conclusion, the research performed here to understand the spindle positioning in the zygote led to two main discoveries; the spindle migration is regulated by cell cycle, and mitosis entry provokes a marked reduction in cortical pulling permitting spindle centration. The centration probably partially relies on cytoplasmic pulling that is able to move the aster, but also on another element that could explain the rapidity of the spindle centration. Based on preliminary data I proposed that the entry into mitosis is not spatially homogenous and that it would spread as a wave as seen in SCWs. Since mitosis stops cortical pulling, a transient asymmetric cortical pulling would appear and drive a fast aster centration. Lastly, even though the centration mechanism is partially understood the question of the spindle orientation is still unresolved. I hypothesized that the presence of a MT repulsive domain at the vegetal pole, maybe originating from the myoplasm, would be sufficient to guide the spindle orientation.

While the asters position, they do not stop performing other functions, such as maintaining the intracellular organization. Apart from the investigation on cytoplasmic pulling, I did not consider this function of MTs, however it is during the zygotic stage that the cytoplasm reorganizes. In the next chapter, I investigated how the polymerization of astral MTs in the zygote impacted the organization of subcellular structures and organelles.

Chapter 2:

Endomembranous organelle accumulation at the sperm aster excludes the yolk

2.1 Introduction

MTs are key elements in the cell. Once organized in an aster, in a mitotic apparatus or even in bundles, they can guide the cell cleavage orientation or organize the cell (Glotzer, 2004; van Bergeijk et al., 2016). Yet, oftentimes these functions are studied separately. The positioning of asters, involved in the cell cleavage orientation, focuses on the asters and MTs mechanical properties while the simultaneous role of asters as cell organizers concentrates on MT transport. The discovery of the cytoplasmic pulling where an aster is moved by the dragging force created by organelle transport (Hamaguchi et al., 1986; Kimura & Kimura, 2011a; Tanimoto et al., 2018), showed that transport and aster movement are connected. However, beyond this connection, the reciprocal influences of the cell organization onto the MTs aster are still largely unknown. Recently this topic started to be tackled and the existence of feedbacks between cell organization and aster properties (movements, MTs repartition or curvature) was shown (Kimura et al., 2017; Pelletier et al., 2020; Sami & Gatlin, 2022; Tikhomirova et al., 2022).

Among all organelles, the contribution of yolk in the positioning of the mitotic apparatus, and thus the interaction between yolk and MTs, needs to be addressed. Indeed, different yolk distribution in eggs lead to different types of cleavage pattern (Gilbert & Barresi, 2016), suggesting a correlation between yolk and spindle position. In many species like zebrafish, the hen *Gallus gallus domesticus*, and *Xenopus,* a striking segregation of the yolk from the rest the cytoplasm occurs, and the spindle mostly forms and resides in a yolk-free area.

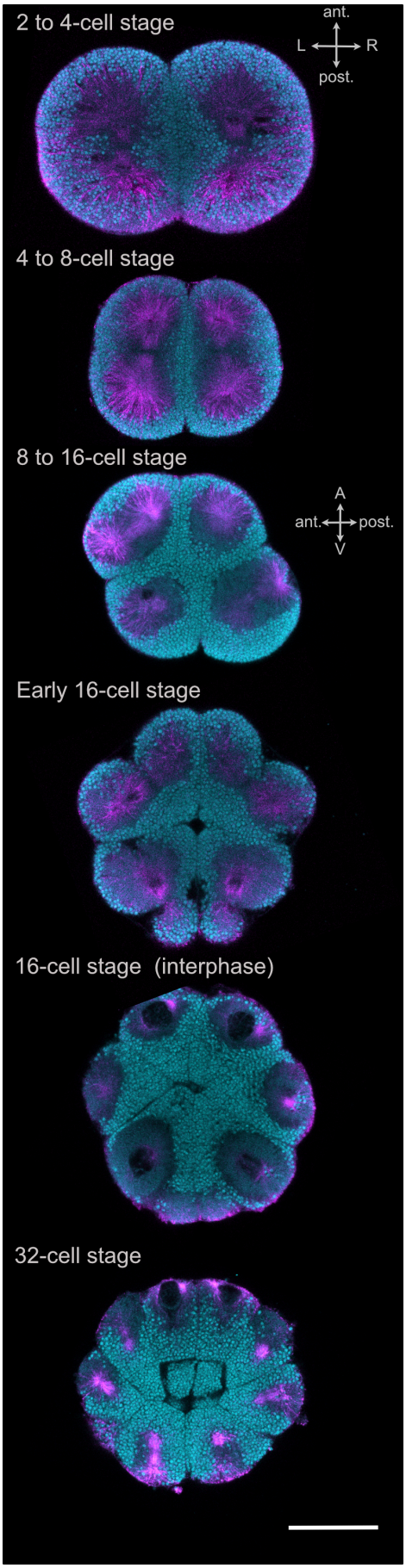

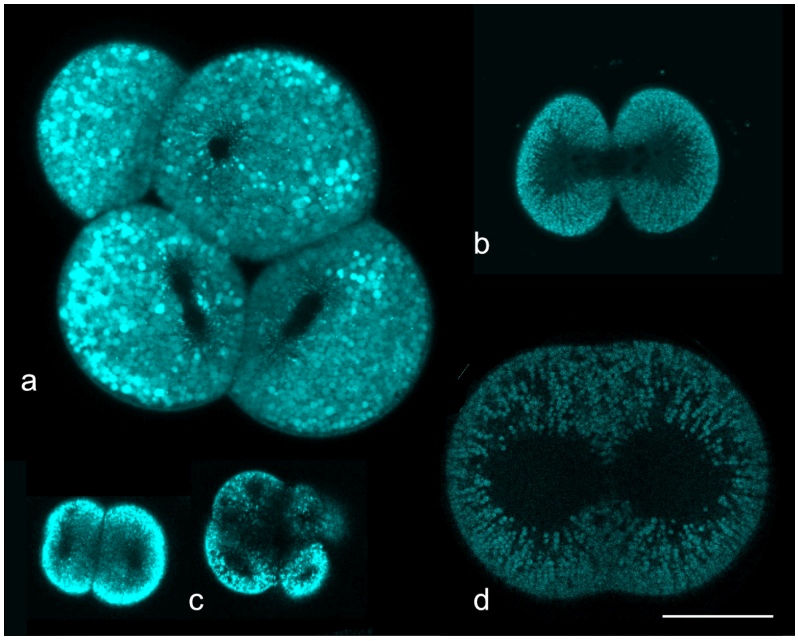

↑

Figure 2.1 : An area of yolk exclusion from the spindle is observed in several species.

Confocal images of yolk exclusion in live embryos from four phyla (a) Cnidarian: *Clytia hemisphaerica*, (b) Echinoderm: *Paracentrotus lividus*, (c) Mollusc: *Mytilus galloprovincialis*, (d) Chordate: *Phallusia mammillata*. Yolk is in cyan. Scale bar is 50 µm.

←

Figure 2.2: Yolk exclusion is preserved during early ascidian development

Confocal images of samples of *P. mammillata* fixed at different stages of early embryo development, and stained for yolk (cyan) and microtubules (magenta). All images are oriented as in the first picture (2 to 4-cell stage) except the third (8 to 16 cell stage). Scale bar is 50 µm.

In metazoan species from jellyfish to lophotrocozoans, echinoderms and ascidian that undergo holoblastic cleavage, I found that although the eggs generally possess a homogeneous distribution of yolk, the yolk also seems segregated from the spindle, like in *Clytia, Paratrocentus, Phallusia* and *Mytilus* (Figure 2.1). This segregation can become drastic (Figure 2.2) (Conklin, 1905a). Thus, in most -if not all- cases, the yolk's distribution seems to anticorrelate with the spindle position and this feeds the intuition that one could influence the other. This is further supported by theorical work that used simulation to show that cleavage pattern of the sea urchin, zebrafish and *Xenopus* was coherent with a spindle position defined by the shape of the yolk-free area (Pierre et al., 2016). Despite the strong anticorrelation between the yolk distribution and spindle position, the mechanism underlying their repulsive interaction in the cell remains overlooked. Hence, to get a better understanding of the reciprocal influences of the cell organization and the aster positioning, I focused on how the yolk abecame excluded from the MT-based aster and mitotic apparatus.

To tackle this question, I exploited the sperm aster formation in the ascidian zygote. Indeed, working on a zygote permits the investigation of the origin of the segregation, and not only its maintenance. *P. mammillata* egg is of an intermediate size (circa 120 µm of diameter), with a homogenous yolk distribution, and is easily accessible for experimentation, and is thus an appropriate model to investigate the mechanism of yolk segregation. In addition, given that the segregation seems more and more drastic at each cell cycle (Figure 2.2), and that ascidians have an invariant cleavage pattern, future studies on the spindle position and yolk segregation putative co-dependency could be pursued in the same species.

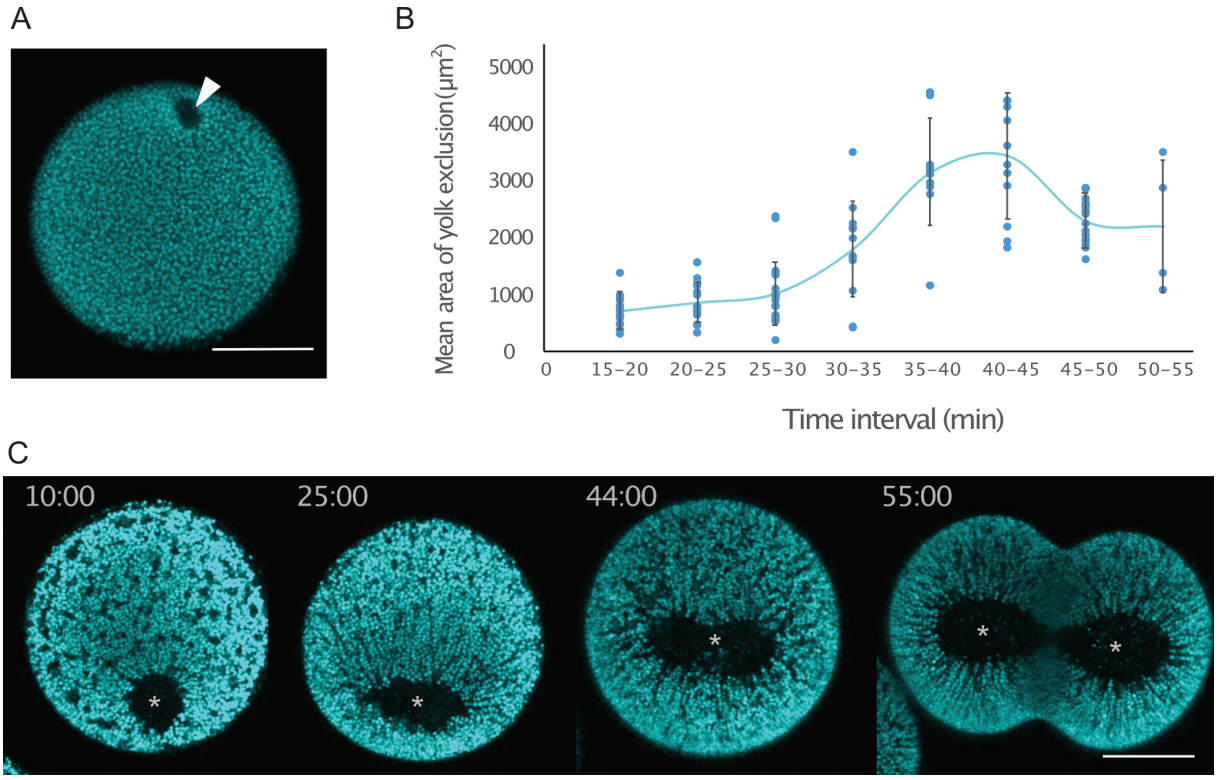

Figure 2.3: Yolk exclusion increases in the zygote with time

A- Image of the homogenous egg yolk. The white arrowhead indicates a yolk exclusion corresponding to the position of the meiotic spindle. B- Surface of the yolk exclusion around the sperm aster in µm², as a function of time. Time points are gathered in interval of 5 min, starting 15mpf. Measurements are done on a total of 20 live embryos. From 45 min, the embryos started dividing, so each future daughter cell was counted as one cell. Bars are ± SD. C- Time lapse of the yolk exclusion in a zygote filmed from around 10 min post fertilization to cytokinesis and labeled with a yolk marker (cyan). The white star indicates the yolk exclusion around the sperm aster and spindle. Scale bar is 50 µm.

2.2 Results

2.2.1 The yolk exclusion forms and grows around the sperm aster

To investigate the formation of the yolk exclusion zone at the sperm aster, I studied through live imaging the evolution of this yolk-free area throughout zygote development (Figure 2.3, Movie 11). Before fertilization, the yolk distribution was completely homogenous, except for an empty spot at the animal pole that corresponded to the meiotic spindle position (Figure 2.3 A). In eggs, the contour of each yolk platelet, also called yolk granule (YG) was visible, this allowed the measurement of their size. With a manual measure, the average YG diameter was of 1.9 ± 0.4 µm (n=64), with an automatic measure the YG diameter was of 1.6 ± 0.3 µm (n=134). A similar result was found in zygotes, 4-cell and 16-cell stage embryos. After fertilization, the yolk homogeneity was disrupted by sperm aster growth. A yolk exclusion zone appeared around the MT structure, and enlarged with time (Figure 2.3 B, C, M). Indeed at 15 mpf the yolk-free area covers a surface of 696 μm^2, but after 40 mpf the exclusion area expanded to reach 3424μm^2 (Figure 2.3 B). This increase seems to correspond to the progressive transformation of the sperm aster into the mitotic apparatus, that is completely formed around 35 to 45 mpf (Figure 2.3 B, C). A 3D measure of the exclusion throughout cell cycle is found in (Figure Sup 2.9). The comparison of the positions of the yolk exclusion and MT structures was possible thanks to the transparency of the ascidian zygote which permits MT visualization in BF. One could also notice the rays that emanated from the area of exclusion and parted the yolk (Figure 2.3 C), they evoke individual or bundles of MTs. By the end of mitosis, the cell started dividing (45 to 55 mpf, Figure 2.3 B C), and the yolk exclusion formed during the zygote development was transmitted to the daughter cells. Therefore, it seems that yok exclusion is not completely reformed *de novo* at each cell division throughout embryo segmentation (Figure 2.2). In parallel to the main yolk exclusion observed around MT structures, yolk homogeneity was also disrupted at fertilization by the apparition of a pattern of small exclusions, that I called microdomains of exclusion (Figure 2.3 A, C), and that did not seem to correspond to any MT-based structure. Two types of yolk exclusions are observed after fertilization; microdomains of exclusion drawing a pattern in the yolk, and a main exclusion that forms and grow around MTs structures, and is transmitted to daughter cells.

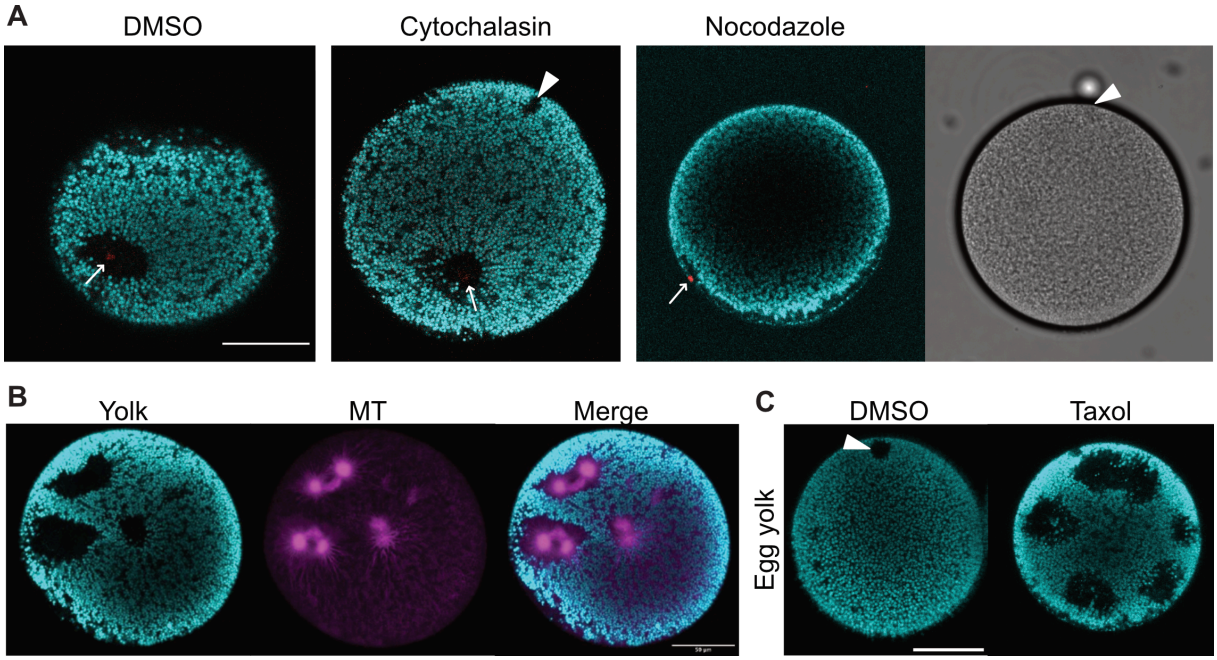

Figure 2.4: MTs are necessary and sufficient to create the yolk exclusion
A-Images of the presence or absence of yolk exclusion in live zygotes treated with either DMSO for controls, or with cytochalasin or nocodazole. DNA is in red and yolk in cyan. White arrows indicate the male DNA label. The white arrowheads indicate the position of the meiotic spindle.
B- Images of yolk exclusion in a live embryo showing abnormal presence of multiple spindles. MT are in magenta, yolk in cyan. C- Images of yolk exclusion in a control egg (DMSO) and in an egg where the formation of several asters is induced by taxol addition. Scale bar is 50 µm.

2.2.2 MTs polymerization initiates the yolk exclusion

Since the main yolk exclusion was found around MT structures, I tested whether MTs were necessary to create the yolk-free area, and if they could induce it. To do so, I counted the occurrence of the formation of a yolk exclusion in zygotes treated with drugs that induced the presence, absence, or abnormal repartition of MTs. The role of microfilaments was also tested since an actin-based yolk reorganization has been previously described in zebrafish (Shamipour et al., 2019). DMSO, cytochalasin or nocodazole were added immediately at fertilization, before sperm aster polymerization. 17/20 zygotes treated with cytochalasin to inhibit F-actin exhibited a yolk exclusion. 21/21 zygotes treated with DMSO for a control treatment showed a yolk exclusion (Figure 2.4 A, first and second panel). After nocodazole treatment, that inhibits MT polymerization, 0/34 zygotes exhibited a yolk exclusion versus 24/26 in embryos treated with DMSO (Figure 2.4 A, first and third panel). The zygotes showing no yolk exclusion after cytochalasin or DMSO treatment did not have an aster. So, in absence of microtubule, there was no yolk exclusion around the male DNA. However, the microdomains were still observed. In the opposite experiment, that is to test if random MT structures could create yolk exclusion, I observed abnormal zygotes that developed several asters and spindles, and saw that for every MT-structure formed, there was a corresponding yolk exclusion area (Figure 2.4 B). The same result was obtained from eggs treated with taxol to stabilize MTs (Figure 2.4 C). In *P. mammillata* eggs, taxol induces the formation of many MT asters (Khetan et al., 2021), in 11/11 zygote treated with taxol, yolk exclusion in areas corresponding to the position asters were observed. Note that as expected from unfertilized eggs, microdomains were absent. To sum up, in all cases the presence of a microtubule aster-like structure resulted in a yolk exclusion, and the inhibition of microtubules before the aster could grow inhibited the formation of the main yolk exclusion area.

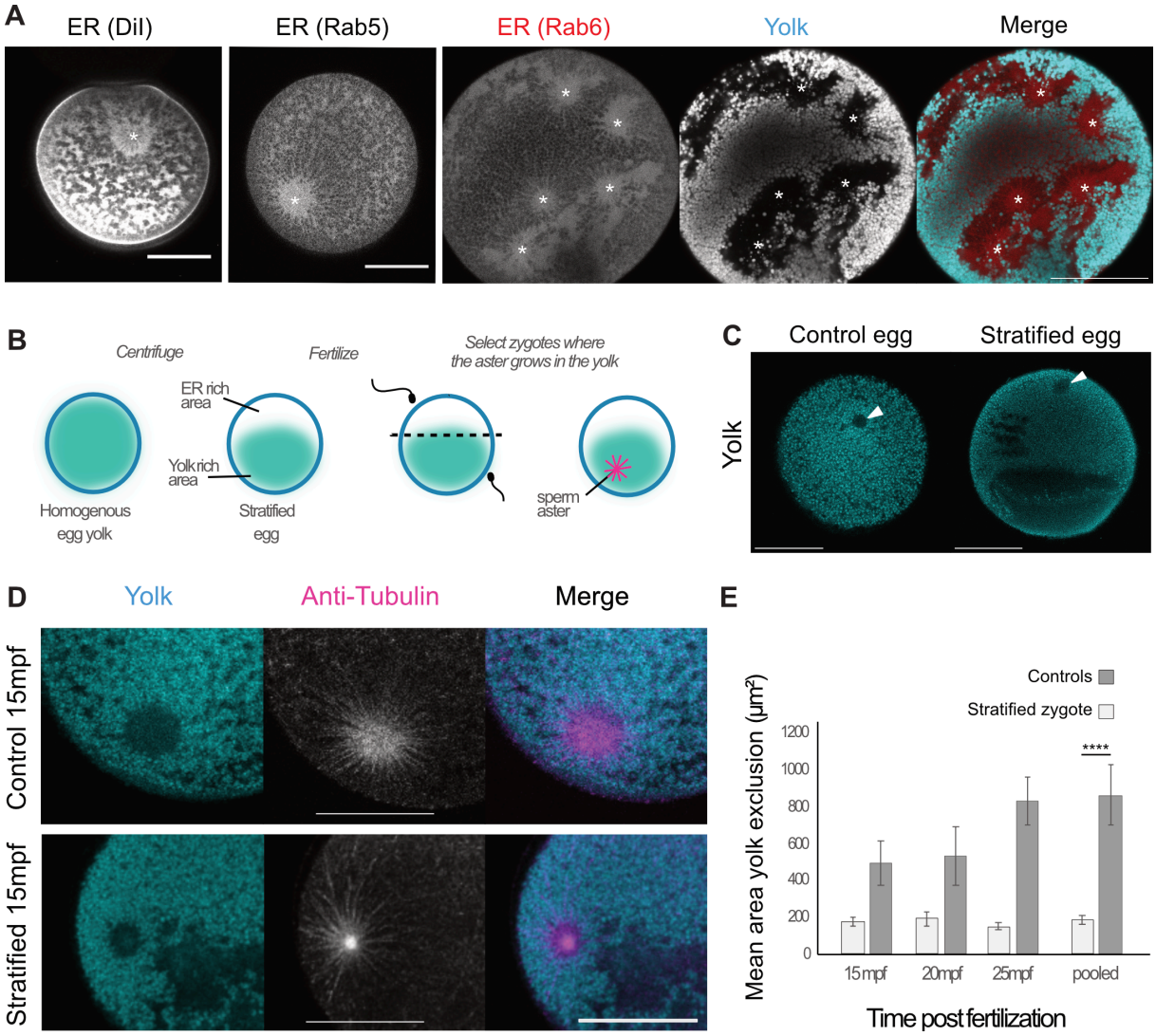

Figure 2.5: Yolk exclusion relies on ER accumulation at the aster

A-Images of the ER labeled with different markers in live zygotes. Left panel shows the ER labeled by injection of the lipophilic dye DiI. Middle panel shows the ER labeled by injection of Rab5::Venus. Right panel shows the ER labeled by injection of Rab6::Venus and the corresponding yolk exclusion. On the merge yolk is in cyan and ER in red. The embryo developed abnormally and shows many asters. White stars indicate aster position. B- Schematic of the experiment of egg stratification. C- Images of the yolk distribution in a control egg and in an egg after stratification (yolk is in cyan) White arrowheads indicate the meiotic spindle position. D- Images of the yolk exclusion around the sperm aster in control and stratified zygote fixed 15mpf. Yolk is in cyan, and microtubules labeled with anti-tubulin are in magenta on the merge. Scale bar is 50 µm. E- Surface of the yolk exclusion around the sperm aster in μm^2, measured on control and stratified zygotes, fixed at 15, 20, and 25 mpf. Measurements are done on a total of n=19 stratified zygotes and n=15 control zygotes. Bars are ± SEM. p-value of Wilcoxon test.

2.2.3 ER accumulation at the aster participates to the yolk exclusion formation and maintenance

For each MT-structure, there was a corresponding yolk exclusion area. However, the zone of exclusion did not perfectly fit the contour of MTs (Figure 2.2, Figure 2.4 B). Furthermore, asters are known to organize organelles, and especially, to accumulate ER (Speksnijder et al., 1993; Terasaki & Jaffe, 1991). Hence, I addressed the presence and the role of the ER in the yolk exclusion mechanism (Figure 2.5). The first challenge was to find an appropriate endomembranous marker (Figure 2.5 A). The dye DiI is routinely used to label the ER in ascidian zygotes (McDougall et al., 2014; Terasaki & Jaffe, 1991). To dye the endomembranous system with DiI a drop of oil saturated with the pigment was injected into the egg. But the pigment is very bright and so are the yolk dyes, therefore co-labeling was difficult. Moreover, the aster often grew near the drop of oil, which impeded a proper visualization of the studied phenomena. The injection of several Rab mRNA with Venus as a fluorescent reporter was also tested. Rab3, Rab5, Rab6, Rab11 did label the endomembranous system, but their injection seemed to perturb normal embryo development. Indeed, a minority of injected embryos underwent a first successful cell division. Subsequent tests showed promising results with the injection of venus::reticulon mRNA (data not shown). All ER markers showed a signal at the aster and in each microdomain of yolk exclusion (Figure 2.5 A). The abnormal embryos that developed after injection of Rab::Venus RNAs sometimes showed several asters, each accumulating ER, and the ER accumulations were found in the area of yolk exclusion (right panel Figure 2.5 A). To determine whether the ER accumulation at the aster participated to create the yolk exclusion zone, I developed a system to obtain growing asters with reduced ER accumulation. I then compared the yolk exclusion around such asters and around control sperm asters (Figure 2.5 B, C, D). Egg centrifugation in a Percoll gradient permitted the creation of an intracellular organelles stratification that separated the endomembranous system from the YG (Figure 2.5 B, C). Some asters were able to develop in the yolk rich area (Figure 2.5 D), thus with a reduced access to organelles. These asters could reach the same size as asters that developed in control condition (Figure 2.5 D). Control and stratified zygotes were fixed at 15, 20 and 25 mpf and stained for yolk and MTs to measure the surface of yolk exclusion in both conditions. The surface of yolk exclusion around asters formed in a yolk-rich area was significantly smaller than in controls (Figure 2.5 D, E, Figure 2.10). The experiment did not include zygotes fixed after 25 mpf because past this time, MTs of the asters

extended enough to have some MTs in contact with the ER-rich area, and this would allow the ER transport to the aster center. In summary, the ER accumulated at the sperm aster and was found in all yolk-free areas. This accumulation most likely participated to the yolk exclusion mechanism.

Since yolk was excluded from the ER microdomains that did not comprise MTs, I wondered whether the organelles accumulated at the aster could be sufficient to maintain the yolk exclusion. To address this question, the aster was left to develop and accumulate organelles for 20 min, time at which a yolk exclusion and ER accumulation were already visible (Figure 2.5 C, D). Then the zygote was treated with nocodazole and imaged during the treatment (Figure 2.6, Movie 12). After more than 1 hour post treatment the yolk exclusion zone was still visible and seemed rather unchanged. On the opposite microdomains did change, they seemed less numerous and bigger; this may be due to the dispersal of the Golgi apparatus that occurs under nocodazole treatment (Minin, 1997).

The results concerning ER accumulation taken together showed that the transport of organelles toward the aster participated to the formation of the yolk exclusion zone around the aster and that organelles alone were sufficient to preserve yolk exclusion areas.

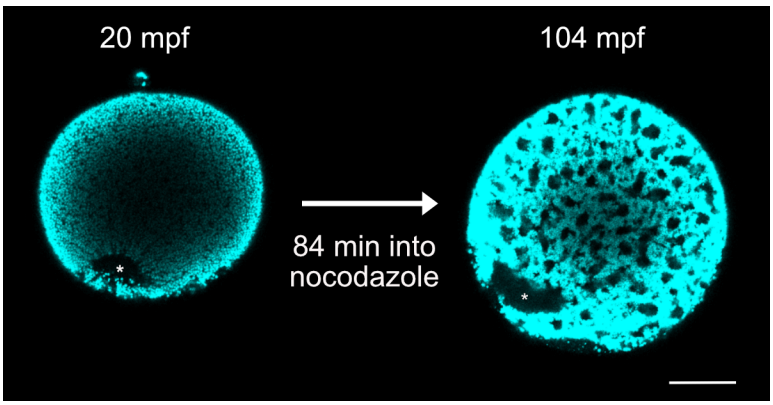

Figure 2.6: MTs are not necessary to maintain the yolk exclusion
Images of the yolk exclusion before and during nocodazole treatment. White stars indicate the initial aster position. Scale bar is 50 µm.

2.2.4 A potential dynein-based mechanism excludes the yolk from the aster

I found that ER accumulation on MT-structures combines with the concomitant exclusion of YGs. I was therefore interested in revealing the mechanism driving YG exclusion from the sperm aster and the ER. I hypothesized that dynein was not present on the surface of

YGs, and that a difference of dynein attachment between ER and YG could cause the yolk segregation.

To determine whether dynein was present on YGs we raised an antibody to *Phallusia* dynein intermediate chain (PhDIC). Dynein was found to label the meiotic spindle area and otherwise it was homogeneously distributed in control eggs (Figure 2.7A). In stratified eggs, the meiotic spindle area was still labeled but the homogenous cytoplasmic label diminished (Figure 2.7A). Instead where ER was enriched at one pole, dynein label was stronger while it was depleted in the YG-enriched domain. When fixation and staining were performed on zygotes, the dynein label was found with the sperm aster and in the ER microdomains. In stratified zygotes, the aster was also labeled, there were no microdomains of exclusion so no label of the microdomains, and a label of the ER-rich area as in eggs (Figure 2.7B). This confirmed that the zygote stratification limited the capture of organelles by the aster, but also and mainly, it supported the hypothesis that there was no dynein bound to the yolk. Next, we studied the movement of YGs to determine whether they interacted with and moved on MTs. Although vesicles and pronuclei can be measured moving towards the center of the sperm aster, YGs neither appear to interact with MTs nor move along MTs (Movie 13). This tended to indicate that YGs do not have dynein on their surface and do not move along MTs.

Although these data are consistent with the exclusion of YGs powered by dynein-based ER accumulation to the center of the sperm aster, I attempted to perturb the mechanism of yolk exclusion by inhibiting dynein activity in the zygote to show that dynein indeed powered exclusion of the yolk from the sperm aster as ER was accumulated. Ciliobrevin D, Ciliobrevin A, dynactin CC1 protein and dynactinCC1::Venus mRNA were used to inhibit dynein activity, but for each test the concentration used did not inhibit dynein while zygotes developed in an aberrant manner. For instance, 50µM of ciliobrevin D, often employed as a pharmacological tool to inhibit dynein, caused severe zygote deformations while minus-end directed transport was still observed by the accumulation of endocytosed vesicles at the aster (Figure Sup 2.11). I speculate that ciliobrevin has off-target effects and should be treated with caution. Given that I was unable to inhibit endogenous dynein, I made a 2D simulation representing the surmised mechanism (Figure 2.7C, Movie 14). The simulation was composed of an aster, of beads that were attached to dynein (green) representing the ER, and of beads that could not attach dynein (red), representing YG. With time, the sole difference of dynein presence on the green ER beads caused the accumulation of green beads to the aster and an efficient exclusion of the red YGs beads from the aster. (Figure 2.7C, Movie 14). Thus, the simulation supported that the proposed

YG exclusion hypothesis based on organelle accumulation reasonable, and could be the main mechanism driving the yolk exclusion, and thus the ER and yolk segregation.

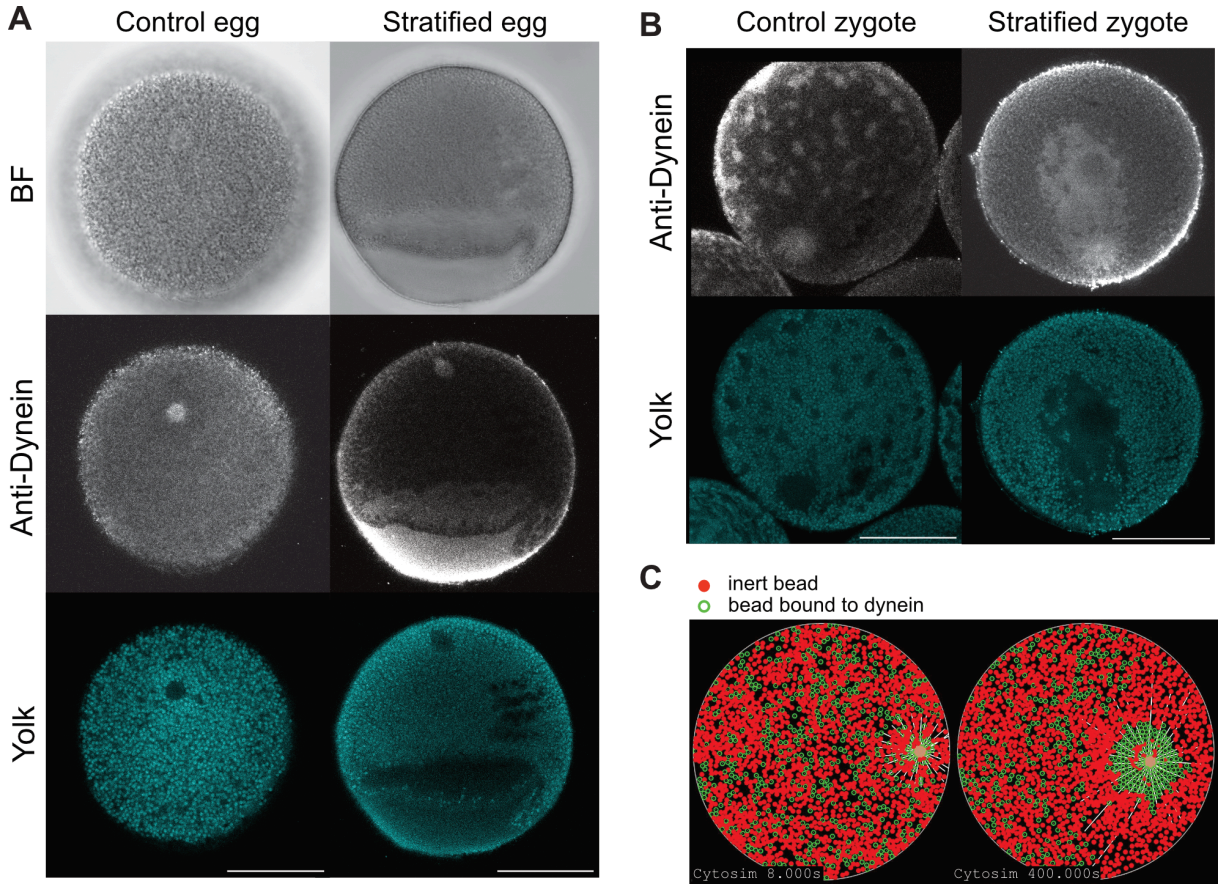

Figure 2.7: A possible absence of dynein on the yolk
Confocal images of control and stratified eggs (A), or zygotes (B), stained with anti-dynein intermediate chain (DIC) (gray) and with a yolk label (cyan). Brightness levels were adjusted. Scale bar is 50 µm. C- Frames from the beginning and the end of a Cytosim simulation representing a possible mechanism of yolk exclusion. Yolk is represented in red as inert beads that do not bind motors. Organelles accumulating at the aster are represented in green as beads bound to minus end directed motor, that go along the MT (white) towards the center of the aster (orange core).

2.3 Discussion

A defined intracellular organization is necessary for multiple reasons, to bias the spindle position and control cell division orientation (Pierre et al., 2016), but also to ensure a proper organelle repartition to daughter cells at cytokinesis, and to localize organelles in specific places to perform specific functions (van Bergeijk et al., 2016). For example, the nuclear envelop formation requires ER near the nucleus (Mukherjee et al., 2019; Voeltz et al., 2002). In turn, organelle repartition can itself impact cell processes. An unequal distribution of organelles able to bind molecular motors can influence the position of MT structures (Kimura & Kimura, 2011a; Negishi & Yasuo, 2015; Sallé et al., 2019). It has also been recently shown that the ER organization around MTs changes the aster properties (Sami & Gatlin, 2022; Tikhomirova et al., 2022). Indeed, MTs curve less when surrounded by ER, and this favors MT pushing mechanism compared to what was theorized from *in vitro* experiments (Sami & Gatlin, 2022). Also, the aster's MTs tend to form bundles when the ER tubular network is not homogenous in the cell (Tikhomirova et al., 2022). The yolk is also thought to influence the mitotic apparatus position by constraining it in yolk-free areas. This function, that seems based on the yolk localization in the cell, is acknowledged but rarely studied. Thus, as a first step to understand how the yolk could constrain the spindle position, I wondered how the yolk is excluded from the areas containing MT-structures, in other words how to reshape intracellular organization. Using ascidian oocytes which possess a homogenous isolecithal yolk, I assessed the yolk exclusion during the zygote development and tested its dependence on the cytoskeleton and on the ER distribution.

The results indicate that the yolk, present in the form of yolk platelets (YG), is progressively re-organized in time, in a MT-dependent fashion. From a homogenous yolk repartition in the egg, an area of exclusion appears and grows with the sperm aster evolution. In the absence of MT no major segregation occurred, only small microdomains of exclusion were visible, that turned out to anticorrelate to ER clusters (also called microdomains or patches) formed after fertilization (Speksnijder et al., 1993; Terasaki et al., 2001; Terasaki & Jaffe, 1991). Any MT-structure can initiate the yolk exclusion, but the exclusion requires the accumulation of organelles like the ER towards the MTs minus end. Once the yolk exclusion is formed and dynein-bound organelles are accumulated on MTs, the yolk exclusion can persist without MTs. During the cell division, the yolk exclusion area that was around the sperm aster is around the mitotic apparatus, and it is transmitted to the daughter cells. The presence of actin

is not necessary for the formation of a yolk exclusion, however its influence past the initiation of the exclusion has not been assessed. Finally, to explain the yolk/ER segregation process, I propose a simple mechanism of spatial exclusion based on the presence of dynein on the ER and the absence of dynein on the YGs. The proposed model of yolk exclusion does not exclude the possibility of other co-existing mechanisms. For example, some YGs could be randomly pushed by polymerizing MTs. The hypothesis of a size selection accumulation was also considered, however small beads injected into the ascidian zygote could go to the aster center (Annex Movie 15), and larger elements such as the female PN or the ER can also be transported to the MT minus-end, thus this hypothesis has been ruled out.

The results obtained are coherent with ER literature. The ER is dynamic and connected to the cytoskeleton; it accumulates at MTs asters thanks to dynein-mediate transport (Sami & Gatlin, 2022; Wang et al., 2013) then the ER spreads outward and expands tracked by MTs plus-end (Schwarz & Blower, 2016; Wang et al., 2013). Despite radical changes during mitosis, the ER network does not disassemble during cell division and it is divided between the daughter cells (Schwarz & Blower, 2016; Voeltz et al., 2002). Note that ER has been reported to only co-localize with spindles poles, and not with the spindle (Wang et al., 2013), this did not reflect in the yolk repartition around the mitotic apparatus. Lastly, the apparition of ER clusters, also called ER microdomains (Speksnijder et al., 1993; Terasaki et al., 2001; Terasaki & Jaffe, 1991) correlated with the yolk distribution. The difficulty faced to find a good ER marker that did not perturb zygotic development is also consistent with the literature; over-expression of ER structural protein (Atlastin, reticulon) frequently provokes abnormal ER organization with unbalanced formation of ER sheets and tubules. The deletion of different Rab proteins caused an increase in ER sheets (Schwarz & Blower, 2016). The injection of Rab mRNAs fused with a fluorescent marker also seemed to cause an increase in ER sheet, therefore they may have played a role of competitive inhibitor.

To sum up, in the ascidian zygote yolk distribution seems to be the negative of the ER localization. Some questions are still unresolved, particularly concerning two points: 1- the interaction between the yolk and dynein, and 2- the preservation of yolk exclusion. Concerning the first point, the simulation performed to illustrate the hypothesis of a dynein-based segregation mechanism uses beads and not a network as a representation of the ER. Thus, the outcome of the simulation with a network-like ER is unknown. In addition, the anti-dynein staining showed a weak concentration of dynein around the YGs, but this is not proof of a lack of interaction between dynein and YG. Indeed, dynein is cytoplasmic and may have been pulled down during centrifugation rather than being stratified because of an attachment with the

endomembranous system. In addition, dynein needs adapter proteins to transport cargos, and even sometimes to activate (Xiang & Qiu, 2020), so rather than estimating the proximity of dynein, it may be more direct to investigate whether the adapter proteins exist that can bind both YGs and dynein. To overcome these limitations and understand the yolk and dynein interaction, a better knowledge of the yolk properties and biochemistry is essential. For instance, to find yolk transmembranous proteins would facilitate the development of molecular tools to manipulate yolk attachment to dynein and then prevent YG exclusion from the aster to determine how this affects further development. Also, since cytoplasmic pulling from organelles is a major mechanism for aligning mitotic spindles (Kimura & Kimura, 2011), it is utmost importance to determine which organelles provide the means for cytoplasmic pulling.

The second point to address is how the preservation of the yolk exclusion could occur over an extended time. I found that yolk is segregated at each stage during ascidian segmentation, and that the yolk segregation is transmitted. Nevertheless, given the ER dynamism, one could wonder to what extent the yolk exclusion is preserved and remodeled at every cell cycle. In addition, the segregation becomes more and more drastic through the cell cycles (Figure 2.2), which could suggest that additional factors add to the equation. Strong candidates to explain the progressive change in the segregation are ER availability and yolk compaction. If part of the ER stays at the asters at each cell cycle, then with time the ER will eventually be depleted from the cell periphery. Without the presence of ER among YGs, and constrained by a bigger accumulation of ER at the asters, YGs would be packed tighter together in the cell periphery, and thus yolk compaction would increase within each cell. A compact yolk may in turn be more difficult to reshape, and maybe it could then influence the position of the mitotic apparatus in ascidian embryos. This question could be addressed *in vitro* by adding an increasing amount of yolk in cell extracts (Shimogama et al., 2022).

To conclude, I suggest that the segregation of organelles (ER and YGs) in the ascidian is driven by the presence or absence of dynein which I term the ER-YG exclusion model. Even though the yolk is quite a universal component of early embryos, it comes in a variety of shapes and structures (Cf. section 0.3, Jorgensen, 2008). Matching this variety, it seems that yolk distribution can be guided by a panel of different mechanisms. YGs are transported to the cell center in a kinesin-dependent manner in *C. elegans* maturing oocyte (McNally et al., 2010). In the zebrafish zygotes YG are pushed on the vegetal side by actin comets (Shamipour et al., 2019), and here we depicted another mechanism that reshape the YGs localization based on the presence of dynein on organelles such as the ER and the absence of dynein on YGs leading to ER accumulation at the aster driving the progressive exclusion of YGs. It is also interesting to

note that YGs are excluded from the mitotic apparatus in jellyfish, molluscs, echinoderms in addition to ascidians. An insight into the origin and the type of yolk in various species could provide avenues to appreciate the conservation of the mechanism and maybe predict the preferential mechanism of yolk segregation in a given species.

2.4 Methods:

Biological material

Phallusia mamillata eggs and embryo were as described in the methods of section 1.2, and mounted as described in section 1.6. Embryos from other species shown in figure 2.1 were handle like *Pm* embryos, except *Clytia* embryos that were mounted between two coverslips fixed with grease (High Vacuum Grease, Dow Corning) on a metal structure to create a wider chamber than the one I used for *Pm*.

Mytilus galloprovincialis were collected in the bay of Villefranche-sur-Mer (France), and embryos were obtained as described in (Kapsenberg et al., 2022).

Paracentrotus lividus were collected in the bay of Villefranche-sur-Mer (France). Gamete collection and fertilization were performed by the EvoInside team as previously described in (Formery et al., 2022).

Clytia hemisphaerica embryos were obtained from permanent laboratory colonies, after gametes release induced by light illumination, and subsequent fertilization performed by the Cnidarian Developmental Mechanism team (Lechable et al., 2020).

Live labelling

YG were labeled indifferently with Nile Red (3013, Sigma, diluted in ethanol circa 1mg/mL to create a saturated solution), Lysotacker Red (L7528, Invitrogen), or Lysotacker Green DND-26 (L7526, Invitrogen), all used at 1:1000 in the MFSW medium. No difference was found between Lysotracker green and Nile red staining, except that Nile Red seemed to penetrate faster into the eggs or embryos (Figure Sup 2.12). To stain DNA, Hoechst 33342 (Sigma) was added in the medium at concentration of 200 µg/ml.

MT or ER labelling required to perform microinjections as described earlier (see section 1.2, McDougall et al., 2014; Yasuo & McDougall, 2018). To label MTs the RNA injected was Ensconsin::Venus. Rab3::Venus, Rab5::Venus, Rab6::Venus, Rab11::Venus or Venus:Reticulon were injected to label the ER. Another way to label the ER was to inject a drop of mineral oil (M8410, Sigma) or of Wesson oil saturated with DiIC16 (D384, Invitrogen) and briefly centrifuged to not inject the pigments. Injected eggs were incubated at 18°C overnight before subsequent fertilization and imaging.

Immunofluorescence

An antibody specific for ascidian dynein was generated against the P. mammillata dynein intermediate chain (PmDIC). The entire PmDIC coding sequence (NCBI CAB3240298.1) fused to His-6 tag was expressed in bacteria from the T7 promoter using the pET-11 plasmid. The PmDIC-His6 fusion protein was purified on a nickel column and used to immunize mice (Covalab, Bron, France). Immune sera showed a single band on western blots of Phallusia protein extract and by immunofluorescence labelled multiple structures in embryonic cells including spindle, membrane, nucleus, kinetochore, and ER.

Eggs and zygotes were fixed in cold methanol (-20°C) and stained as described (section 1. 6, , Patalano et al., 2006)with anti-tubulin (rat monoclonal YL1/2 (Sigma, 1:200) or with anti-PmDIC (1:50). After incubation with appropriate secondary antibodies and consecutive washes including the Hoechst staining (5 to 10 µg/ml in PBS-Tween 0,1%), an additional wash complemented with Nile Red (1:1000) was performed to stain the yolk, then two PBS-Tween washes were added to remove the dyes.

Egg stratification

1mL of dechorionated eggs in MFSW were placed on a cushion of 1mL 50% Percoll (PLUS/Percoll, GE Healthcare) in MFSW, and centrifuged for 50 min at 300g. After centrifugation, eggs were washed in a petri dish until all the percoll was removed from the medium, that is, until eggs could settle at the bottom of the dish. Fertilization was immediately performed.

Chemical treatments

Several chemical inhibitors diluted in DMSO were used throughout the study, they were used at the final concentration of 5 µM for the Cytochalasin B (6762, Sigma), and at 10 µM for

Nocodazole (1404, Sigma) or Taxol (Paclitaxel T7402, Sigma) treatment. Ciliobrevin A (Sigma; as HPI-4, gifted by Hitoyoshi Yasuo) and Ciliobrevin D (250401, MEMD Millipore) were used at 50 µM.

Taxol was added on eggs, Cytochalasin B and the two types Ciliobrevin were added just after fertilization (when the egg made a contraction pole), and nocodazole was either added just after fertilization or 20mpf after apparition of a yolk exclusion.

Microscopy imaging

All experiments were imaged using the Leica TCS SP8 inverted microscope, and 40×/1.1NA water objective lens.

Image analysis

The software Fiji, was used for image analysis. The surface of YG was measure using by 1- selecting a z were YG seemed distinguishable, 2- adjusting the brightness to visually separate the YG from each other, and creating a binary mask, 3- using the function "Analyse particles" set to detect shape pf a size between 0 and $5\mu m^2$, and a circularity between 0.80 and 1. The YGs diameters were inferred from the measured surfaces. The manual measurement consisted into tracing a line on the YG diameter. The 2D area of exclusion, was found by selecting the z where the yolk exclusion was the clearest and the biggest. Then the brightness threshold was adjusted with Huang method by "convert to mask", which created a binary image from the new threshold. On the binary image contours of the area of exclusion were neat, so they could be selected and measured using the magic wand tool. For the 3D measurement, the previous procedure was applied on every z where the yolk exclusion was visible, and all the measurements were summed. Since the z-step is not continuous μm^3 cannot be used, thus the unity of this measure is in arbitrary unit.

Simulation

The simulation was performed in 2D using Cytosim (https://gitlab.com/f-nedelec/cytosim) with standard parameters values inspired from the Cytosim tutorial. The parameters are details in (Table 2.8). The simulation was run with equal amount of the two types of beads; 1000 "ER" beads each attached to 1 dynein, and 1000 "yolk beads".

2.5 Supplementary material

General parameters	
Time step	0,01
Number of run	40000
Cell diameter	10
Viscosity	1
Beads	
Radius	0,16
Steric	1
Dynein attached to beads	
Binding rate	5
Binding range	0,1
Unbinding rate	0,1
Unbinding force	10
Bind also end	1
Activity	move
Max Speed	-0,5
Stall force	5
Hold growing end	0
MT	
Rigidity	20
Segmentation	0,5
Activity	classic
Total polymer	200
Growing speed	0,5
Growing force	5
Shrinking speed	-0,085
Catastrophe rate	0,05
Rescue rate	0,5
Min length	0,6
Aster	
Radius	0,5
number of fibers	30
Fiber length	1
Stiffness	1000, 1000
Nucleation rate	1

Table 2.8: Cytosim parameters values for the yolk exclusion simulation.

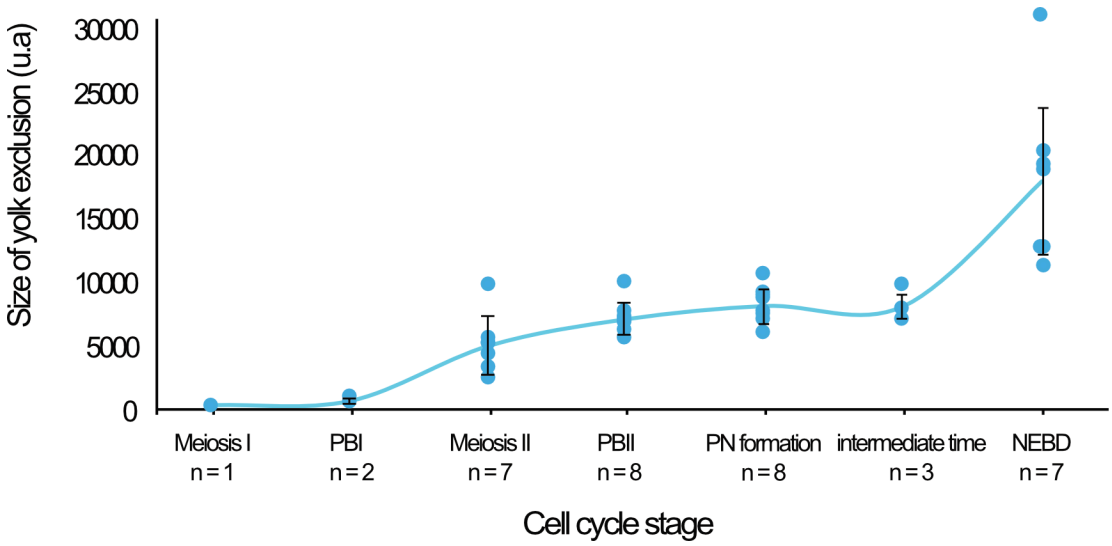

Figure 2.9: Yolk exclusion size increases throughout first cell cycle
3D measurements of the yolk exclusion's size around the sperm aster in arbitrary unit, at several cell cycle events representative of the first cell cycle stage. Bars are ± SD.

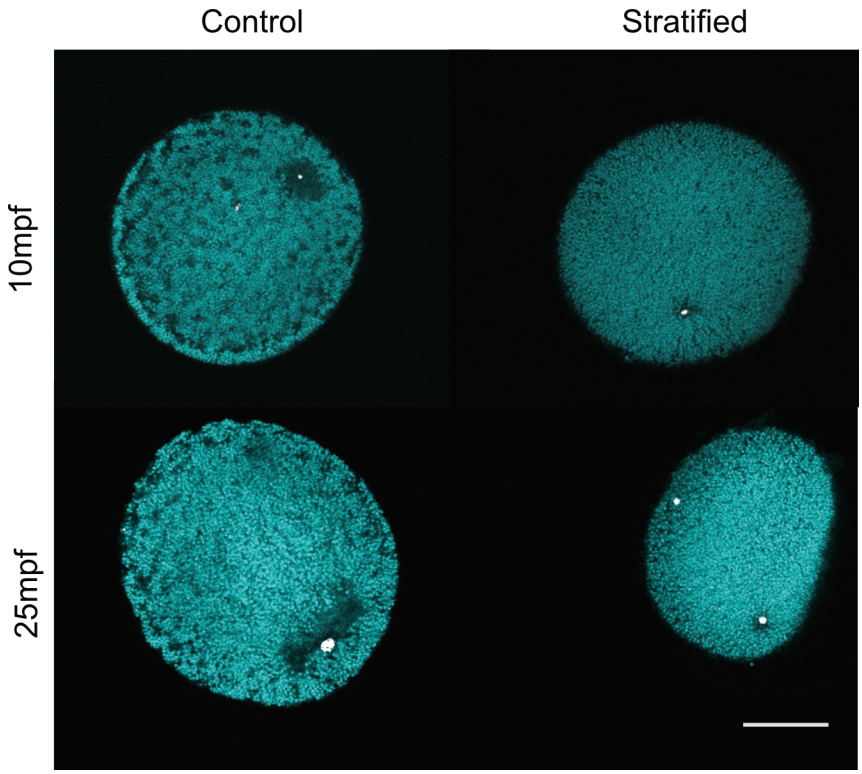

Figure 2.10: Yolk exclusion area around male DNA is reduced in stratified zygotes
Confocal images of the yolk exclusion around the sperm aster in control and stratified zygote fixed at 10 mpf (top row) or 25mpf (bottom row). Yolk is in cyan. Scale bar is 50 µm.

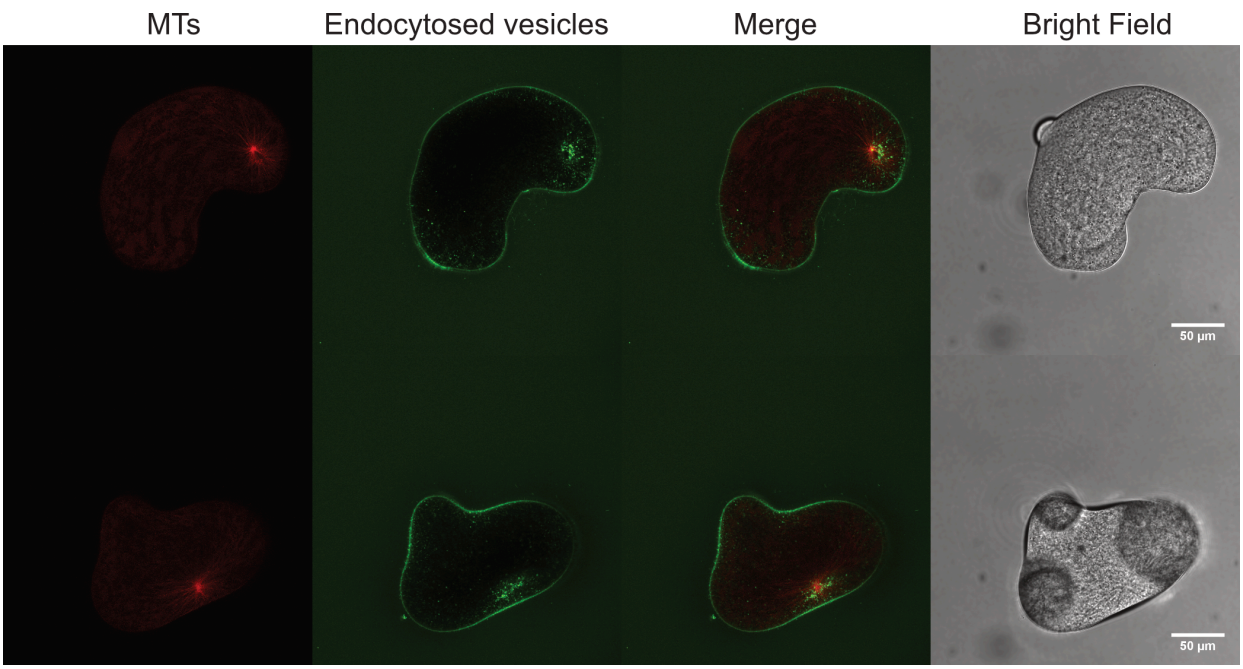

Figure 2.11: Effects of 50 µM ciliobrevin D on the zygote.
Confocal images of two zygotes treated with 50 µM ciliobrevin D. MT are in red (leftmost column), vesicles endocytosed from the membrane that were labeled to assess the presence of minus-end directed transport are in green (second column from the left), the merge is shown on the third column, and the associated BF on the rightmost column. Scale bar is 50 µm.

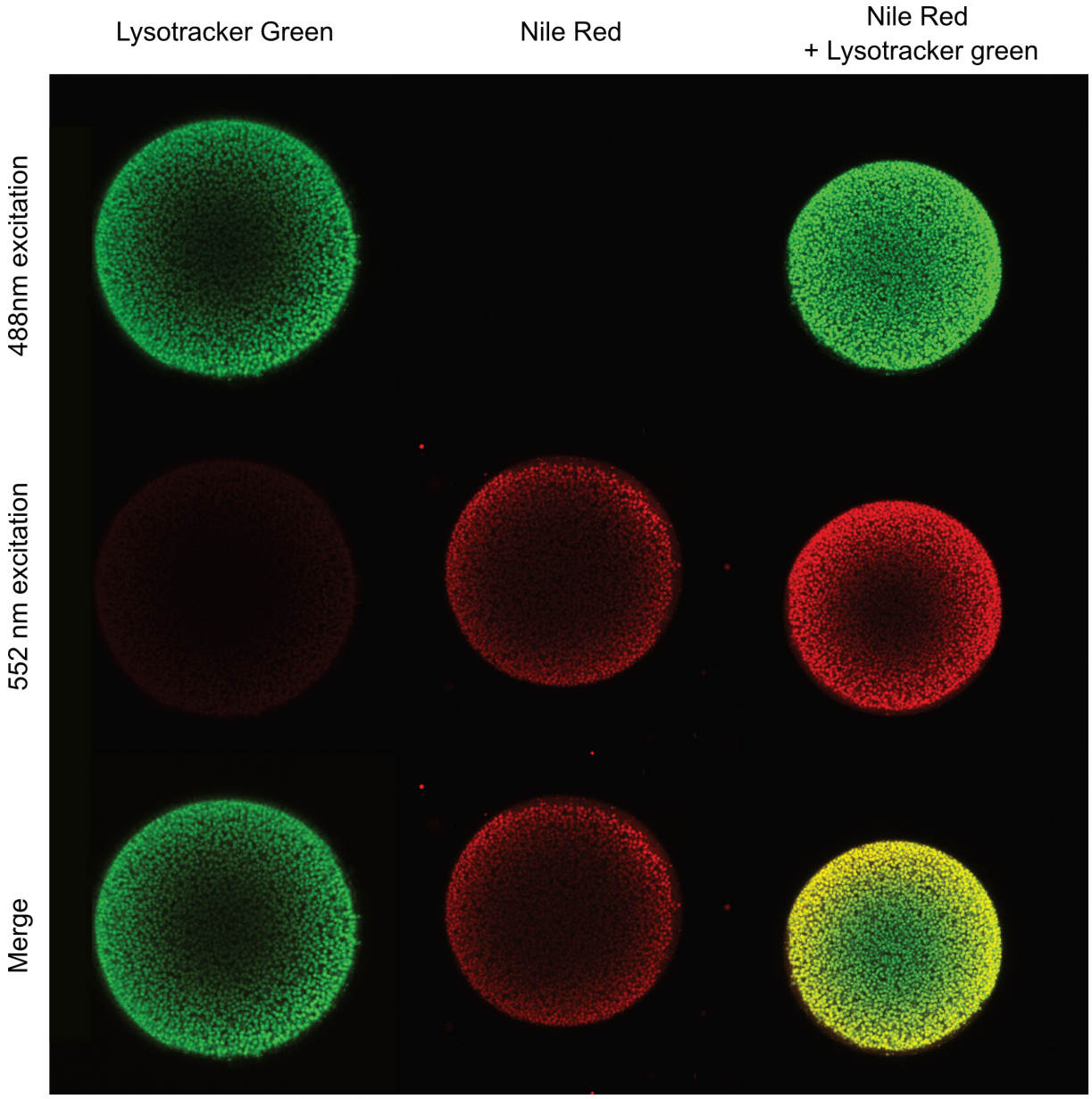

Figure 2.12: Comparison of the yolk labels
Confocal images of live eggs stained with, Lysotracker green, Nile Red, or both, and imaged with different wavelength of excitation. Images captured after 488 nm excitation are in green (first row), images captured after 552nm excitation are in red (second row), and the merge of both pictures in their respective colors is shown in the third row.

General conclusion

The thesis general aim was to understand how the spindle positions in the zygote and how it interacts with the other cellular components, especially with the yolk, to get a better understanding of the basic mechanisms susceptible of being involved in spindle positioning throughout the whole embryo segmentation. Accordingly, two objectives were defined; 1- find the mechanism(s) that position the spindle in the zygote**,** 2- find the mechanism(s) by which the yolk and spindle are segregated from each other.

Conclusion on the objectives

To answer the first objective and find the mechanisms of spindle positioning, I first described the process of aster migration and tested the contribution in aster and spindle centration of three known mechanisms: cytoplasmic pulling, cortical pushing and cortical pulling. With this approach I discovered that each mechanism is involved in the aster migration throughout the first cell cycle, and that mitosis entry, driven by increasing CDK1/CycB activity, causes the arrest of cortical pulling and therefore allows the centering of the spindle by cytoplasmic pulling. However, the trajectory of a spindle centering by cytoplasmic pulling does not exactly fit the migration trajectory observed. This suggests that the complete mechanism of centration has not been deciphered. I propose that, in addition to the major role of cytoplasmic pulling, a second element participates in the spindle centration. Based on numerical simulation and preliminary data, I propose that this second mechanism may be a spatio-temporal regulation of the cortical pulling at the moment of mitosis entry. This could be achieved by a local activation of CDK1/CycB that decreases the cortical actin and propagates through the cell, much like in the phenomenon of the SCW. The data concerning this complementary mechanism could be either developed to pursue this project on spindle centration or used to build an interesting stand-alone project about a SCW in the ascidian zygote. With the discovery of the contraction wave, a second hypothesis appears; the zygote contraction in mitosis could create

cytoplasmic flows that may displace the spindle. However, this avenue has not yet been investigated. Lastly, even though the centration mechanism is partially understood the question of the spindle orientation remains unresolved. I hypothesized that the presence of a MT repulsive domain at the vegetal pole may be sufficient to guide the spindle orientation.

Concerning the second objective, I studied the formation of a region of yolk exclusion around the sperm aster in different conditions in order to find the mechanism(s) by which the yolk and spindle are segregated from each other. I found that the yolk granules (YGs) distribution is the complement of the endomembranous system localization. Microdomains of yolk exclusion are associated with ER clusters, and the main yolk exclusion zone around the sperm aster was found to depend on the accumulation of endomembranous compartment. Hence, I suggested that the mechanism that reshapes YGs localization is based on the attachment of dynein on organelles, such as the ER, and on the absence of dynein interaction with YGs, leading to an ER accumulation at the aster driving the progressive exclusion of YGs. With some modifications, this work could generate an article.

The two objectives were partially answered, however the question of spindle position was limited by the depth and the complexity of the project that raised numerous avenues, and the project on the yolk segregation was limited by the tools available. Nevertheless, both objectives led to concrete discoveries and new hypotheses that contribute to a better understanding of how the spindle can move in the cell and interact with its surroundings. Furthermore, since the actors studied here in the ascidian are quite universal (yolk, MTs, actin, ER, ...), the new findings described in the manuscript may inspire the research performed on other organisms.

Conclusions on the zygote

I established a model for the aster and spindle migration in the ascidian zygote without having to include the yolk in the story. Reciprocally, the formation of the yolk segregation from the aster is independent of the aster migration, although yolk localization correlates inversely with the aster and spindle position. Thus, it seems that at the zygotic stage the yolk segregation does not influence the spindle position. However, the accumulation of ER at the aster could be crucial in the aster migration since it may change aster properties (Sami & Gatlin, 2022). And

a proper ER accumulation could rely, in turn, on the precise regulation of the amount of yolk near the aster (Shimogama et al., 2022). The yolk also has an important background role; it crowds the cytoplasm and therefore likely participates to mechanical properties of the cytoplasm such as its viscosity or compressibility (Shamipour et al., 2019). Cytoplasm viscosity is a key element in the cytoplasmic pulling model since the pulling force created by the organelles transport depends on the dragging force of each organelle (Tanimoto et al., 2018). In addition, I still have not ruled out whether a cytoplasmic streaming following the zygote change of shape could affect spindle position. One could wonder whether the presence of yolk in the cell can affect cytoplasmic flows as well. In this context, aster and spindle migration are linked through the mechanical properties of the cytoplasm.

On the opposite extreme, in zebrafish or *Xenopus Laevis*, which are known to have a dense yolk, yolk localization limits spindle position (Pierre et al., 2016). It would be interesting to find what are the thresholds, probably in terms of yolk density or yolk compaction, that determine how restrictive the yolk is toward the spindle movement, and thus that influence directly the cleavage pattern of early embryos.

The ascidian zygote happened to be an interesting and challenging system. Indeed, many events and elements superimpose in a short time period. At NEB especially, when the spindle centers, a contraction wave appears, the myoplasm reshapes while embryo axes are already defined and the cell cycle continues. This gives an opportunity to investigate both the inter-dependency of all processes together at the whole cellular scale, and to study specific interactions that are not always seen in other models, like the actin cortex dynamics and the aster centration, or the formation of the anterio-posterior axis and spindle orientation, etc... The downsides are that any perturbation affects simultaneously many processes and that the number of elements to take into account to study one phenomenon is considerable. Nonetheless, my present work on *P. mammillata* zygote was necessary to fill a gap in our knowledge of the ascidian development. Indeed, the oocyte's reorganization and fertilization, as well as the first contractions were previously described (Roegiers et al., 1995, 1999; Sardet et al., 1989; Sawada & Osanai, 1981; Yoshida et al., 2003), as were the cleavage pattern (Hotta et al., 2007) and noticeable events that dictate this pattern (McDougall et al., 2019; Nishikata et al., 1999; Prodon et al., 2010), but the knowledge about the ascidian zygote during mitosis was scarce and often especially focused on the myoplasm reorganization (Ishii et al., 2017; Roegiers et al., 1999). This latter point may actually differ according to the ascidian species studied since results on

the presence of a MT cortical array that moves the myoplasm in *Ciona* may not be reproducible in *P. mammillata* (see Chapter 1 Discussion). I used the term ascidian zygote for convenience to talk about *P. mammillata* zygote development, but note that it may be inaccurate because of potential differences between ascidian zygotes.

Conclusions on the embryo

The initial reason for studying the zygote was to find basic mechanisms that could be involved in positioning the spindle to shape the embryo during cleavage division. I found that spindle position in the zygote is independent of the yolk. However, given the uncovered mechanism of yolk segregation that relies on a progressive accumulation of organelles at the aster, and the observation of an increasingly drastic segregation at each cell cycle, I hypothesize that the yolk becomes more compacted throughout development. While yolk segregation is increasingly drastic, the yolk is also more and more localized at the basolateral side of blastomeres (section 2.1, Figure 2.2). During the whole segmentation, thus until gastrulation, all cells possess an apical side, and it has been shown that the spindle aligns with the longest axis of the apical side (Dumollard et al., 2017). Thus, the presence of a compact yolk mass near the basolateral cortex could influence spindle position at the apical side. Whether a compacted yolk could influence the spindle position is unknown but it brings back the idea of testing yolk properties to find criterion of the yolk capacity to constrain the spindle position. Yolk quantity can be determined in different cells and at different stages thanks to the intensity and shape of a yolk fluorescent label. Cytoplasm viscosity in areas containing yolk could be measured by the injection of a magnetic bead of large enough size and the estimation of the forces required to move the bead (Hiramoto, 1969; Tanimoto et al., 2018), or by measurement of the YGs mean square displacement (Khatri et al., 2022). Yolk distribution could also be, like in the zygote, a simple consequence of the apical localization of the spindle. Indeed, at least until 32-cell stage, the nuclei migrate from the site of cytokinesis towards the apical surface of the blastomeres during interphase (unpublished data). The migration is more obvious in smaller cells where nuclei reach the cell surface. According to what was found in the zygote in interphase, the nuclei may migrate towards the surface by cortical pulling. This must be confirmed, and further explanation about how nuclei target the apical membrane and not the basolateral membrane are required. It is interesting to note that nuclei leave the cortex in prophase, much like in the zygote. Furthermore, unlike what was found in other species, the blastomeres of *P.mammillata*

undergo a mitotic rounding while decreasing cell tension, and not increasing cell tension (Godard et al., 2020). This is also consistent with zygote development where a cortical relaxation wave was found at mitosis entry. One open question is how entry into mitosis leads to less cortical tension. This question may be easier to address in the zygote than in embryos since the zygote offers a larger and thus more accessible surface, and also more time (due to meiosis) to set the experiments before the entry into interphase and then into mitosis. Finally, I hypothesized the presence of a MT-repulsive domain in the zygote similar to that found in 4-cell stage embryos (Godard et al., 2021). It would be interesting to extend this idea to assess how a MT-repulsive domain could affect the whole ascidian cleavage pattern, and to study when this domain is active, whether it is a permanent or transient domain, and what it is made of. In brief, some cues coming from my work on the zygote can be exploited to further investigate spindle position during embryo cleavage stages, as well as other events such as mitotic softening. The nuclei migration during interphase of the cleavage stages seems to be especially consistent with a cell cycle regulated cortical pulling mechanism and is an interesting candidate to explore further for the question of spindle positioning throughout ascidian embryo cleavage cycles.

In few words

In conclusion, my thesis work provides an overview of the events involving the sperm aster and the spindle at the cellular-scale in *P.mammillata* zygote. This overview sheds light on ascidian early development. The precise cellular mechanisms I discovered answered my initial aims only partially, but they generated concrete results that contribute to a better understanding of the mechanisms of spindle positioning. Moreover, these results are exploitable and comparable to other species thanks to the universality of the elements studied. Finally, many precise research paths stem from preliminary data and hypotheses proposed throughout this manuscript.

References

Abreu, L. A., Valle, D., Manso, P. P. A., Façanha, A. R., Pelajo-Machado, M., Masuda, H., Masuda, A., Vaz, I., Lenzi, H., Oliveira, P. L., & Logullo, C. (2004). Proteolytic activity of Boophilus microplus Yolk pro-Cathepsin D (BYC) is coincident with cortical acidification during embryogenesis. *Insect Biochemistry and Molecular Biology*, *34*(5), 443–449. https://doi.org/10.1016/J.IBMB.2004.01.006

Akasaka, M., Kato, K. H., Kitajima, K., & Sawada, H. (2013). Identification of novel isoforms of vitellogenin expressed in ascidian eggs. *Journal of Experimental Zoology Part B: Molecular and Developmental Evolution*, *320*(2), 118–128. https://doi.org/10.1002/jez.b.22488

Alberts, B. (2014). Molecular biology of the cell. *Alberts - Molecular Biology o of the Cell*, *5*, 406.

Alberts, B., Bray, D., Hopkins, K., Johnson, A., Lewis, J., Raff, M., Roberts, K., & Walter, P. (2014). Essential Cell Biology Essential Cell Biology. *Garland Science*, 728.

Alié, A., Hiebert, L. S., Simion, P., Scelzo, M., Prünster, M. M., Lotito, S., Delsuc, F., Douzery, E. J. P., Dantec, C., Lemaire, P., Darras, S., Kawamura, K., Brown, F. D., & Tiozzo, S. (2018). Convergent Acquisition of Nonembryonic Development in Styelid Ascidians. *Molecular Biology and Evolution*, *35*(7), 1728–1743. https://doi.org/10.1093

Amiel, A., & Houliston, E. (2009). Three distinct RNA localization mechanisms contribute to oocyte polarity establishment in the cnidarian Clytia hemisphærica. *Developmental Biology*, *327*(1), 191–203. https://doi.org/10.1016/J.YDBIO.2008.12.007

Anton, M. (2013). Egg yolk: Structures, functionalities and processes. *Journal of the Science of Food and Agriculture*, *93*(12), 2871–2880. https://doi.org/10.1002/JSFA.6247

Ban, S., Harada, Y., Yokosawa, H., & Sawada, H. (2005). Highly polymorphic vitelline-coat protein HaVC80 from the ascidian, Halocynthia aurantium: Structural analysis and involvement in self/nonself recognition during fertilization. *Developmental Biology*, *286*(2), 440–451. https://doi.org/10.1016/J.YDBIO.2005.08.004

Berg, W. E., & Humphreys, W. J. (1960). Electron microscopy of four-cell stages of the ascidians Ciona and Styela. *Developmental Biology*, *2*(1), 42–60. https://doi.org/10.1016/0012-1606(60)90015-4

Bezanilla, M., & Wadsworth, P. (2009). Spindle Positioning: Actin Mediates Pushing and Pulling. *Current Biology*, *19*(4), R168–R169. https://doi.org/10.1016/J.CUB.2008.12.026

Bhavsar-Jog, Y. P., & Bi, E. (2017). Mechanics and regulation of cytokinesis in budding yeast. *Seminars in Cell & Developmental Biology*, *66*, 107. https://doi.org/10.1016/J.SEMCDB.2016.12.010

Bischof, J., Brand, C. A., Somogyi, K., Májer, I., Thome, S., Mori, M., Schwarz, U. S., & Lénárt, P. (2017). A cdk1 gradient guides surface contraction waves in oocytes. *Nature Communications 2017 8:1*, *8*(1), 1–10. https://doi.org/10.1038/s41467-017-00979-6

Bosveld, F., Markova, O., Guirao, B., Martin, C., Wang, Z., Pierre, A., Balakireva, M., Gaugue, I., Ainslie, A., Christophorou, N., Lubensky, D. K., Minc, N., & Bellaiche, Y. (2016). Epithelial tricellular junctions act as interphase cell shape sensors to orient mitosis. *Nature*, *530*(7591), 495–498. https://doi.org/10.1038/NATURE16970

Bun, P., Liu, J., Turlier, H., Liu, Z., Uriot, K., Joanny, J. F., & Coppey-Moisan, M. (2014). Mechanical checkpoint for persistent cell polarization in adhesion-naive fibroblasts. *Biophysical Journal*, *107*(2), 324–335. https://doi.org/10.1016/j.bpj.2014.05.041

Chaigne, A., Campillo, C., Voituriez, R., Gov, N. S., Sykes, C., Verlhac, M. H., & Terret, M. E. (2016). F-actin mechanics control spindle centring in the mouse zygote. *Nature Communications 2016 7:1*, *7*(1), 1–14. https://doi.org/10.1038/ncomms10253

Chambon, J.-P., Touati, S. A., Berneau, S., Cladière, D., Hebras, C., Groeme, R., McDougall, A., & Wassmann, K. (2013). The PP2A Inhibitor I2PP2A Is Essential for Sister Chromatid Segregation in Oocyte Meiosis II. *Current Biology*, *23*(6), 485–490. https://doi.org/10.1016/j.cub.2013.02.004

Chenevert, J., Roca, M., Besnardeau, L., Ruggiero, A., Nabi, D., McDougall, A., Copley, R. R., Christians, E., & Castagnetti, S. (2020). The Spindle Assembly Checkpoint Functions during Early Development in Non-Chordate Embryos. *Cells 2020, Vol. 9, Page 1087*, *9*(5), 1087. https://doi.org/10.3390/CELLS9051087

Chugh, P., & Paluch, E. K. (2018). The actin cortex at a glance. *Journal of Cell Science*, *131*(14). https://doi.org/10.1242/JCS.186254/56817

Conklin, E. G. (1905a). *The Organization and Cell-lineage of the Ascidian Egg* (Academy of Natural Science, Ed.). Université du Michigan.

Conklin, E. G. (1905b). Mosaic development in ascidian eggs. *Journal of Experimental Zoology*, *2*(2), 145–223. https://doi.org/10.1002/JEZ.1400020202

Cooper, G. M., & Hausman, R. (2013). *The Cell: A Molecular Approach*. 832.

Costache, V., Hebras, C., Pruliere, G., Besnardeau, L., Failla, M., Copley, R. R., Burgess, D., Chenevert, J., & McDougall, A. (2017). Kif2 localizes to a subdomain of cortical endoplasmic reticulum that drives asymmetric spindle position. *Nature Communications*, *8*(1). https://doi.org/10.1038/s41467-017-01048-8

Cuvier, G. L. (1815). *Memoire sur les ascidies et sur leur anatomique*. Mem. Mus. Hist. Nat. Paris 2.

Davidson, P. M., & Cadot, B. (2021). Actin on and around the Nucleus. *Trends in Cell Biology*, *31*(3), 211–223. https://doi.org/10.1016/J.TCB.2020.11.009

D'Avino, P. P., Giansanti, M. G., & Petronczki, M. (2015). Cytokinesis in animal cells. *Cold Spring Harbor Perspectives in Biology*, *7*(4). https://doi.org/10.1101/CSHPERSPECT.A015834

De Simone, A., Spahr, A., Busso, C., & Gönczy, P. (2018). Uncovering the balance of forces driving microtubule aster migration in C. elegans zygotes. *Nature Communications 2018 9:1*, *9*(1), 1–9. https://doi.org/10.1038/s41467-018-03118-x

Delsuc, F., Philippe, H., Tsagkogeorga, G., Simion, P., Tilak, M. K., Turon, X., López-Legentil, S., Piette, J., Lemaire, P., & Douzery, E. J. P. (2018). A phylogenomic framework and timescale for comparative studies of tunicates. *BMC Biology*, *16*(1). https://doi.org/10.1186/S12915-018-0499-2

Desnitskiy, A. G., & Litvinchuk, S. N. (2015). Comparative and phylogenetic perspectives of the cleavage process in tailed amphibians. *Zygote*, *23*(5), 722–731. https://doi.org/10.1017/S0967199414000379

di Pietro, F., Echard, A., & Morin, X. (2016). Regulation of mitotic spindle orientation: an integrated view. *EMBO Reports*, *17*(8), 1106–1130. https://doi.org/10.15252/embr.201642292

Dobrzynska, A., Gonzalo, S., Shanahan, C., & Askjaer, P. (2016). The nuclear lamina in health and disease. *Http://Dx.Doi.Org/10.1080/19491034.2016.1183848*, *7*(3), 233–248. https://doi.org/10.1080/19491034.2016.1183848

Dogterom, M., Kerssemakers, J. W. J., Romet-Lemonne, G., & Janson, M. E. (2005). Force generation by dynamic microtubules. *Current Opinion in Cell Biology*, *17*(1), 67–74. https://doi.org/10.1016/J.CEB.2004.12.011

Dumollard, R., Levasseur, M., Hebras, C., Huitorel, P., Carroll, M., Chambon, J.-P., & McDougall, A. (2011). Mos limits the number of meiotic divisions in urochordate eggs. *Development*, *138*(5), 885–895. https://doi.org/10.1242/dev.057133

Dumollard, R., Minc, N., Salez, G., Aicha, S. Ben, Bekkouche, F., Hebras, C., Besnardeau, L., & McDougall, A. (2017). The invariant cleavage pattern displayed by ascidian embryos depends on spindle positioning along the cell's longest axis in the apical plane and relies on asynchronous cell divisions. *ELife*, *6*. https://doi.org/10.7554/eLife.19290

Dunkley, S., Scheffler, K., & Mogessie, B. (2022). Cytoskeletal form and function in mammalian oocytes and zygotes. *Current Opinion in Cell Biology*, *75*, 102073. https://doi.org/10.1016/J.CEB.2022.02.007

Esposito, R., Yasuo, H., Sirour, C., Palladino, A., Spagnuolo, A., & Hudson, C. (2017). Patterning of brain precursors in ascidian embryos. *Development*, *144*(2), 258–264. https://doi.org/10.1242/dev.142307

Etienne-Manneville, S. (2018). Cytoplasmic Intermediate Filaments in Cell Biology. *Https://Doi.Org/10.1146/Annurev-Cellbio-100617-062534*, *34*, 1–28. https://doi.org/10.1146/ANNUREV-CELLBIO-100617-062534

Fagotto, F. (1995). Regulation of yolk degradation, or how to make sleepy lysosomes. In *Journal of Cell Science* (Vol. 108, Issue 12, pp. 3645–3647). https://doi.org/10.1242/jcs.108.12.3645

Fagotto, F., & Maxfield, F. R. (1994). Changes in yolk platelet pH during Xenopus laevis development correlate with yolk utilization. A quantitative confocal microscopy study. *Journal of Cell Science*, *107 (Pt 12)*(12), 3325–3337. https://doi.org/10.1242/JCS.107.12.3325

Finegan, T. M., Na, D., Cammarota, C., Skeeters, A. V, Nádasi, T. J., Dawney, N. S., Fletcher, A. G., Oakes, P. W., & Bergstralh, D. T. (2019). Tissue tension and not interphase cell shape determines cell division orientation in the Drosophila follicular epithelium. *The EMBO Journal*, *38*(3), e100072. https://doi.org/10.15252/embj.2018100072

Fisher, J.-L., & Smith, J. (1984). FRENCH EMBRYOLOGY AND THE « MECHANICS OF DEVELOPMENT » FROM 1887 TO 1910: L. CHABRY, Y. DELAGE & E. BATAILLON on JSTOR. In *History and Philosophy of the Life Sciences* (no. 1, Vol. 6, pp. 25–39). Anton Dohrn . https://www.jstor.org/stable/23328333#metadata_info_tab_contents

Formery, L., Wakefield, A., Gesson, M., Toisoul, L., Lhomond, G., Gilletta, L., Lasbleiz, R., Schubert, M., & Croce, J. C. (2022). Developmental atlas of the indirect-developing sea urchin Paracentrotus lividus: From fertilization to juvenile stages. *Frontiers in Cell and Developmental Biology*, *10*. https://doi.org/10.3389/FCELL.2022.966408

Foucrier, J., Franquinet, Raphaël., & Vervoort, Michel. (2019). *Atlas d'embryologie descriptive* (4th ed.).

Franchet, C., Goudeau, M., & Goudeau, H. (1997). Mercuric Ions Impair the Fertilization Potential, the Resumption of Meiosis, the Formation of Male Pronucleus, and Increase Polyspermy, in the Egg of the Ascidian Phallusia mammillata. *The Journal Of Experimental Zoology*, *278*, 255–272. https://doi.org/10.1002/(SICI)1097-010X(19970701)278:4

Fujii, Y., Koizumi, W. C., Imai, T., Yokobori, M., Matsuo, T., Oka, K., Hotta, K., & Okajima, T. (2021). Spatiotemporal dynamics of single cell stiffness in the early developing ascidian chordate embryo. *Communications Biology 2021 4:1*, *4*(1), 1–12. https://doi.org/10.1038/s42003-021-01869-w

G., J. (1928). Experimental Embryology. *Nature 1928 122:3078*, *122*(3078), 640–641. https://doi.org/10.1038/122640b0

Gilbert, S. F., & Barresi, M. J. F. (2016). *Developmental biology* (11th ed.).
Glotzer, M. (2004). Cleavage furrow positioning. In *Journal of Cell Biology* (Vol. 164, Issue 3, pp. 347–351). The Rockefeller University Press. https://doi.org/10.1083/jcb.200310112
Godard, B. G., Dumollard, R., Heisenberg, C. P., & McDougall, A. (2021). Combined effect of cell geometry and polarity domains determines the orientation of unequal division. *ELife*, *10*. https://doi.org/10.7554/ELIFE.75639
Godard, B. G., Dumollard, R., Munro, E., Chenevert, J., Hebras, C., McDougall, A., & Heisenberg, C. P. (2020). Apical Relaxation during Mitotic Rounding Promotes Tension-Oriented Cell Division. *Developmental Cell*, *55*(6), 695-706.e4. https://doi.org/10.1016/J.DEVCEL.2020.10.016
Godsave, S. F., Anderton, B. H., Heasman, J., & Wylie, C. C. (1984). Oocytes and early embryos of Xenopus laevis contain intermediate filaments which react with anti-mammalian vimentin antibodies. *Development*, *83*(1), 169–187. https://doi.org/10.1242/DEV.83.1.169
Gomes, I. D. L., Gazo, I., Besnardeau, L., Hebras, C., McDougall, A., & Dumollard, R. (2019). Potential roles of nuclear receptors in mediating neurodevelopmental toxicity of known endocrine-disrupting chemicals in ascidian embryos. *Molecular Reproduction and Development*, *86*(10), 1333–1347. https://doi.org/10.1002/MRD.23219
Goodbody, I. (1975). The Physiology of Ascidians. *Advances in Marine Biology*, *12*(C), 1–149. https://doi.org/10.1016/S0065-2881(08)60457-5
Goto, T., Kanda, K., & Nishikata, T. (2019). Non-centrosomal microtubule structures regulated by egg activation signaling contribute to cytoplasmic and cortical reorganization in the ascidian egg. *Developmental Biology*, *448*(2), 161–172. https://doi.org/10.1016/J.YDBIO.2018.10.014
Goto, T., Torii, S., Kondo, A., Kanda, K., Kawakami, J., Kataoka, Y., & Nishikata, T. (2022). Actin Filament in the First Cell Cycle Contributes to the Determination of the Anteroposterior Axis in Ascidian Development. *Journal of Developmental Biology*, *10*(1). https://doi.org/10.3390/JDB10010010
Gotta, M., Dong, Y., Peterson, Y. K., Lanier, S. M., & Ahringer, J. (2003). Asymmetrically Distributed C. elegans Homologs of AGS3/PINS Control Spindle Position in the Early Embryo. *Current Biology*, *13*(12), 1029–1037. https://doi.org/10.1016/S0960-9822(03)00371-3
Grill, S. W., Gönczy, P., Stelzer, E. H. K., & Hyman, A. A. (2001). Polarity controls forces governing asymmetric spindle positioning in the Caenorhabditis elegans embryo. *Nature*, *409*(6820), 630–633. https://doi.org/10.1038/35054572
Guevorkian, K., & Maître, J. L. (2017). Micropipette aspiration: A unique tool for exploring cell and tissue mechanics in vivo. *Methods in Cell Biology*, *139*, 187–201. https://doi.org/10.1016/BS.MCB.2016.11.012
Guignard, L., Fiúza, U. M., Leggio, B., Laussu, J., Faure, E., Michelin, G., Biasuz, K., Hufnagel, L., Malandain, G., Godin, C., & Lemaire, P. (2020). Contact area-dependent cell communication and the morphological invariance of ascidian embryogenesis. *Science*, *369*(6500). https://doi.org/10.1126/SCIENCE.AAR5663/SUPPL_FILE/AAR5663_S4.MOV
Hagting, A., Karlsson, C., Clute, P., Jackman, M., & Pines, J. (1998). MPF localization is controlled by nuclear export. *The EMBO Journal*, *17*(14), 4127–4138. https://doi.org/10.1093/EMBOJ/17.14.4127
Hamaguchi, M. S., Hamaguchi, Y., & Hiramoto, Y. (1986). Microinjected Polystyrene Beads Move Along Astral Rays in Sand Dollar Eggs. *Development, Growth and Differentiation*, *28*(5), 461–470. https://doi.org/10.1111/j.1440-169X.1986.00461.x

Harant, H., & Vernières, P. (1933). *Faune De France N° 27, Tuniciers: Vol. Fascicule 1 : Ascidie*

Hibino, T., Nishikata, T., & Nishida, H. (1998). Centrosome-attracting body: A novel structure closely related to unequal cleavages in the ascidian embryo. *Development Growth and Differentiation*, *40*(1), 85–95. https://doi.org/10.1046/J.1440-169X.1998.T01-5-00010.X

Hiramatsu, N., Todo, T., Sullivan, C. V., Schilling, J., Reading, B. J., Matsubara, T., Ryu, Y. W., Mizuta, H., Luo, W., Nishimiya, O., Wu, M., Mushirobira, Y., Yilmaz, O., & Hara, A. (2015). Ovarian yolk formation in fishes: Molecular mechanisms underlying formation of lipid droplets and vitellogenin-derived yolk proteins. *General and Comparative Endocrinology*, *221*, 9–15. https://doi.org/10.1016/J.YGCEN.2015.01.025

Hiramoto, Y. (1969). Mechanical properties of the protoplasm of the sea urchin egg: II. Fertilized egg. *Experimental Cell Research*, *56*(2–3), 209–218. https://doi.org/10.1016/0014-4827(69)90004-4

Holy, T. E., Dogterom, M., Yurke, B., & Leibler, S. (1997). Assembly and positioning of microtubule asters in microfabricated chambers. *Proceedings of the National Academy of Sciences of the United States of America*, *94*(12), 6228–6231. https://doi.org/10.1073/pnas.94.12.6228

Honegger, T. G., & Koyanagi, R. (2008). The ascidian egg envelope in fertilization: structural and molecular features. *The International Journal of Developmental Biology*, *52*(5–6), 527–533. https://doi.org/10.1387/IJDB.072547TH

Hotta, K., Dauga, D., & Manni, L. (2020). The ontology of the anatomy and development of the solitary ascidian Ciona: the swimming larva and its metamorphosis. *Scientific Reports 2020 10:1*, *10*(1), 1–16. https://doi.org/10.1038/s41598-020-73544-9

Hotta, K., Mitsuhara, K., Takahashi, H., Inaba, K., Oka, K., Gojobori, T., & Ikeo, K. (2007). A web-based interactive developmental table for the ascidian Ciona intestinalis, including 3D real-image embryo reconstructions: I. From fertilized egg to hatching larva. *Developmental Dynamics*, *236*(7), 1790–1805. https://doi.org/10.1002/DVDY.21188

Ikenouchi, J., & Aoki, K. (2022). A Clockwork Bleb: cytoskeleton, calcium, and cytoplasmic fluidity. *The FEBS Journal*, *289*(24), 7907–7917. https://doi.org/10.1111/FEBS.16220

Ishii, H., Goto, T., & Nishikata, T. (2017). Microtubule array observed in the posterior-vegetal cortex during cytoplasmic and cortical reorganization of the ascidian egg. *Development, Growth & Differentiation*, *59*(8), 648–656. https://doi.org/10.1111/DGD.12405

Ishii, H., Shirai, T., Makino, C., & Nishikata, T. (2014). Mitochondrial inhibitor sodium azide inhibits the reorganization of mitochondria-rich cytoplasm and the establishment of the anteroposterior axis in ascidian embryo. *Development Growth and Differentiation*, *56*(2), 175–188. https://doi.org/10.1111/dgd.12117

Jackson, C. L. (2019). Lipid droplet biogenesis. *Current Opinion in Cell Biology*, *59*, 88–96. https://doi.org/10.1016/J.CEB.2019.03.018

Jessus, C., Munro, C., & Houliston, E. (2020). Managing the Oocyte Meiotic Arrest—Lessons from Frogs and Jellyfish. *Cells*, *9*(5). https://doi.org/10.3390/CELLS9051150

Jorgensen, P. (2008). Yolk. In *Current Biology* (Vol. 18, Issue 3, pp. R103–R104). Cell Press. https://doi.org/10.1016/j.cub.2007.10.037

Jorgensen, P., Steen, J. A. J., Steen, H., & Kirschner, M. W. (2009). The mechanism and pattern of yolk consumption provide insight into embryonic nutrition in Xenopus. *Development (Cambridge, England)*, *136*(9), 1539. https://doi.org/10.1242/DEV.032425

Kapsenberg, L., Bitter, M. C., Miglioli, A., Aparicio-Estalella, C., Pelejero, C., Gattuso, J. P., & Dumollard, R. (2022). Molecular basis of ocean acidification sensitivity and

adaptation in Mytilus galloprovincialis. *IScience*, *25*(8). https://doi.org/10.1016/J.ISCI.2022.104677

Karasaki, S. (1963). Studies on amphibian yolk: 5. Electron microscopic observations on the utilization of yolk platelets during embryogenesis. *Journal of Ultrastructure Research*, *9*(3–4), 225–247. https://doi.org/10.1016/S0022-5320(63)80004-0

Kawashima, T., Maruyama, D., Shagirov, M., Li, J., Hamamura, Y., Yelagandula, R., Toyama, Y., & Berger, F. (2014). Dynamic F-actin movement is essential for fertilization in Arabidopsis thaliana. *ELife*, *3*. https://doi.org/10.7554/ELIFE.04501

Kelkar, M., Bohec, P., & Charras, G. (2020). Mechanics of the cellular actin cortex: From signalling to shape change. *Current Opinion in Cell Biology*, *66*, 69–78. https://doi.org/10.1016/J.CEB.2020.05.008

Kessel, R. G. (1966). Electron microscope studies on the origin and maturation of yolk in oocytes of the tunicate, Ciona intestinalis. *Zeitschrift Für Zellforschung Und Mikroskopische Anatomie 1966 71:4*, *71*(4), 525–544. https://doi.org/10.1007/BF00349612

Kessel, R. G. (1968). Electron microscope studies on developing oocytes of a coelenterate medusa with special reference to vitellogenesis. *Journal of Morphology*, *126*(2), 211–247. https://doi.org/10.1002/JMOR.1051260205

Khatri, D., Brugière, T., Athale, C. A., & Delattre, M. (2022). Evolutionary divergence of anaphase spindle mechanics in nematode embryos constrained by antagonistic pulling and viscous forces. *Molecular Biology of the Cell*, *33*(6), ar61. https://doi.org/10.1091/MBC.E21-10-0532

Khetan, N., Pruliere, G., Hebras, C., Chenevert, J., & Athale, C. A. (2021). Self-organized optimal packing of kinesin-5-driven microtubule asters scales with cell size. *Journal of Cell Science*, *134*(10). https://doi.org/10.1242/JCS.257543/VIDEO-4

Kimura, K., & Kimura, A. (2011a). Intracellular organelles mediate cytoplasmic pulling force for centrosome centration in the Caenorhabditis elegans early embryo. *Proceedings of the National Academy of Sciences of the United States of America*, *108*(1), 137–142. https://doi.org/10.1073/pnas.1013275108

Kimura, K., & Kimura, A. (2011b). A novel mechanism of microtubule length-dependent force to pull centrosomes toward the cell center. *Bioarchitecture*, *1*(2), 74–79. https://doi.org/10.4161/bioa.1.2.15549

Kimura, K., Mamane, A., Sasaki, T., Sato, K., Takagi, J., Niwayama, R., Hufnagel, L., Shimamoto, Y., Joanny, J. F., Uchida, S., & Kimura, A. (2017). Endoplasmic-reticulum-mediated microtubule alignment governs cytoplasmic streaming. *Nature Cell Biology 2017 19:4*, *19*(4), 399–406. https://doi.org/10.1038/ncb3490

Ko, C. S., Kalakuntla, P., & Martin, A. C. (2020). Apical Constriction Reversal upon Mitotic Entry Underlies Different Morphogenetic Outcomes of Cell Division. *Molecular Biology of the Cell*, *31*(16), 1663–1674. https://doi.org/10.1091/MBC.E19-12-0673

Kocot, K. M., Tassia, M. G., Halanych, K. M., & Swalla, B. J. (2018). Phylogenomics offers resolution of major tunicate relationships. *Molecular Phylogenetics and Evolution*, *121*, 166–173. https://doi.org/10.1016/J.YMPEV.2018.01.005

Koné, M. (2016). *Nucléologenèse et régulation de l'expression de l'hétérochromatine péricentromérique dans l'embryon précoce de souris*. 203 p

Kroiher, M., Siefker, B., & Berking, S. (2000). Induction of segmentation in polyps of Aurelia aurita (Scyphozoa, Cnidaria) into medusae and formation of mirror-image medusa anlagen. *International Journal of Developmental Biology*, *44*(5), 485–490. https://doi.org/10.1387/IJDB.11032183

Kumano, G., & Nishida, H. (2007). Ascidian embryonic development: An emerging model system for the study of cell fate specification in chordates. *Developmental Dynamics*, *236*(7), 1732–1747. https://doi.org/10.1002/DVDY.21108

Laan, L., Roth, S., & Dogterom, M. (2012). End-on microtubule-dynein interactions and pulling-based positioning of microtubule organizing centers. *Cell Cycle*, *11*(20), 3750–3757. https://doi.org/10.4161/cc.21753

Lacroix, B., & Dumont, J. (2022). Spatial and Temporal Scaling of Microtubules and Mitotic Spindles. *Cells 2022, Vol. 11, Page 248*, *11*(2), 248. https://doi.org/10.3390/CELLS11020248

Lechable, M., Jan, A., Duchene, A., Uveira, J., Weissbourd, B., Gissat, L., Collet, S., Gilletta, L., Chevalier, S., Leclère, L., Peron, S., Barreau, C., Lasbleiz, R., Houliston, E., & Momose, T. (2020). An improved whole life cycle culture protocol for the hydrozoan genetic model Clytia hemisphaerica. *Biology Open*, *9*(11). https://doi.org/10.1242/BIO.051268/266442

Lecuit, T., & Lenne, P. F. (2007). Cell surface mechanics and the control of cell shape, tissue patterns and morphogenesis. *Nature Reviews Molecular Cell Biology 2007 8:8*, *8*(8), 633–644. https://doi.org/10.1038/nrm2222

Levasseur, M., Carroll, M., Jones, K. J., & McDougall, A. (2007). A novel mechanism controls the Ca2+ oscillations triggered by activation of ascidian eggs and has an absolute requirement for Cdk1 activity. *Journal of Cell Science*, *120*(10), 1763–1771. https://doi.org/10.1242/JCS.003012

Levasseur, M., & McDougall, A. (2000). Sperm-induced calcium oscillations at fertilisation in ascidians are controlled by cyclin B1-dependent kinase activity. *Development*, *127*(3), 631–641. https://doi.org/10.1242/DEV.127.3.631

Longhini, K. M., & Glotzer, M. (2022). Aurora A and cortical flows promote polarization and cytokinesis by inducing asymmetric ECT-2 accumulation. *ELife*, *11*. https://doi.org/10.7554/ELIFE.83992

Markova, M., Nikolova, V., Chakarova, I., & Zhivkova RS. (2015). Intermediate filament distribution patterns in maturing mouse oocytes and cumulus cells. *Biocell*.

McDougall, A., Chenevert, J., & Dumollard, R. (2012). Cell-Cycle Control in Oocytes and During Early Embryonic Cleavage Cycles in Ascidians. In *International Review of Cell and Molecular Biology* (Vol. 297, pp. 235–264). Elsevier.

McDougall, A., Chenevert, J., Godard, B. G., & Dumollard, R. (2019). Emergence of Embryo Shape During Cleavage Divisions. *Results and Problems in Cell Differentiation*, *68*, 127–154. https://doi.org/10.1007/978-3-030-23459-1_6

McDougall, A., Chenevert, J., Pruliere, G., Costache, V., Hebras, C., Salez, G., & Dumollard, R. (2015). Centrosomes and spindles in ascidian embryos and eggs. In *Methods in Cell Biology* (Vol. 129, pp. 317–339). Elsevier. https://linkinghub.elsevier.com/retrieve/pii/S0091679X15000783

McDougall, A., Lee, K. W., & Dumollard, R. (2014a). Microinjection and 4D Fluorescence Imaging in the Eggs and Embryos of the Ascidian Phallusia mammillata. In D. J. Carroll & S. A. Stricker (Eds.), *Developmental Biology of the Sea Urchin and Other Marine Invertebrates: Methods and Protocols* (pp. 175–185). Humana Press. https://doi.org/10.1007/978-1-62703-974-1_11

McDougall, A., & Levasseur, M. (1998). Sperm-triggered calcium oscillations during meiosis in ascidian oocytes first pause, restart, then stop: Correlations with cell cycle kinase activity. *Development*, *125*(22), 4451–4459.

McDougall, A., & Sardet, C. (1995). Function and characteristics of repetitive calcium waves associated with meiosis. *Current Biology*, *5*(3), 318–328. https://doi.org/10.1016/S0960-9822(95)00062-5

McNally, K. L., Martin, J. L., Ellefson, M., & McNally, F. J. (2010). Kinesin-dependent transport results in polarized migration of the nucleus in oocytes and inward movement of yolk granules in meiotic embryos. *Developmental Biology*, *339*(1), 126–140. https://doi.org/10.1016/J.YDBIO.2009.12.021

Meaders, J. L., de Matos, S. N., & Burgess, D. R. (2020). A Pushing Mechanism for Microtubule Aster Positioning in a Large Cell Type. *Cell Reports*, *33*(1). https://doi.org/10.1016/j.celrep.2020.108213

Minc, N., Burgess, D., & Chang, F. (2011). Influence of Cell Geometry on Division-Plane Positioning. *Cell*, *144*(3), 414–426. https://doi.org/10.1016/j.cell.2011.01.016

Minin, A. A. (1997). Dispersal of Golgi apparatus in nocodazole-treated fibroblasts is a kinesin-driven process. *Journal of Cell Science*, *110*(19), 2495–2505. https://doi.org/10.1242/JCS.110.19.2495

Mitchinson, J. M., & Swann, M. M. (1954). The Mechanical Properties of the Cell Surface I. The Cell Elastimeter. *Journal of Experimental Biology*, *31*(3), 443–460. https://doi.org/10.1242/JEB.31.3.443

Mitchison, T., & Kirschner, M. (1984). Dynamic instability of microtubule growth. *Nature*, *312*(5991), 237–242. https://doi.org/10.1038/312237a0

Mogessie, B., & Schuh, M. (2017). Actin protects mammalian eggs against chromosome segregation errors. *Science (New York, N.Y.)*, *357*(6353). https://doi.org/10.1126/SCIENCE.AAL1647

Morgan, T. H. (1927). *Experimental embryology*. Columbia University Press,.

Mukherjee, R. N., Sallé, J., Dmitrieff, S., Nelson, K., Oakey, J., Minc, N., & Levy, D. L. (2019). The perinuclear ER scales nuclear size independently of cell size in early embryos. *BioRxiv*, 818724. https://doi.org/10.1101/818724

Negishi, T., Takada, T., Kawai, N., & Nishida, H. (2007). Localized PEM mRNA and Protein Are Involved in Cleavage-Plane Orientation and Unequal Cell Divisions in Ascidians. *Current Biology*, *17*(12), 1014–1025. https://doi.org/10.1016/j.cub.2007.05.047

Negishi, T., & Yasuo, H. (2015). Distinct modes of mitotic spindle orientation align cells in the dorsal midline of ascidian embryos. *Developmental Biology*, *408*(1), 66–78. https://doi.org/10.1016/j.ydbio.2015.09.019

Newport, J., & Kirschner, M. (1982). A major developmental transition in early xenopus embryos: I. characterization and timing of cellular changes at the midblastula stage. *Cell*, *30*(3), 675–686. https://doi.org/10.1016/0092-8674(82)90272-0

Nishida, H. (1987). Cell lineage analysis in ascidian embryos by intracellular injection of a tracer enzyme: III. Up to the tissue restricted stage. *Developmental Biology*, *121*(2), 526–541. https://doi.org/10.1016/0012-1606(87)90188-6

Nishida, H. (2002). Specification of developmental fates in ascidian embryos: Molecular approach to maternal determinants and signaling molecules. *International Review of Cytology*, *217*, 227–276. https://doi.org/10.1016/S0074-7696(02)17016-1

Nishida, H. (2005). Specification of embryonic axis and mosaic development in ascidians. *Developmental Dynamics*, *233*(4), 1177–1193. https://doi.org/10.1002/DVDY.20469

Nishikata, T., Hibino, T., & Nishida, H. (1999). The Centrosome-Attracting Body, Microtubule System, and Posterior Egg Cytoplasm Are Involved in Positioning of Cleavage Planes in the Ascidian Embryo. *Developmental Biology*, *209*(1), 72–85. https://doi.org/10.1006/dbio.1999.9244

Nomura, M., Nakajima, A., & Inaba, K. (2009). Proteomic profiles of embryonic development in the ascidian Ciona intestinalis. *Developmental Biology*, *325*(2), 468–481. https://doi.org/10.1016/j.ydbio.2008.10.038

Patalano, S., Prulière, G., Prodon, F., Paix, A., Dru, P., Sardet, C., & Chenevert, J. (2006). The aPKC–PAR-6–PAR-3 cell polarity complex localizes to the centrosome attracting

body, a macroscopic cortical structure responsible for asymmetric divisions in the early ascidian embryo. *Journal of Cell Science*, *119*(8), 1592–1603. https://doi.org/10.1242/jcs.02873

Pavin, N., & Tolíc-Nørrelykke, I. M. (2013). Dynein, microtubule and cargo: A ménage à trois. *Biochemical Society Transactions*, *41*(6), 1731–1735. https://doi.org/10.1042/BST20130235

Pelletier, J. F., Field, C. M., Fürthauer, S., Sonnett, M., & Mitchison, T. J. (2020). Co-movement of astral microtubules, organelles and f-actin by dynein and actomyosin forces in frog egg cytoplasm. *ELife*, *9*, 1–30. https://doi.org/10.7554/ELIFE.60047

Perez, M. F., & Lehner, B. (2019). Vitellogenins - Yolk Gene Function and Regulation in Caenorhabditis elegans. *Frontiers in Physiology*, *10*, 1067. https://doi.org/10.3389/FPHYS.2019.01067/BIBTEX

Pérez-Mongiovi, D., Chang, P., & Houliston, E. (1998). A propagated wave of MPF activation accompanies surface contraction waves at first mitosis in Xenopus. *Journal of Cell Science*, *111*(3), 385–393. https://doi.org/10.1242/JCS.111.3.385

Petry, S., Groen, A. C., Ishihara, K., Mitchison, T. J., & Vale, R. D. (2013). Branching microtubule nucleation in Xenopus egg extracts mediated by augmin and TPX2. *Cell*, *152*(4), 768–777. https://doi.org/10.1016/J.CELL.2012.12.044

Pierre, A., Sallé, J., Wühr, M., & Minc, N. (2016). Generic Theoretical Models to Predict Division Patterns of Cleaving Embryos. *Developmental Cell*, *39*(6), 667–682. https://doi.org/10.1016/J.DEVCEL.2016.11.018

Postlethwait, J. H., & Giorgi, F. (1985). Vitellogenesis in insects. *Developmental Biology (New York, N.Y. : 1985)*, *1*, 85–126. https://doi.org/10.1007/978-1-4615-6814-8_2/COVER

Prodon, F., Chenevert, J., Hebras, C., Dumollard, R., Faure, E., Gonzalez-Garcia, J., Nishida, H., Sardet, C., & McDougall, A. (2010). Dual mechanism controls asymmetric spindle position in ascidian germ cell precursors. *Development*, *137*(12), 2011–2021. https://doi.org/10.1242/dev.047845

Prodon, F., Chenevert, J., & Sardet, C. (2006). Establishment of animal–vegetal polarity during maturation in ascidian oocytes. *Developmental Biology*, *290*(2), 297–311. https://doi.org/10.1016/J.YDBIO.2005.11.025

Prodon, F., Dru, P., Roegiers, F., & Sardet, C. (2005). Polarity of the ascidian egg cortex and relocalization of cER and mRNAs in the early embryo. *Journal of Cell Science*, *118*(11), 2393–2404. https://doi.org/10.1242/jcs.02366

Prodon, F., Sardet, C., & Nishida, H. (2008). Cortical and cytoplasmic flows driven by actin microfilaments polarize the cortical ER-mRNA domain along the a–v axis in ascidian oocytes. *Developmental Biology*, *313*(2), 682–699. https://doi.org/10.1016/J.YDBIO.2007.11.001

Ramanathan, S. P., Helenius, J., Stewart, M. P., Cattin, C. J., Hyman, A. A., & Muller, D. J. (2015). Cdk1-dependent mitotic enrichment of cortical myosin II promotes cell rounding against confinement. *Nature Cell Biology*, *17*(2), 148–159. https://doi.org/10.1038/NCB3098

Ramos, I., Machado, E., Masuda, H., & Gomes, F. (2022). Open questions on the functional biology of the yolk granules during embryo development. *Molecular Reproduction and Development*, *89*(2), 86–94. https://doi.org/10.1002/MRD.23555

Rankin, S., & Kirschner, M. W. (1997). The surface contraction waves of Xenopus eggs reflect the metachronous cell-cycle state of the cytoplasm. *Current Biology*, *7*(6), 451–454. https://doi.org/10.1016/S0960-9822(06)00192-8

Rappaport, R. (1961). Experiments concerning the cleavage stimulus in sand dollar eggs. *Journal of Experimental Zoology*, *148*(1), 81–89. https://doi.org/10.1002/JEZ.1401480107

Redemann, S., Pecreaux, J., Goehring, N., Khairy, K., Stelzer, E., Hyman, A., & Howard, J. (2010). Membrane Invaginations Reveal Cortical Sites that Pull on Mitotic Spindles in One-Cell C. elegans Embryos. *PloS One*, *5*, e12301. https://doi.org/10.1371/journal.pone.0012301

Reguieg, A., Kupfer, M., & Sittler, A.-P. (2021). *Phallusia mammillata (Cuvier 1815)*.

Reinsch, S., & Gönczy, P. (1998). Mechanisms of nuclear positioning. In *Journal of Cell Science* (Vol. 111, Issue 16, pp. 2283–2295). The Company of Biologists. https://doi.org/10.1242/jcs.111.16.2283

Reymann, A. C., Staniscia, F., Erzberger, A., Salbreux, G., & Grill, S. W. (2016). Cortical flow aligns actin filaments to form a furrow. *ELife*, https://doi.org/10.7554/ELIFE.17807

Riedl, J., Crevenna, A. H., Kessenbrock, K., Yu, J. H., Neukirchen, D., Bista, M., Bradke, F., Jenne, D., Holak, T. A., Werb, Z., Sixt, M., & Wedlich-Soldner, R. (2008). Lifeact: a versatile marker to visualize F-actin. *Nature Methods 2008 5:7*, *5*(7), 605–607. https://doi.org/10.1038/nmeth.1220

Roegiers, F., Djediat, C., Dumollard, R., Rouviere, C., & Sardet, C. (1999). Phases of cytoplasmic and cortical reorganizations of the ascidian zygote between fertilization and first division. *Development*, *126*(14).

Roegiers, F., McDougall, A., & Sardet, C. (1995). The sperm entry point defines the orientation of the calcium-induced contraction wave that directs the first phase of cytoplasmic reorganization in the ascidian egg. *Development 121*(10), 3457–3466. https://doi.org/10.1242/DEV.121.10.3457

Roth, T. F., & Porter, K. R. (1964). Yolk Protein Uptake in the Oocyte of the Mosquito Aedes aegypti. L. *The Journal of Cell Biology*, *20*(2), 313–332. https://doi.org/10.1083/JCB.20.2.313

Rusan, N. M., Fagerstrom, C. J., Yvon, A. M. C., & Wadsworth, P. (2001). Cell cycle-dependent changes in microtubule dynamics in living cells expressing green fluorescent protein-α tubulin. *Molecular Biology of the Cell*, *12*(4), 971–980. https://doi.org/10.1091/MBC.12.4.971

Sallé, J., Xie, J., Ershov, D., Lacassin, M., Dmitrieff, S., & Minc, N. (2019). Asymmetric division through a reduction of microtubule centering forces. *The Journal of Cell Biology*, *218*(3), 771–782. https://doi.org/10.1083/JCB.201807102

Sami, A. B., & Gatlin, J. C. (2022). Dynein-dependent collection of membranes defines the architecture and position of microtubule asters in isolated, geometrically confined volumes of cell-free extracts. *Molecular Biology of the Cell*, *33*(11), br20. https://doi.org/10.1091/MBC.E22-03-0074

Sardet, C., Dru, P., & Ois Prodon, F. (2005). Maternal determinants and mRNAs in the cortex of ascidian oocytes, zygotes and embryos. *Biology of the Cell*, *97*(1), 35–49. https://doi.org/10.1042/BC20040126

Sardet, C., McDougall, A., & Houliston, E. (1994). Cytoplasmic domains in eggs. *Trends in Cell Biology*, *4*(5), 166–172. https://doi.org/10.1016/0962-8924(94)90201-1

Sardet, C., Paix, A., Prodon, F., Dru, P., & Chenevert, J. (2007). From oocyte to 16-cell stage: Cytoplasmic and cortical reorganizations that pattern the ascidian embryo. *Developmental Dynamics*, *236*(7), 1716–1731. https://doi.org/10.1002/dvdy.21136

Sardet, C., Prodon, F., Dumollard, R., Chang, P., & Chênevert, J. (2002). Structure and Function of the Egg Cortex from Oogenesis through Fertilization. *Developmental Biology*, *241*(1), 1–23. https://doi.org/10.1006/DBIO.2001.0474

Sardet, C., Speksnijder, J., Inoue, S., & Jaffe, L. (1989). Fertilization and ooplasmic movements in the ascidian egg. *Development*, *105*(2), 237–249. https://doi.org/10.1242/DEV.105.2.237

Sathananthan, A. H., Selvaraj, K., Lakshmi Girijashankar, M., Ganesh, V., Selvaraj, P., & Trounson, A. O. (2006). From Oogonia to Mature Oocytes: Inactivation of the Maternal Centrosome in Humans. *Microscopy Research And Technique*, *69*, 396–407. https://doi.org/10.1002/jemt.20299

Sawada, T. o., & Osanai, K. (1981). The cortical contraction related to the ooplasmic segregation inCiona intestinalis eggs. *Wilhelm Roux's Archives of Developmental Biology*, *190*(4), 208–214. https://doi.org/10.1007/BF00848304

Sawada, T., & Schatten, G. (1988). Microtubules in ascidian eggs during meiosis, fertilization, and mitosis. *Cell Motility and the Cytoskeleton*, *9*(3), 219–230. https://doi.org/10.1002/cm.970090304

Scarpa, E., Finet, C., Blanchard, G. B., & Sanson, B. (2018). Actomyosin-Driven Tension at Compartmental Boundaries Orients Cell Division Independently of Cell Geometry In Vivo. *Developmental Cell*, *47*(6), 727-740.e6. https://doi.org/10.1016/J.DEVCEL.2018.10.029

Schuh, M., & Ellenberg, J. (2008). A New Model for Asymmetric Spindle Positioning in Mouse Oocytes. *Current Biology*, *18*(24), 1986–1992. https://doi.org/10.1016/J.CUB.2008.11.022

Schwarz, D. S., & Blower, M. D. (2016). The endoplasmic reticulum: Structure, function and response to cellular signaling. In *Cellular and Molecular Life Sciences* (Vol. 73, Issue 1, pp. 79–94). Birkhauser Verlag AG. https://doi.org/10.1007/s00018-015-2052-6

Selman, K., Wallace, R. A., Sarka, A., & Qi, X. (1993). Stages of oocyte development in the zebrafish, Brachydanio rerio. *Journal of Morphology*, *218*(2), 203–224. https://doi.org/10.1002/JMOR.1052180209

Shamipour, S., Hofmann, L., Steccari, I., Kardos, R., & Heisenberg, C.-P. (2022). Yolk granule fusion and microtubule aster formation regulate cortical granule translocation and exocytosis in zebrafish oocytes. *BioRxiv*, 2022.08.10.503442. https://doi.org/10.1101/2022.08.10.503442

Shamipour, S., Kardos, R., Xue, S.-L., Hof, B., Hannezo, E., & Heisenberg, C.-P. (2019). Bulk Actin Dynamics Drive Phase Segregation in Zebrafish Oocytes. *Cell*, *0*(0). https://doi.org/10.1016/j.cell.2019.04.030

Shimogama, S., Iwao, Y., & Hara, Y. (2022). Yolk platelets impede nuclear expansion in Xenopus embryos. *Developmental Biology*, *482*, 101–113. https://doi.org/10.1016/J.YDBIO.2021.12.003

Slack, J. M. W. (1991). From Egg to Embryo: Regional Specification in Early Development. *From Egg to Embryo*. https://doi.org/10.1017/CBO9780511525322

Speksnijder, J. E., Terasaki, M., Hage, W. J., Jaffe, L. F., & Sardet, C. (1993). Polarity and reorganization of the endoplasmic reticulum during fertilization and ooplasmic segregation in the ascidian egg. *Journal of Cell Biology*, *120*(6), 1337–1346. https://doi.org/10.1083/jcb.120.6.1337

Stewart, M. P., Helenius, J., Toyoda, Y., Ramanathan, S. P., Muller, D. J., & Hyman, A. A. (2011). Hydrostatic pressure and the actomyosin cortex drive mitotic cell rounding. *Nature 2010 469:7329*, *469*(7329), 226–230. https://doi.org/10.1038/nature09642

Stolfi, A., & Brown, F. D. (2015). Tunicata. *Evolutionary Developmental Biology of Invertebrates 6: Deuterostomia*, 135–204. https://doi.org/10.1007/978-3-7091-1856-6_4

Strome, S. (1993). Determination of cleavage planes. In *Cell* (Vol. 72, Issue 1, pp. 3–6). Cell Press. https://doi.org/10.1016/0092-8674(93)90041-N

Svitkina, T. M. (2020). Actin Cell Cortex: Structure and Molecular Organization. *Trends in Cell Biology*, *30*(7), 556. https://doi.org/10.1016/J.TCB.2020.03.005

Tanimoto, H., Sallé, J., Dodin, L., & Minc, N. (2018). Physical forces determining the persistency and centring precision of microtubule asters. *Nature Physics*, *14*(8), 848–854. https://doi.org/10.1038/s41567-018-0154-4

Terasaki, M. (2000). Dynamics of the endoplasmic reticulum and Golgi apparatus during early sea urchin development. *Molecular Biology of the Cell*, *11*(3), 897–914. https://doi.org/10.1091/mbc.11.3.897

Terasaki, M., & Jaffe, L. A. (1991). Organization of the sea urchin egg endoplasmic reticulum and its reorganization at fertilization. *Journal of Cell Biology*, *114*(5), 929–940. https://doi.org/10.1083/jcb.114.5.929

Terasaki, M., Okumura, E. I., Hinkle, B., & Kishimoto, T. (2003). Localization and Dynamics of Cdc2-Cyclin B during Meiotic Reinitiation in Starfish Oocytes. *Molecular Biology of the Cell*, *14*(11), 4685–4694. https://doi.org/10.1091/MBC.E03-04-0249

Terasaki, M., Runft, L. L., & Hand, A. R. (2001). Changes in Organization of the Endoplasmic Reticulum during Xenopus Oocyte Maturation and Activation. *Molecular Biology of the Cell*, *12*(4), 1103–1116. https://doi.org/10.1091/mbc.12.4.1103

Thompson, D. W. (1942). On growth and form. *Cambridge University Press*, *Vol. 2,* 470.

Tikhomirova, M. S., Kadosh, A., Saukko-Paavola, A. J., Shemesh, T., & Klemm, R. W. (2022). A role for endoplasmic reticulum dynamics in the cellular distribution of microtubules. *Proceedings of the National Academy of Sciences of the United States of America*, *119*(15), e2104309119. https://doi.org/10.1073/PNAS.2104309119

Tolić-Nørrelykke, I. M. (2008). Push-me-pull-you: How microtubules organize the cell interior. *European Biophysics Journal*, *37*(7), 1271–1278. https://doi.org/10.1007/s00249-008-0321-0

Tsagkogeorga, G., Turon, X., Hopcroft, R. R., Tilak, M. K., Feldstein, T., Shenkar, N., Loya, Y., Huchon, D., Douzery, E. J., & Delsuc, F. (2009). An updated 18S rRNA phylogeny of tunicates based on mixture and secondary structure models. *BMC Evolutionary Biology*, *9*(1). https://doi.org/10.1186/1471-2148-9-187

Turlier, H., Audoly, B., Prost, J., & Joanny, J. F. (2014). Furrow constriction in animal cell cytokinesis. *Biophysical Journal*, *106*(1), 114–123. https://doi.org/10.1016/J.BPJ.2013.11.014

van Bergeijk, P., Hoogenraad, C. C., & Kapitein, L. C. (2016). Right Time, Right Place: Probing the Functions of Organelle Positioning. *Trends in Cell Biology*, *26*(2), 121–134. https://doi.org/10.1016/J.TCB.2015.10.001

van Leen, E. V., di Pietro, F., & Bellaïche, Y. (2019). Oriented cell divisions in epithelia: from force generation to force anisotropy by tension, shape and vertices. *Current Opinion in Cell Biology*, *62*, 9–16. https://doi.org/10.1016/j.ceb.2019.07.013

Voeltz, G. K., Rolls, M. M., & Rapoport, T. A. (2002). Structural organization of the endoplasmic reticulum. *EMBO Reports*, *3*(10), 944–950. https://doi.org/10.1093/EMBO-REPORTS/KVF202

Wakatsuki, T., Schwab, B., Thompson, N. C., & Elson, E. L. (2001). Effects of cytochalasin D and latrunculin B on mechanical properties of cells. *Journal of Cell Science*, *114*(5), 1025–1036. https://doi.org/10.1242/JCS.114.5.1025

Wallace, R. A. (1985). Vitellogenesis and oocyte growth in nonmammalian vertebrates. *Developmental Biology*, *1*, 127–177. https://doi.org/10.1007/978-1-4615-6814-8_3

Wallace, R. A., Opresko, L., Wiley, H. S., & Selman, K. (1983). The oocyte as an endocytic cell. *Ciba Foundation Symposium*, *98*, 228–248. https://doi.org/10.1002/9780470720790.CH13

Wang, S., Romano, F. B., Field, C. M., Mitchison, T. J., & Rapoport, T. A. (2013). Multiple mechanisms determine ER network morphology during the cell cycle in Xenopus egg extracts. *Journal of Cell Biology*, *203*(5), 801–814. https://doi.org/10.1083/jcb.201308001

Williaume, G., de Buyl, S., Sirour, C., Haupaix, N., Bettoni, R., Imai, K. S., Satou, Y., Dupont, G., Hudson, C., & Yasuo, H. (2021). Cell geometry, signal dampening, and a bimodal transcriptional response underlie the spatial precision of an ERK-mediated embryonic induction. *Developmental Cell*, *56*(21), 2966-2979.e10. https://doi.org/10.1016/J.DEVCEL.2021.09.025

Wulff, J. L. (1991). Asexual fragmentation, genotype success, and population dynamics of erect branching sponges. *Journal of Experimental Marine Biology and Ecology*, *149*(2), 227–247. https://doi.org/10.1016/0022-0981(91)90047-Z

Xiang, X., & Qiu, R. (2020). Cargo-Mediated Activation of Cytoplasmic Dynein in vivo. *Frontiers in Cell and Developmental Biology*, *8*, 1212. https://doi.org/10.3389/FCELL.2020.598952/BIBTEX

Yamamoto, K., & Kimura, A. (2017). An asymmetric attraction model for the diversity and robustness of cell arrangement in nematodes. *Development*, *144*(23), 4437–4449. https://doi.org/10.1242/DEV.154609

Yamamoto, K., & Oota, I. (1967). An electron microscope study of the formation of the yolk globule in the oocyte of zebrafish, Brachydanio rerio. . 北海道大學水産學部研究彙報, *17*, 165-174.

Yamamoto, S., Gaillard, J., Vianay, B., Guerin, C., Orhant-Prioux, M., Blanchoin, L., & Théry, M. (2022). Actin network architecture can ensure robust centering or sensitive decentering of the centrosome. *The EMBO Journal*, *41*(20), e111631. https://doi.org/10.15252/EMBJ.2022111631

Yasuo, H., & McDougall, A. (2018). Practical guide for ascidian microinjection: Phallusia mammillata. *Advances in Experimental Medicine and Biology*, *1029*, 15–24. https://doi.org/10.1007/978-981-10-7545-2_3

Yoneda, M., Kobayakawa, Y., Kubota, H. Y., & Sakai, M. (1982). Surface contraction waves in amphibian eggs. *Journal of Cell Science*, *54*(1), 35–46. https://doi.org/10.1242/JCS.54.1.35

Yoshida, M., Horiuchi, Y., Sensui, N., & Morisawa, M. (2003). Signaling pathway from [Ca2+]i transients to ooplasmic segregation involves small GTPase rho in the ascidian egg. *Development, Growth & Differentiation*, *45*(3), 275–281. https://doi.org/10.1046/J.1524-4725.2003.695.X

Yoshizaki, N., Soga, M., Ito, Y., Kun, M. M., Sultana, F., & Yonezawa, S. (2004). Two-step consumption of yolk granules during the development of quail embryos. *Development, Growth & Differentiation*, *46*(3), 229–238. https://doi.org/10.1111/J.1440-169X.2004.00740.X

Yüce, Ö., Piekny, A., & Glotzer, M. (2005). An ECT2-centralspindlin complex regulates the localization and function of RhoA. *Journal of Cell Biology*, *170*(4), 571–582. https://doi.org/10.1083/JCB.200501097/VIDEO-10

Annexes

Annex 1: Movie legend and additional movies

In chapter 1:
Movie 8. Drastic example of cell deformation and actin loss in mitosis

Sum of several confocal z-section from a timelapse series showing the F-actin in grey, from mid-interphase to beginning of cytokinesis. NEB at 13:00. Time in min:sec. F-actin is labelled with LifeAct:RFP.

Movie 9. Micropipette aspiration

Bright field timelapse of the zygote deformation in a micropipette applying a constant negative pressure. **A-** At the vegetal pole, **B-** At the animal hemisphere. Time in min:sec.

Movie 10. Simulation of the aster migration with a transient asymmetric pulling at mitosis entry.

2D simulation of the aster migration from mid-meiosis to mitosis. The aster core (centrosome) is represented by a purple dot at the center of the MTs structure. MTs are in white, they are set to become more stable in interphase and when they touch the cortex. The purple cell border illustrates the activity of cortical dyneins. At entry in mitosis, half of cortical dyneins are inactivated on the aster side. The grey are cytoplasmic dyneins. They become green when attached to MTs.

In chapter 2:
Movie 11. Yolk exclusion around the DNA
Selected confocal z-section of a xyzt acquisition of yolk (cyan) and DNA (grey) in a zygote from meiosis II to cytokinesis. Yolk Time in hour:min. Yolk is labelled with nile red, DNA with hoescht.

Movie 12. Inhibition of MTs after yolk segregation formation
Selected confocal z-section of a xyzt acquisition of yolk (grey) before and after addition of nocodazole around 35 mpf. MTs were inhibited after the yolk has been excluded from the spermaster. Time post fertilization in hour:min

Movie 13. Yolk granules are passive
Confocal z-section of a zygote at the end of Meiosis II/beginning of interphase, showing yolk granules (green, labelled with LysoTracker red), and MTs (red, labelled with Ens:Venus).The aster grows. Several yolk granules near and far from the aster center were circled in white as examples, none showed directional transport, through the 15 min of the movie. Time in min:sec

Movie 14. Simulation of ER-YG exclusion model

2D simulation of the ER-YG exclusion model. The aster core (centrosome) is represented by a orange dot at the center of the MTs structure. MTs are in white. Red beads represent yolk granules that do not attach to motors. Green beads represent the ER, they are all tethered to a minus-end directed motor

Supplementary movies:

Throughout my thesis I attempted several experiments that revealed to be too challenging to pursue, among which the injection of fluorescent bead and laser ablation of the sperm aster.

Movie 15. Fluoresent beads injected in the zygote

Fluorescent beads (in red) of A-1μm and B- 0.2 μm diameter were injected in the zygote to test a size exclusion model for the yolk granules exclusion around the sperm aster. YG diameter is 1.6 μm. Time in min:sec. Injection of bigger beads failed as they block the injection pipette.

Movie 16. Laser ablation of interphasic MTs

Laser ablation of interphasic MTs (in grey) between the aster and the cortex, performed with ZEIZZ 780 on zygotes injected with Ensconsin::Venus. By ablating MTs between the cortex and the aster in interphase, I tested whether cortical attachment was responsible for a lack of migration during interphase. The ablation was successful, but done in 1z. I discarded this experiment because of the poor quality of the embryo at the time, and because given the 3D aster and embryo, a lack of aster migration after ablation could be due to MTs attachment to the cortex on other z, or could be a result, and I lacked controls to determine between the hypotheses. I am grateful to Matteo Rauzi and his team who welcomed me in their lab to use their equipment for this experiment.

Movie 17. Second example of MT pushing on plasma membrane in meiosis/inter/mitosis. Confocal timeseries of zygote with microtubules (magenta) labelled with Ensconsin::3GFP and the plasma membrane labelled with Cell Mask Orange (cyan) and treated with latrunculin. Time in min:sec. Scale bar is 10μm.

Annex 2: Aster speed throughout cell cycle

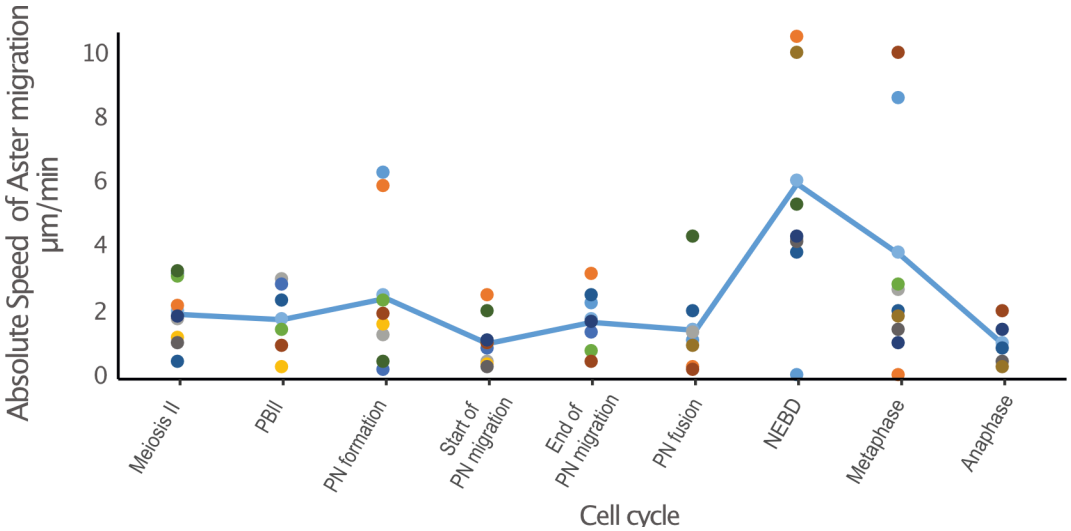

Figure A1: Aster speed throughout cell cycle

Graph of the speed of the aster in µm/min computed from the data shown in Figure 1 of the DNA distance to the cell center. The x-axis shows the cell cycle stages.

Annex 3: Aspect ratio of individual zygotes

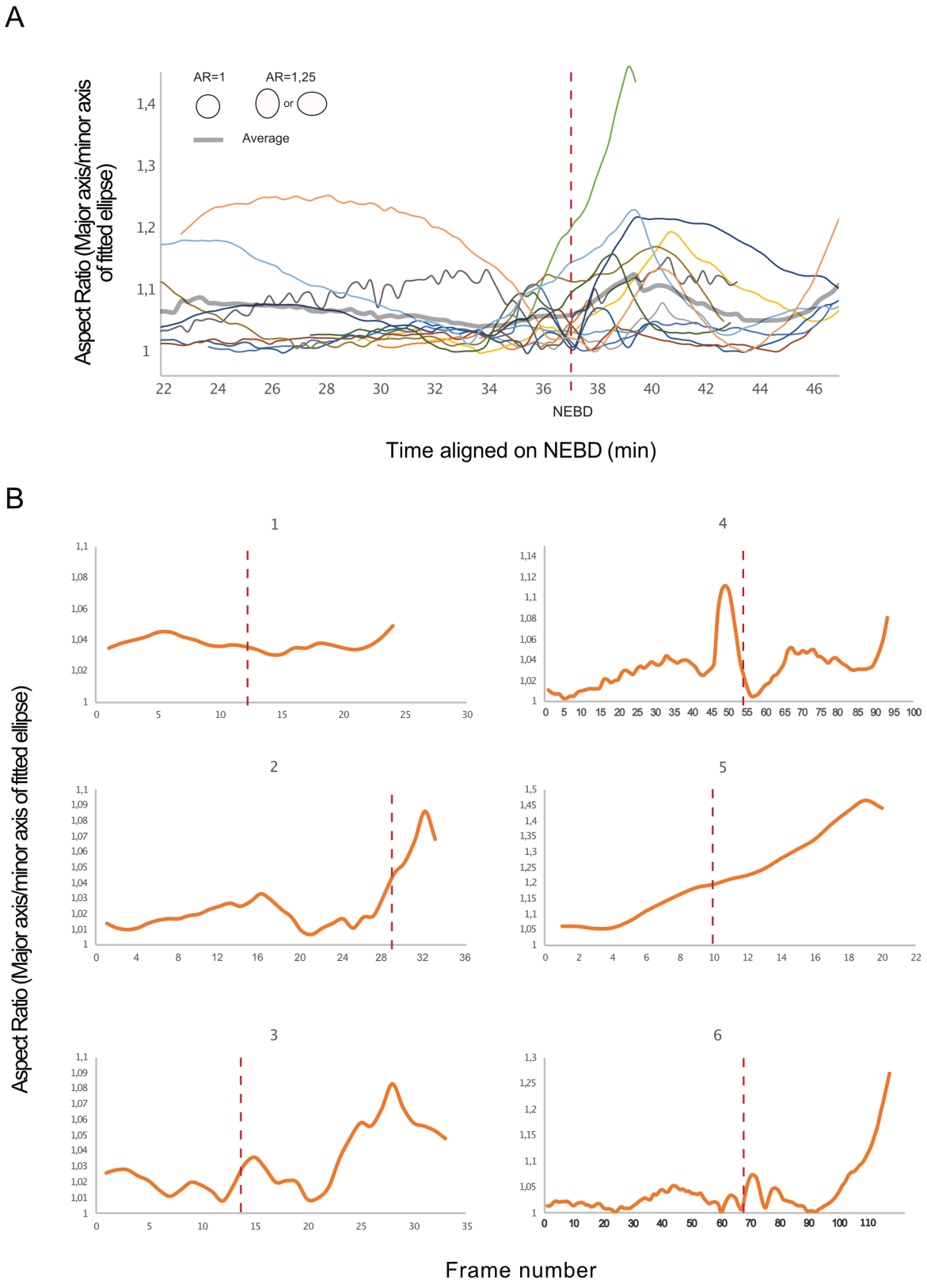

Figure A2: Aspect ratio of individual zygotes around their time of NEB

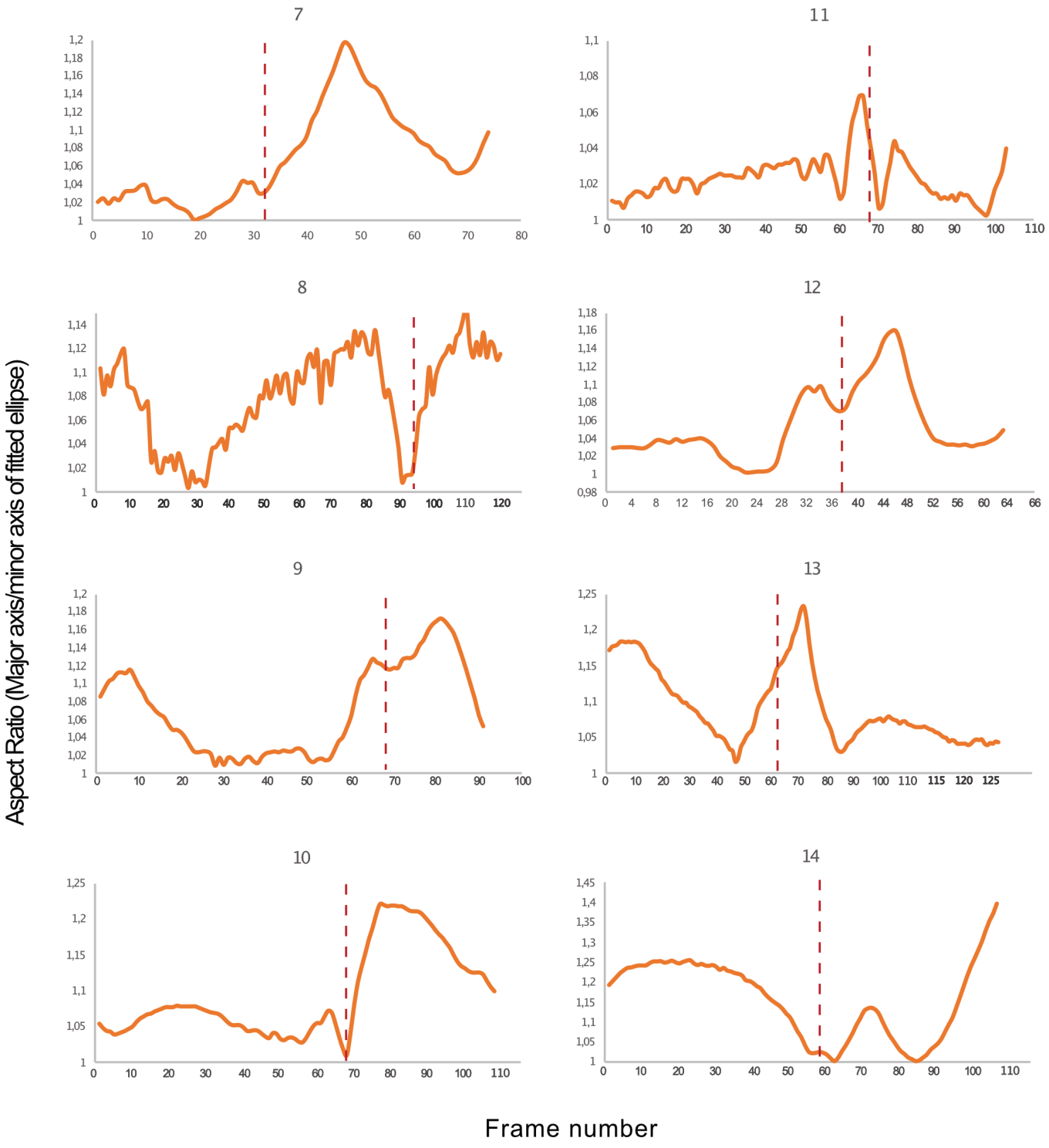

Figure A2 (continuation): Aspect ratio of individual zygotes around their time of NEB

A- Aspect ratio (AR) of the 2D ellipse that best fit the zygote shape as a function of time. Curves are aligned with respect to the time of NEB (dotted line). The average AR of 14 zygotes is represented in thick grey. Colored curves represent the AR of individual zygotes. B- For clarity individual curves are displayed, the red dotted line represents time of NEB, x-axis is the frame number of the movie analysed, all movies were taken with a time-step of 15seconds.